UCLA
UCLA Electronic Theses and Dissertations

Title
Polymeric Materials for Enhancing Therapeutic Biologics

Permalink
https://escholarship.org/uc/item/9pg8h84h

Author
Puente, Ellie Grace

Publication Date
2024

Peer reviewed|Thesis/dissertation

eScholarship.org Powered by the California Digital Library
University of California

UNIVERSITY OF CALIFORNIA

Los Angeles

Polymeric Materials for Enhancing Therapeutic Biologics

A dissertation submitted in partial satisfaction of the

requirements for the degree Doctor of Philosophy

in Chemistry

by

Ellie Grace Puente

2024

ABSTRACT OF THE DISSERTATION

Polymeric Materials for Enhancing Therapeutic Biologics

by

Ellie Grace Puente

Doctor of Philosophy in Chemistry

University of California, Los Angeles, 2024

Professor Heather D. Maynard, Chair

Peptide and protein therapeutics are a growing and diverse field of medicine for the treatment of numerous diseases. Compared to small molecule therapeutics, protein and peptide therapeutics offer high specificity towards their target, minimizing off-target effects. However, translation of these therapeutics to the clinic is limited by their poor stability, pharmacokinetics, and immunogenetic concerns. Polymeric materials have been used to stabilize and deliver these biologics as excipients, conjugates, and nanoparticles. Herein, challenges with the stability of protein and peptide therapeutics will be discussed as well as polymeric delivery strategies with an

emphasis on polymeric nanoparticles, covalent conjugation of PEG, known as PEGylation, and biodegradable polymers. My research focuses on 1) the exploration of polymeric nanoparticles to stabilize and deliver the therapeutic peptide glucagon, 2) the comparison of polymer protein homo dimerization via cysteine bioconjugation, 3) the comparison of polymer protein multimerization with Au (III) reagents via cysteine bioconjugation, and 4) the synthesis and characterization of degradable sulfonated polymers.

Glucagon is a peptide hormone that acts via receptor-mediated signaling predominantly in the liver to raise glucose levels by hepatic glycogen breakdown or conversion of noncarbohydrate, 3 carbon precursors to glucose by gluconeogenesis. Glucagon is administered to reverse severe hypoglycemia, a clinical complication associated with type 1 diabetes. However, due to low stability and solubility at neutral pH, there are limitations in the current formulations of glucagon. In Chapter 2, trehalose methacrylate-based nanoparticles were utilized as the stabilizing and solubilizing moiety; glucagon was site-selectively modified to contain a cysteine at amino acid number 24 to covalently attach to the methacrylate-based polymer containing pyridyl disulfide side chains. PEG_{2000} dithiol was employed as the crosslinker to form uniform nanoparticles. Glucagon nanogels were monitored in Dulbecco's phosphate-buffered saline (DPBS) pH 7.4 at various temperatures to determine its long-term stability in solution. Glucagon nanogels were stable up to at least 5 months by size uniformity when stored at −20 °C and 4 °C, up to 5 days at 25 °C, and less than 12 hours at 37 °C. When glucagon stability was studied by either HPLC or thioflavin T assays, the glucagon was intact for at least 5 months at −20 °C and 4 °C within the nanoparticles at −20 °C and 4 °C and up to 2 days at 25 °C. Additionally, the glucagon nanogels were studied for toxicity and efficacy using various assays *in vitro*. The findings indicate that the nanogels were nontoxic to fibroblast cells and nonhemolytic to red blood cells. The glucagon in

the nanogels was as active as glucagon alone. These results demonstrate the utility of trehalose nanogels towards a glucagon formulation with improved stability and solubility in aqueous solutions, particularly useful for storage at cold temperatures.

Protein self-assembly into dimers and higher order structures in biological systems can be essential for protein function and activity, however, many of these complexes are unstable *in vivo*. Polymeric linkers with reactive handles for protein bioconjugation can stabilize protein higher order structures and improve their pharmacokinetics. In Chapter 3, cysteine bioconjugation strategies are explored with poly(ethylene) glycol (PEG) reagents to dimerize the model protein T4 lysozyme (V131C), containing a single surface exposed cysteine. Dimer conversion with dicyclohexylphosphine (PCy_2) P,N ligated PEG2000 Au(III), di-1-adamantylphophine (PAd_2) P,N ligated PEG2000 Au(III), $(maleimide)_2$, and $(vinyl\ sulfone)_2$ bifunctionalized PEG were compared at pH 6.0, pH 7.5, and 9.0 and their stability evaluated. This work adds to the growing body of literature on protein dimerization.

The work towards investigating higher order oligomeric protein polymer structures is expanded on utilizing the therapeutic protein basic fibroblast growth factor 2 (FGF-2) in Chapter 4. The multimerization conversion from monomeric FGF-2 is investigated at various equivalents, temperatures, and reaction times. This work adds to the growing body of literature on protein multimerization.

Polycaprolactone is a widely used biocompatible and degradable polymer. However, the polymer is hydrophobic, and not soluble in water. There are advantages to rendering the polymer soluble in aqueous solutions. In Chapter 5, allyl functionalized caprolactone underwent anionic ring-opening polymerization (ROP) and post-polymerization modification *via* thiol-ene click chemistry with 3-mercaptopropane sulfonate. ROP of ally caprolactone to yield poly (allyl-

caprolactone) with molecular weights from 6.3 - 81.2 kDa and poly (sulfonate-caprolactone) with molecular weights from 12.2 - 163.3 kDa after functionalization *via* thiol-ene. The synthetic approaches taken to access high molecular weights of poly (sulfonate-caprolactone), mechanical properties, and degradability of these materials are discussed.

Chapter 2 is published as: Puente, E. G.; Sivasankaran, R.; Vinciguerra, D.; Yang, J.; Lower, H. C.; Hevener, A.; Maynard, H. D. "Uniform Trehalose Nanogels for Glucagon Stabilization." *RSC Appl. Polym*. 2024, 2, 473. Chapter 3 is in preparation for publication as: Puente, E. G.; Polite, M. F.; Meckes, F. A.; Spokoyny, A. M.; Maynard, H. D. "Comparison of Polymer Protein Homo Dimerization via Cysteine Bioconjugation." *In Preparation*. Chapter 5 is in preparation for publication as: Puente, E. G.; Snell, K. M.; Maynard, H. D. "Degradable Sulfonate Polymers by Thiol-ene Click Chemistry." *In Preparation*.

This dissertation of Ellie Grace Puente is approved.

Andrea L. Hevener

Jose A. Rodriguez

Alexander M. Spokoyny

Heather D. Maynard, Committee Chair

University of California, Los Angeles

2024

Esta tesis está dedicada a mí misma, por persistir cuando el miedo me perseguía, y por descubrir la resiliencia que tenía dentro de mí

Table of Contents

List of Figures

List of Tables

List of Abbreviations

Ad	Adamantyl
AIBN	Azobisisobutyronitrile
ATRP	Atom Transfer Radical Polymerization
AUC	Area under the curve
BME	b-mercaptoethanol
Cy	Cyclohexyl
Cys	Cysteine
DCM	Dichloromethane
DI	Deionized
DLS	Dynamic Light Scattering
DMSO	Dimethyl Sulfoxide
DI	Deionized
DLS	Dynamic Light Scattering
DMF	Dimethylformamide
DPBS	Dulbeco's Phosphate Buffered Saline
DSC	Differential Scanning
E. coli	Escherichia Coli
ESI	Electrospray Ionization
Eq.	Equivalents
FBS	Fetal Bovine Serum
FGF-2	Fibroblast growth factor 2

FPLC	Fast Protein Liquid Chromatography
FDA	Food and Drug Administration
FGF-2	Fibroblast growth factor 2
FPLC	Fast Protein Liquid Chromatography
FTIR	Fourier Transform Infrared Spectroscopy
GPC	Gel Permeation Chromatography
GSH	Glutathione
HPLC	High Performance Liquid Chromatography
IPTG	Isopropyl- β-D-thiogalactopyranoside
kDa	kilodalton
LCMS	Liquid Chromatography-Mass Spectrometry
MeCN	Acetonitrile
MeOH	Methanol
MTBD	7-methyl-1,5,7-triazabicyclo(4.4.0)dec-5-ene
NMR	Nuclear Magnetic Resonance
OA	Oxidative Addition
OACs	Oxidative Addition Complexes
PCL	Poly(caprolactone)
PDSOH	Pyridyl disulfide ethyl alcohol
PDSMA	Pyridyl disulfide ethyl methacrylate
PEG	Poly(Ethylene Glycol)
PGA	Poly(glycolic acid)
PLA	Poly(lactic acid)

RE	Reductive Elimination
ROP	Ring-opening polymerization
SDS-PAGE	Sodium Dodecylsulfate-Polyacrylamide Gel Electrophoresis
SEC	Size Exclusion Chromatography
T4L	T4 Lysozyme
TCEP	Tris(2-carboxyethyl)phosphine
TCEP·HCl	Tris(2-carboxyethyl)phosphine hydrochloride
TEA	Triethylamine
TEM	Transmission Electron Microscopy
TGA	Thermogravimetric analysis
ThT	Thioflavin T
TrMA	Trehalose methacrylate
UV	Ultraviolet Transmission Electron Microscopy
3-O	1-(3,5-bis(trifluoromethyl)phenyl)-3-cyclohexylthiourea

Acknowledgments

My thesis represents the culmination of years of hard work and dedication, and it would not have been possible without the support, guidance, and encouragement of many individuals. I would like to express my heartfelt gratitude and deepest appreciation to all those who have contributed to this journey.

To my parents, your unwavering love, encouragement, and belief in me, even during the most challenging times, did not go unnoticed. I am truly fortunate to have parents who have always inspired me to pursue my dreams and never give up, no matter the obstacles. Mom, thank you for listening and trying your best to understand the trials and tribulations of my time as a graduate student. Dad, thank you for supporting me and encouraging me through the hard times, and celebrating with me when deserved. Kate, thank you for providing comedic relief during some of the most demanding time. I hope I can continue answering all of yours and Cam's science related questions for years to come. My desire to pursue a PhD at UCLA is rooted from the many roles it has played in my family's life. To my Grandma Carolyn and Grandpa Bob who spent time at UCLA as undergraduates, with my grandpa playing football, you paved the way and drew importance on the value of education, learning, and knowledge. To my namesake, Dr. Elliot, your kindness and intelligence during your time at UCLA Mattel Hospital to cure my brother from leukemia inspired me to pursue a career where I could also make a difference. Jordan, your perseverance and ability to dream big inspires me to do the same. Yolo, thank you for always believing and supporting me, I appreciated it greatly. To my Grandma Chelia and Grandpa Pablo- you are both the definition of what hard work can accomplish and inspire. You taught our family the value in working hard to provide for your family and I think about you both daily.

To my best friends, Cat Gang, Eyo, Jenny, and Hayley – thank all for being understanding and empathetic with me during my time in graduate school. Our friendship means the world to me, and I will forever cherish all the times I was able to shut out the stress of school and take workout classes, girls trips, and giggle together. To my emotional support animals Chesney and Mer, thank you for providing so much more than emotional support over the past years and for all the years to come. To my community at CorePower yoga and my fellow teachers, thank you for allowing me to grow spiritually, mentally, and physically and simultaneously become an instructor myself.

To my high school chemistry teacher Mr. Iverson, thank you for sparking my interest and curiosity in chemistry and all it could do. To my undergraduate mentor Dr. Alexander Malinick, your passion and excitement for research inspired me to pursue my PhD. To my advisor Prof. Heather Maynard, thank you for providing me with the space to grow into the scientist I am today. I would like to thank all the members of my committee, especially those who I have had the opportunity to collaborate with and learn from - Prof. Alexander Spokoyny and Prof. Andrea Hevener. During my time at UCLA, I have had the pleasure of being a teaching assistant to many undergraduates; thank you specifically Dr. Nicholas Deifel for supporting me as a teacher as well as providing mentorship outside of the classroom.

I would not have been able to get up each day and step foot into to lab without the graduate students and friends I've made along the way at UCLA. I would like to thank my first grad school mentor- Dr. Jane Yang, your tough love approach pushed me to work hard and become a better scientist each day. Dr. Daniele Vinciguerra- thank you for introducing me to the world of polymers and providing guidance during my first couple years. Dr. Mikayla Tan- the vibes we cultivated in 4230 with our music blasting and coffee brewing made getting to work at the crack of dawn doable. Haillie Lower- we started this crazy journey together and I wouldn't have wanted it any other way.

I am so thankful for having you by my side in the lab being silly first years just trying to make polymers to all our friendship have grown in to today. Dr. Hayden Montgomery - thank you for becoming a mentor to me and teaching me all the things about bioconjugation; I am also so grateful for all our memories both inside and outside of lab from the infamous griddle days to Jonas Brother concerts. Dr. Grace Kunkel - I remember meeting you at recruitment and being so excited to join lab with you because you were so funny- thank you for filling the lab with laughter and for our speakers to somehow be in sync from labs away. Dr. Billy Treacy - thank you for all your help throughout my time in the lab, even if it didn't seem like it, I appreciated it. Katie Snell, whether it was working next to you in our hoods, all our time spent in 4230, or at yoga, having you by my side while we tried daily to get our ducks in a row made the daily grind so much better. Felix Fu, I am so glad I forced you to move to 4230 with me and provide comedic relief when it felt like the world was on fire. Brock Hosier - your youthful stories, presence, and sense of humor elevated the 4230 office and I can't wait to see all you accomplish in graduate school and beyond. To my undergraduate mentee Alex Meckes, your excitement and curiosity for research made mentoring you so much fun. To Ricky Ruiz- you are the backbone of our department, and I truly appreciate all the times you went out of your way to help and support me. To the next generation of chemists, Maggie Polite, Ryan Lai, and Ben Miller – I can't wait to see all you accomplish and the incredible chemists I know you will all become. Thank you to all the past and current members of the Maynard lab that I had the pleasure of overlapping with.

To all the women and women of color in STEM that have come before me and will come after me, never less we persist.

Vita

Education

University of California, Los Angeles, Los Angeles, CA

Doctor of Philosophy in Chemistry — Expected: December 2024

Master of Science in Chemistry — March 2022

Bachelor of Science in Biochemistry — June 2020

Publications

- **Puente, E. G**.; Snell, K. M.; Maynard, H. D. "Degradable Sulfonate Polymers by Thiol-ene Click Chemistry." *In Preparation*.
- **Puente, E. G**.; Polite, M. F.; Meckes, F. A.; Spokoyny, A. M.; Maynard, H. D. "Comparison of Polymer Protein Homo Dimerization via Cysteine Bioconjugation." *In Preparation*.
- **Puente, E. G**.; Sivasankaran, R.; Vinciguerra, D.; Yang, J.; Lower, H. C.; Hevener, A.; Maynard, H. D. "Uniform Trehalose Nanogels for Glucagon Stabilization." *RSC Appl. Polym*. **2024,** 2, 473.
- Kunkel, G. E.; Treacy, J. W.; Montgomery, H. R.; **Puente, E. G**.; Doud, E. A.; Spokoyny, A. M.; Maynard, H. D*. "Efficient end-group functionalization and diblock copolymer synthesis via Au(III) polymer reagents." *Chem. Commun.* 60, **2024**, 79-82.
- Yang, J.; Gelb, M. B.; Tamshen, K.; Forsythe, N. L.; Ko, J. H.; **Puente, E. G.**; Pelegri-O'Day, E.; Jamieson, S. M. J.; Perry, J. K.; Maynard, H. D. "Site-Selective Zwitterionic Poly(caprolactone-carboxybetaine)-Growth Hormone Receptor Antagonist Conjugate: Synthesis and Biological Evaluation. "*Biomacromolecules*. **2024**. Accepted.
- Sivasankaran, R. P.; Snell, K.; Kunkel, G.; Georgiou, P.; **Puente, E. G**.; Maynard, H.D. "Polymer-mediated Protein/Peptide Therapeutic Stabilization: Current Progress and Future Directions." *Prog. Polym. Sci.* **2024**, 156, 101867.
- Malinick, A. S.; Lambert, A. S.; Stuart, D. D.; Li, B.; **Puente, E**.; Cheng, Q. "Detection of Multiple Sclerosis Biomarkers in Serum by Ganglioside Microarrays and Surface Plasmon Resonance Imaging." *ACS Sens.* **2020**, *5* (11), 3617–3626.

Presentations

- "Uniform Trehalose Nanogels for Glucagon Stabilization" UCCS, Lake Arrowhead, CA, March 2024 (presentation).
- "Uniform Trehalose Nanogels for Glucagon Stabilization" Seaborg Symposium, UCLA, Los Angeles, CA, January 2024 (poster).
- "Uniform Trehalose Nanogels Improve Long Term Glucagon Stability" UCCS, Lake Arrowhead, CA April 2023 (poster). "

Awards

- Michael E. Jung Excellence in Teaching Award, 2024.
- Kuwana and Sawyer Undergraduate Award in Analytical Chemistry, 2020.
- Chancellor's and Dean's Honor's List University of California, Riverside, 2018, 2019, 2020.

Teaching Experience

Teaching Assistant – September 2020 – December 2024

UCLA Department of Chemistry and Biochemistry

- General Chemistry for Life Sciences Laboratories (CHEM14B and CHEM14CL)
- Organic Chemistry for Life Sciences (CHEM20L)
- Organic Chemistry for Physical Sciences Laboratories (CHEM30AL and CHEM30BL)

Leadership and Service

- California NanoSystems Institute (CNSI) Nanoscience Outreach 2020 – 2022
- Organization for Cultural Diversity in Science (OCDS)
    - *Professional Development Chair* 2021 – 2022
    - *Member* 2020 – 2024

Chapter 1

Polymeric Strategies for Protein Delivery and Stabilization[†]

1.1 Introduction

Therapeutic biologics are a growing and diverse field of medicine derived from a biological source and include monoclonal antibodies, growth factors, proteins and peptides.[1] The United States Food and Drug Administration (FDA)-approved biologics have increased in the past century, gaining a large interest, with recent advances such as CRISPR–Cas9-edited cell therapy and antibody-based therapies.[2] Compared to small molecule therapeutics, protein and peptide therapeutics offer high specificity towards their target, minimizing off-target effects. *In vivo*, proteins and peptides often experience low cell membrane permeability, degradation and denaturation, and rapid metabolism, resulting in decreased bioavailability.[3,4] Proteins and peptides face additional stability challenges through manufacturing, formulation, and cold chain transportation.[5,6] Polymeric materials have been used to stabilize and deliver these biologics as excipients, conjugates, and nanoparticles. Herein, challenges with the stability of protein and peptide therapeutics will be discussed as well as polymeric delivery strategies with an emphasis on polymeric nanoparticles, covalent conjugation of PEG, known as PEGylation, and biodegradable polymers.

1.2 Challenges with Stability of Protein and Peptide Therapeutics

1.2.1 Mechanisms of Instability: Degradation, Fibrillation, Aggregation

Protein and peptide stability in biologics is a challenge that the biopharmaceutical industry faces. Proteins experience many changes to their environments during the manufacturing process, formulation, and cold chain transportation.[5,6] Stress factors that can affect the stability of the protein include temperature, pH, and agitation.[7,8] Countries with poor access to refrigeration and in regions with elevated climatic temperatures have attempted to delay the degradation of these biologics by using handmade cold storage devices; however, these attempts are temporary and are

not sustainable.[9,10] The stresses of the bioprocessing system such as temperature fluctuations, pH variations, shear forces, and interactions with container surfaces affect protein formulation stability and efficacy, and ultimately lead to alterations in the pharmacokinetic profile, reduction in bioavailability, and pose a threat to the patient health. Therefore, it is important to understand the mechanisms and causes of biologic instability to further improve their formulation stability.[11] The mechanism of instability of a protein generally falls in the two categories: physical or chemical instability.

1.2.2. Physical Instability

Proteins that exhibit physical instability undergo a transformation in their higher-order structure, thereby altering the protein itself. Protein denaturation is one of the most common physical changes. Denaturation is a process in which a protein unfolds, resulting in the disruption of secondary and/or tertiary structure. Proteins subjected to increased temperatures undergo thermal denaturation, a process usually irreversible in nature. When proteins are properly folded, their hydrophobic patches are buried deeply, minimizing their exposure to water. Once denatured, the unfolded protein becomes highly disordered, forming higher-ordered structures such as dimers and oligomers that lead to soluble and insoluble aggregates in solution.[11–14] The model protein lysozyme has been shown to denature at temperatures at or above 65 °C, resulting in the formation aggregation and fibrils.[15] The pathway of aggregation can be classified as unfolding, chemical linkage, self-association, and degradation.[16] Insulin undergoes an approximately 10-fold increase in degradation for every 10 °C rise at temperatures above 25 °C.[9] Even the clinical formulations of insulin are prone to fibrillation and aggregation at low pH and high temperature, resulting in a decrease in helical content and generation of insulin fibers.[9,17,18] Glucagonlike peptide-1 (GLP-1) and its C-terminal amide derivative, GLP-1Am, are known to aggregate into amyloid fibrils over

time when exposed to elevated temperatures.[19] However, the low molecular weight oligomers formed by an off-pathway mechanism, which competes with amyloid fibril formation, were shown to be stable.[19] During bioprocessing, proteins adsorb at the air/water interface, which increases the exposure of hydrophobic regions, enhancing aggregation; this was studied for various proteins such as bovine serum albumin, catalase, lipase, lysozyme, and papain.[20]

1.2.3. Chemical Instability

Proteins that exhibit chemical instability undergo a covalent modification through the breaking or forming of bonds in the first order structure. Therapeutic biomolecules are susceptible to hydrolysis, which is unfavorable when formulating them in aqueous solution. At pH 2.7, bovine serum albumin (BSA) can readily undergo hydrolysis or interact with metal ions, resulting in a denatured protein.[21] The aspartic acid-proline (Asp-Pro) amino acid sequence of proteins is commonly susceptible to hydrolysis due to the catalysis of the carbonyl group of the Asp residue.[22] Deamidation occurs via the hydrolysis of the side-chain amide linkage in asparagine (Asn), especially asparagine-glycine (Asn-Gly) and asparagine-serine (Asn-Ser) and glutamine (Gln), leading to the formation of a free carboxylic acid.[23,24] The conversion of a neutral residue to a negatively charged residue can reduce bioactivity if it affects the active site or the structural conformation of the protein. Oxidation of a protein can occur with changes to pH, exposure to light, atmospheric oxygen, or redox-active metal ions (Cu2+, Fe2+).[25–27] Oxidation is known to impact the structure, functionality, and biological activity of the therapeutic depending on the site of oxidation.[26] Oxidation typically occurs in methionine (Met), histidine (His), lysine (Lys), tryptophan (Trp), and tyrosine (Tyr) residues in proteins [40]. For example, the recombinant human vascular endothelial growth factor (rhVEGF) has been shown to be susceptible to oxidation and deamidation, leading to a reduction in its overall efficacy.[28]

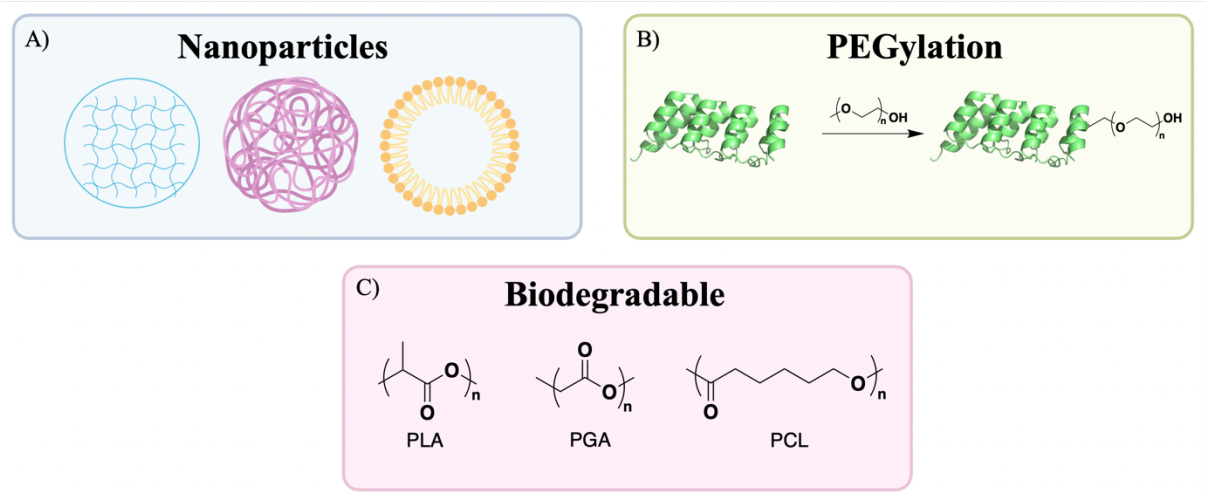

Figure 1.1 Polymeric materials used for stabilization and delivery of therapeutic biologics include, but are not limited to, A) polymeric nanoparticles, B) PEGylation, and C) biodegradable polymers.

1.3 Polymeric Delivery Strategies

1.3.1 Polymeric Nanoparticles

Protein and peptide-containing nano-formulations have been used in the clinical setting and have demonstrated enhanced efficacy and reduced side effects upon delivery due to their nanoscale confinement.[29–32] A variety of natural, synthetic or composite nanomaterials have thus far been investigated as potential candidates for protein stabilization and delivery, such as carbon nanotubes,[33] inorganic-based materials such as mesoporous silica,[34] metallic nanoparticles,[35] and many others. These nanocarriers, however, demonstrate significant limitations, including low encapsulation efficiency, physical instability and inherent toxicity to cells or tissues.[36,37] Notable nanocarriers in biomolecule stabilization include lipid-containing, colloidal systems (i.e. lipid nanoparticles),[38] liposomes,[39] protein-based carriers,[40] and polymeric nanoparticles.[41] Polymeric nanocarriers have gained a particular interest as vehicles for protein delivery and stabilization thanks to their multifunctionality along with shell, protecting proteins from hydrolytic, enzymatic,

or chemical degradation, enabling targeted delivery of potentially fragile proteins.[42–44] Protein and peptide cargoes can be loaded into various nanocarriers using different strategies. The most prevalent include covalent conjugation approaches, physical adsorption/complexation (non-covalent) including electrostatic interactions, hydrophobic interactions, hydrogen bonding, and physical encapsulation/confinement.

Amphiphilic block copolymers have been used extensively in nanoparticle engineering owing to their structural adaptability, chemical composition, and flexibility. They exhibit a self-assembly behavior in selective solvents forming high-ordered nanostructures.[45] Moreover, their variable molecular weight and tunable chemical properties can be tailored to the requirements of each protein.[46,47] Polyelectrolytes, amphiphilic block copolymers comprising of at least one polyelectrolyte block, and surfactants are also an interesting class of synthetic macromolecules for protein stabilization.[48,49] Polyion complex micelles (PICs) are formed when a negatively or positively charged block copolymer containing a hydrophilic non-ionic block is mixed with an oppositely charged homopolymer or block copolymer through electrostatic interactions and van der Waals forces. During this approach, the use of an organic solvent is avoided, eliminating the side effects caused by the organic solvent and providing PICs as appropriate candidates for the stabilization of proteins and nucleic acids due to their varying charge.[50,51]

Most common polymeric architectures involved in peptide stabilization and delivery include micelles, nanogels, hydrogels and vesicles (**Figure 1.1A**). In this regard, several properties of polymeric nanoparticles, including shape, size, structure, and surface must be considered. These factors play a critical role in the protein's stability, targeting specificity, release kinetics and, thus, therapeutic efficacy. Nanogels are classified as crosslinked materials at high water content with nanoscale size. The water-containing cavity is environmentally beneficial for the localization and

delivery of proteins and other cargo. Specifically, their crosslinked network can restrict the free movement of the cargo, thereby decreasing aggregation and increasing stability.[52,53] Nanogels have been extensively deployed for the long-term stabilization and storage of therapeutic proteins and other biological cargoes. Nanogels provide a protective shell against proteases and enhance the protein transmembrane and intracellular delivery.[54] Various natural and synthetic building blocks, including polysaccharides and vinyl-derived polymers, have been used in nanogel design.[55,56] Functionalization with ligand moieties or incorporation of responsive materials can enhance the protein delivery and therapeutic efficacy through temporal and distribution control like other nanoparticle systems discussed previously.

Two main approaches have been used to design biomolecule-nanogel formulations. These include graft-to through protein post-modification using pre-synthesized polymers and crosslinkers, or graft-from which involves the localization of monomers and crosslinkers (covalent/non-covalent) around the surface of the protein followed by polymerization to yield a protective, polymeric shell.[57] Although nanogels containing a singular enzyme (known as enzyme nanogels, ENGs) are a versatile platform for industrial catalysis and biomedical applications, they are mainly limited to enzymes with small molecule substrates. The polymer around the protein prevents the latter from interacting with other biomacromolecules. Therefore, this system cannot be freely translated to proteins that interact with other macromolecule substrates, such as growth factors, cytokines, and antibodies. In addition, this strategy involves the direct modification of the protein, which can lead to a reduction in activity and even denaturation. To address these challenges, several approaches for non-covalent formation of protein-stabilized nanogels have been developed including the localization of positively charged monomers around a charged protein and the employment of degradable cross-linkers.[58–65] Our group conjugated photocleavable

polymerization handles to phenylalanine ammonia lyase (PAL) to synthesize a nanogel around the protein by graft-from. The covalent bonds between nanogel and protein was cleaved using light after encapsulation, restoring enzyme activity.[66] Lu and co-workers reported the synthesis of organophosphorus hydrolase nanogels exhibiting significantly improved stability at elevated temperature, in organic solvents, after freeze-thaw cycles, and prolonged storage up to seven months.[67] Segura et al. developed a graft-from ATRP approach to grow poly(2-(dimethylamino)ethyl methacrylate) p(DMA)-based homopolymers on ribonuclease (RNase), showing enhancement in enzyme stability compared to RNase alone. This enzyme was proposed as a candidate drug for cancer therapeutics owning to its capability to cease rapid division of tumor cells.[68]

1.3.2 PEGylation

PEGylation is one of the most widely incorporated polymer strategy for stabilizing and delivering protein and peptide therapeutics with 31 FDA-approved PEGylated biologics on the market (**Figure 1.1B**). Formulating biologics with PEG has been shown to increase pharmacokinetics, improve stability, reduce renal clearance, and minimize immunogenicity *in vivo*.[69] Upon PEGylation of proteins in aqueous solutions, the hydrodynamic radius increases, which provides anti-fouling and stealth benefits to protect the biologic towards immune responses.[70–72] Due to these stealth properties and inert polyether backbone, PEG has historically been regarded as non-immunogenic and non-antigenic, and is also generally regarded as safe by the FDA. [73] Additionally, these characteristics tend to improve with larger PEG sizes, however accumulation of PEG molecules greater than 20 kDa interact more strongly with the glomerular filtration membrane, slowing their renal clearance.[74]

Conjugation chemistry between proteins and polymers can often be challenging bringing two large molecules together. Additionally, the efficiency, conversion, and yield of conjugation can limit the translatability of these therapeutics to clinical use. The relative ease of synthesis to prepare amine, thiol, and numerous "click" reactive PEG reagents offers an advantageous approach in synthesizing versatile and scalable protein polymer conjugates.[75–78] PEGylation of interleukin-2 (IL-2) via copper-free click reaction significantly improved the pharmacokinetics and half-life and could offer a more general approach to improving the therapeutic performance to treat autoimmune diseases.[79] Site-specific conjugation with varying PEG sizes to growth hormone receptor antagonist B2036-alkyne through copper mediated click chemistry significantly improved the bioactivity of this therapeutic.[80] Molecular dynamics simulations of insulin and lysozyme reveal that PEG likely stabilizes the proteins at higher temperatures by shielding the hydrophobic regions of the biomolecules from water molecules, thereby stabilizing their secondary structure.[81]

Over the recent decades, there has been an increasing concern regarding the immunogenicity potential of PEGylated therapeutics. Patients who were previously or continuously treated with PEGylated therapeutics can form anti-PEG antibodies, which can unfortunately result in reduced efficacy and hypersensitivity.[82–87] It has been found that some individuals who have not received a PEGylated therapeutic before can exhibit pre-existing anti-PEG antibodies, potentially due to the increase in everyday consumer goods containing PEG products.[88–90] At the same time, PEG alternatives such as poly(glycerol)s, trehalose-based polymers, poly(carboxybetaines), and others have gained increased interest as researchers search for polymers that provide similar stabilizing and enhanced pharmacokinetic properties.[91–95]

1.3.3 Biodegradable Polymers

Biodegradable polymers are made from renewable resources such as corn, sugarcane, and potato that can degrade into non-toxic compounds when exposed to water, air, and microbes.[96] The physical properties such as glass transition temperature (T_g) of biodegradable polymers offer mechanical properties that allow for varying delivery applications such as drug delivery, wound healing, and implants. The most common synthetic biodegradable polymers, also used in biologic therapeutic delivery, include poly(lactic acid) (PLA), poly(glycolic acid) (PGA), and poly(caprolactone) PCL (**Figure 1.1C)**.[97] Synthetic polymers often require the use of environmental conditions, such as temperature, humidity, pH, and high-oxygen conditions to degrade. PCL for example requires the use of strong acids or bases and/or high temperatures to degrade via environmental conditions and otherwise can take a long time *in vivo*. Alternatively, natural polymers based on polypeptides and polysaccharides exhibit biocompatibility and low cost, however, they can be difficult to functionalize and modify compared to synthetic polymers.[98]

The ability to functionalize and modify biodegradable polymers with relative ease and flexibility gives access to a range of synthetically accessible novel properties and applications. Biodegradable polymers can either be functionalized on the monomer or contain a functional handle to access post-polymerization to give access to conjugation handles or stabilization moieties. Conjugation of a macroinitiator to a lipase enzyme and subsequential enzymatic ring opening polymerization with ε-caprolactone yielded biodegradable protein–PCL conjugates, which degraded faster than PCL alone without the presence of the lipase enzyme.[99] The field of protein-polypeptide (PEPylation) conjugations is growing due to the tunable degradation and versatility in side chain functionalities.[100] For example, grafting from poly-L-proline (PLP) from enhanced green fluorescent protein (EGFP) bearing an N-cysteine, dihydrofolate reductase (DHFR), and ASNase, demonstrated improved stability to heat and organic solvent in the case of

DHFR.[101] The thermoresponsive, degradable, and self-immolative poly(ethyl glyoxylate) has been utilized in hydrogels and diblock copolymers to study the degradation properties through a variety of triggers based on both endcap and backbone unit.[102–104] The Wurm group has led the field in the synthesis and application of poly(phosphoesters) (PPEs) with myoglobin-PPE conjugates bearing hydrophilic pendant groups, protecting against thermally induced aggregation and proteolytic degradation, whereas hydrophobic PPEs led to protein destabilization.[105]

Due to its biodegradability, biocompatibility, and versatility, PCL has attracted increasing attention as a promising material for broad applications. PCL has been used in the development of nano-drug delivery systems when copolymerized with hydrophilic counterparts to deliver therapeutic biologics, and furthermore as electrospun materials for wound and tissue therapies.[106–110] For example, PCL-chitosan microparticles increased the loading capacity and extended the release of anti-vascular endothelial growth factor (VEGF).[109] PCL was electrospun and coated with chitosan-based nanogels for a controlled release platform of growth factors bone morphogenetic protein 2 (BMP-2) and transforming growth factor-β_3 (TGF-β_3).[111] While there have been many advances implementing PCL with other polymers as a biodegradable material, our group has worked towards synthesizing a easy to functionalize PCL with allyl side chains to allow for thiol-ene post polymerization to click on stabilizing and water solubilizing side chains stabilize insulin and granulocyte colony stimulating factor (G-CSF).[112,113]

In this thesis, chapter 2 will demonstrate the improvement of stability on the therapeutic peptide, glucagon using a polymeric nanoparticle; chapter 3 and chapter 4 will utilizing PEGylation to prepare protein dimers and multimers; and chapter 5 will explore the degradation and mechanical properties of a PCL derivative.

1.4 Conclusion and Future Perspectives

Polymeric materials act as a protective shield for biomolecule therapeutics, providing improvements in stability during formulation and transportation caused by environmental stressors and in activity *in vivo.* The polymeric delivery strategies outlined herein have shown rapid and evolving progress towards improving the stability and activity of therapeutic biologics. As these therapeutics move towards clinical use, challenges of purification and characterization of these polymeric systems remain. Additionally, developing biodegradable polymers which degrade more quickly or with predictability in biologically relevant conditions will help improve the area of degradable biologics. Innovative advancements through academic research in protein engineering and chemistry continue to progress the field with new possibilities to meet the demand of improved biologics. Scientists should continue to explore new polymers in hopes of discovering novel properties and modes of stabilization while also building on the extensive foundation and learning from our challenges.

1.5 References

†Parts of this chapter, with copyright permission from Elsevier, contains portions of a review article published as: Sivasankaran, R.P.; Snell, K.; Kunkel, G.E.; Georgiou, P.; **Puente, E. G.**; Maynard, H. D. Polymer- mediated Protein/Peptide Therapeutic Stabilization: Current Progress and Future Directions. *Prog. Polym. Sci*. **2024**, 156, 101867.

(1) Research, C. for D. E. and. *Therapeutic Biologics Applications (BLA)*. FDA. https://www.fda.gov/drugs/types-applications/therapeutic-biologics-applications-bla (accessed 2024-08-30).

(2) Senior, M. Fresh from the Biotech Pipeline: Record-Breaking FDA Approvals. *Nat. Biotechnol.* **2024**, *42* (3), 355–361. https://doi.org/10.1038/s41587-024-02166-7.

(3) Wu, J.; Sahoo, J. K.; Li, Y.; Xu, Q.; Kaplan, D. L. Challenges in Delivering Therapeutic Peptides and Proteins: A Silk-Based Solution. *J. Controlled Release* **2022**, *345*, 176–189. https://doi.org/10.1016/j.jconrel.2022.02.011.

(4) Muheem, A.; Shakeel, F.; Jahangir, M. A.; Anwar, M.; Mallick, N.; Jain, G. K.; Warsi, M. H.; Ahmad, F. J. A Review on the Strategies for Oral Delivery of Proteins and Peptides and Their Clinical Perspectives. *Saudi Pharm. J.* **2016**, *24* (4), 413–428. https://doi.org/10.1016/j.jsps.2014.06.004.

(5) Frokjaer, S.; Otzen, D. E. Protein Drug Stability: A Formulation Challenge. *Nat. Rev. Drug Discov.* **2005**, *4* (4), 298–306. https://doi.org/10.1038/nrd1695.

(6) Manning, M. C.; Chou, D. K.; Murphy, B. M.; Payne, R. W.; Katayama, D. S. Stability of Protein Pharmaceuticals: An Update. *Pharm. Res.* **2010**, *27* (4), 544–575. https://doi.org/10.1007/s11095-009-0045-6.

(7) Nielsen, L.; Khurana, R.; Coats, A.; Frokjaer, S.; Brange, J.; Vyas, S.; Uversky, V. N.; Fink, A. L. Effect of Environmental Factors on the Kinetics of Insulin Fibril Formation: Elucidation of the Molecular Mechanism. *Biochemistry* **2001**, *40* (20), 6036–6046. https://doi.org/10.1021/bi002555c.

(8) Hill, E. K.; Krebs, B.; Goodall, D. G.; Howlett, G. J.; Dunstan, D. E. Shear Flow Induces Amyloid Fibril Formation. *Biomacromolecules* **2006**, *7* (1), 10–13. https://doi.org/10.1021/bm0505078.

(9) Sen, S.; Ali, R.; Onkar, A.; Ganesh, S.; Verma, S. Strategies for Interference of Insulin Fibrillogenesis: Challenges and Advances. *ChemBioChem* **2022**, *23* (11), e202100678. https://doi.org/10.1002/cbic.202100678.

(10) Ogle, G. D.; Abdullah, M.; Mason, D.; Januszewski, A. S.; Besançon, S. Insulin Storage in Hot Climates without Refrigeration: Temperature Reduction Efficacy of Clay Pots and Other Techniques. *Diabet. Med.* **2016**, *33* (11), 1544–1553. https://doi.org/10.1111/dme.13194.

(11) Pandey, L. M. Physicochemical Factors of Bioprocessing Impact the Stability of Therapeutic Proteins. *Biotechnol. Adv.* **2022**, *55*, 107909. https://doi.org/10.1016/j.biotechadv.2022.107909.

(12) Simpson, L. W.; Good, T. A.; Leach, J. B. Protein Folding and Assembly in Confined Environments: Implications for Protein Aggregation in Hydrogels and Tissues. *Biotechnol. Adv.* **2020**, *42*, 107573. https://doi.org/10.1016/j.biotechadv.2020.107573.

(13) Roberts, C. J. Protein Aggregation and Its Impact on Product Quality. *Curr. Opin. Biotechnol.* **2014**, *30*, 211–217. https://doi.org/10.1016/j.copbio.2014.08.001.

(14) Dolui, S.; Roy, A.; Pal, U.; Saha, A.; Maiti, N. C. Structural Insight of Amyloidogenic Intermediates of Human Insulin. *ACS Omega* **2018**, *3* (2), 2452–2462. https://doi.org/10.1021/acsomega.7b01776.

(15) Liu, L.; Li, X.; Chen, N.; Chen, X.; Xing, L.; Zhou, X.; Liu, S. Influence of Cadmium Ion on Denaturation Kinetics of Hen Egg White-Lysozyme under Thermal and Acidic Conditions. *Spectrochim. Acta. A. Mol. Biomol. Spectrosc.* **2023**, *296*, 122650. https://doi.org/10.1016/j.saa.2023.122650.

(16) Wang, W.; Nema, S.; Teagarden, D. Protein Aggregation—Pathways and Influencing Factors. *Int. J. Pharm.* **2010**, *390* (2), 89–99. https://doi.org/10.1016/j.ijpharm.2010.02.025.

(17) Qafary, M.; Rashno, F.; Khajeh, K.; Khaledi, M.; Moosavi-Movahedi, A. A. Insulin Fibrillation: Strategies for Inhibition. *Prog. Biophys. Mol. Biol.* **2022**, *175*, 49–62. https://doi.org/10.1016/j.pbiomolbio.2022.09.001.

(18) Das, A.; Shah, M.; Saraogi, I. Molecular Aspects of Insulin Aggregation and Various Therapeutic Interventions. *ACS Bio Med Chem Au* **2022**, *2* (3), 205–221. https://doi.org/10.1021/acsbiomedchemau.1c00054.

(19) Přáda Brichtová, E.; Krupová, M.; Bouř, P.; Lindo, V.; Gomes Dos Santos, A.; Jackson, S. E. Glucagon-like Peptide 1 Aggregates into Low-Molecular-Weight Oligomers off-Pathway to Fibrillation. *Biophys. J.* **2023**, *122* (12), 2475–2488. https://doi.org/10.1016/j.bpj.2023.04.027.

(20) Xiao, H.; Huang, L.; Zhang, W.; Yin, Z. Damage of Proteins at the Air/Water Interface: Surface Tension Characterizes Globulin Interface Stability. *Int. J. Pharm.* **2020**, *584*, 119445. https://doi.org/10.1016/j.ijpharm.2020.119445.

(21) Lusci, G.; Pivetta, T.; Carucci, C.; Parsons, D. F.; Salis, A.; Monduzzi, M. BSA Fragmentation Specifically Induced by Added Electrolytes: An Electrospray Ionization Mass Spectrometry Investigation. *Colloids Surf. B Biointerfaces* **2022**, *218*, 112726. https://doi.org/10.1016/j.colsurfb.2022.112726.

(22) Butreddy, A.; Janga, K. Y.; Ajjarapu, S.; Sarabu, S.; Dudhipala, N. Instability of Therapeutic Proteins — An Overview of Stresses, Stabilization Mechanisms and Analytical Techniques Involved in Lyophilized Proteins. *Int. J. Biol. Macromol.* **2021**, *167*, 309–325. https://doi.org/10.1016/j.ijbiomac.2020.11.188.

(23) Kato, K.; Nakayoshi, T.; Kurimoto, E.; Oda, A. Mechanisms of Deamidation of Asparagine Residues and Effects of Main-Chain Conformation on Activation Energy. *Int. J. Mol. Sci.* **2020**, *21* (19), 7035. https://doi.org/10.3390/ijms21197035.

(24) Yang, H.; Zubarev, R. A. Mass Spectrometric Analysis of Asparagine Deamidation and Aspartate Isomerization in Polypeptides. *ELECTROPHORESIS* **2010**, *31* (11), 1764–1772. https://doi.org/10.1002/elps.201000027.

(25) Hawkins, C. L.; Davies, M. J. Detection, Identification, and Quantification of Oxidative Protein Modifications. *J. Biol. Chem.* **2019**, *294* (51), 19683–19708. https://doi.org/10.1074/jbc.REV119.006217.

(26) Gupta, S.; Jiskoot, W.; Schöneich, C.; Rathore, A. S. Oxidation and Deamidation of Monoclonal Antibody Products: Potential Impact on Stability, Biological Activity, and Efficacy. *J. Pharm. Sci.* **2022**, *111* (4), 903–918. https://doi.org/10.1016/j.xphs.2021.11.024.

(27) Kehm, R.; Baldensperger, T.; Raupbach, J.; Höhn, A. Protein Oxidation - Formation Mechanisms, Detection and Relevance as Biomarkers in Human Diseases. *Redox Biol.* **2021**, *42*, 101901. https://doi.org/10.1016/j.redox.2021.101901.

(28) Beheshtizadeh, N.; Gharibshahian, M.; Bayati, M.; Maleki, R.; Strachan, H.; Doughty, S.; Tayebi, L. Vascular Endothelial Growth Factor (VEGF) Delivery Approaches in Regenerative Medicine. *Biomed. Pharmacother.* **2023**, *166*, 115301. https://doi.org/10.1016/j.biopha.2023.115301.

(29) Mitchell, M. J.; Billingsley, M. M.; Haley, R. M.; Wechsler, M. E.; Peppas, N. A.; Langer, R. Engineering Precision Nanoparticles for Drug Delivery. *Nat. Rev. Drug Discov.* **2021**, *20* (2), 101–124. https://doi.org/10.1038/s41573-020-0090-8.

(30) Vargason, A. M.; Anselmo, A. C.; Mitragotri, S. The Evolution of Commercial Drug Delivery Technologies. *Nat. Biomed. Eng.* **2021**, *5* (9), 951–967. https://doi.org/10.1038/s41551-021-00698-w.

(31) Davis, M. E.; Chen, Z. (Georgia); Shin, D. M. Nanoparticle Therapeutics: An Emerging Treatment Modality for Cancer. *Nat. Rev. Drug Discov.* **2008**, *7* (9), 771–782. https://doi.org/10.1038/nrd2614.

(32) Peer, D.; Karp, J. M.; Hong, S.; Farokhzad, O. C.; Margalit, R.; Langer, R. Nanocarriers as an Emerging Platform for Cancer Therapy. *Nat. Nanotechnol.* **2007**, *2* (12), 751–760. https://doi.org/10.1038/nnano.2007.387.

(33) Saito, N.; Haniu, H.; Usui, Y.; Aoki, K.; Hara, K.; Takanashi, S.; Shimizu, M.; Narita, N.; Okamoto, M.; Kobayashi, S.; Nomura, H.; Kato, H.; Nishimura, N.; Taruta, S.; Endo, M. Safe Clinical Use of Carbon Nanotubes as Innovative Biomaterials. *Chem. Rev.* **2014**, *114* (11), 6040–6079. https://doi.org/10.1021/cr400341h.

(34) Xu, C.; Lei, C.; Yu, C. Mesoporous Silica Nanoparticles for Protein Protection and Delivery. *Front. Chem.* **2019**, *7*. https://doi.org/10.3389/fchem.2019.00290.

(35) Chandrakala, V.; Aruna, V.; Angajala, G. Review on Metal Nanoparticles as Nanocarriers: Current Challenges and Perspectives in Drug Delivery Systems. *Emergent Mater.* **2022**, *5* (6), 1593–1615. https://doi.org/10.1007/s42247-021-00335-x.

(36) Pisal, D. S.; Kosloski, M. P.; Balu-Iyer, S. V. Delivery of Therapeutic Proteins. *J. Pharm. Sci.* **2010**, *99* (6), 2557–2575. https://doi.org/10.1002/jps.22054.

(37) Tan, M. L.; Choong, P. F. M.; Dass, C. R. Recent Developments in Liposomes, Microparticles and Nanoparticles for Protein and Peptide Drug Delivery. *Peptides* **2010**, *31* (1), 184–193. https://doi.org/10.1016/j.peptides.2009.10.002.

(38) Hirai, Y.; Hirose, H.; Imanishi, M.; Asai, T.; Futaki, S. Cytosolic Protein Delivery Using pH-Responsive, Charge-Reversible Lipid Nanoparticles. *Sci. Rep.* **2021**, *11* (1), 19896. https://doi.org/10.1038/s41598-021-99180-5.

(39) Jash, A.; Ubeyitogullari, A.; Rizvi, S. S. H. Liposomes for Oral Delivery of Protein and Peptide-Based Therapeutics: Challenges, Formulation Strategies, and Advances. *J Mater Chem B* **2021**, *9* (24), 4773–4792. https://doi.org/10.1039/D1TB00126D.

(40) Kaltbeitzel, J.; Wich, P. R. Protein-Based Nanoparticles: From Drug Delivery to Imaging, Nanocatalysis and Protein Therapy. *Angew. Chem. Int. Ed.* **2023**, *62* (44), e202216097. https://doi.org/10.1002/anie.202216097.

(41) Vardaxi, A.; Kafetzi, M.; Pispas, S. Polymeric Nanostructures Containing Proteins and Peptides for Pharmaceutical Applications. *Polymers* **2022**, *14* (4), 777. https://doi.org/10.3390/polym14040777.

(42) Muhammad Sajid Hamid Akash, K. R.; Chen, S. Natural and Synthetic Polymers as Drug Carriers for Delivery of Therapeutic Proteins. *Polym. Rev.* **2015**, *55* (3), 371–406. https://doi.org/10.1080/15583724.2014.995806.

(43) Bertrand, N.; Wu, J.; Xu, X.; Kamaly, N.; Farokhzad, O. C. Cancer Nanotechnology: The Impact of Passive and Active Targeting in the Era of Modern Cancer Biology. *Adv. Drug Deliv. Rev.* **2014**, *66*, 2–25. https://doi.org/10.1016/j.addr.2013.11.009.

(44) Kiran, P.; Khan, A.; Neekhra, S.; Pallod, S.; Srivastava, R. Nanohybrids as Protein-Polymer Conjugate Multimodal Therapeutics. *Front. Med. Technol.* **2021**, *3*. https://doi.org/10.3389/fmedt.2021.676025.

(45) Perin, F.; Motta, A.; Maniglio, D. Amphiphilic Copolymers in Biomedical Applications: Synthesis Routes and Property Control. *Mater. Sci. Eng. C* **2021**, *123*, 111952. https://doi.org/10.1016/j.msec.2021.111952.

(46) Agrahari, V.; Agrahari, V. Advances and Applications of Block-Copolymer-Based Nanoformulations. *Drug Discov. Today* **2018**, *23* (5), 1139–1151. https://doi.org/10.1016/j.drudis.2018.03.004.

(47) Stevens, C. A.; Kaur, K.; Klok, H.-A. Self-Assembly of Protein-Polymer Conjugates for Drug Delivery. *Adv. Drug Deliv. Rev.* **2021**, *174*, 447–460. https://doi.org/10.1016/j.addr.2021.05.002.

(48) Zhao, H.; Lin, Z. Y.; Yildirimer, L.; Dhinakar, A.; Zhao, X.; Wu, J. Polymer-Based Nanoparticles for Protein Delivery: Design, Strategies and Applications. *J Mater Chem B* **2016**, *4* (23), 4060–4071. https://doi.org/10.1039/C6TB00308G.

(49) Gao, S.; Holkar, A.; Srivastava, S. Protein–Polyelectrolyte Complexes and Micellar Assemblies. *Polymers* **2019**, *11* (7). https://doi.org/10.3390/polym11071097.

(50) Chen, F.; Stenzel, M. H. Polyion Complex Micelles for Protein Delivery*. *Aust. J. Chem.* **2018**, *71* (10), 768–780.

(51) Sun, J.; Li, Z. Polyion Complexes via Electrostatic Interaction of Oppositely Charged Block Copolymers. *Macromolecules* **2020**, *53* (20), 8737–8740. https://doi.org/10.1021/acs.macromol.0c02031.

(52) Sasaki, Y.; Akiyoshi, K. Nanogel Engineering for New Nanobiomaterials: From Chaperoning Engineering to Biomedical Applications. *Chem. Rec.* **2010**, *10* (6), 366–376. https://doi.org/10.1002/tcr.201000008.

(53) Xu, X.; Shen, S.; Mo, R. Bioresponsive Nanogels for Protein Delivery. *VIEW* **2022**, *3* (1), 20200136. https://doi.org/10.1002/VIW.20200136.

(54) Cuggino, J. C.; Blanco, E. R. O.; Gugliotta, L. M.; Igarzabal, C. I. A.; Calderón, M. Crossing Biological Barriers with Nanogels to Improve Drug Delivery Performance. *J. Controlled Release* **2019**, *307*, 221–246. https://doi.org/10.1016/j.jconrel.2019.06.005.

(55) Ding, Y.-F.; Wei, J.; Li, S.; Pan, Y.-T.; Wang, L.-H.; Wang, R. Host–Guest Interactions Initiated Supramolecular Chitosan Nanogels for Selective Intracellular Drug Delivery. *ACS Appl. Mater. Interfaces* **2019**, *11* (32), 28665–28670. https://doi.org/10.1021/acsami.9b09059.

(56) Li, B.; Yuan, Z.; Zhang, P.; Sinclair, A.; Jain, P.; Wu, K.; Tsao, C.; Xie, J.; Hung, H.-C.; Lin, X.; Bai, T.; Jiang, S. Zwitterionic Nanocages Overcome the Efficacy Loss of Biologic Drugs. *Adv. Mater.* **2018**, *30* (14), 1705728. https://doi.org/10.1002/adma.201705728.

(57) Jia, X.; Wang, L.; Du, J. In Situ Polymerization on Biomacromolecules for Nanomedicines. *Nano Res.* **2018**, *11* (10), 5028–5048. https://doi.org/10.1007/s12274-018-2080-2.

(58) Gu, Z.; Yan, M.; Hu, B.; Joo, K.-I.; Biswas, A.; Huang, Y.; Lu, Y.; Wang, P.; Tang, Y. Protein Nanocapsule Weaved with Enzymatically Degradable Polymeric Network. *Nano Lett.* **2009**, *9* (12), 4533–4538. https://doi.org/10.1021/nl902935b.

(59) Zhao, M.; Biswas, A.; Hu, B.; Joo, K.-I.; Wang, P.; Gu, Z.; Tang, Y. Redox-Responsive Nanocapsules for Intracellular Protein Delivery. *Biomaterials* **2011**, *32* (22), 5223–5230. https://doi.org/10.1016/j.biomaterials.2011.03.060.

(60) Wen, J.; Anderson, S. M.; Du, J.; Yan, M.; Wang, J.; Shen, M.; Lu, Y.; Segura, T. Controlled Protein Delivery Based on Enzyme-Responsive Nanocapsules. *Adv. Mater.* **2011**, *23* (39), 4549–4553. https://doi.org/10.1002/adma.201101771.

(61) Beloqui, A.; Kobitski, A. Y.; Nienhaus, G. U.; Delaittre, G. A Simple Route to Highly Active Single-Enzyme Nanogels. *Chem Sci* **2018**, *9* (4), 1006–1013. https://doi.org/10.1039/C7SC04438K.

(62) Xiaomei Wang, L. L., Dan Cheng; Li, X. Development of Poly(Hydroxyethyl Methacrylate) Nanogel for Effective Oral Insulin Delivery. *Pharm. Dev. Technol.* **2018**, *23* (4), 351–357. https://doi.org/10.1080/10837450.2017.1295064.

(63) Biswas, A.; Joo, K.-I.; Liu, J.; Zhao, M.; Fan, G.; Wang, P.; Gu, Z.; Tang, Y. Endoprotease-Mediated Intracellular Protein Delivery Using Nanocapsules. *ACS Nano* **2011**, *5* (2), 1385–1394. https://doi.org/10.1021/nn1031005.

(64) Zhao, M.; Liu, Y.; Hsieh, R. S.; Wang, N.; Tai, W.; Joo, K.-I.; Wang, P.; Gu, Z.; Tang, Y. Clickable Protein Nanocapsules for Targeted Delivery of Recombinant P53 Protein. *J. Am. Chem. Soc.* **2014**, *136* (43), 15319–15325. https://doi.org/10.1021/ja508083g.

(65) Biswas, A.; Liu, Y.; Liu, T.; Fan, G.; Tang, Y. Polyethylene Glycol-Based Protein Nanocapsules for Functional Delivery of a Differentiation Transcription Factor. *Biomaterials* **2012**, *33* (21), 5459–5467. https://doi.org/10.1016/j.biomaterials.2012.04.012.

(66) Forsythe, N. L.; Tan, M. F.; Vinciguerra, D.; Woodford, J.; Stieg, A. Z.; Maynard, H. D. Noncovalent Enzyme Nanogels via a Photocleavable Linkage. *Macromolecules* **2022**, *55* (22), 9925–9933. https://doi.org/10.1021/acs.macromol.2c01334.

(67) Wei, W.; Du, J.; Li, J.; Yan, M.; Zhu, Q.; Jin, X.; Zhu, X.; Hu, Z.; Tang, Y.; Lu, Y. Construction of Robust Enzyme Nanocapsules for Effective Organophosphate Decontamination, Detoxification, and Protection. *Adv. Mater.* **2013**, *25* (15), 2212–2218. https://doi.org/10.1002/adma.201205138.

(68) Zhang, J.; Du, J.; Yan, M.; Dhaliwal, A.; Wen, J.; Liu, F.; Segura, T.; Lu, Y. Synthesis of Protein Nano-Conjugates for Cancer Therapy. *Nano Res.* **2011**, *4* (5), 425–433. https://doi.org/10.1007/s12274-011-0098-9.

(69) Santhanakrishnan, K. R.; Koilpillai, J.; Narayanasamy, D. PEGylation in Pharmaceutical Development: Current Status and Emerging Trends in Macromolecular and Immunotherapeutic Drugs. *Cureus* **2024**. https://doi.org/10.7759/cureus.66669.

(70) Branca, C.; Magazù, S.; Maisano, G.; Migliardo, F.; Migliardo, P.; Romeo, G. Hydration Study of PEG/Water Mixtures by Quasi Elastic Light Scattering, Acoustic and Rheological Measurements. *J. Phys. Chem. B* **2002**, *106* (39), 10272–10276. https://doi.org/10.1021/jp014345v.

(71) Rozza, A. M.; Vanpoucke, D. E. P.; Krammer, E.-M.; Bouckaert, J.; Blossey, R.; Lensink, M. F.; Ondrechen, M. J.; Bakó, I.; Oláh, J.; Roos, G. Hydration Sphere Structure of Architectural Molecules: Polyethylene Glycol and Polyoxymethylene Oligomers. *J. Mol. Liq.* **2023**, *384*, 122172. https://doi.org/10.1016/j.molliq.2023.122172.

(72) Arakawa, T.; Timasheff, S. N. Mechanism of Poly(Ethylene Glycol) Interaction with Proteins. *Biochemistry* **1985**, *24* (24), 6756–6762. https://doi.org/10.1021/bi00345a005.

(73) Pasut, G.; Veronese, F. M. State of the Art in PEGylation: The Great Versatility Achieved after Forty Years of Research. *J. Controlled Release* **2012**, *161* (2), 461–472. https://doi.org/10.1016/j.jconrel.2011.10.037.

(74) Du, B.; Jiang, X.; Huang, Y.; Li, S.; Lin, J. C.; Yu, M.; Zheng, J. Tailoring Kidney Transport of Organic Dyes with Low-Molecular-Weight PEGylation. *Bioconjug. Chem.* **2020**, *31* (2), 241–247. https://doi.org/10.1021/acs.bioconjchem.9b00707.

(75) Montgomery, H. R.; Messina, M. S.; Doud, E. A.; Spokoyny, A. M.; Maynard, H. D. Organometallic S-Arylation Reagents for Rapid PEGylation of Biomolecules. *Bioconjug. Chem.* **2022**, *33* (8), 1536–1542. https://doi.org/10.1021/acs.bioconjchem.2c00280.

(76) Edward Semple, J.; Sullivan, B.; Vojkovsky, T.; Sill, K. N. Synthesis and Facile End-group Quantification of Functionalized PEG Azides. *J. Polym. Sci. Part Polym. Chem.* **2016**, *54* (18), 2888–2895. https://doi.org/10.1002/pola.28174.

(77) Morpurgo, M.; Veronese, F. M.; Kachensky, D.; Harris, J. M. Preparation and Characterization of Poly(Ethylene Glycol) Vinyl Sulfone. *Bioconjug. Chem.* **1996**, *7* (3), 363–368. https://doi.org/10.1021/bc9600224.

(78) Lee, H.-Y.; Cha, S.-H. Enhancement of Self-Healing Property by Introducing Ethylene Glycol Group into Thermally Reversible Diels-Alder Reaction Based Self-Healable Materials. *Macromol. Res.* **2017**, *25* (6), 640–647. https://doi.org/10.1007/s13233-017-5120-y.

(79) Zhang, B.; Sun, J.; Wang, Y.; Ji, D.; Yuan, Y.; Li, S.; Sun, Y.; Hou, Y.; Li, P.; Zhao, L.; Yu, F.; Ma, W.; Cheng, B.; Wu, L.; Hu, J.; Wang, M.; Song, W.; Li, X.; Li, H.; Fei, Y.; Chen, H.; Zhang, L.; Tsokos, G. C.; Zhou, D.; Zhang, X. Site-Specific PEGylation of Interleukin-2

Enhances Immunosuppression via the Sustained Activation of Regulatory T Cells. *Nat. Biomed. Eng.* **2021**, *5* (11), 1288–1305. https://doi.org/10.1038/s41551-021-00797-8.

(80) Tamshen, K.; Wang, Y.; Jamieson, S. M. F.; Perry, J. K.; Maynard, H. D. Genetic Code Expansion Enables Site-Specific PEGylation of a Human Growth Hormone Receptor Antagonist through Click Chemistry. *Bioconjug. Chem.* **2020**, *31* (9), 2179–2190. https://doi.org/10.1021/acs.bioconjchem.0c00365.

(81) Jia, Y.; Fernandez, A.; Sampath, J. PEGylation of Insulin and Lysozyme To Stabilize against Thermal Denaturation: A Molecular Dynamics Simulation Study. *J. Phys. Chem. B* **2023**, *127* (31), 6856–6866. https://doi.org/10.1021/acs.jpcb.3c01289.

(82) Ganson, N. J.; Povsic, T. J.; Sullenger, B. A.; Alexander, J. H.; Zelenkofske, S. L.; Sailstad, J. M.; Rusconi, C. P.; Hershfield, M. S. Pre-Existing Anti-Polyethylene Glycol Antibody Linked to First-Exposure Allergic Reactions to Pegnivacogin, a PEGylated RNA Aptamer. *J. Allergy Clin. Immunol.* **2016**, *137* (5), 1610-1613.e7. https://doi.org/10.1016/j.jaci.2015.10.034.

(83) Povsic, T. J.; Lawrence, M. G.; Lincoff, A. M.; Mehran, R.; Rusconi, C. P.; Zelenkofske, S. L.; Huang, Z.; Sailstad, J.; Armstrong, P. W.; Steg, P. G.; Bode, C.; Becker, R. C.; Alexander, J. H.; Adkinson, N. F.; Levinson, A. I. Pre-Existing Anti-PEG Antibodies Are Associated with Severe Immediate Allergic Reactions to Pegnivacogin, a PEGylated Aptamer. *J. Allergy Clin. Immunol.* **2016**, *138* (6), 1712–1715. https://doi.org/10.1016/j.jaci.2016.04.058.

(84) Lipsky, P. E.; Calabrese, L. H.; Kavanaugh, A.; Sundy, J. S.; Wright, D.; Wolfson, M.; Becker, M. A. Pegloticase Immunogenicity: The Relationship between Efficacy and

Antibody Development in Patients Treated for Refractory Chronic Gout. *Arthritis Res. Ther.* **2014**, *16* (2), R60. https://doi.org/10.1186/ar4497.

(85) Hershfield, M. S.; Ganson, N. J.; Kelly, S. J.; Scarlett, E. L.; Jaggers, D. A.; Sundy, J. S. Induced and Pre-Existing Anti-Polyethylene Glycol Antibody in a Trial of Every 3-Week Dosing of Pegloticase for Refractory Gout, Including in Organ Transplant Recipients. *Arthritis Res. Ther.* **2014**, *16* (2), R63. https://doi.org/10.1186/ar4500.

(86) Sundy, J. S.; Ganson, N. J.; Kelly, S. J.; Scarlett, E. L.; Rehrig, C. D.; Huang, W.; Hershfield, M. S. Pharmacokinetics and Pharmacodynamics of Intravenous PEGylated Recombinant Mammalian Urate Oxidase in Patients with Refractory Gout. *Arthritis Rheum.* **2007**, *56* (3), 1021–1028. https://doi.org/10.1002/art.22403.

(87) Ganson, N. J.; Kelly, S. J.; Scarlett, E.; Sundy, J. S.; Hershfield, M. S. Control of Hyperuricemia in Subjects with Refractory Gout, and Induction of Antibody against Poly(Ethylene Glycol) (PEG), in a Phase I Trial of Subcutaneous PEGylated Urate Oxidase. *Arthritis Res. Ther.* **2006**, *8* (1), R12. https://doi.org/10.1186/ar1861.

(88) Armstrong, J. K. The Occurrence, Induction, Specificity and Potential Effect of Antibodies against Poly(Ethylene Glycol). In *PEGylated Protein Drugs: Basic Science and Clinical Applications*; Veronese, F. M., Ed.; Milestones in Drug Therapy; Birkhäuser: Basel, 2009; pp 147–168. https://doi.org/10.1007/978-3-7643-8679-5_9.

(89) Yang, Q.; Jacobs, T. M.; McCallen, J. D.; Moore, D. T.; Huckaby, J. T.; Edelstein, J. N.; Lai, S. K. Analysis of Pre-Existing IgG and IgM Antibodies against Polyethylene Glycol (PEG) in the General Population. *Anal. Chem.* **2016**, *88* (23), 11804–11812. https://doi.org/10.1021/acs.analchem.6b03437.

(90) Fruijtier-Pölloth, C. Safety Assessment on Polyethylene Glycols (PEGs) and Their Derivatives as Used in Cosmetic Products. *Toxicology* **2005**, *214* (1–2), 1–38. https://doi.org/10.1016/j.tox.2005.06.001.

(91) Pelegri-O'Day, E. M.; Lin, E.-W.; Maynard, H. D. Therapeutic Protein–Polymer Conjugates: Advancing Beyond PEGylation. *J. Am. Chem. Soc.* **2014**, *136* (41), 14323–14332. https://doi.org/10.1021/ja504390x.

(92) Shi, D.; Beasock, D.; Fessler, A.; Szebeni, J.; Ljubimova, J. Y.; Afonin, K. A.; Dobrovolskaia, M. A. To PEGylate or Not to PEGylate: Immunological Properties of Nanomedicine's Most Popular Component, Polyethylene Glycol and Its Alternatives. *Adv. Drug Deliv. Rev.* **2022**, *180*, 114079. https://doi.org/10.1016/j.addr.2021.114079.

(93) Barz, M.; Luxenhofer, R.; Zentel, R.; Vicent, M. J. Overcoming the PEG-Addiction: Well-Defined Alternatives to PEG, from Structure–Property Relationships to Better Defined Therapeutics. *Polym. Chem.* **2011**, *2* (9), 1900–1918. https://doi.org/10.1039/C0PY00406E.

(94) Qi, Y.; Chilkoti, A. Protein–Polymer Conjugation — Moving beyond PEGylation. *Curr. Opin. Chem. Biol.* **2015**, *28*, 181–193. https://doi.org/10.1016/j.cbpa.2015.08.009.

(95) Zhang, P.; Sun, F.; Liu, S.; Jiang, S. Anti-PEG Antibodies in the Clinic: Current Issues and beyond PEGylation. *J. Controlled Release* **2016**, *244*, 184–193. https://doi.org/10.1016/j.jconrel.2016.06.040.

(96) Sushma, M. V.; kadam, A.; Kumar, D.; Mutreja, I. Biodegradable Polymers. In *Biomaterials and Biopolymers*; Domb, A., Mizrahi, B., Farah, S., Eds.; Springer International Publishing: Cham, 2023; pp 33–54. https://doi.org/10.1007/978-3-031-36135-7_2.

(97) Henke, M.; Tessmar, J.; Göpferich, A. 9.18 - Biomimetic Polymers (for Biomedical Applications). In *Polymer Science: A Comprehensive Reference*; Matyjaszewski, K., Möller,

M., Eds.; Elsevier: Amsterdam, 2012; pp 339–361. https://doi.org/10.1016/B978-0-444-53349-4.00222-3.

(98) Gelb, M. B.; Messina, K. M. M.; Vinciguerra, D.; Ko, J. H.; Collins, J.; Tamboline, M.; Xu, S.; Ibarrondo, F. J.; Maynard, H. D. Poly(Trehalose Methacrylate) as an Excipient for Insulin Stabilization: Mechanism and Safety. *ACS Appl. Mater. Interfaces* **2022**, *14* (33), 37410–37423. https://doi.org/10.1021/acsami.2c09301.

(99) Bao, C.; Xu, X.; Chen, J.; Zhang, Q. Synthesis of Biodegradable Protein–Poly(ε-Caprolactone) Conjugates via Enzymatic Ring Opening Polymerization. *Polym. Chem.* **2020**, *11* (3), 682–686. https://doi.org/10.1039/C9PY01464K.

(100) Hou, Y.; Lu, H. Protein PEPylation: A New Paradigm of Protein–Polymer Conjugation. *Bioconjug. Chem.* **2019**, *30* (6), 1604–1616. https://doi.org/10.1021/acs.bioconjchem.9b00236.

(101) Hu, Y.; Tian, Z.-Y.; Xiong, W.; Wang, D.; Zhao, R.; Xie, Y.; Song, Y.-Q.; Zhu, J.; Lu, H. Water-Assisted and Protein-Initiated Fast and Controlled Ring-Opening Polymerization of Proline N-Carboxyanhydride. *Natl. Sci. Rev.* **2022**, *9* (8), nwac033. https://doi.org/10.1093/nsr/nwac033.

(102) Maschmeyer, P. G.; Liang, X.; Hung, A.; Ahmadzai, O.; Kenny, A. L.; Luong, Y. C.; Forder, T. N.; Zeng, H.; Gillies, E. R.; Roberts, D. A. Post-Polymerization 'Click' End-Capping of Polyglyoxylate Self-Immolative Polymers. *Polym. Chem.* **2021**, *12* (47), 6824–6831. https://doi.org/10.1039/D1PY01169C.

(103) Gong, J.; Tavsanli, B.; Gillies, E. R. Self-Immolative Polymers: From Synthesis to Applications. *Annu. Rev. Mater. Res.* **2024**, *54* (1), null. https://doi.org/10.1146/annurev-matsci-080222-104556.

(104) Sirianni, Q. E. A.; Liang, X.; Such, G. K.; Gillies, E. R. Polyglyoxylamides with a pH-Mediated Solubility and Depolymerization Switch. *Macromolecules* **2021**, *54* (22), 10547–10556. https://doi.org/10.1021/acs.macromol.1c01796.

(105) Pelosi, C.; Duce, C.; Wurm, F. R.; Tinè, M. R. Effect of Polymer Hydrophilicity and Molar Mass on the Properties of the Protein in Protein–Polymer Conjugates: The Case of PPEylated Myoglobin. *Biomacromolecules* **2021**, *22* (5), 1932–1943. https://doi.org/10.1021/acs.biomac.1c00058.

(106) Azari, A.; Golchin, A.; Mahmoodinia Maymand, M.; Mansouri, F.; Ardeshirylajimi, A. Electrospun Polycaprolactone Nanofibers: Current Research and Applications in Biomedical Application. *Adv. Pharm. Bull.* **2022**, *12* (4), 658–672. https://doi.org/10.34172/apb.2022.070.

(107) El Yousfi, R.; Brahmi, M.; Dalli, M.; Achalhi, N.; Azougagh, O.; Tahani, A.; Touzani, R.; El Idrissi, A. Recent Advances in Nanoparticle Development for Drug Delivery: A Comprehensive Review of Polycaprolactone-Based Multi-Arm Architectures. *Polymers* **2023**, *15* (8), 1835. https://doi.org/10.3390/polym15081835.

(108) Hassankhani Rad, A.; Asiaee, F.; Jafari, S.; Shayanfar, A.; Lavasanifar, A.; Molavi, O. Poly(Ethylene Glycol)-Poly(ε-Caprolactone)-Based Micelles for Solubilization and Tumor-Targeted Delivery of Silibinin. *BioImpacts BI* **2020**, *10* (2), 87–95. https://doi.org/10.34172/bi.2020.11.

(109) Jiang, P.; Jacobs, K. M.; Ohr, M. P.; Swindle-Reilly, K. E. Chitosan–Polycaprolactone Core–Shell Microparticles for Sustained Delivery of Bevacizumab. *Mol. Pharm.* **2020**, *17* (7), 2570–2584. https://doi.org/10.1021/acs.molpharmaceut.0c00260.

(110) Rafiei, M.; Jooybar, E.; Abdekhodaie, M. J.; Alvi, M. Construction of 3D Fibrous PCL Scaffolds by Coaxial Electrospinning for Protein Delivery. *Mater. Sci. Eng. C Mater. Biol. Appl.* **2020**, *113*, 110913. https://doi.org/10.1016/j.msec.2020.110913.

(111) Sundermann, J.; Sydow, S.; Burmeister, L.; Hoffmann, A.; Menzel, H.; Bunjes, H. Spatially and Temporally Controllable BMP-2 and TGF-B3 Double Release From Polycaprolactone Fiber Scaffolds via Chitosan-Based Polyelectrolyte Coatings. *ACS Biomater. Sci. Eng.* **2024**, *10* (1), 89–98. https://doi.org/10.1021/acsbiomaterials.1c01585.

(112) Pelegri-O'Day, E. M.; Bhattacharya, A.; Theopold, N.; Ko, J. H.; Maynard, H. D. Synthesis of Zwitterionic and Trehalose Polymers with Variable Degradation Rates and Stabilization of Insulin. *Biomacromolecules* **2020**, *21* (6), 2147–2154. https://doi.org/10.1021/acs.biomac.0c00133.`

(113) Pelegri-O'Day, E. M.; Paluck, S. J.; Maynard, H. D. Substituted Polyesters by Thiol–Ene Modification: Rapid Diversification for Therapeutic Protein Stabilization. *J. Am. Chem. Soc.* **2017**, *139* (3), 1145–1154. https://doi.org/10.1021/jacs.6b10776.

Chapter 2

Uniform Trehalose Nanogels for Glucagon Stabilization†

2.1 Introduction

Individuals with type 1 diabetes regularly inject insulin to manage blood glucose levels; however, insulin overdose and irregular eating schedules can lead to hypoglycemia.[1] Severe hypoglycemia occurs when blood glucose levels fall below 50 mg dL−1, with complications ranging from weakness, difficulty walking, vision impairment, confusion, and seizures.[1–3] Glucagon is currently administered to treat emergency hypoglycemic episodes.[4] Glucagon increases blood glucose concentration through binding to hepatic glucagon receptors, which stimulate glycogen breakdown and release of glucose from the liver.[5–7] Due to low stability, low solubility at physiological pH, and tendency to form toxic fibrils, glucagon formulations for emergency delivery remain a challenge.[8–10]

New glucagon formulations have been developed within the past few years, with some receiving FDA approval. In 2019, Eli Lilly released the first nasal rescue glucagon, BAQSIMI™, formulated as a 3 mg dry powder.[11–13] Later that year, Xeris Pharmaceuticals released the GVOKE HypoPen® formulated as a solution of glucagon in sulfuric acid and dimethyl sulfoxide (DMSO) in an automatic injector.[14,15] In 2021, Zealand Pharma released their automatic injector ZEGALOGUE™, which contains a glucagon analogue, dasiglucagon.[16–18] Although these formulations demonstrate great progress and effort towards a stable and efficacious glucagon formulation, their stability in an aqueous pH 7.4 solution at a range of temperatures is limited. For example, BAQSIMI™ is only stable up to 30 °C as a dry powder and cannot be exposed to moisture. GVOKE HypoPen® is only stable up to 25 °C, is formulated in organic solvent, and could cause pain at the injection site from the sulfuric acid. ZEGALOGUE™ is only stable up to 25 °C.[11,15,16] Thus, there is still a need for glucagon formulations stable in aqueous solution. Glucagon has been stabilized by various strategies including chemical modification, covalent

attachment of poly(ethylene glycol) (PEG), and addition of excipients including salts, surfactants, and sugars.[19–22] However, even with these excipients in solution, glucagon is still susceptible to degradation at neutral or slightly acidic pH (5–7) within ~26 h in solution.[23] During manufacture, storage, and cold chain transport, many biomolecules experience environmental stressors necessitating stabilization.[21,24,25] In particular, trehalose has been used as an excipient for RNA, enzymes, insulin, and other proteins, including glucagon in the GVOKE HypoPen®.[25–29] Trehalose stabilizes proteins in both solution and lyophilized form;[30–32] which is hypothesized to be achieved through vitrification, water entrapment, and/or water replacement mechanisms.[33–35] Properties that make trehalose a good stabilizer are its high solubility in water, large hydration number, and a high glass transition temperature (Tg).[36] Trehalose polymers, where the disaccharide is a side chain, exhibit superior stabilizing capabilities compared to trehalose.[37–41] We have previously shown that proteins retain greater bioactivity against heat and lyophilization in the presence of trehalose polymers as either an excipient, conjugate, hydrogel, or nanogel compared to trehalose.[37–39,42] Others have reported that nanoformulations of trehalose polymers are considerably more stable than other nanoparticles in cell culture media and upon storage to deliver RNA and DNA in vivo.[27]

We previously synthesized a trehalose nanoparticle by utilizing a chemically modified glucagon, thiolated at N-terminus and Lys12. This modification stabilized a glucagon nanoparticle in aqueous solution (pH 7.4) for up to three weeks.[29] However, these trehalose nanoparticles were non-uniform in size and morphology when employing glucagon as a crosslinker.[29] To translate a formulation to human use, it is desirable that nanoparticles be synthesized with a high level of purity and uniformity.[43] In the study described herein, we aimed to investigate an alternative crosslinker to create uniform trehalose nanoparticles and evaluate the long-term stabilization of

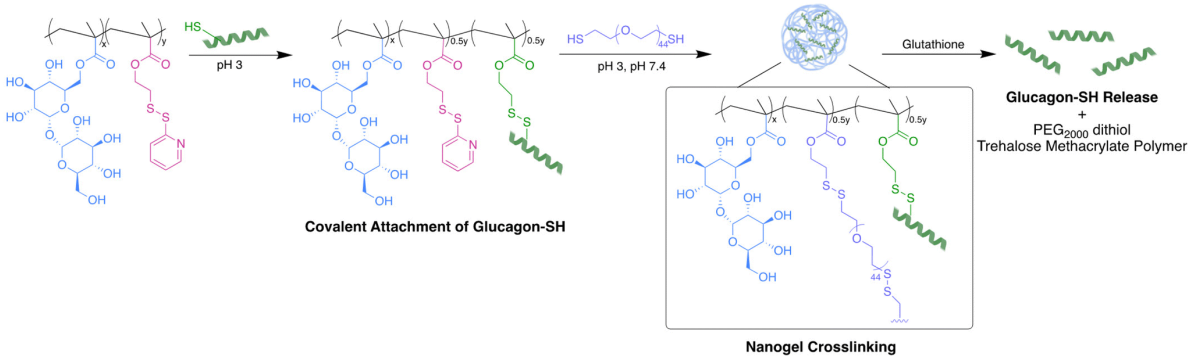

Figure 2.1 Glucagon nanogel formation begins with the covalent attachment of glucagon-SH to poly(PDSMA-*co*-TrMA), followed by crosslinking with PEG_{2000} dithiol. In the presence of glutathione, glucagon-SH was released as well as PEG_{2000} dithiol and trehalose methacrylate polymer.

glucagon in aqueous solutions over a range of relevant temperatures. Glucagon was site-selectively modified to contain a cysteine at glutamine (Gln) 24 to create a thiol reactive handle for ease of conjugation (glucagon–SH). Previously, Gln24 was replaced with alanine, yielding potency similar to the native peptide.[44] Additionally, a crystal structure of a glucagon analogue binding to its receptor including a substitution at Gln24 showed that the modification did not significantly influence receptor binding.[45] We copolymerized methacrylate functionalized trehalose with pyridyl disulfide ethyl methacrylate using free radical polymerization conditions forming trehalose polymers with thiol reactive handles. Glucagon–SH was conjugated via a PDS disulfide exchange, followed by crosslinking with PEG_{2000} dithiol to give pH 7.4 soluble and stable glucagon nanogels uniform in size. The glucagon stability and nanogel uniformity was thoroughly investigated at temperatures mimicking environmental stressors as well as the in vitro biocompatibility and efficacy.

2.2 Results and Discussion

2.2.1 Optimization of Glucagon Nanogel Synthesis.

TrMA and PDSMA were copolymerized using free radical polymerization with a feed ratio of 1 : 1 to yield poly(PDSMA-*co*-TrMA) with a molecular weight of 9.8 kDa and Đ of 1.9 (**Figure 2.14 and 2.15**).[29] We first wanted to understand the time course of the disulfide exchange between glucagon–SH and the PDS group of poly(PDSMA-*co*-TrMA) using the cysteine installed glucagon–SH. We monitored the kinetics via HPLC (**Figure 2.16**). A solution of poly(PDSMA-*co*-TrMA) and glucagon– SH in 10 mM HCl were mixed at 4 °C to observe 50% conjugation within 15 minutes and 82% conjugation after 3 h, reaching a plateau. Release of glucagon–SH was confirmed by HPLC, SDS-PAGE, and LC-MS by comparing the purified glucagon nanogel peak to the reduced nanogel peak (**Figure 2.17-2.19**). A nanoparticle <200 nm was targeted for optimal release of glucagon, clearance, and circulation.[46–48] Glucagon nanogel synthesis was first attempted through crosslinking with 10, 20, 30, 40, and 50% PEG_{2000} dithiol (by PDS group) followed by the covalent attachment of glucagon–SH (to the remaining PDS groups) in 1 : 1 50 mM DPBS pH 7.4 : 10 mM HCl and purified by microdialysis using a 20 kDa MWCO filter against 50 mM DPBS pH 7.4 (**Figure 2.20**). Crosslinking percentages of 10–50% yielded nanogels with sizes >200 nm, with increasing crosslinking percentages yielding smaller nanogel sizes. We hypothesize this was due to the glucagon conjugation to the outside of the nanoparticle; the glucagon could aggregate, causing an increase in nanoparticle size. Although the 50% crosslinking yielded nanogels of 640 nm, we used this percentage in subsequent optimization to synthesize nanogels with 50% glucagon loading (half of the pyridyl disulfide groups). Using a 50% crosslinking, nanogel formation was next attempted with simultaneous glucagon–SH conjugation by mixing both PEG_{2000} dithiol and glucagon–SH in 1: 1 50 mM DPBS pH 7.4 : 10 mM HCl and purified by microdialysis using a 20 kDa MWCO filter against 50 mM DPBS pH 7.4 (**Figure 2.21**). This yielded a uniform glucagon nanogel of 360 nm, which led us to believe a smaller size

could be achieved by attaching the glucagon–SH first and then crosslinking. To prevent the glucagon from aggregating in solution, the reaction solvent was changed to HCl to ensure any free glucagon in solution would remain soluble throughout purification. Glucagon–SH was then conjugated to poly(PDSMA-*co*-TrMA) followed by the crosslinking with varying PEG dithiol sizes (600, 1000, and 2000 Da) yielding nanogel sizes of 3190, 310, 150 nm, respectively (**Figure 2.22-2.24**). As the crosslinker length increased, the nanogel size decreased. This could be due to the ability of the larger PEG to better encapsulate the glucagon attached to the trehalose polymer. Thus, PEG_{2000} dithiol was used as the crosslinker going forward, with adding the glucagon first to minimize aggregation. With glucagon nanoparticles of 150 nm, the nanogel stability and uniformity to lyophilization was investigated. Lyophilization removes water through sublimation of ice under high vacuum, which has been known to offer a longer shelf-life and ease of transportation of many pharmaceutical products.[24,49,50] DLS and TEM images show the uniformity of the nanogels after lyophilization, reconstituted in 50 mM DPBS pH 7.4, with sizes comparable to the non-lyophilized solution form (**Figure 2.25 and 2.26**). Although the lyophilization of the glucagon nanogel could offer additional stabilizing properties, for the scope of this paper we aimed to focus on the solution-based formulation. Formulating the nanogel to be stored in solution removes the reconstitution step for a patient or caregiver during an emergency hypoglycemic event. We see this as clinically advantageous. The optimized nanogel synthesis using a 50% glucagon–SH conjugation followed by crosslinking with 50% PEG_{2000} in HCl, buffer exchanged to DPBS pH 7.4 was moved forward for the short- and long-term stability experiments (**Figure 2.1**). The glucagon nanogels were stored at −20 °C, 4 °C, 25 °C, and 37 °C to mimic cold chain transport, refrigeration, room temperature, and body temperature. The nanogel uniformity was

assessed using DLS and TEM, while the glucagon stability was assessed using HPLC to monitor degradation and ThT to monitor fibrillation.

2.2.2 Characterization of Glucagon Nanogel Size.

The size and uniformity of the glucagon nanogel was monitored over 5 months at −20 °C and 4 °C, 5 days at 25 °C, and 12 h at 37 °C using DLS and TEM (**Figure 2.2**). At day 0, the glucagon nanogels *Z*-average (d nm) was 150 by DLS. The glucagon nanogels at −20 °C and 4 °C underwent a small shift in size after day 0 but did not exhibit significant changes in size and uniformity by DLS and TEM (**Figure 2.2A-D**) over time and therefore were deemed stable in size up to 5 months, which was the longest time tested. We attempted to obtain TEM images with more particles in the frame by concentrating the nanogels, however, this caused the nanogels to aggregate. A wider frame of the nanogels at their final time point shows uniformity in size distribution of the nanogels at −20 °C and 4 °C (**Figure 2.27**). The glucagon nanogel stored at 25

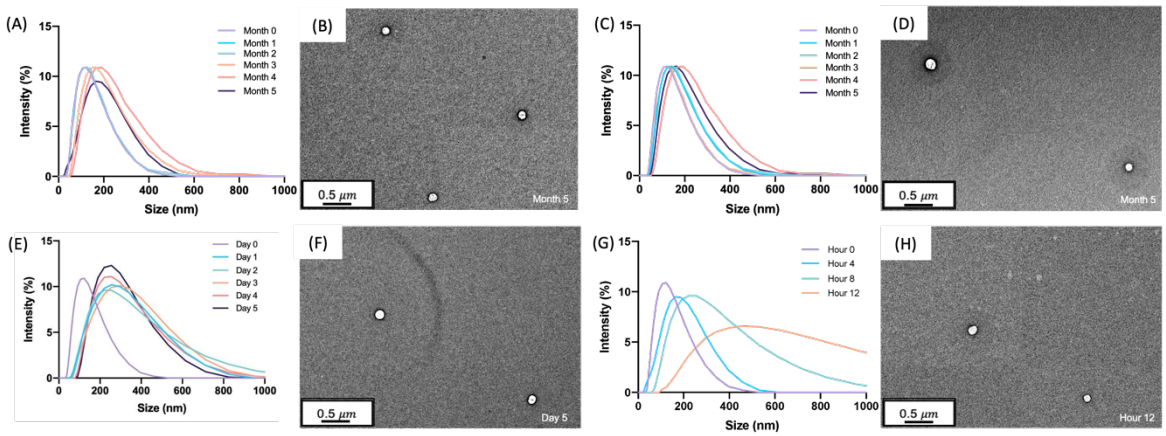

Figure 2.2 a) Glucagon nanogels (1 mg mL−1) were analyzed by DLS after being stored at (A) −20 °C, (C) 4 °C, (E) 25 °C, and (G) 37 °C for the indicated times. TEM images were taken at the final time point after storage at (B) −20 °C for 5 months, (D) 4 °C for 5 months, (F) 25 °C for 5 days, and (H) 37 °C for 12 hours. DLS intensity was measured at 25 °C. TEM images were taken using a 2% uranyl acetate negative stain.

°C exhibited an increased shift of approximately 100 nm after 1 day by DLS, however, after 5 days the glucagon nanogels remained of similar size by both DLS and TEM (**Figure 2.2E and F**). After 12 h at 37 °C, the glucagon nanogels size began shifting dramatically with a large size distribution by DLS (**Figure 2.2G**). However, by TEM, an increase in size was not observed. In a wider frame by TEM, some potential fibrils can be seen after 5 days at 25 °C and after 12 h at 37 °C (**Figure 2.27**). The discrepancy is likely due to DLS intensity putting an emphasis on larger particle sizes.[51] It has been observed that nanoparticles increase in size at increased temperatures due to aggregation.[52–54] However, trehalose polymers have been shown to prevent this aggregation.[55] Therefore, the glucagon either internally or near the surface could be causing the aggregation observed at 37 °C. The glucagon nanogels at −20 °C and 4 °C can be studied past 5 months to evaluate additional time points; however, the glucagon nanogels formulation at 25 °C and 37 °C will likely need be reformulated before evaluating at longer time points. A larger PEG dithiol crosslinker could potentially be employed to create smaller nanoparticles and improve the stability at higher temperatures, glucagon loading could be lowered, or the trehalose polymer size or trehalose content could be increased. These studies are planned for the future.

2.2.3 Degradation and Fibrillation of Glucagon.

The degradation and fibrillation of the glucagon in the optimized glucagon nanogel formulation was also monitored over 5 months at −20 °C and 4 °C, 5 days at 25 °C, and 12 h at 37 °C using HPLC and ThT assay. A quantitative assessment of glucagon–SH degradation was made by integrating the AUC of the glucagon nanogel after reducing with TCEP, for simplicity, compared to free glucagon–SH at the same temperature and time point. After 2 months at −20 °C, the free glucagon began to degrade significantly more than glucagon in the nanogel (**Figure 2.3A**). After only 1 month at 4 °C, the free glucagon began to degrade significantly more than glucagon

nanogel (**Figure 2.3B**). In contrast, the glucagon released from the glucagon nanogel at −20 °C and 4 °C remained above 95% up to 5 months. After 3 days at 25 °C, the free glucagon began to degrade significantly more than glucagon nanogel; however, the glucagon from the nanogel was 63% intact after 3 days (**Figure 2.3C**). After 4 h at 37 °C, the free glucagon began to degrade significantly more than glucagon nanogel; however, the glucagon from the nanogel was also degrading after 4 h (**Figure 2.3D**). Glucagon is known to form fibrils in acidic and alkaline pH solutions within hours at 25 °C.[56] Glucagon fibrillation can be assessed qualitatively by measuring the fluorescence with ThT, a fluorescence dye that is known to bind to amyloid fibrils *in vitro* and can be used to monitor the formation of fibrils in a 96-well plate.[8,56] Since the ThT fluorescence is dependent on both acidic and basic pH, inducing a significant decrease in ThT absorbance, a

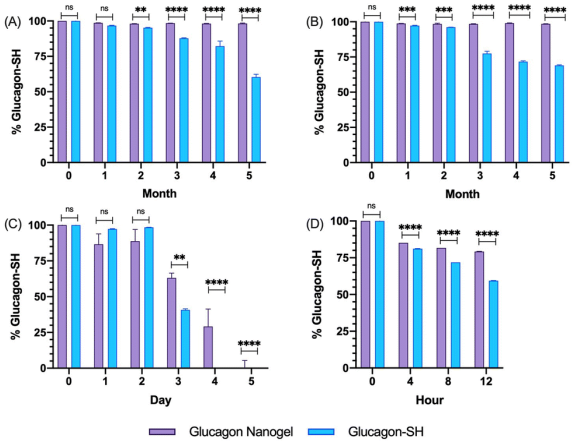

Figure 2.3 Glucagon–SH degradation was assessed by integrating the AUC of the released glucagon–SH using HPLC for glucagon nanogels stored at (A) −20 °C, (B) 4 °C, (C) 25 °C, and (D) 37 °C at various time points. Normalization was done by comparing all samples against t_0. Statistical significance was determined by comparing the glucagon–SH released from nanogel to the glucagon–SH control at the respective time and storage temperatures. Statistical significance was determined *via* a one-way ANOVA with multiple comparisons ($p = 0.1$ (ns), $p < 0.01$ (**), $p < 0.001$ (***), $p < 0.0001$ (****)) ($n = 6$).

soluble solution of glucagon–SH at either acidic or basic pH was not suitable to be used as a positive control.[57] Thus, bovine serum albumin (BSA) fibrils was used as a positive control through induced fibrillation by heating to 80 °C before incubating with ThT, since in this case neutral pH was utilized.[58] Both the glucagon released as described above from the nanogels stored at −20 °C and 4 °C exhibited no statistically significant increase in fluorescence over the 5 months of monitoring, indicating no fibril formation (**Figure 2.4A and B**). However, after 5 days at 25 °C, the glucagon nanogels exhibited a significant increase in fluorescence compared to the control and day 0, indicating fibril formation (**Figure 2.4C**). Additionally, after 12 h at 37 °C, the glucagon

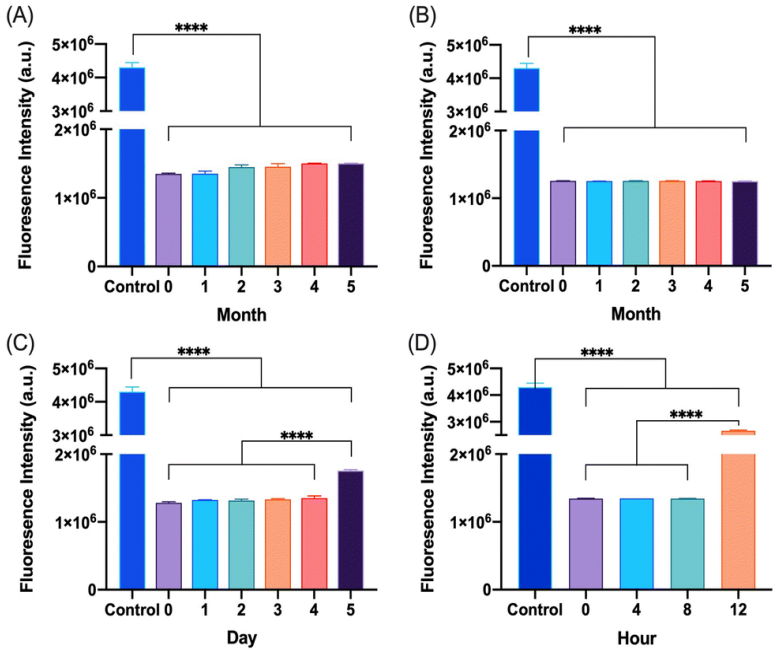

Figure 2.4 Glucagon–SH fibrillation was assessed by measuring the ThT fluorescence of glucagon nanogels stored at (A) −20 °C, (B) 4 °C, (C) 25 °C, and (D) 37 °C at various time points. Statistical significance was determined by comparing each sample to t_0 at the respective time and storage temperatures. Unless annotated, there is no statistical significance between t_0 and other time points. Statistical significance was determined *via* a one-way ANOVA with multiple comparisons (****$p \leq 0.0001$.) ($n = 6$).

nanogels exhibited a statistically significant increase in fluorescence compared to the control and day 0, indicating fibril formation (**Figure 2.4D**). We hypothesize that glucagon started forming small molecular weight aggregates that were not detectable by the ThT assays at 3 days at 25 °C, and by day 5 detectable fibrils had begun to form. Likewise, after 4 h at 37 °C less glucagon was observed by HPLC and by 12 h fibrils were observed. It is also possible that some of the glucagon degrades and therefore it not detected at earlier time points. From these studies, it can be concluded that improved glucagon stability against degradation and fibrillation was observed at all temperatures studied. The glucagon nanogels at −20 °C and 4 °C exhibited no significant degradation or fibrillation up to 5 months and are promising for further studied to increase cold chain stability of glucagon.

2.2.4 Nanogel Stability in Cell Media Conditions.

Glucagon nanogel stability was assessed in cell media conditions before beginning *in vitro* experiments.[59] The glucagon nanogels were incubated with 10% FBS and stored at 4 °C, 25 °C, and 37 °C and analyzed by DLS. DLS measurements were taken up to 3 days for the glucagon nanogels stored at 4 °C and 25 °C and 12 h for the glucagon nanogel at 37 °C. The glucagon nanogels did not exhibit any significant change in size at any of the temperatures and time points

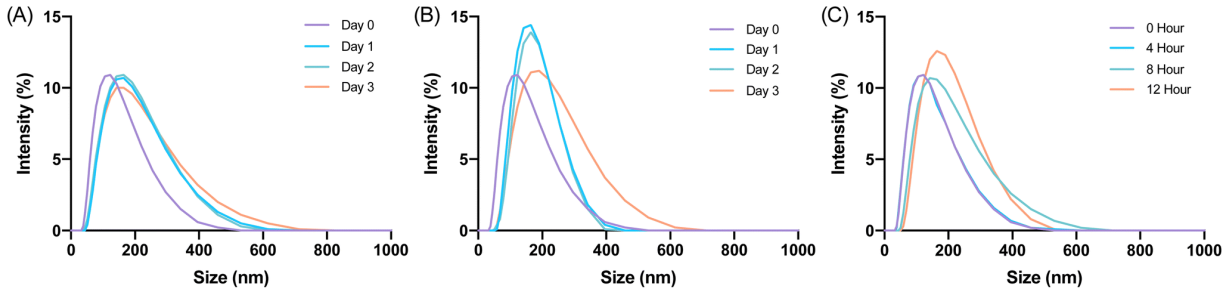

Figure 2.5. Glucagon nanogels were treated with 10% FBS and visualized by DLS for the respective storage temperatures (A) 4 ºC, (B) 25 ºC, (C) 37 ºC at various time points. DLS intensity was measured at 25 ºC.

(**Figure 2.5**). Additionally, the glucagon nanogel remained uniform up until 12 h at 37 °C with 10% FBS, which differs from its DLS size measurement in (**Figure 2.5C vs. 2.5G**). It is possible the proteins and other components in FBS helped to stabilize the aggregation of the nanogels at 37 °C.[60]

2.2.5 *In vitro* Biocompatibility.

The *in vitro* biocompatibility of the empty nanogel and glucagon nanogels (freshly prepared, 4 °C for 3 months, and −20 °C for 3 months) were evaluated for 24 h in mouse embryonic fibroblasts, NIH 3T3, by performing the colorimetric MTT (3-(4,5-dimethylthiazol-2-yl)-2,5-diphenyl-2*H*-tetrazolium bromide) assay. The *in vitro biocompatibility* was evaluated at 24 h at increasing concentrations of nanogel 10–1000 μg mL^{-1}. The cell viability exposed to empty nanogel and glucagon nanogels were not statistically different from the control except for glucagon nanogels stored for 4 °C for 3 months at 1 mg mL^{-1}, and −20 °C for 3 months at greater than 0.5

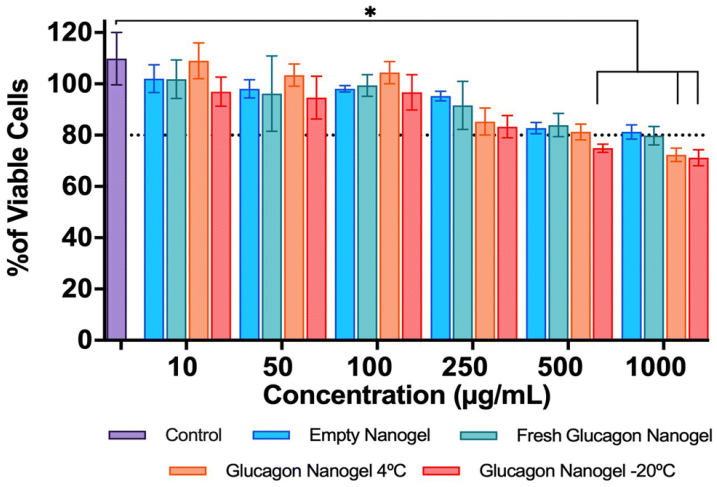

Figure 2.6. *In vitro* biocompatibility was evaluated after 24 h in mouse embryonic fibroblasts, NIH3T3 by performing the colorimetric MTT assay. Data are represented as mean ± SEM (n = 3). Statistical significance was determined *via* a one-way ANOVA with multiple comparisons $p < 0.05$ (*).

mg mL^{-1} after 24 h, indicating good *in vitro* biocompatibility of the material (**Figure 2.6**). Further, a live/dead assay was used to evaluate the biocompatibility of empty nanogel and freshly prepared glucagon nanogel qualitatively for 24 h (**Figure 2.7**). The calcein AM stains the live cells green and ethidium homodimer-1 stains the dead cells red. The green fluorescence and very minimal red

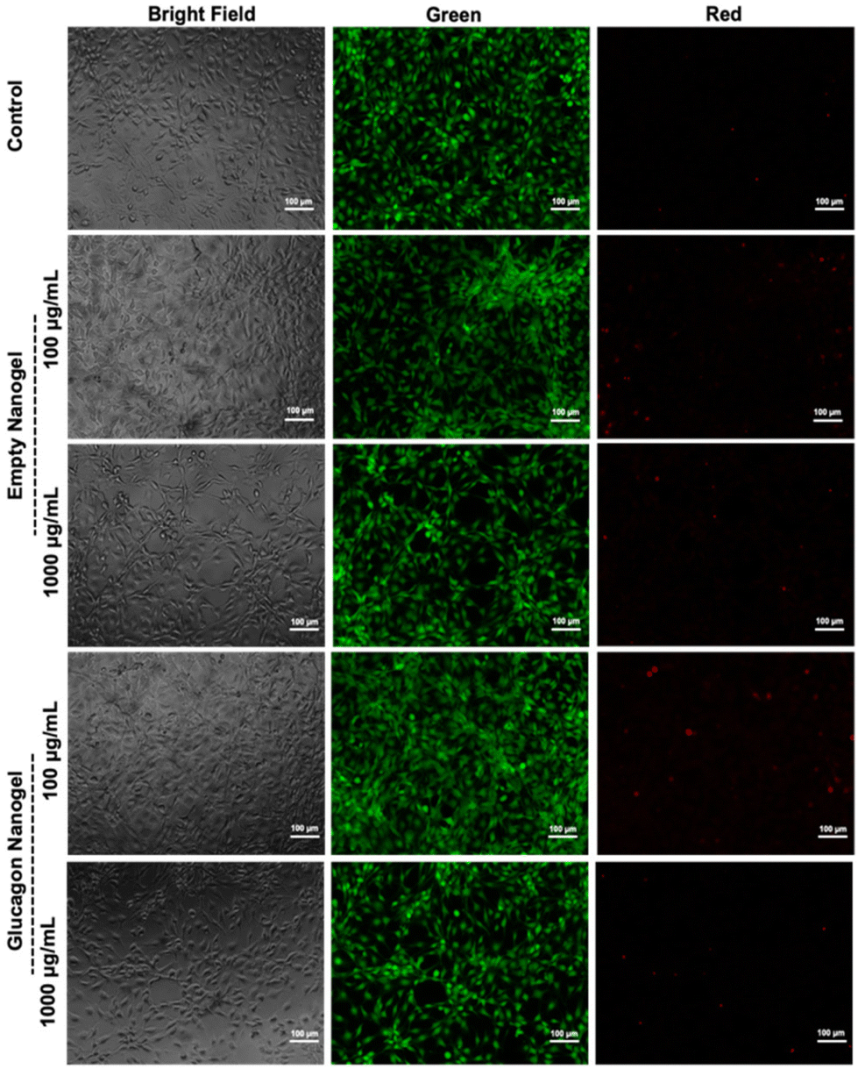

Figure 2.7 *In vitro* biocompatibility was evaluated after 24 hours in mouse embryonic fibroblasts, NIH 3T3 by performing a live/dead assay using calcein AM and ethidium homodimer. The cells exposed to the empty nanogel and glucagon nanogel were imaged using a bright field and fluorescent microscope (scale bar: 100 µm).

fluorescence indicate the empty nanogel and glucagon nanogel are biocompatible at 10, 100, 500, and 1000 μg mL^{-1} (**Figure 2.7 and Figure 2.28**).

2.2.6 *In vitro* Efficacy.

The in vitro efficacy of the glucagon nanogel was evaluated by comparing the levels of lactate produced when treated with empty nanogel, glucagon–SH and glucagon nanogel. Glucagon is known to promote the conversion of glycogen to glucose in the liver, producing lactate as a by-product of glycogenolysis (breakdown of the glucose).[5] Herein, a liver cell model, HepG2 cells were starved with media containing low glucose, resembling hypoglycemic conditions. After starvation, media was replaced containing normal levels of glucose along with empty nanogel, glucagon–SH and glucagon nanogel. The levels of lactate were measured at different time points from 2–72 h using bioluminescence (**Figure 2.8**). The results show that cells treated with glucagon–SH and glucagon nanogel produce significantly higher levels of lactate than the control and empty nanogel. Further, a color change of the cell culture media was observed (phenol red to

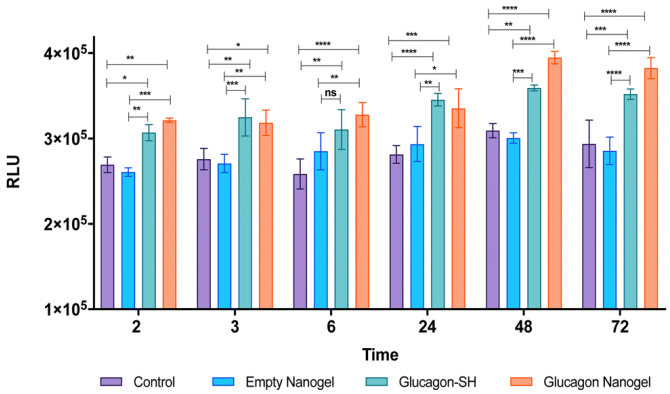

Figure 2.8 *In vitro* efficacy evaluated in a liver cell line model, HepG2 by comparing the levels of lactate produced from 2–72 h by observing bioluminescence. Statistical significance was determined *via* a one-way ANOVA with multiple comparisons (p = 0.1 (ns), $p < 0.05$ (*), $p < 0.01$ (**), $p < 0.001$ (***), $p < 0.0001$ (****)) (n = 3).

golden yellow) in samples treated with native glucagon, glucagon–SH, and glucagon nanogel when compared to the control (**Figure 2.29**). The color change is due to the production of the lactate, an acidic bioproduct of glycogenolysis. These cell studies indicate the activity of the glucagon–SH both free and conjugated to the nanogel, confirming our hypothesis that the modified glucagon is active as native glucagon.

2.2.7 Hemocompatibility.

The toxicity of the glucagon nanogels and its components to cells were assessed by measuring the destruction of red blood cells (RBCs). The concentrations of 200–500 μg active ingredient (glucagon) tested were chosen to mimick future and past in vivo experiments.29 Using sheep RBCs, the glucagon nanogels, PEG_{2000} dithiol, poly(PDSMA-*co*-TrMA), and glucagon–SH all showed ≤3% hemolysis, indicating the samples are not disrupting the cells (**Figure 2.9**). This is also understood qualitatively by observing a clear supernatant for the samples tested (**Figure 2.30**). The results show that the nanoparticles, loaded or empty, are non-hemolytic.

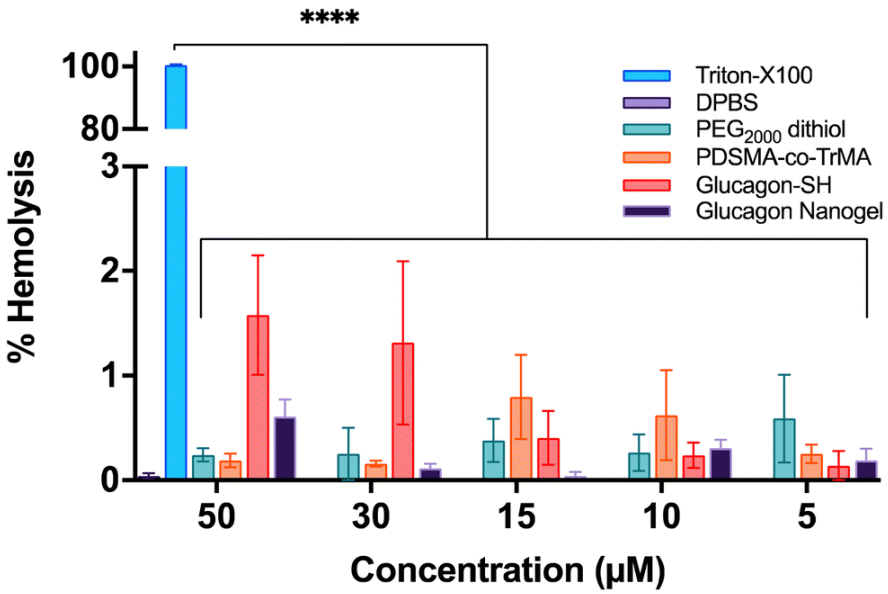

Figure 2.9 Hemocompatibility of the glucagon nanogel and its components were assessed in sheep RBCs. Data are represented as mean ± SEM (n = 3).

2.2.8 Viscosity.

For the emergency delivery of glucagon, a subcutaneous (SC) route is typically used.[15,17] When considering SC injectable therapeutics, one factor to consider is the viscosity of the solution.[61–63] The viscosity of formulations that can be SC injected within 10 seconds into humans without pain tolerance concerns is up to 15–20 centipoise (cp).[63] At a concentration of 1 mg mL−1 active ingredient (glucagon), the viscosities of the empty and loaded nanogel were measured. At 25 °C with a shear rate of 5000 s−1, viscosity of the empty nanogel was 1.38 ± 0.19 cp and the glucagon nanogel was 1.31 ± 0.06 cp, well below 15–20 cp. These results suggest that viscosities of the nanogels are acceptable for subcutaneous injection of the nanogel formulation into humans.[61]

2.3 Conclusion

In conclusion, we prepared and evaluated a uniform nanogel formulation that solubilized glucagon in aqueous solution at pH 7.4 for long term stabilization at −20 °C and 4 °C. The system was optimized by varying the crosslinker size, crosslinking percentage, and order of addition of the components to yield uniform glucagon loaded nanogels of ∼150 nm in size. The glucagon nanogels were shown to be biocompatible and efficacious in vitro by comprehensive study of hemolysis, colorimetric MTT assay, live/dead assay, and lactate assay. Additionally, this formulation exhibited viscosity suitable for subcutaneous delivery in humans, meaning that the viscosity was much lower than would cause pain tolerance concerns.

2.4 Experimental

2.4.1 Materials

Trehalose was purchased from The Healthy Essential Management Corporation (Houston, TX) and was azeotropically dried with ethanol and kept under vacuum until use. Unless otherwise

noted, all materials were of analytical grade and purchased and used as received from Fisher Scientific, Acros Organics, Oakwood Chemicals and Sigma Aldrich. Anhydrous compounds were dried over molecular sieves. Azobis(isobutryronitrile) (AIBN) was recrystallized from acetone before use. DMSO was dried using molecular sieves and kept under an inert atmosphere. Spectra/Por3 regenerated cellulose membrane (MWCO 1.0 or 3.5 kDa) was purchased from Spectrum Chemical (New Brunswick, NJ) for polymer dialysis. Thiolated glucagon (GCG-SH, sequence: HSQGTFTSDYSKYLDSRRAQDFVCWLMNT) and native GCG (sequence: HSQGTFTSDYSKYLDSRRAQDFVQWLMNT) were purchased from Biomatik at >90% purity. MilliporeSigma™ Millex™ hydrophilic PTFE filters were used for all glucagon nanogel experiments. Sheep red blood cells (RBCs) were purchased from Innovative Research (lot # 39841). Dulbecco's Phosphate buffer saline (DPBS) (pH 7.4), Dulbecco's Modified Eagle's Medium (DMEM) cell culture media, and Pen Strep (Penicillin and Streptomycin) were procured from Gibco, ThermoFisher Scientific. Fetal bovine serum (FBS) was procured from Sigma-Aldrich. Trypsin was purchased from MP Biomedicals. MTT (3-(4,5-dimethylthiazol-2-yl)-2,5-diphenyltetrazolium bromide) was procured from RPI (Research Product International Corp.). DMSO was procured from VWR chemicals. Glo TM Calcein AM and ethidium homodimer-1 were purchased from Invitrogen. Lactate- Glo^{TM} assay was purchased from Promega.

2.4.2 Analytical Techniques

Nuclear magnetic resonance (NMR) spectra were obtained using a Bruker AV 400 MHz spectrometer and the data was analyzed using MestRenova v12 software. Deuterated solvents obtained from Cambridge Isotope Laboratories were used for all NMR spectroscopic analyses. A Biotage Isolera Prime equipped with KP-SNAP Ultra Biotage columns was used for all flash column chromatography. Analytical reverse-phase high performance liquid chromatography

(HPLC) was carried out on an Agilent 1260 Infinity II HPLC system equipped with an autosampler and a UV detector using a Zorbax 300SB-C18 (analytical: 3.5 μm, 3.0 × 150 mm) with monitoring at λ = 220 nm and with a flow rate of 0.8 mL/min, using a gradient 30-45% of solvent B (A: H 2 O + 0.1% TFA; B: CAN + 0.1% TFA) over 18 minutes. Preparatory HPLC purification was performed on a Shimadzu HPLC system equipped with a UV detector using a Luna 5 μm C18 100 Å column (preparatory: 5 μm, 250 × 21.2 mm) with monitoring at λ = 215 and 254 nm. Gradient solvent system (H_2O:MeOH = 90:10 to 40:60 over 20 min) was used as the mobile phase at a flow rate of 20 mL/min. Gel permeation chromatography (GPC) using a size exclusion chromatography (SEC) measurements were performed in DMF on an Infinity 1260 II HPLC system from Agilent equipped with a multiangle light scattering detector MALS and a diode array detector DAD and differential refractive index detector dRI from Wyatt technology. Polymers were separated on two Plgel Mixed-D gel columns PL1110–6504 (300 × 7.5 mm) at a flow rate of 0.6 mL min–1 . Column temperatures were held at 40 °C in DMF with LiBr (0.1 M). Molar masses were calculated from the dn/dc. Absorbance and fluorescence readings were measured using the SpectraMax iD3Multi-Mode Microplate Reader from Molecular Devices.Electrospray ionization (ESI) mass spectra were obtained using an Agilent 6530 QTOF-ESI in tandem with a 1260 Infinity LC. Dynamic light scattering (DLS) measurements were carried out using a Malvern Zetasizer Nano at polymer concentrations of 1 mg/mL. Transmission electron microscopy (TEM) images were acquired on a FEI T12 instrument using formvar/carbon coated grids (200 mesh, Cu, Ted Pella). Grids were glow discharged for 15 seconds. 5 μL of sample (1 mg/mL) were placed on the grid and allowed to adhere for 5 minutes. After, the grids were stained with 3 μL of 2% uranyl acetate for 3 minutes. Infrared absorption spectra were recorded using a PerkinElmer FT-IR equipped with an ATR accessory. For SDS-PAGE gels, samples were loaded using 2X Laemmli sample buffer and run on

Mini-Protean TGX, Any kD gels (Bio-Rad) at 195V for 35 minutes using Tris/Glycine/SDS buffer (Bio-Rad). Gels were stained with Coomassie. SDS-PAGE protein standards were obtained from Bio-Rad (Precision Plus Protein Prestained Standards). fluorescence Microscopy. The fluorescence images were taken using Zeiss Viscosity was measured using a RheoSense microVisc.

2.4.3 Methods

Synthesis of trehalose methacrylate monomer[3]

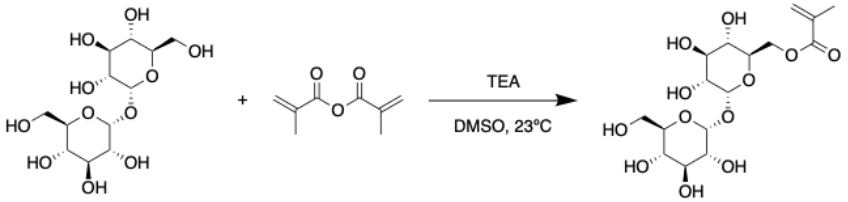

Anhydrous trehalose (5.02 g, 14.6 mmol, 5 eq) was dissolved in dry DMSO (60 mL) in a dry round bottom flask (250 mL) equipped with a stir bar. The solution was stirred under argon until most of the trehalose dissolved. Under argon, dry triethylamine (6.1 mL, 43.8 mmol, 15 eq) was added followed by methacrylic anhydride (0.43 mL, 2.92 mmol, 1 eq). The solution was left to stir at room temperature for 72 hours. The solution was added dropwise to ice-cold 8:2 hexanes: dichloromethane (2000 mL) with gradual stirring over 10 minutes. A sticky yellow oil was left at the bottom of the flask. The organic layer was poured off to leave the oil and some remaining solvent. The solution was transferred to a round bottom flask (1000 mL) to remove any remaining organic solvent via a rotary evaporator. The sticky solid was re-dissolved in deionized water. The material was purified via HPLC (C18 column, 10-60% MeOH). The pure fractions were collected and transferred to a round bottom flask containing MEHQ solution (10 µL, 4 mg/mL in water) to prevent autopolymerization. The methanol was removed by blowing air into the round bottom for 18 hours. The material was rinsed with distilled water and transferred to a tared falcon tube and

lyophilized to yield a white fluffy solid (Yield: 38 %). ^{1}H NMR (400 MHz, D_2O) δ 6.15 (p, J = 1.0 Hz, 1H), 5.74 (p, J = 1.5 Hz, 1H), 5.16 (dd, J = 13.5, 3.9 Hz, 2H), 4.49 (dd, J = 12.3, 2.2 Hz, 1H), 4.36 (dd, J = 12.3, 5.2 Hz, 1H), 4.07 (ddd, J = 10.1, 5.1, 2.1 Hz, 1H), 3.88 – 3.40 (m, 11H), 1.93 (dd, J = 1.6, 1.0 Hz, 3H). Spectrum matched published one.

Synthesis of PDSMA monomer

Synthesis of pyridyl disulfide ethyl alcohol[64]

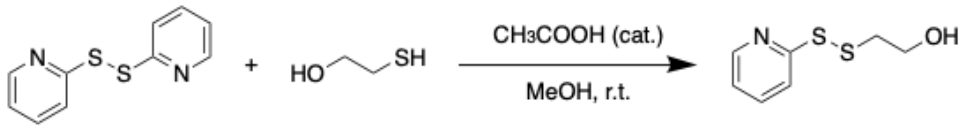

2-2 dipyridyl disulfide, (5.052 g, 22.9 mmol) was dissolved in 25 mL of methanol. Glacial acetic acid (330 µL) was added to the mixture. 2-mercaptoethanol (800 µL, 11.4 mmol) was added to the mixture drop-wise at room temperature making a yellow solution. The reaction was stirred at 4 hours at room temperature. The solution was concentrated down to a yellow oil by removing the methanol. The oil was redissolved in dichloromethane and washed with sodium bicarbonate (30 mL), distilled water (30 mL), and brine (30 mL). The organic layer was dried over magnesium sulfate. The material was purified by flash chromatography using a 25% ethyl acetate: hexanes isocratic method to remove the 2,2-dipyridyl disulfide peak first and then increased to a gradient of 25%-40% ethyl acetate: hexanes to elute the product peak. The pure fractions were collected and rotovapped to remove the solvent. The product was concentrated to a clear oil (Yield: 72%). ^{1}H NMR (400 MHz, $CDCl_3$) δ 8.36 (ddd, J = 6.0, 2.0, 1.1 Hz, 1H), 7.43 (dddd, J = 8.0, 7.4, 1.8, 0.7 Hz, 1H), 7.25 (dt, J = 8.1, 1.0 Hz, 1H), 7.00 (ddt, J = 7.2, 5.0, 1.1 Hz, 1H), 3.68 – 3.61 (m, 2H), 2.82 – 2.76 (m, 2H). FT-IR (film) λ= 3307 cm-1, 2853 cm-1, 2842cm-1, 1573 cm-1, 1406 cm-1, 1042 cm-1. NMR spectrum matched published one.

Synthesis of pyridyl disulfide ethyl methacrylate monomer[64]

Pyridyl disulfide ethyl alcohol (500 mg) was dissolved dry dichloromethane (2 mL) in a dry round bottom flask with a stir bar. Dry triethylamine (483 µL) was added and the mixture was stirred in an ice-bath under argon. Methacryloyl chloride (260 µL) was diluted in dry dichloromethane (800 µL) then added drop-wise with continuous stirring to the reaction flask. The reaction mixture was then stirred at room temperature for 6 hours. The stirring was stopped, and the reaction mixture was washed with sodium bicarbonate (3x30 mL), distilled water (3x30 mL), and brine (30 mL). The organic layer was collected and dried over anhydrous magnesium sulfate. The product was purified via flash column chromatography using a 20% isocratic method. The product eluted first and was concentrated to yield a clear oil (Yield: 56 %). ^{1}H NMR (400 MHz, $CDCl_3$) δ 8.46 (ddd, J = 4.9, 1.8, 0.9 Hz, 1H), 7.70 – 7.59 (m, 2H), 7.09 (ddd, J = 7.3, 4.9, 1.2 Hz, 1H), 6.12 (dq, J = 2.0, 1.0 Hz, 1H), 5.58 (p, J = 1.6 Hz, 1H), 4.39 (t, J = 6.4 Hz, 2H), 3.09 (t, J = 6.4 Hz, 2H), 1.93 (dd, J = 1.6, 1.0 Hz, 3H). Spectrum matched literature.

Free radical polymerization of PDSMA and TrMA

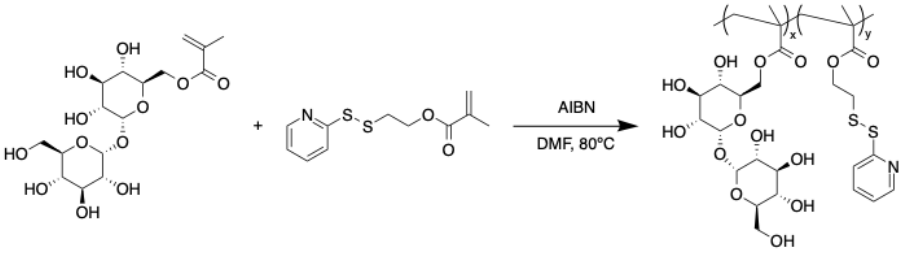

For a 1:1 PDSMA:TrMA feed ratio, TrMA (50 mg, 122 µmol), PDSMA (31.1 mg, 122 µmol), and azobisisobutyronitrile (AIBN) (1 mg, 6 µmol) were dissolved in dry dimethylformamide (0.80 mL) to give a [TrMA]:[PDSMA]:[initiator] ratio of 20:20:1. The solutions were degassed by freezepump–thawing five times. The polymerization reaction vessel

was then put under argon to stir for 5 hours at 80 ºC in an oil bath. The polymerization stopped at 5 hours by exposing to air. The polymerization was purified by precipitating in ethyl acetate and dialyzing for 3 days against deionized water using 1 kDa MWCO tubing. The polymer was lyophilized for 2 days to yield a white fluffy solid (Yield: 53%). ^{1}H NMR (400 MHz, DMSO) δ 8.46 (s, 1H), 7.79 (s, 2H), 7.24 (s, 1H), 4.85 (d, J = 41.0 Hz, 10H), 1.81 (s, 4H), 0.87 (d, J = 69.0 Hz, 8H).

Empty nanogel synthesis

Poly(PDSMA-*co*-TrMA) (1.0 mg) was dissolved in 500 µL 10 mM HCl in a 1.5 mL lo bind Eppendorf tube equipped with a micro stir bar. PEG_{2000} dithiol (0.63 mg, 50% of PDS side chain) was dissolved in 250 µL 10 mM HCl, added to the reaction vial dropwise, and left to stir at 8000 rpm, 4 °C for 3 h. The crude empty nanogel solution was purified against DPBS 50 mM pH 7.4 using a 20 kDa MWCO microdialysis cup at 4 °C for 2 days. After purification, the empty nanogels were filtered using a 0.2 µm PTFE filter until further analysis and stored at 4 °C.

Glucagon nanogel synthesis

Poly(PDSMA-*co*-TrMA) (1.0 mg) was dissolved in 500 µL 10 mM HCl in a 1.5 mL lo bind Eppendorf tube equipped with a micro stir bar. Glucagon–SH (2.2 mg, 50% of PDS side chain) was dissolved in 250 µL 10 mM HCl and added to the reaction vial. The vial was left to stir at 8000 rpm, 4 °C for 2 h. PEG_{2000} dithiol (0.63 mg, 50% of PDS side chain) was dissolved in 250 µL 10 mM HCl, added to the reaction vial dropwise, and left to stir at 8000 rpm, 4 °C for 3 h. The crude glucagon nanogel was purified against DPBS 50 mM pH 7.4 using a 20 kDa MWCO microdialysis cup at 4 °C for 2 days. After purification, the glucagon nanogels were filtered using a 0.2 µm PTFE filter and stored at either −20 °C, 4 °C, 25 °C, or 37 °C. All glucagon nanogels were stored at 1 mg mL^{-1} (polymer) in a solution of DPBS 50 mM pH 7.4 unless otherwise noted

for all subsequential experiments. All glucagon nanogels were used immediately unless otherwise noted.

HPLC glucagon quantification

Glucagon incorporation and conjugation was monitored *via* the disappearance of the glucagon peak during the nanogel formation and reappearance after reducing with tris(2-carboxyethyl)phosphine (TCEP) 100 equiv. using the AUC of the glucagon peak (**Figure 2.17**) at 220 nm using high performance liquid chromatography (HPLC). Glucagon–SH controls were dissolved in minimal 10 mM HCl then brought to pH 7.4 with 50 mM DPBS.

Thioflavin T (ThT) assay

BSA fibrils prepared at 1 mg mL^{-1} were used as the positive control by inducing fibrils by heating to 80 °C for 1 h.[46] Empty nanogels at 1 mg mL^{-1} (polymer) in DPBS 50 mM pH 7.4 with 100 equiv. TCEP was used as the negative control. Glucagon nanogels were incubated with 100 equiv. TCEP for 15 min at 4 °C before analysis. 250 µL of ThT solution at 50 µM (in DPBS) was added into a black plate followed by the addition of 50 µL of either glucagon nanogel, empty nanogel, or BSA. The solutions were covered in the dark and incubated at 25 °C for 20 min. Fluorescence intensity was then measured using a plate reader (λ_{ex} = 450 nm, λ_{em} = 482 nm).[47]

Fetal bovine serum (FBS) glucagon nanogel stability

Glucagon nanogels were incubated with 10% FBS. DLS measurements were taken at 0, 1, 2, and 3 days for samples stored at 4 °C and 25 °C and at 0, 4, 8, and 12 h for samples stored at 37 °C.

Cell lines and maintenance

The mouse embryonic fibroblasts, NIH 3T3 were provided by Professor Andrea M Kasko, Engineering V, University of California Los Angeles and the human liver cancer cells, HepG2,

from Professor Yu-Pei, California NanoSystem Institute, UCLA. The mouse embryonic fibroblasts, NIH 3T3, and human liver cancer cells, HepG2, were cultured in Dulbecco's modified Eagle's medium (DMEM) media supplemented with 10% FBS (v/v), 1% Pen Strep, and antibiotics at 37 °C in a standard humidified atmosphere containing 5% carbon dioxide (CO_2).

***In vitro* biocompatibility**

The *in vitro* biocompatibility of empty nanogels and glucagon nanogels were evaluated for 24 h in mouse embryonic fibroblasts, NIH 3T3, by performing the colorimetric MTT (3-(4,5-dimethylthiazol-2-yl)-2,5-diphenyl-2*H*-tetrazolium bromide) assay. The MTT assay was evaluated for different concentrations: 10, 50, 100, 250, 500, 1000 μg mL^{-1} for 24 h. 0.7×10^4 cells per well were counted using hemocytometer, seeded in 96-well plates, and incubated at 37 °C overnight. The next day, the cells were treated with different concentrations of the empty nanogel and glucagon nanogel (freshly prepared, 3 month at 4 °C, and 3 months at −20 °C) and incubated at 37 °C for 24 h. Media supplemented with FBS served as a control. After incubation, cell culture media was replaced with serum-free media containing MTT reagent (5 mg per 10 mL) and incubated at 37 °C for 3 h. The MTT-containing media was removed, a solubilizing agent, DMSO, was added to dissolve the formazan crystals, and the absorbance was measured at 570 nm using a plate reader. For normalizing, the absorbance was measured at 630 nm.

Live/dead cell assay

The *in vitro* biocompatibility of empty nanogels and glucagon nanogels were evaluated for 24 h in mouse embryonic fibroblasts, NIH 3T3, by performing a microscopic live/dead assay. The live/dead assay was evaluated at 4 different concentrations: 10, 100, 500, 1000 μg mL^{-1}. 0.7×10^4 cells per well were counted using a hemocytometer, seeded in 96-well plates, and incubated at 37 °C for 12 h. The next day, the cells were treated with different concentrations of the empty

nanogel and glucagon nanogel and incubated for 24 h at 37 °C. After 24 h, the cell culture media was replaced with fresh media and fluorescent probes calcein AM (green fluorescence) and ethidium homodimer-1 (red fluorescence) were added, incubated for 20 min at 37 °C, and imaged using a fluorescent microscope.

***In vitro* efficacy study**

The *in vitro* efficacy of the glucagon nanogel was evaluated by comparing the level of lactate produced using a Lactate-Glo™ assay kit, Promega. The liver model cell line, HepG2 was used for evaluating the levels of lactate produced. Cells (0.7×10^4 per well) were plated in a 96-well plate and incubated overnight at 37 °C. The next day, the cell culture media was replaced with 1 mg of glucose containing media without FBS and starved for 4 h. After 4 h, the media was replaced with 4.5 mg of glucose containing media with 10% FBS along with the empty nanogel, glucagon–SH (20 μg) and glucagon nanogel (20 μg). The sample of the medium at experimental time points (2, 3, 6, 24, 48, and 72 h) were collected by diluting 4 μl into 96 μl DPBS. The samples were collected and frozen at −20 °C until ready to perform the assay. The samples were thawed and 50 μl was transferred to a white 96-well assay plate. 50 μL of Lactate Detection Reagent (Lactate-Glo™ assay, Promega) was added and incubated for 60 min at 25 °C. Luminescence was recorded using the plate reader.

Metabolic activity

The metabolic activity of the glucagon nanogels were evaluated qualitatively by monitoring the color change of the cell culture media in a liver model cell line, HepG2. Cells (0.3×10^6 per well) were plated into 35 mm cell culture dishes and incubated for 12 h at 37 °C. The next day, the cell culture media was replaced with 1 g L^{-1} of glucose containing media without FBS and starved for 4 h. The control for the experiment was the cells cultured in the cell culture

media supplemented with FBS. After 4 h, the media was replaced with 4.5 g L^{-1} of glucose containing media with 10% FBS along with native glucagon, glucagon–SH (20 μg mL^{-1}) and glucagon nanogel (20 μg mL^{-1}). The media color change was observed every day and imaged after 72 h.

Hemocompatibility

Hemolytic effects of the glucagon nanogels were determined following a previous report.[65] Sheep red blood cells (RBCs) (1 mL, 100%) were resuspended in 5 mL of DPBS (50 mM, pH = 7.4) and centrifuged at 3000 rpm, 4 °C for 10 min. The supernatant was discarded and replenished with more DPBS. This wash was repeated 3–5 more times until the supernatant was visibly clear. The RBCs were resuspended to 8 mL with DPBS. The cells were counted using a hemacytometer and diluted to 2.0×10^7 cells per mL. 250 μL of diluted RBCs were added to clear lo bind Eppendorf tubes followed by the addition of 750 μL of sample. PEG_{2000} dithiol, poly(PDSMA-*co*-TrMA), glucagon–SH, and glucagon nanogel at concentrations 5–50 μM were tested ($n = 3$). Concentrations were based on glucagon–SH. 50 mM DPBS was used as the negative control and 20% Triton X-100 in DPBS was used as the positive control. The samples were incubated at 37 °C for 1 h. Then, the samples were centrifuged at 3000 rpm, 4 °C, for 10 min. 100 μL of supernatant of each sample were aliquoted in a 96-well plate. The absorbance was measured at 540 nm. To determine the hemolysis percentage, we used the following equation: % hemolysis $= 100(A - A_0)/(A_{TX} - A_0)$ where A is the absorbance reading of the sample, A_0 is the negative hemolysis control, and A_{TX} is the positive hemolysis control.

Viscosity measurements

The empty nanogel and glucagon nanogel were prepared as mentioned above and then loaded into a Rheosense syringe. Air bubbles were carefully removed from the syringe. Syringe

was loaded into the viscometer and allowed to equilibrate at the measurement temperature for 20 min.

Statistical analysis

All experimental values are reported as the mean ± SD. Graph Pad Prism 8 software was used for statistical analyses. One-way analysis of variance (ANOVA) followed by Turkey's multiple comparison test was employed to compare the means and determine the significance. Statistical significance is denoted by $p < 0.05$ (*), $p < 0.01$ (**), $p < 0.001$ (***), $p < 0.0001$ (****).

2.5 Appendix I

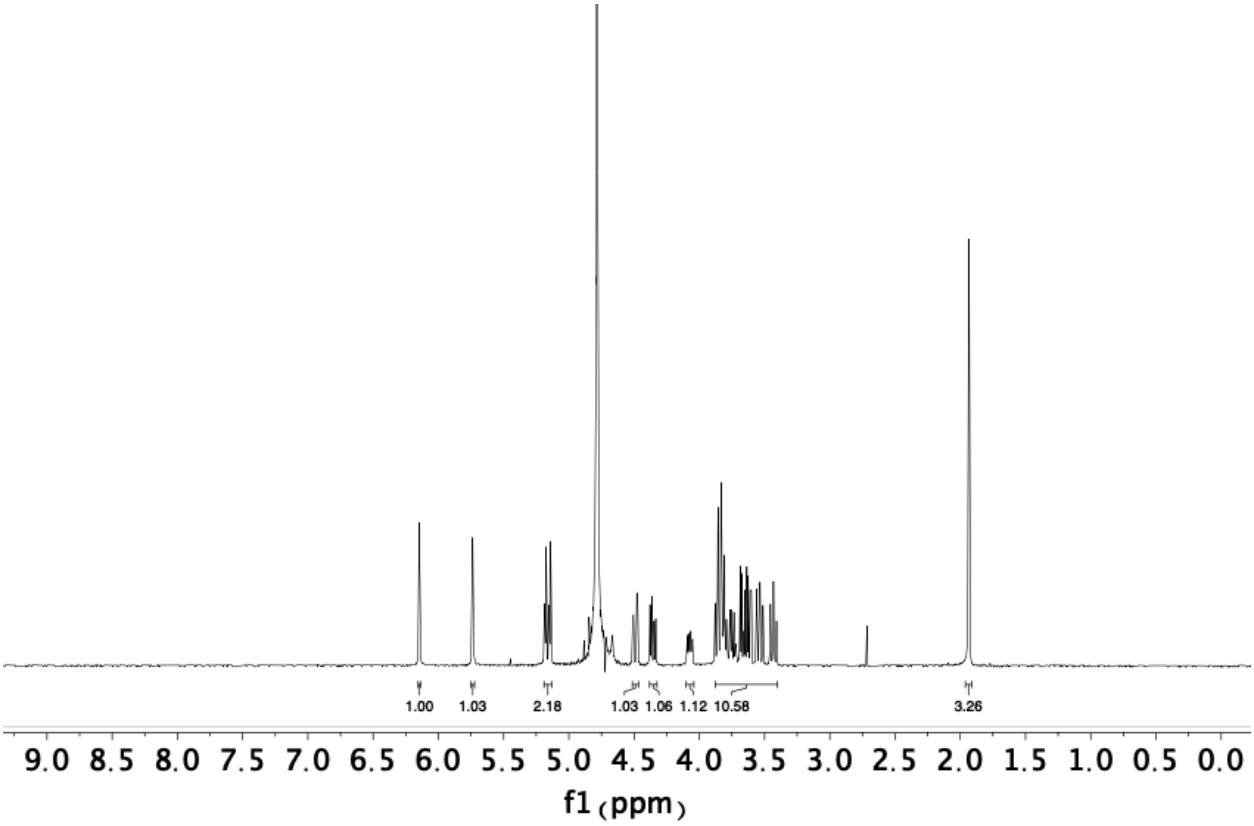

Figure 2.10. ^{1}H NMR spectrum of TrMA (400 MHz in D_2O).

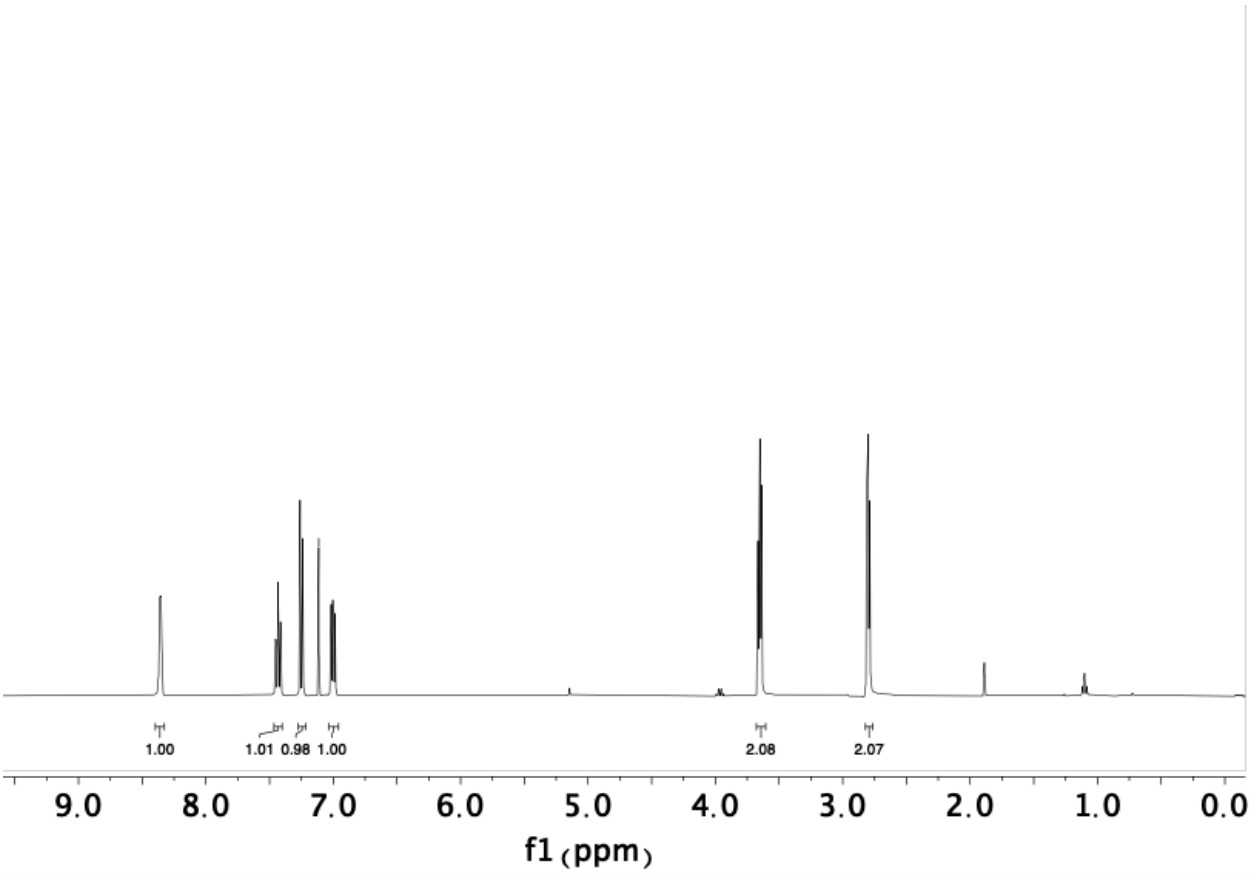

Figure 2.11. ^{1}H NMR spectrum of PDSOH (400 MHz in $CDCl_3$).

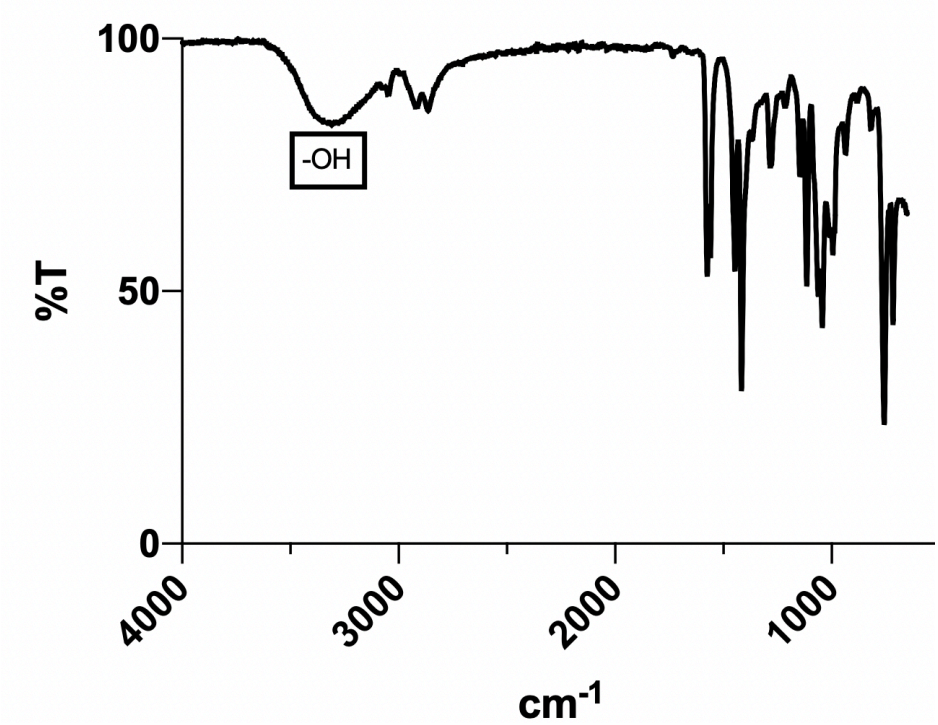

Figure 2.12. FT-IR spectrum of PDSOH.

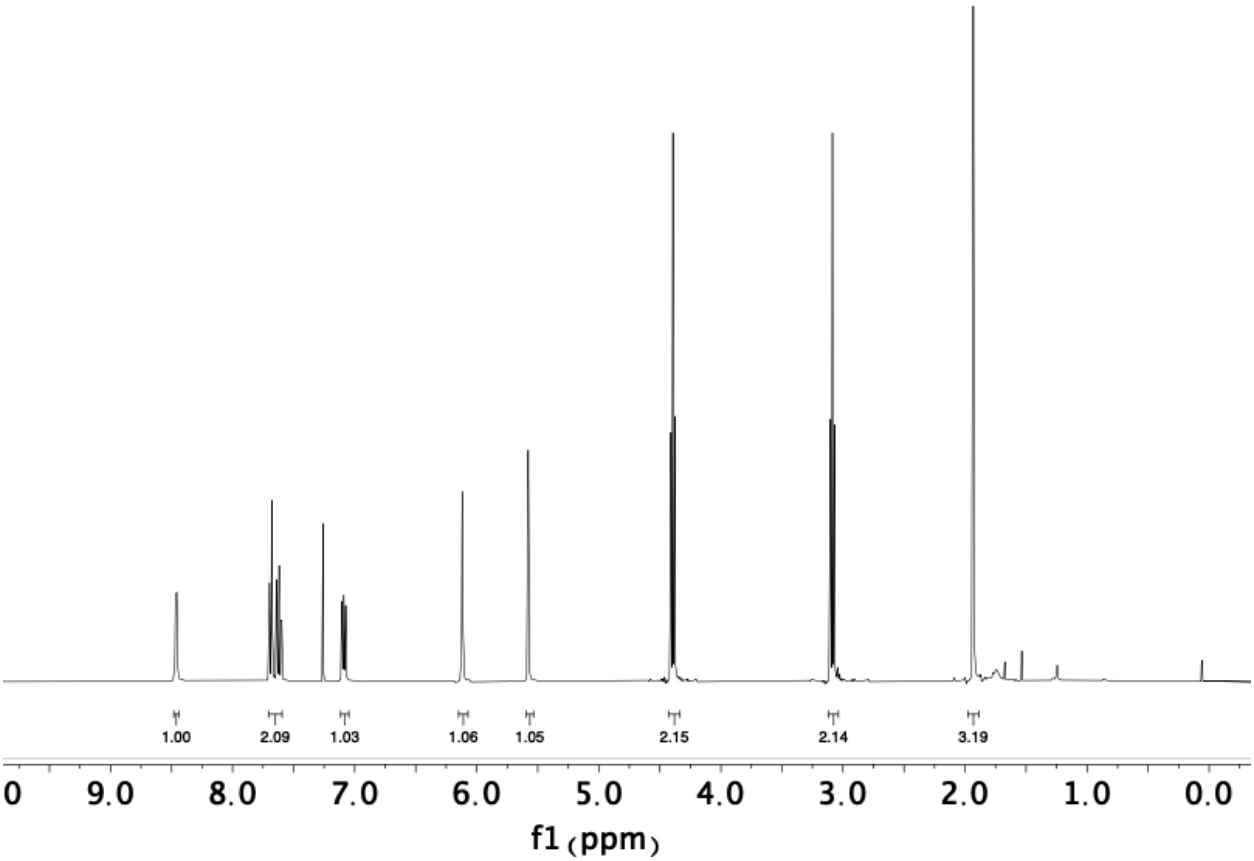

Figure 2.13. ^{1}H NMR spectrum of PDSMA (400 MHz in $CDCl_3$).

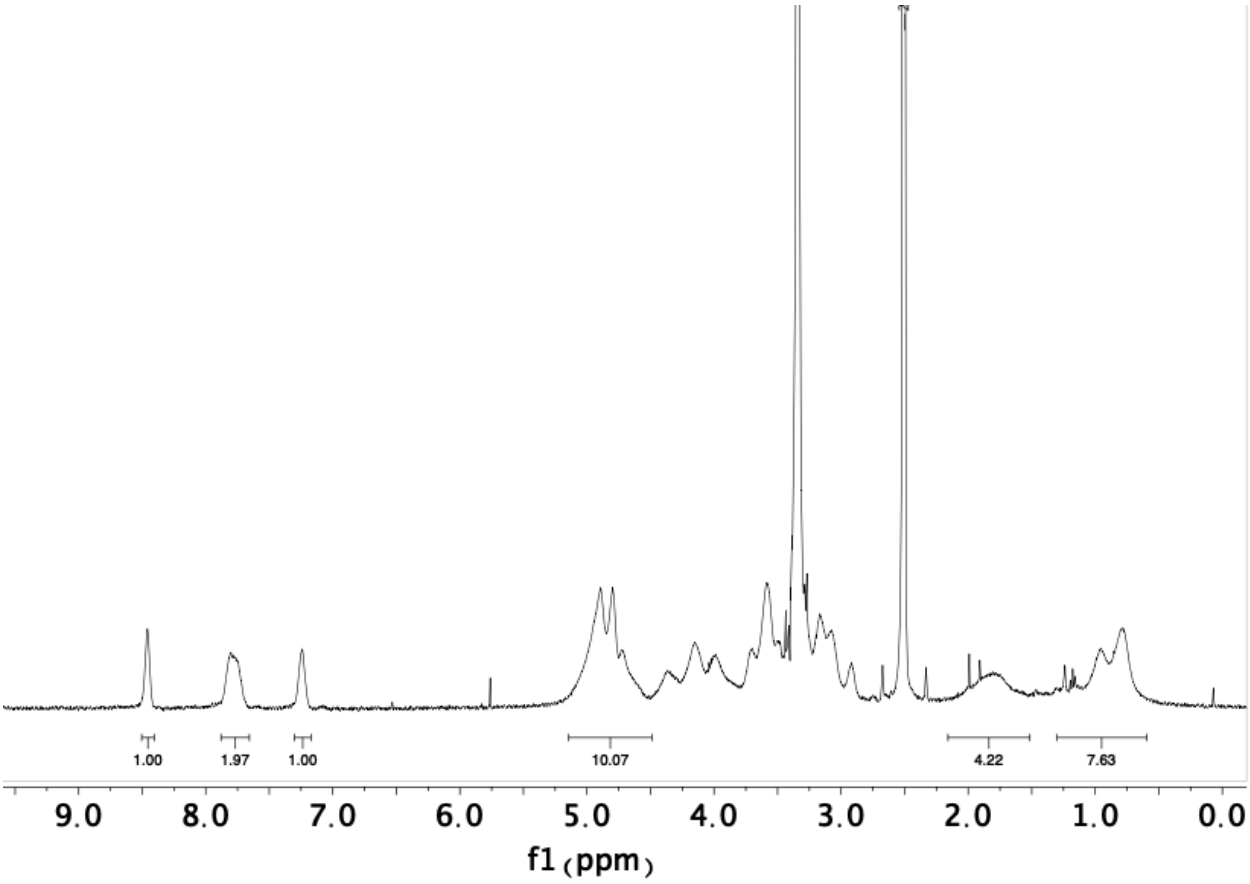

Figure 2.14. ^{1}H NMR spectrum of poly(PDSMA-*co*-TrMA (400 MHz in DMSO-d_6).

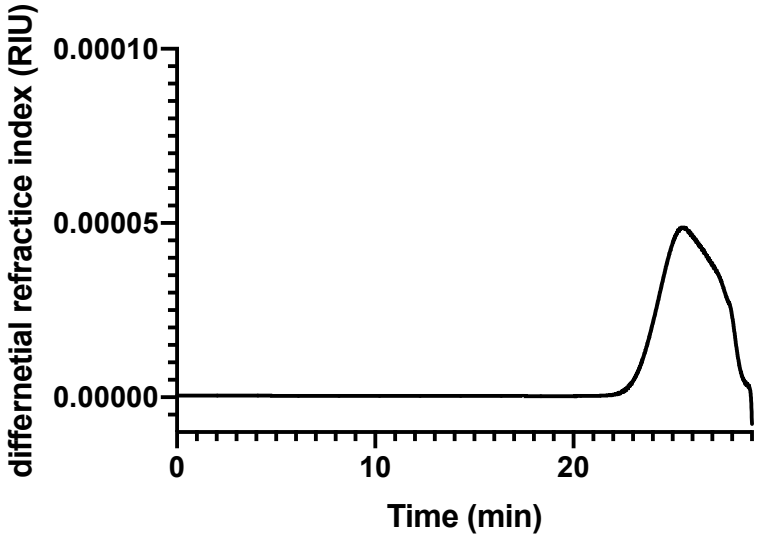

Figure 2.15. GPC of poly(PDSMA-*co*-TrMA) in DMF (M_n = 9820; Đ = 1.9).

Hour	% Consumption
0	0
0.2	52
1	65
2	73
3	82

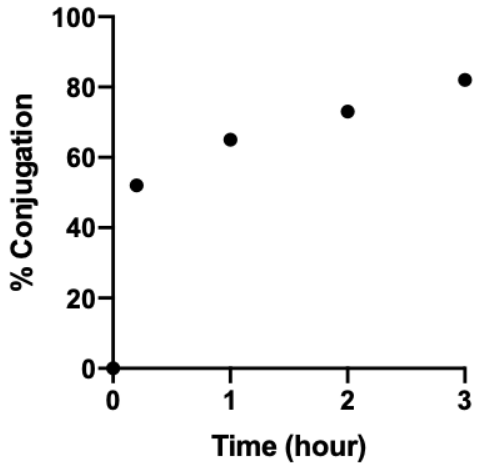

Figure 2.16. Glucagon-SH conjugation kinetics to poly(PDSMA-*co*-TrMA) was monitored via HPLC over 3 hours.

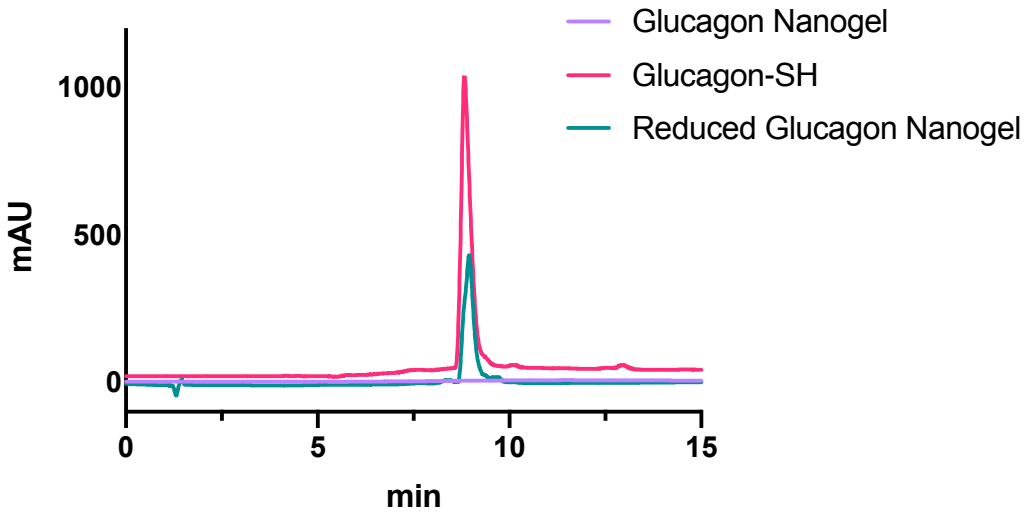

Figure 2.17. Representative HPLC traces of glucagon-SH conjugation and release from the glucagon nanogel.

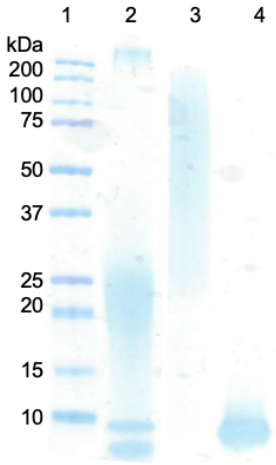

Figure 2.18. Representative SDS-PAGE of glucagon-SH conjugation and release from the glucagon nanogel. Lane 1: protein ladder; lane 2: crude glucagon nanogel; lane 3: purified glucagon nanogel; lane 4: glucagon nanogel from lane 3 reduced with TCEP (100 eq).

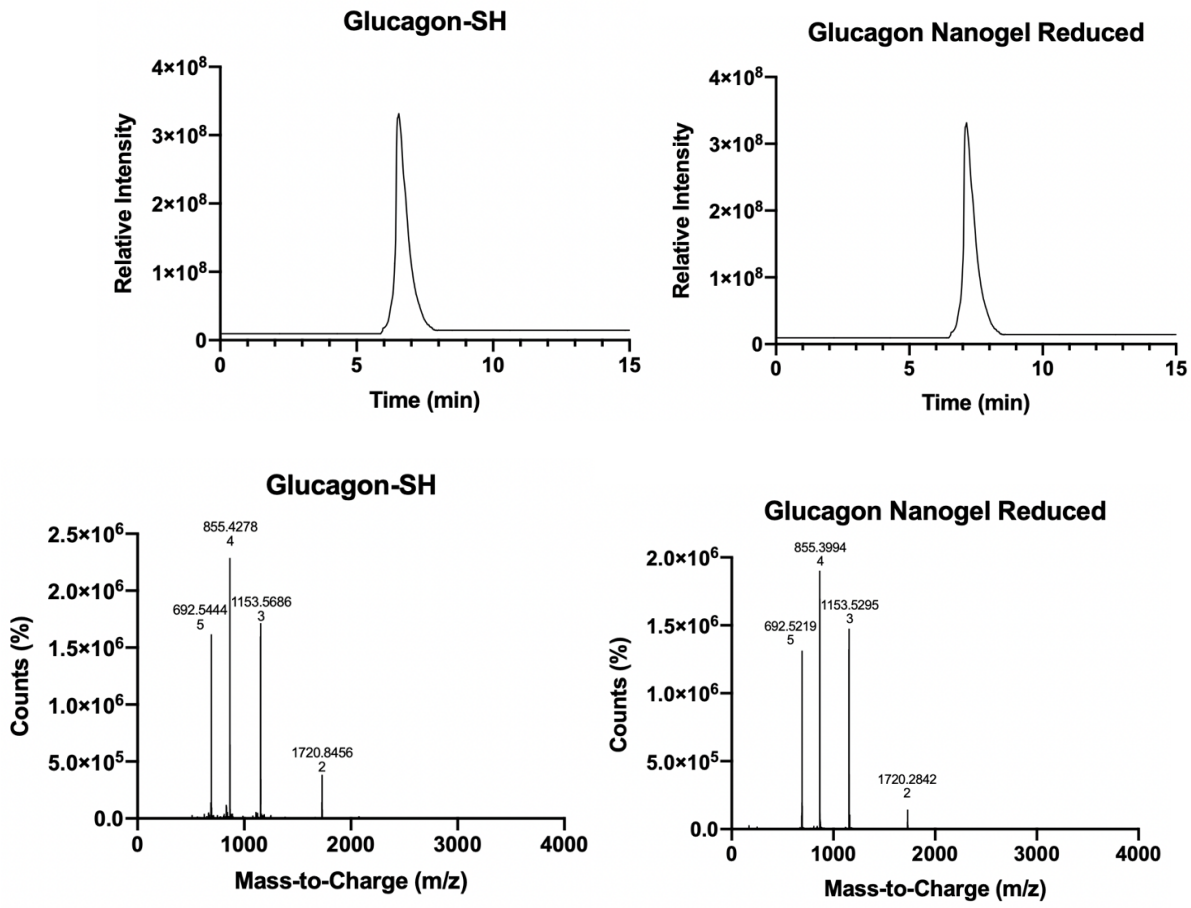

Figure 2.19. Representative LC-MS trace of glucagon-SH standard compared to reduced glucagon nanogels show no degradation in fresh glucagon-SH or immediately after reduction. Calculated m/z= 3460, observed m/z=3460, retention time= 6.3 minutes.

Crosslinking %	Empty Nanogel Z-average (d.nm)	Glucagon nanogel Z-average (d.nm)	Glucagon nanogel Z-average (d.nm), 24 hours 4°C	DLS results
10	7.2	1408	1374	poor
20	7.5	196.0	2981	poor
30	7.6	1333	2326	poor
40	7.8	649.2	973.4	**good**
50	8.6	643.3	660.9	**good**

Figure 2.20. Varying percentages of PEG_{2000} dithiol varied the glucagon nanogel size by DLS.

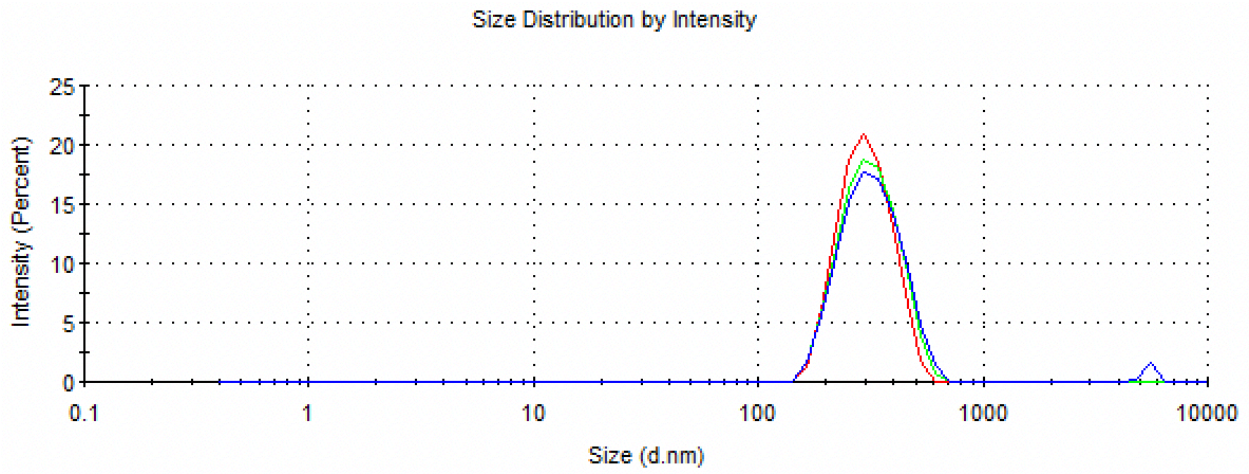

Figure 2.21. DLS of simultaneous crosslinking of PEG_{2000} dithiol and glucagon-SH PDI: 0.427 Z-average (d.nm): 360.0. with microdialysis purification.

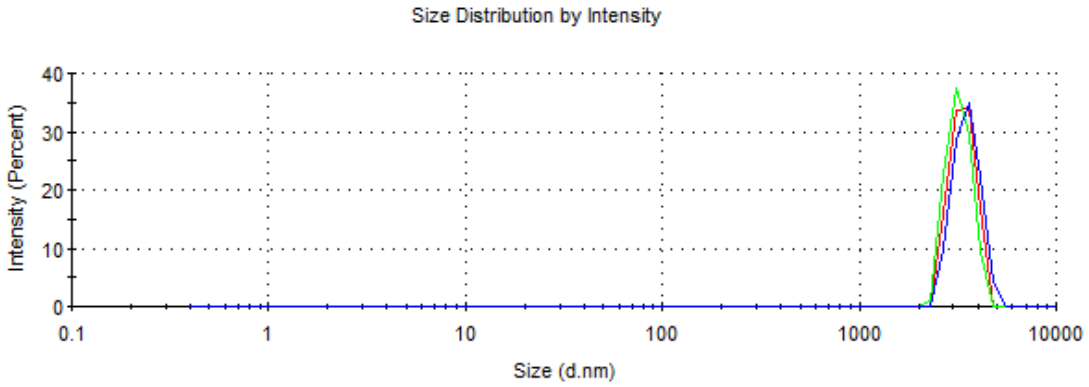

Figure 2.22. DLS of covalent attachment of glucagon-SH followed by crosslinking of PEG_{600} dithiol in 10 mM HCl, buffer exchanged to DPBS pH 7.4, purified by microdialysis. PDI: 0.02, Z-average (d.nm): 3189.

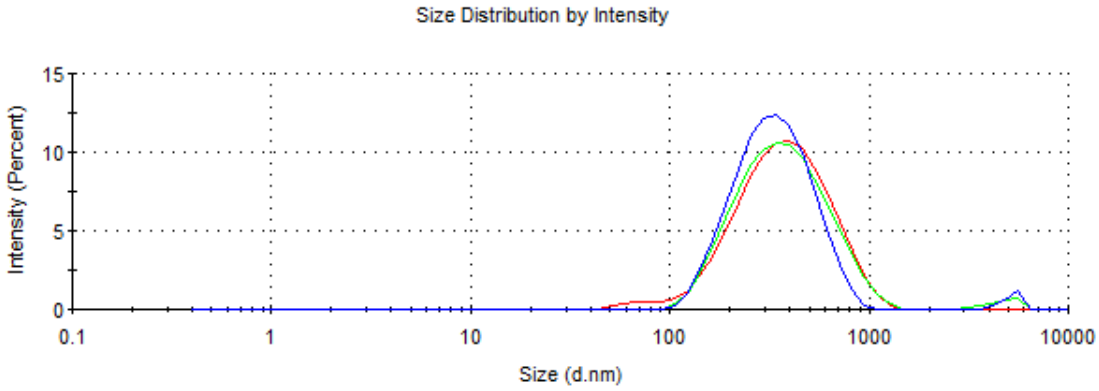

Figure 2.23. DLS of covalent attachment of glucagon-SH followed by crosslinking of PEG_{1000} dithiol in 10 mM HCl, buffer exchanged to DPBS pH 7.4 and purified by microdialysis. PDI: 0.23, Z-average (d.nm): 312.4.

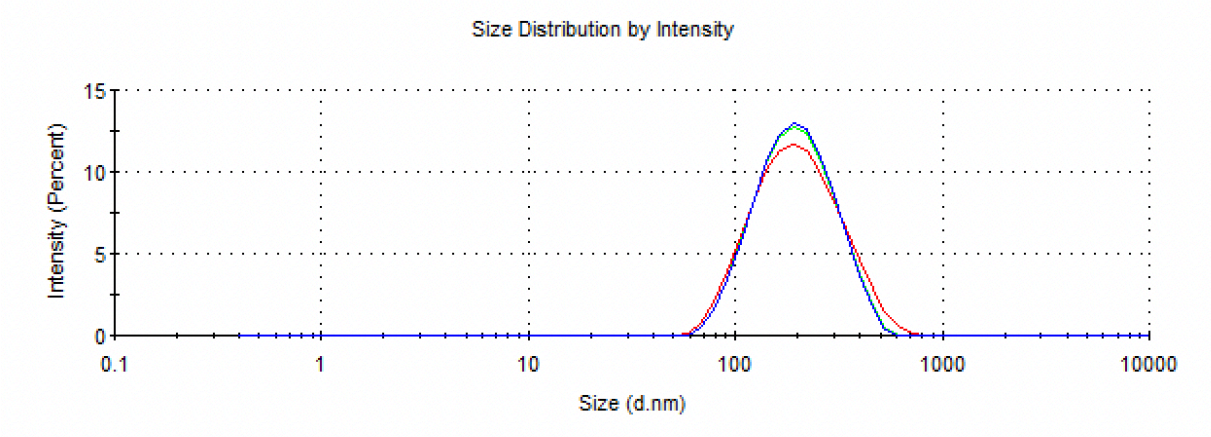

Figure 2.24. DLS of covalent attachment of glucagon-SH followed by crosslinking of PEG_{2000} dithiol in 10 mM HCl, buffer exchanged to DPBS pH 7.4 and purified by microdialysis. PDI: 0.18, Z-average (d.nm) 149.1.

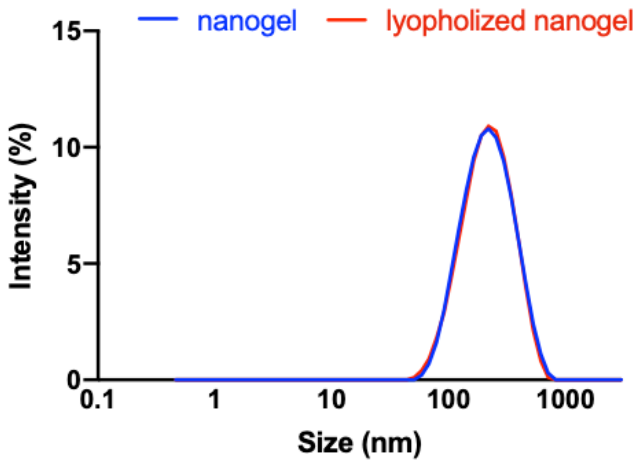

Figure 2.25. DLS of glucagon nanogels 1 mg/mL lyophilized versus in solution show comparable sizes of 149.1 nm (nanogel) and 155.2 nm (lyophilized nanogel).

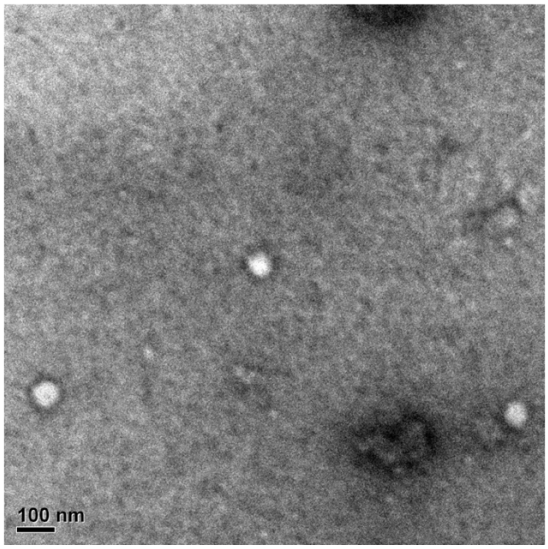

Figure 2.26. Transmission electron microscopy image of glucagon nanogels 1 mg/mL lyophilized.

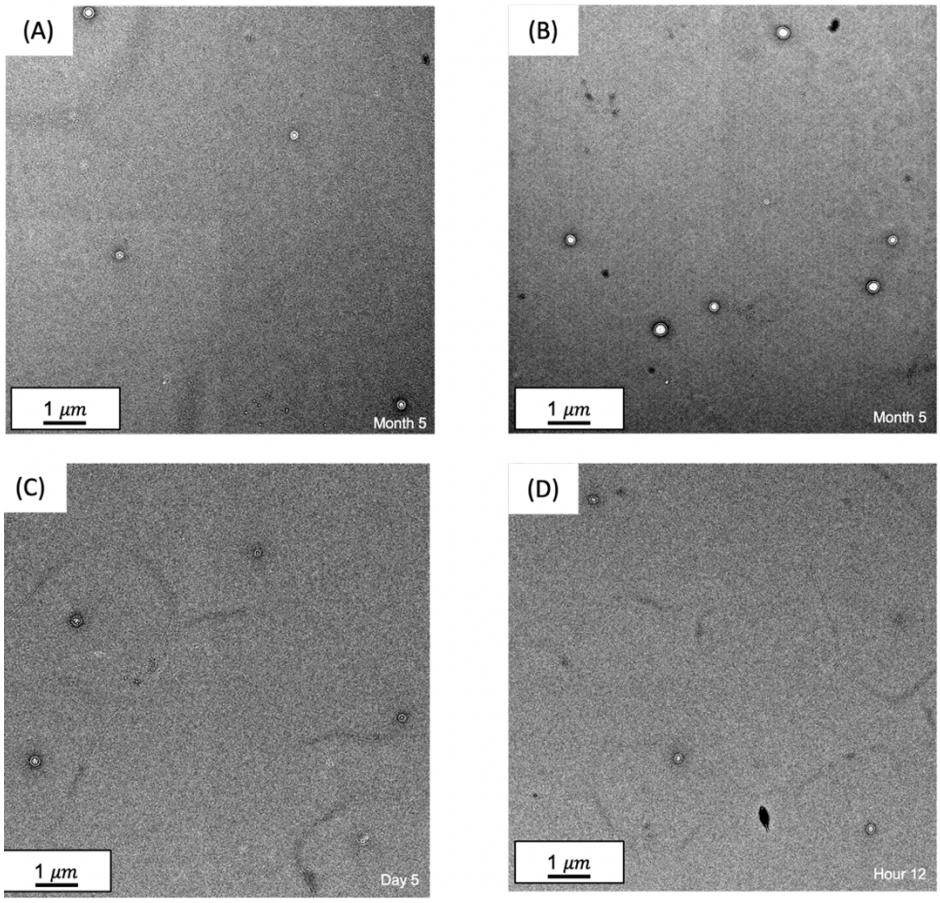

Figure 2.27. Zoomed out TEM of the glucagon nanogels at A) -20 ºC for 5 months, B) 4 ºC for 5 months, C) 25 ºC for 5 days, and D) 37 ºC for 12 hours.

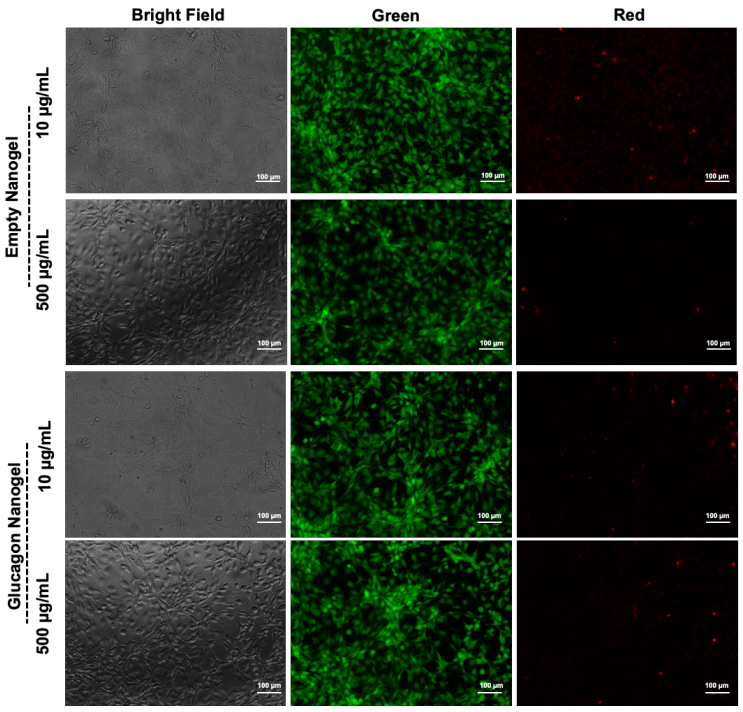

Figure 2.28. *In vitro* biocompatibility was evaluated after 24 hours in mouse embryonic fibroblasts, NIH3T3 by performing a live/dead assay using calcein AM and ethidium homodimer-1. The empty nanogel and glucagon nanogel are biocompatible at 500 µg/mL and 10 µg/mL.

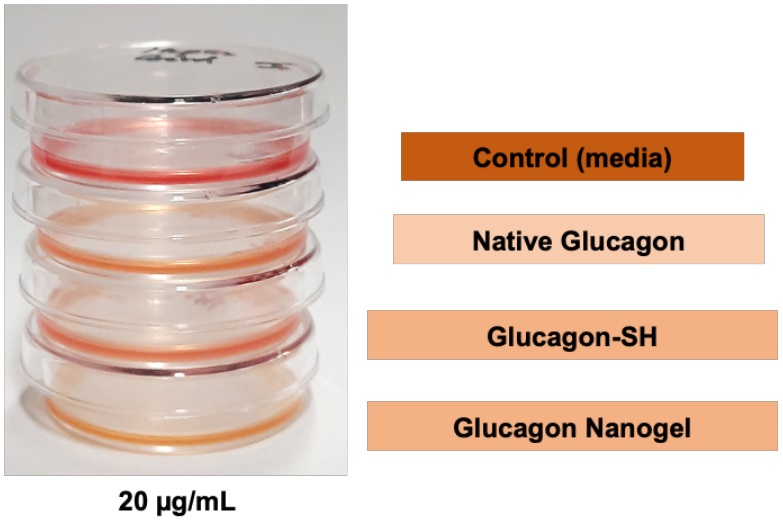

Figure 2.98. Metabolic activity was qualitatively evaluated after 24 hours in a liver cell model, HepG2 cells by visualizing a color change of golden yellow to phenol red of the control compared to the glucagon containing samples. 0.3×10^6 cells/well were counted using hemocytometer.

Glucagon-SH:

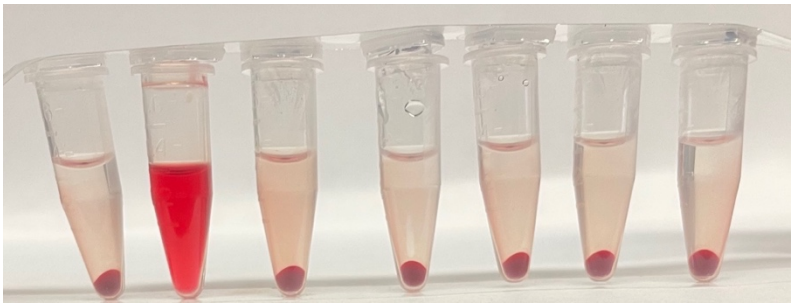

Glucagon Nanogel:

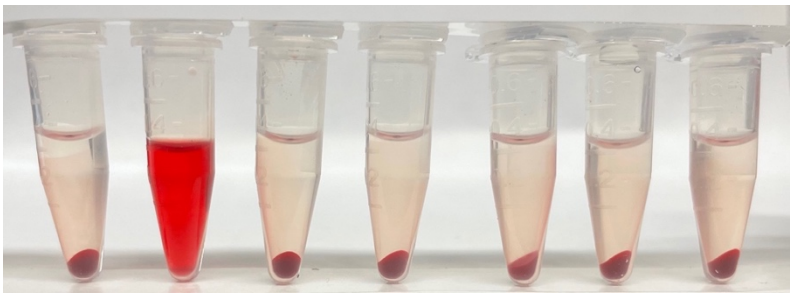

PEG_{2000} dithiol:

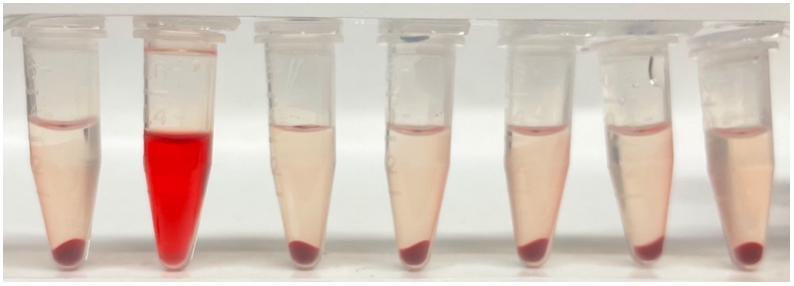

PDSMA-co-TrMA:

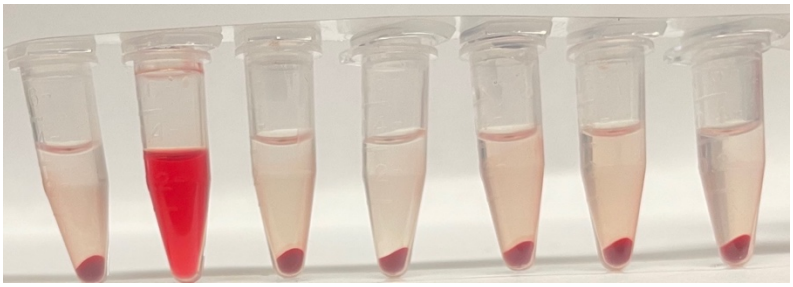

Figure 2.30. Qualitative hemolysis results left to right: DPBS, 20% Triton-X, 0 μM , 5 μM, 10 μM, 25 μM, 50 μM.

2.6 References

†This chapter, with copyright permission from RSC, contains a paper published as: **Puente, E. G**.; Sivasankaran, R.; Vinciguerra, D.; Yang, J.; Lower, H. C.; Hevener, A.; Maynard, H. Uniform Trehalose Nanogels for Glucagon Stabilization. *RSC Appl. Polym*. **2024,** 2, 473.

(1) CDC. *Low Blood Sugar (Hypoglycemia)*. Centers for Disease Control and Prevention. https://www.cdc.gov/diabetes/basics/low-blood-sugar.html (accessed 2023-03-06).

(2) CDC. *How to Treat Low Blood Sugar (Hypoglycemia)*. Centers for Disease Control and Prevention. https://www.cdc.gov/diabetes/basics/low-blood-sugar-treatment.html (accessed 2023-03-06).

(3) Morales, J.; Schneider, D. Hypoglycemia. *Am. J. Med.* **2014**, *127* (10, Supplement), S17–S24. https://doi.org/10.1016/j.amjmed.2014.07.004.

(4) *Glucagon & Other Emergency Glucose Products | ADA*. https://diabetes.org/healthy-living/medication-treatments/glucagon-other-emergency-glucose-products (accessed 2023-03-06).

(5) Mattedi, G.; Acosta-Gutiérrez, S.; Clark, T.; Gervasio, F. L. A Combined Activation Mechanism for the Glucagon Receptor. *Proc. Natl. Acad. Sci.* **2020**, *117* (27), 15414–15422. https://doi.org/10.1073/pnas.1921851117.

(6) Jelinek, L.; Lok, S.; Rosenberg, G.; Smith, R.; Grant, F.; Biggs, S.; Bensch, P.; Kuijper, J.; Sheppard, P.; Sprecher, C.; Et, Al. Expression Cloning and Signaling Properties of the Rat Glucagon Receptor. *Science* **1993**, *259* (5101), 1614–1616. https://doi.org/10.1126/science.8384375.

(7) Müller, T. D.; Finan, B.; Clemmensen, C.; DiMarchi, R. D.; Tschöp, M. H. The New Biology and Pharmacology of Glucagon. *Physiol. Rev.* **2017**, *97* (2), 721–766. https://doi.org/10.1152/physrev.00025.2016.

(8) Onoue, S.; Ohshima, K.; Debari, K.; Koh, K.; Shioda, S.; Iwasa, S.; Kashimoto, K.; Yajima, T. Mishandling of the Therapeutic Peptide Glucagon Generates Cytotoxic Amyloidogenic Fibrils. *Pharm. Res.* **2004**, *21* (7), 1274–1283. https://doi.org/10.1023/B:PHAM.0000033016.36825.2c.

(9) Caputo, N.; Castle, J. R.; Bergstrom, C. P.; Carroll, J. M.; Bakhtiani, P. A.; Jackson, M. A.; Roberts, C. T.; David, L. L.; Ward, W. K. Mechanisms of Glucagon Degradation at Alkaline pH. *Peptides* **2013**, *45*, 40–47. https://doi.org/10.1016/j.peptides.2013.04.005.

(10) Caputo, N.; Jackson, M. A.; Castle, J. R.; El Youssef, J.; Bakhtiani, P. A.; Bergstrom, C. P.; Carroll, J. M.; Breen, M. E.; Leonard, G. L.; David, L. L.; Roberts, C. T.; Ward, W. K. Biochemical Stabilization of Glucagon at Alkaline pH. *Diabetes Technol. Ther.* **2014**, *16* (11), 747–758. https://doi.org/10.1089/dia.2014.0047.

(11) *BAQSIMI® (glucagon) nasal powder | Severe Hypoglycemia Treatment*. https://www.baqsimi.com/ (accessed 2023-03-07).

(12) Singh-Franco, D.; Moreau, C.; Levin, A. D.; Rosa, D. D. L.; Johnson, M. Efficacy and Usability of Intranasal Glucagon for the Management of Hypoglycemia in Patients With Diabetes: A Systematic Review. *Clin. Ther.* **2020**, *42* (9), e177–e208. https://doi.org/10.1016/j.clinthera.2020.06.024.

(13) Suico, J. G.; Hövelmann, U.; Zhang, S.; Shen, T.; Bergman, B.; Sherr, J.; Zijlstra, E.; Frier, B. M.; Plum-Mörschel, L. Glucagon Administration by Nasal and Intramuscular Routes in Adults With Type 1 Diabetes During Insulin-Induced Hypoglycaemia: A Randomised,

Open-Label, Crossover Study. *Diabetes Ther.* **2020**, *11* (7), 1591–1603. https://doi.org/10.1007/s13300-020-00845-7.

(14) Christiansen, M. P.; Cummins, M.; Prestrelski, S.; Close, N. C.; Nguyen, A.; Junaidi, K. Comparison of a Ready-to-Use Liquid Glucagon Injection Administered by Autoinjector to Glucagon Emergency Kit for the Symptomatic Relief of Severe Hypoglycemia: Two Randomized Crossover Non-Inferiority Studies. *BMJ Open Diabetes Res. Care* **2021**, *9* (1), e002137. https://doi.org/10.1136/bmjdrc-2021-002137.

(15) *Gvoke™ (glucagon injection) | Patient Information*. GVOKE. https://gvokeglucagon.com (accessed 2023-03-07).

(16) *Dasiglucagon for BHAP systems*. Zealand pharma. https://www.zealandpharma.com/dasiglucagon-pump (accessed 2023-03-07).

(17) Bailey, N. C.; Dimsits, J.; Hammer, M.; Kendall, D. M.; Bailey, T. S. A Comparative Study of Dasiglucagon Ready-to-Use Autoinjector and Glucagon Emergency Kit During Rescue from Simulated Severe Hypoglycemia. *Diabetes Technol. Ther.* **2022**, *24* (4), 231–240. https://doi.org/10.1089/dia.2021.0367.

(18) Battelino, T.; Tehranchi, R.; Bailey, T.; Dovc, K.; Melgaard, A.; Stone, J. Y.; Woerner, S.; Von Dem Berg, T.; DiMeglio, L. A.; Kendall, D.; Danne, T. Dasiglucagon, a Ready-To-Use Glucagon Analog, For Rapid And Effective Treatment of Severe Hypoglycemia: A Phase 3, Randomized Controlled Trial in Children With Type 1 Diabetes. *Metabolism* **2021**, *116*, 154507. https://doi.org/10.1016/j.metabol.2020.154507.

(19) Stigsnaes, P.; Frokjaer, S.; Bjerregaard, S.; Van De Weert, M.; Kingshott, P.; Moeller, E. H. Characterisation and Physical Stability of PEGylated Glucagon. *Int. J. Pharm.* **2007**, *330* (1–2), 89–98. https://doi.org/10.1016/j.ijpharm.2006.09.002.

(20) Matilainen, L.; Larsen, K. L.; Wimmer, R.; Keski-Rahkonen, P.; Auriola, S.; Järvinen, T.; Jarho, P. The Effect of Cyclodextrins on Chemical and Physical Stability of Glucagon and Characterization of Glucagon/γ-CD Inclusion Complexes. *J. Pharm. Sci.* **2008**, *97* (7), 2720–2729. https://doi.org/10.1002/jps.21209.

(21) Crommelin, D. J. A.; Anchordoquy, T. J.; Volkin, D. B.; Jiskoot, W.; Mastrobattista, E. Addressing the Cold Reality of mRNA Vaccine Stability. *J. Pharm. Sci.* **2021**, *110* (3), 997–1001. https://doi.org/10.1016/j.xphs.2020.12.006.

(22) Chabenne, J. R.; DiMarchi, M. A.; Gelfanov, V. M.; DiMarchi, R. D. Optimization of the Native Glucagon Sequence for Medicinal Purposes. *J. Diabetes Sci. Technol.* **2010**, *4* (6), 1322–1331. https://doi.org/10.1177/193229681000400605.

(23) Joshi, A. B.; Rus, E.; Kirsch, L. E. The Degradation Pathways of Glucagon in Acidic Solutions. *Int. J. Pharm.* **2000**, *203* (1–2), 115–125. https://doi.org/10.1016/s0378-5173(00)00438-5.

(24) Ojha, T.; Hu, Q.; Colombo, C.; Wit, J.; van Geijn, M.; van Steenbergen, M. J.; Bagheri, M.; Königs-Werner, H.; Buhl, E. M.; Bansal, R.; Shi, Y.; Hennink, W. E.; Storm, G.; Rijcken, C. J. F.; Lammers, T. Lyophilization Stabilizes Clinical-Stage Core-Crosslinked Polymeric Micelles to Overcome Cold Chain Supply Challenges. *Biotechnol. J.* **2021**, *16* (6), 2000212. https://doi.org/10.1002/biot.202000212.

(25) Gelb, M. B.; Messina, K. M. M.; Vinciguerra, D.; Ko, J. H.; Collins, J.; Tamboline, M.; Xu, S.; Ibarrondo, F. J.; Maynard, H. D. Poly(Trehalose Methacrylate) as an Excipient for Insulin Stabilization: Mechanism and Safety. *ACS Appl. Mater. Interfaces* **2022**, *14* (33), 37410–37423. https://doi.org/10.1021/acsami.2c09301.

(26) Liu, M.; Zhao, P.; Uddin, M. H.; Li, W.; Lin, F.; Chandrashekar, C.; Nishiuchi, Y.; Kajihara, Y.; Forbes, B. E.; Wootten, D.; Wade, J. D.; Hossain, M. A. Chemical Synthesis and Characterization of a Nonfibrillating Glycoglucagon. *Bioconjug. Chem.* **2021**, *32* (10), 2148–2153. https://doi.org/10.1021/acs.bioconjchem.1c00419.

(27) Tolstyka, Z. P.; Phillips, H.; Cortez, M.; Wu, Y.; Ingle, N.; Bell, J. B.; Hackett, P. B.; Reineke, T. M. Trehalose-Based Block Copolycations Promote Polyplex Stabilization for Lyophilization and in Vivo pDNA Delivery. *ACS Biomater. Sci. Eng.* **2016**, *2* (1), 43–55. https://doi.org/10.1021/acsbiomaterials.5b00312.

(28) Jones, K. L.; Drane, D.; Gowans, E. J. Long-Term Storage of DNA-Free RNA for Use in Vaccine Studies. *BioTechniques* **2007**, *43* (5), 675–681. https://doi.org/10.2144/000112593.

(29) Boehnke, N.; Kammeyer, J. K.; Damoiseaux, R.; Maynard, H. D. Stabilization of Glucagon by Trehalose Glycopolymer Nanogels. *Adv. Funct. Mater.* **2018**, *28* (10), 1705475. https://doi.org/10.1002/adfm.201705475.

(30) Crilly, C. J.; Brom, J. A.; Kowalewski, M. E.; Piszkiewicz, S.; Pielak, G. J. Dried Protein Structure Revealed at the Residue Level by Liquid-Observed Vapor Exchange NMR. *Biochemistry* **2021**, *60* (2), 152–159. https://doi.org/10.1021/acs.biochem.0c00863.

(31) Colaço, C.; Sen, S.; Thangavelu, M.; Pinder, S.; Roser, B. Extraordinary Stability of Enzymes Dried in Trehalose: Simplified Molecular Biology. *Nat. Biotechnol.* **1992**, *10* (9), 1007–1011. https://doi.org/10.1038/nbt0992-1007.

(32) Olsson, C.; Jansson, H.; Swenson, J. The Role of Trehalose for the Stabilization of Proteins. *J. Phys. Chem. B* **2016**, *120* (20), 4723–4731. https://doi.org/10.1021/acs.jpcb.6b02517.

(33) Chang, L. (Lucy); Pikal, M. J. Mechanisms of Protein Stabilization in the Solid State. *J. Pharm. Sci.* **2009**, *98* (9), 2886–2908. https://doi.org/10.1002/jps.21825.

(34) Mensink, M. A.; Frijlink, H. W.; Van Der Voort Maarschalk, K.; Hinrichs, W. L. J. How Sugars Protect Proteins in the Solid State and during Drying (Review): Mechanisms of Stabilization in Relation to Stress Conditions. *Eur. J. Pharm. Biopharm.* **2017**, *114*, 288–295. https://doi.org/10.1016/j.ejpb.2017.01.024.

(35) Lerbret, A.; Affouard, F.; Hédoux, A.; Krenzlin, S.; Siepmann, J.; Bellissent-Funel, M.-C.; Descamps, M. How Strongly Does Trehalose Interact with Lysozyme in the Solid State? Insights from Molecular Dynamics Simulation and Inelastic Neutron Scattering. *J. Phys. Chem. B* **2012**, *116* (36), 11103–11116. https://doi.org/10.1021/jp3058096.

(36) Olsson, C.; Swenson, J. Structural Comparison between Sucrose and Trehalose in Aqueous Solution. *J. Phys. Chem. B* **2020**, *124* (15), 3074–3082. https://doi.org/10.1021/acs.jpcb.9b09701.

(37) Mancini, R. J.; Lee, J.; Maynard, H. D. Trehalose Glycopolymers for Stabilization of Protein Conjugates to Environmental Stressors. *J. Am. Chem. Soc.* **2012**, *134* (20), 8474–8479. https://doi.org/10.1021/ja2120234.

(38) Pelegri-O'Day, E. M.; Paluck, S. J.; Maynard, H. D. Substituted Polyesters by Thiol–Ene Modification: Rapid Diversification for Therapeutic Protein Stabilization. *J. Am. Chem. Soc.* **2017**, *139* (3), 1145–1154. https://doi.org/10.1021/jacs.6b10776.

(39) Pradhan, N.; Shekhar, S.; Jana, N. R.; Jana, N. R. Sugar-Terminated Nanoparticle Chaperones Are 102–105 Times Better Than Molecular Sugars in Inhibiting Protein Aggregation and Reducing Amyloidogenic Cytotoxicity. *ACS Appl. Mater. Interfaces* **2017**, *9* (12), 10554–10566. https://doi.org/10.1021/acsami.7b01886.

(40) Diaz-Dussan, D.; Peng, Y.-Y.; Sengupta, J.; Zabludowski, R.; Adam, M. K.; Acker, J. P.; Ben, R. N.; Kumar, P.; Narain, R. Trehalose-Based Polyethers for Cryopreservation and

Three-Dimensional Cell Scaffolds. *Biomacromolecules* **2020**, *21* (3), 1264–1273. https://doi.org/10.1021/acs.biomac.0c00018.

(41) Debnath, K.; Sarkar, A. K.; Jana, N. R.; Jana, N. R. Inhibiting Protein Aggregation by Small Molecule-Based Colloidal Nanoparticles. *Acc. Mater. Res.* **2022**, *3* (1), 54–66. https://doi.org/10.1021/accountsmr.1c00193.

(42) Panescu, P. H.; Ko, J. H.; Maynard, H. D. Scalable Trehalose-Functionalized Hydrogel Synthesis for High-Temperature Protection of Enzymes. *Macromol. Mater. Eng.* **2019**, *304* (6), 1800782. https://doi.org/10.1002/mame.201800782.

(43) *Nanoparticle Uniformity*. News-Medical.net. https://www.news-medical.net/life-sciences/Nanoparticle-Uniformity.aspx (accessed 2023-03-07).

(44) Chabenne, J.; Chabenne, M. D.; Zhao, Y.; Levy, J.; Smiley, D.; Gelfanov, V.; DiMarchi, R. A Glucagon Analog Chemically Stabilized for Immediate Treatment of Life-Threatening Hypoglycemia. *Mol. Metab.* **2014**, *3* (3), 293–300. https://doi.org/10.1016/j.molmet.2014.01.006.

(45) Zhang, H.; Qiao, A.; Yang, L.; Van Eps, N.; Frederiksen, K. S.; Yang, D.; Dai, A.; Cai, X.; Zhang, H.; Yi, C.; Cao, C.; He, L.; Yang, H.; Lau, J.; Ernst, O. P.; Hanson, M. A.; Stevens, R. C.; Wang, M.-W.; Reedtz-Runge, S.; Jiang, H.; Zhao, Q.; Wu, B. Structure of the Glucagon Receptor in Complex with a Glucagon Analogue. *Nature* **2018**, *553* (7686), 106–110. https://doi.org/10.1038/nature25153.

(46) Kulkarni, S. A.; Feng, S.-S. Effects of Particle Size and Surface Modification on Cellular Uptake and Biodistribution of Polymeric Nanoparticles for Drug Delivery. *Pharm. Res.* **2013**, *30* (10), 2512–2522. https://doi.org/10.1007/s11095-012-0958-3.

(47) Banik, B. L.; Fattahi, P.; Brown, J. L. Polymeric Nanoparticles: The Future of Nanomedicine. *WIREs Nanomedicine Nanobiotechnology* **2016**, *8* (2), 271–299. https://doi.org/10.1002/wnan.1364.

(48) Poon, W.; Zhang, Y.-N.; Ouyang, B.; Kingston, B. R.; Wu, J. L. Y.; Wilhelm, S.; Chan, W. C. W. Elimination Pathways of Nanoparticles. *ACS Nano* **2019**, *13* (5), 5785–5798. https://doi.org/10.1021/acsnano.9b01383.

(49) Abdelwahed, W.; Degobert, G.; Stainmesse, S.; Fessi, H. Freeze-Drying of Nanoparticles: Formulation, Process and Storage Considerations. *Adv. Drug Deliv. Rev.* **2006**, *58* (15), 1688–1713. https://doi.org/10.1016/j.addr.2006.09.017.

(50) Talsma, H.; Cherng, J.; Lehrmann, H.; Kursa, M.; Ogris, M.; Hennink, W. E.; Cotten, M.; Wagner, E. Stabilization of Gene Delivery Systems by Freeze-Drying. *Int. J. Pharm.* **1997**, *157* (2), 233–238. https://doi.org/10.1016/s0378-5173(97)00244-5.

(51) Souza, T. G. F.; Ciminelli, V. S. T.; Mohallem, N. D. S. A Comparison of TEM and DLS Methods to Characterize Size Distribution of Ceramic Nanoparticles. *J. Phys. Conf. Ser.* **2016**, *733* (1), 012039. https://doi.org/10.1088/1742-6596/733/1/012039.

(52) Kwon, I. K.; Matsuda, T. Co-Electrospun Nanofiber Fabrics of Poly(l-Lactide-Co-ε-Caprolactone) with Type I Collagen or Heparin. *Biomacromolecules* **2005**, *6* (4), 2096–2105. https://doi.org/10.1021/bm050086u.

(53) Yu, W.; Liu, R.; Zhou, Y.; Gao, H. Size-Tunable Strategies for a Tumor Targeted Drug Delivery System. *ACS Cent. Sci.* **2020**, *6* (2), 100–116. https://doi.org/10.1021/acscentsci.9b01139.

(54) Pang, L.; Pei, Y.; Uzunalli, G.; Hyun, H.; Lyle, L. T.; Yeo, Y. Surface Modification of Polymeric Nanoparticles with M2pep Peptide for Drug Delivery to Tumor-Associated Macrophages. *Pharm. Res.* **2019**, *36* (4), 65. https://doi.org/10.1007/s11095-019-2596-5.

(55) Srinivasachari, S.; Liu, Y.; Zhang, G.; Prevette, L.; Reineke, T. M. Trehalose Click Polymers Inhibit Nanoparticle Aggregation and Promote pDNA Delivery in Serum. *J. Am. Chem. Soc.* **2006**, *128* (25), 8176–8184. https://doi.org/10.1021/ja0585580.

(56) Gelenter, M. D.; Smith, K. J.; Liao, S.-Y.; Mandala, V. S.; Dregni, A. J.; Lamm, M. S.; Tian, Y.; Xu, W.; Pochan, D. J.; Tucker, T. J.; Su, Y.; Hong, M. The Peptide Hormone Glucagon Forms Amyloid Fibrils with Two Coexisting β-Strand Conformations. *Nat. Struct. Mol. Biol.* **2019**, *26* (7), 592–598. https://doi.org/10.1038/s41594-019-0238-6.

(57) Hackl, E. V.; Darkwah, J.; Smith, G.; Ermolina, I. Effect of Acidic and Basic pH on Thioflavin T Absorbance and Fluorescence. *Eur. Biophys. J.* **2015**, *44* (4), 249–261. https://doi.org/10.1007/s00249-015-1019-8.

(58) How, S.-C.; Lin, T.-H.; Chang, C.-C.; Wang, S. S.-S. Examining the Effect of Bovine Serum Albumin on the Properties and Drug Release Behavior of β-Lactoglobulin-Derived Amyloid Fibril-Based Hydrogels. *Int. J. Biol. Macromol.* **2021**, *184*, 79–91. https://doi.org/10.1016/j.ijbiomac.2021.06.003.

(59) Ekkelenkamp, A. E.; Jansman, M. M. T.; Roelofs, K.; Engbersen, J. F. J.; Paulusse, J. M. J. Surfactant-Free Preparation of Highly Stable Zwitterionic Poly(Amido Amine) Nanogels with Minimal Cytotoxicity. *Acta Biomater.* **2016**, *30*, 126–134. https://doi.org/10.1016/j.actbio.2015.10.037.

(60) Moore, T. L.; Rodriguez-Lorenzo, L.; Hirsch, V.; Balog, S.; Urban, D.; Jud, C.; Rothen-Rutishauser, B.; Lattuada, M.; Petri-Fink, A. Nanoparticle Colloidal Stability in Cell Culture

Media and Impact on Cellular Interactions. *Chem. Soc. Rev.* **2015**, *44* (17), 6287–6305. https://doi.org/10.1039/C4CS00487F.

(61) Shire, S. J. Formulation and Manufacturability of Biologics. *Curr. Opin. Biotechnol.* **2009**, *20* (6), 708–714. https://doi.org/10.1016/j.copbio.2009.10.006.

(62) Shire, S. J.; Shahrokh, Z.; Liu, J. Challenges in the Development of High Protein Concentration Formulations. *J. Pharm. Sci.* **2004**, *93* (6), 1390–1402. https://doi.org/10.1002/jps.20079.

(63) Berteau, C.; Filipe-Santos, O.; Wang, T.; Rojas, H. E.; Granger, C.; Schwarzenbach, F. Evaluation of the Impact of Viscosity, Injection Volume, and Injection Flow Rate on Subcutaneous Injection Tolerance. *Med. Devices Auckl. NZ* **2015**, *8*, 473–484. https://doi.org/10.2147/MDER.S91019.

(64) Ghosh, S.; Basu, S.; Thayumanavan, S. Simultaneous and Reversible Functionalization of Copolymers for Biological Applications. *Macromolecules* **2006**, *39* (17), 5595–5597. https://doi.org/10.1021/ma061420x.

(65) Evans, B. C.; Nelson, C. E.; Yu, S. S.; Beavers, K. R.; Kim, A. J.; Li, H.; Nelson, H. M.; Giorgio, T. D.; Duvall, C. L. Ex Vivo Red Blood Cell Hemolysis Assay for the Evaluation of pH-Responsive Endosomolytic Agents for Cytosolic Delivery of Biomacromolecular Drugs. *J. Vis. Exp.* **2013**, No. 73, 50166. https://doi.org/10.3791/50166.

Chapter 3

Comparison of Protein Homo Dimerization with PEG Linkers *via* Cysteine Bioconjugation

3.1 Introduction

Protein dimerization and oligomerization is a widespread phenomenon in biology, providing crucial improvements in stability compared to monomer , regulation of activity, and increased complexity.[1–3] Homodimers of therapeutic proteins are used to treat diseases such as diabetes, cancer, and SARS-CoV-2, demonstrating the demand for the development of novel, multivalent therapeutic biologics.[4–8] However, some of these dimers which are assembled *via* disulfide bonds, can assemble and disassemble in an uncontrolled manner, leading to undefined and unpredictable function and toxicity.[3,9,10] Techniques to synthesize stable protein homodimers would improve the understanding and applicability of these potential therapeutics. Notably, conjugation of polymers to proteins can stabilize, increase circulation time, and reduce immunogenicity.[11,12] Specifically, attachment of poly(ethylene) glycol or (PEGylation), is the only FDA approved polymer for conjugation to therapeutic proteins.[12–14] Currently, over 30 PEGylated biologics have been approved with a range of polymer sizes and conjugation linkages, offering versatility in its application.[15] Thus, utilizing PEG as the dimerization linker *via* stable thiol-ether bonds can afford additional favorable properties.

Bioconjugation to cysteines residues is a widely employed strategy due to their relatively low abundance and high nucleophilicity compared to other amino acids.[16,17] Cysteine bioconjugation techniques commonly include thiol-reactive groups such as maleimides, pyridyl disulfides, and vinyl sulfones. Although these conjugation chemistries are essential to the field, disulfide and maleimide Michael addition products can be labile *in vivo*. This can be a negative if undesired.[18] Cysteine S-arylation is a promising bioconjugation technique due to the potentially more stable S-C(sp^2) bond *in vivo*.[19,20] The Spokoyny and Maynard groups have developed

organometallic oxidative addition complexes (OACs) to perform S-arylation of biomolecules with various polymers and polymer sizes.[21–26,20]

Exploiting the rapid kinetics, facile synthesis, and versatility of Au OACs to prepare homodimers of proteins linked by polymers is a promising approach that has yet to be explored. Protein activity is dependent on proper protein conformation and stability; however, changes in pH can alter these properties, posing a challenge when synthesizing dimers *in vitro*.[27–30] Thus, the pH employed for protein dimerization should be considered when preparing these biologics. In addition, a major challenge with protein-polymer-protein formation is low conversion. For example, the model protein, T4 lysozyme (T4L) (V131C), containing a single surface exposed cysteine, has been previously used to prepare protein homodimers with a bifunctional maleimide poly(N-isopropylacrylamide) in only 21% yield after 16 h at 4 ºC using maleimide addition.[31,32]

In this work, dimerization of a model protein utilizing Au(III) OACs was investigated at various pHs and compared to commonly used Michael acceptors. Specifically, the protein homo-dimerization conversion of T4L with bifunctional dicyclohexylphosphine (PCy_2) P,N ligated PEG_{2000} Au(III) OAC and di-1-adamantylphophine (PAd_2) P,N ligated PEG_{2000} OAC was investigated. The conversions of T4L PEG_{2000} dimers with the Au (III) reagents at pH 6.0, 7.5 and 9.0 were directly compared to conversion to dimerization with a bifunctional maleimide PEG_{2000} and bifunctional vinyl sulfone PEG_{2000}. Additionally, the stabilities of the resulting S-arylated T4L PEG_{2000} dimers were assessed for comparison to known values reported in literature for small molecule substrates.

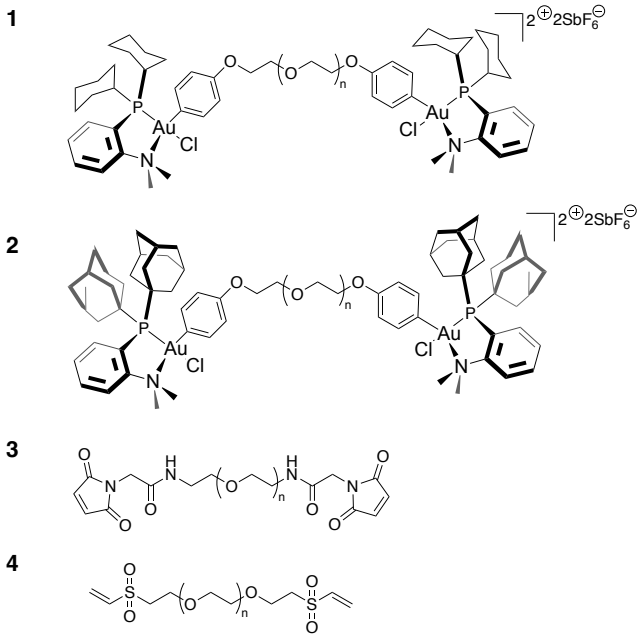

Figure 3.1 Telechelic cysteine-reactive PEG_{2000} reagents explored in this study.

3.2 Results and Discussion

3.2.1 Synthesis of homo-bifunctional PEG_{2000} reagents.

Homo-bifunctional PEG_{2000} linkers capped by dicyclohexylphosphine (PCy_2) P,N ligated Au (III) or di-1-adamantylphophine (PAd_2) P,N ligated Au (III) (**Figure 3.1**, **1** and **2** respectively) were prepared from the respective bis-*para*-iodobenzene end-functionalized polymers (see SI for details).[23] PEG reagents for the cysteine bioconjugation of protein dimers with PEG reagents are well known and some are commercially available;[32–37] thus comparison to the commonly used Michael acceptors was undertaken. To that end, bismaleimide PEG_{2000} (**3**) was purchased from JenKem USA and divinyl sulfonate PEG_{2000} (**4**) was synthesized as previously reported.[38] Although the kinetic rates of Au (III) $(PAd)_2$ and $(PCy)_2$ have been well studied with small molecules and peptides, the direct comparison between these reagents and more common cysteine bioconjugation polymer reagents has not been reported.[21]

3.2.2 Bioconjugation Screening.

We have previously shown that our Au (III) $(PAd)_2$ complex reaches full conversion with glutathione (GSH) or a small molecule respectively at pH 0.5-14.0 and with the model protein, DARPin at pH 5.5 within 1 minute.[23,24] Thus, we anticipated that conjugation in various pHs would be effective, despite the steric hinderance encountered by bringing together three macromolecules. Specifically, conjugations in pHs 6.0, 7.5 and 9.0 were undertaken and the samples run on SDS PAGE to quantify dimer formation by ImageJ analysis.

First, T4L controls in Tris buffer pH 6.0, pH 7.5 and pH 9.0 were prepared and incubated at 37 °C for 18 h. No change in band intensity was observed relative to each other in these conditions (**Figure 3.11**). Therefore, for all future experiments, the T4L control was run at pH 7.5. Initially, reactions using 0.5 eq of PEG linkers **1-4**, respectively, to 1 eq T4L, at 25 °C for 12 h were undertaken (**Figure 3.12**). For **4**, 6 % of T4L was converted to dimer in pH 9.0 and 0% at pH 6.0 and pH 7.5. Dimerization with **3** showed similar conversions at all three pHs, ranging 35% to 43%. While **1** and **2** showed the highest conversion to dimer at pH 6.0, of 71 % and 54 % respectively, with the next highest at pH 7.5 of 54% and 44%, and the lowest conversion (34% and 6%) to dimer at pH 9.0 for **1** and **2**, respectively. The results clearly demonstrate that the PEG with the kinetically faster Au(III) cyclohexane complex had the highest yields of all the samples, and higher than the slower Me-DalPhos Au(III) complex and faster than the Michael acceptors (**Table 3.3**). Specifically, our conversions were much higher with both **1** and **2** compared to our previously reported T4L dimers with bis-tetrazine pNIPAAm and bis-tetrazine-PEG, yielding 38

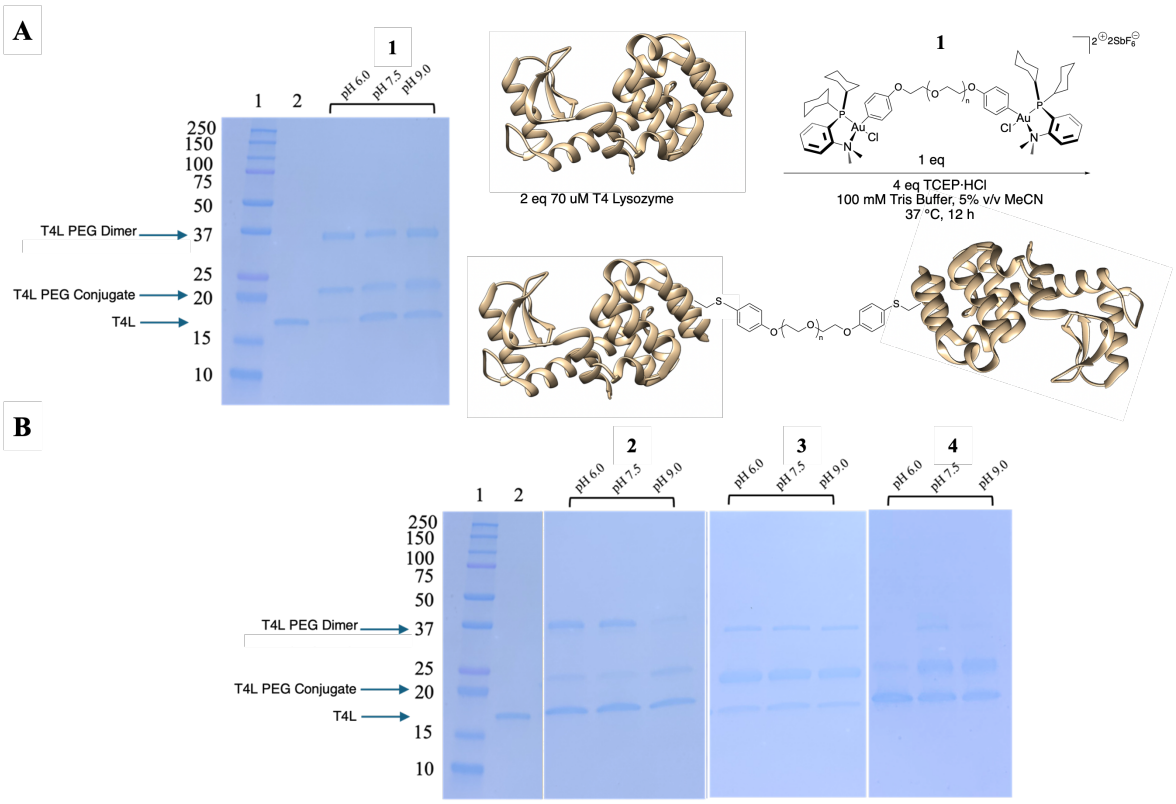

Figure 3.2 A) T4L PEG dimerization scheme and SDS-PAGE after 12 h at 37 ºC. Lane 1: ladder, Lane 2: T4L control, T4L with **1** at pH 6.0, 7.5 and 9.0 converted to 73%, 54%, and 36% respectively. % Conversion calculated with ImageJ. B) SDS-PAGE after 12 h at 37 ºC. Lane 1: ladder, Lane 2: T4L control, T4L with either **2, 3, or 4** at pH 6.0, 7.5 and 9.0.for 12 h. Percent Conversion calculated by Image J with n= 2 and the range is listed.

% and 37% respectively.[32] However, the results are not directly comparable since the polymer is different, which can affect the conjugation percentage. The pH dependance for the Au(III) OACs was unexpected because our work with small molecules clearly showed no dependence on conversion.[24] We hypothesized the Au (III) reagents are slower at the higher pH due to negatively charged amino acid residues or neutral amine residues on the proteins coordinating to the Au (III), either reacting with the end group or slowing down the process. To test this, we subjected the T4L dimers prepared with **1**, with citric acid or glutamic acid, however no significant difference in conversion was observed (**Figure 3.13**). Regardless, the results clearly show that **1** gave superior

Table 3.1 T4L-PEG-T4L dimer conversions with 0.5 equivalents of PEG reagent at 37 ºC for 12 h. Percent Conversion calculated by Image J with n= 2 and the range is listed.

PEG_{2000} Reagent	**% Conversion pH 6.0**	**% Conversion pH 7.5**	**% Conversion pH 9.0**
1	72-75	53-57	50-56
2	55-57	45-48	4-6
3	35-38	47-49	39-43
4	0	5-7	3-5

dimerization yields of 73% compared that with tetrazine click ligation, but without the need for incorporation of an artificial amino acid.

In a recent study, T4L linear and cyclic PEG_{2000} conjugates were prepared using the Au (III) $(Ad)_2$ reagent, reaching full conversion in 18 h at 37 °C.[22] Therefore to increase the yield further, the temperature was increased to 37 °C using 0.5 eq PEG linker to 1 eq T4L (**Figure 3.2**). Dimerization conversion slightly increased for **3** and **4;** more dimer conjugate was formed at pH 9.0 and 7.5 with **4** and at all pHs with **3**. However, only a slight increase was observed at 37 °C with **1** or **2**. Dimerization percent conversion for all reagents with 0.5 eq at 37 °C are summarized in **Table 3.1**.Even though we obtained higher yields were obtained at this higher temperature, we also observed that with **1** and **2** at 18 hours at 37 °C, higher molecular weight bands appeared (**Figure 3.14**). Similar types of higher molecular weight bands were seen previously with T4L using a trans- cylcooctene polymer reagent.[32] The origin of these bands is unknown, but suggest a multimerization product.

In summary, the highest conversion to T4L PEG dimers is observed with **1** at pH 6.0, 7.5 and 9.0 compared to the other reagents at the same pH. The best conversion for **1** was at a slightly acidic pH of 6. Also, a 12 h conjugation time was better than 18 h, since the latter gave higher molecular weight bands in the SDS PAGE gel, suggesting multimerization. It should be noted that a low conversion was observed at pH 9 for reagent **2**. Since this contrasts what was observed for

small molecules in organic solvents, it does suggest that the Me-DalPhos Au (III) reactivity is negatively affected by the presence of the T4L. Yet at neutral pH 2 was the same as maleimide with regard to conversion. Vinyl sulfone end functionalized PEG performed poorly in the dimerization reaction at all pHs tested.

3.2.3 Stability of S-arylated T4L-PEG-T4L dimers.

Stability of the S-Ar bond has been studied for small molecules, but not for polymers.[39] To study the stability of the polymer, the S-arylated T4L PEG_{2000} dimers, we subjected them to either acidic, basic, or oxidative reagents under the same condtions as the small molcules. After 2 days at 25 ºC then 4 days at 37 ºC, the T4L PEG_{2000} dimers were anlayzed by LC-MS comparing the area under the curve to the initial, unperturbed dimer (**Table 3.2**). In the presence of both acid and base, there was approximately a 25 % decrease in dimer while in the presence of oxidative condtions, a 10% decrease was observed. These results were comparable to the small molecule conjugates, demonstrating that the polymer or protein does not have an appreciable effect on stability.

Table 3.2 Stability of S-aryl T4L PEG_{2000} dimers.

Conditions	**Acid**	**Base**	**Oxidation**
% T4L-PEG-T4L	72.9%	74.2%	91.1%

3.3 Conclusion

In conclusion, pH, temperature, and time, were screened to gain an understanding of the homodimer conversion of T4L with cysteine bioconjugation using bifunctional vinyl sulfone, maleimide, Au (III) $(PAd)_2$, and Au (III) $(PCy)_2$ PEG_{2000} reagents. The Au (III) $(PCy)_2$ PEG_{2000} reagent resulted in the highest conversions at pH 6.0, 7.5, and 9.0 compared to other polymers. The S-arylated T4L PEG_{2000} dimers were comparable to reported stabilities for small molecule-

peptide conjugates under acidic, basic, and oxidative conditions. These results show that Me-DalPhos Au (III) bis functionalized PEG is promising for protein dimerization.

3.4 Experimental

3.4.1 Materials

Unless otherwise noted, all materials were of analytical grade and purchased and used as received from Fisher Scientific, Acros Organics, Oakwood Chemicals or Sigma Aldrich. The silver hexafluoroantimonate ($AgSbF_6$) was stored in the glovebox under an atmosphere of N_2 and removed prior to use. Milli-Q water was used for all experiments. Fisher Water Optima™ LC-MS Grade and Fisher Acetonitrile Optima™ LC-MS Grade were used exclusively for LC-MS mobile phase solvents. Protein was expressed and purified from the plasmid pET29c(+)hFGF-2, which was kindly provided by Professor Thomas Scheper from the Helmholtz Centre for Infection Research (Braunschweig, Germany) according to Chen et al.[31]

3.4.2 Analytical Techniques

NMR spectra were recorded on AV 400 Bruker spectrometers at 400 MHz (^1H) and 121 MHz ($^{31}P\{^1H\}$). Spectra are reported in δ (parts per million) relative to residual proteo-solvent signals for ^1H and H_3PO_4 (δ 0.00 ppm) for $^{31}P\{^1H\}$. Deuterated solvents (Cambridge Isotope Laboratories) were used for all NMR experiments. ^1H NMR spectra for all polymers, spectra were acquired with a relaxation delay of 4 seconds. Data was analyzed using MestRenova v12 software. A Biotage Isolera Prime equipped with KP-SNAP Ultra Biotage columns was used for all flash column chromatography.

Protein and protein conjugates were purified by FPLC on a Bio-Rad BioLogic DuoFlow chromatography system. All purifications were carried out at 4 °C. All buffers were freshly prepared and filtered over a Thermo Scientific Nalgene 565-0020 Filter Unit, 0.2um PES prior to

use. Size exclusion chromatography (SEC) purifications were performed using a Superdex 75 Increase 10/300 GL column. All protein purifications were monitored at wavelengths of 254 nm and 280 nm. A standard isocratic method was used for all sampled (20 mM Tris, 150 mM NaCl buffer, pH 7.5 over 50 minutes). Protein concentration measurements were determined on a NanoDrop 2000 UV-Vis spectrophotometer at 280 nm (Extinction coefficient = 16,055 M^{-1} cm^{-1}).

Sodium dodecyl sulfate-polyacrylamide gel electrophoresis (SDS-PAGE) was carried out in a Mini-PROTEAN Tetra Cell system (Bio-Rad) connected to a PowerPac HC (BioRad) power supply using Bio-Rad Any kD™ Mini-PROTEAN® TGX™ Precast Gels at 195 V and 3 A for 30 minutes in a running buffer (25 mM Tris, 192 mM Glycine, 0.1% (w/v) SDS, pH 8.3). Precision Plus Protein™ Dual Xtra Prestained Protein Standards (2 µL) were used as protein ladder in all SDS-PAGE analysis. Laemmli 2x Concentrate (Sigma) containing 4% SDS, 20% glycerol, 0.004% bromophenol blue and 0.125 M Tris HCl at a pH of approximately 6.8 was used to load all protein and conjugate samples. Protein bands were visualized by staining the gels in an aqueous solution (0.1% Coomassie Brilliant Blue R 250, 45% MeOH, 9% acetic acid) and microwaving for 30 seconds followed by agitation for 15 minutes. Destaining was carried out by submerging the gels in an aqueous destaining solution (10% MeOH, 14% acetic acid), microwaving for 30 seconds, and agitating for several hours until the background of the gel became fully destained. ImageJ was used to calculate conversion by optical densitometry.

3.4.3 Methods

Synthesis of ditosyl PEG_{2000}

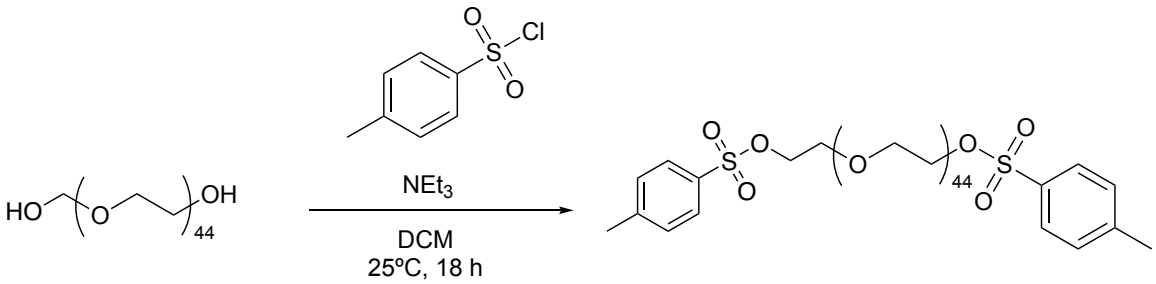

Adapted from Montgomery, et. al. [23] PEG_{2000} dihydroxy (1000 mg, 1 eq) was added to a round bottom equipped with a stir bar and DCM (10 mL). TEA (151.8 mg, 209 µL, 3 eq) was added slowly, stirred for 5 min, and subsequently cooled to 0 °C. 4-methylbenzenesulfonyl chloride (286.0 mg, 3 eq) was dissolved in DCM (10 mL) and added dropwise to the reaction flask. The reaction was allowed to warm to 25 ºC and stir for 16 h. The reaction was concentrated under reduced pressure. The off-white sticky solid was dissolved in minimal DCM and purified by precipitation in ice cold diethyl ether 3 times. The product was dried by vacuum to yield a white solid in 72% yield. ^{1}H NMR (400 MHz, $CDCl_3$) δ 7.76 (dd, J = 7.8, 5.9 Hz, 4H), 7.35 – 7.29 (m, 3H), 7.17 – 7.12 (m, 1H), 4.15 – 4.10 (m, 3H), 3.62 (s, 180H), 3.34 (t, 1H), 2.42 (s, 5H).

Synthesis of bis *para*- iodobenzene PEG_{2000}

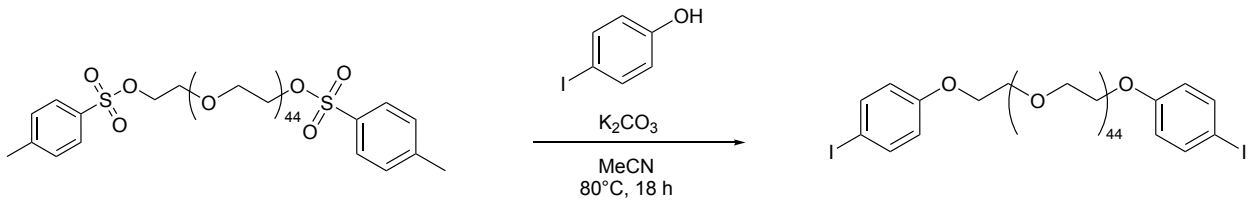

Adapted from Montgomery, et. al. [23] Ditosyl PEG_{2000} (300 mg, 1 eq) and 4-iodophenol (278 mg, 10 eq) were added to an oven-dried round bottom flask equipped with a stir bar and dissolved in anhydrous MeCN (10 mL). K_2CO_3 (175 mg, 10 eq) was then added to the solution while stirring. The reaction mixture was heated to 80 °C and was stirred for 12 hours at reflux. The solvent was removed under reduced pressure to afford an orange oil. The crude mixture was dissolved in DCM

and filtered to remove excess carbonate. The DCM was removed under vacuum and the remaining solids were dissolved in a small amount of water, and the basic solution was neutralized to pH 7-8 with 1 M NH_4OAc buffer. The aqueous solution was removed by lyophilization to provide white solids. These solids were resuspended in DCM and filtered to remove undissolved salts. The DCM solution was concentrated under reduced pressure and precipitated from cold diethyl ether 3 times. The precipitate was then run using 100% DCM to elute the aryl/tosyl peaks and then a gradient to 10% MeOH to elute the product as a white solid in 64% yield. ^1H NMR (400 MHz, $CDCl_3$) δ 7.58 – 7.50 (m, 4H), 6.73 – 6.67 (m, 3H), 4.08 (dd, J = 5.7, 4.0 Hz, 4H), 3.89 – 3.79 (m, 5H), 3.64 (s, 160H).

Synthesis of bis *para*- Au (III) $(Cy)_2$ PEG_{2000} (1)

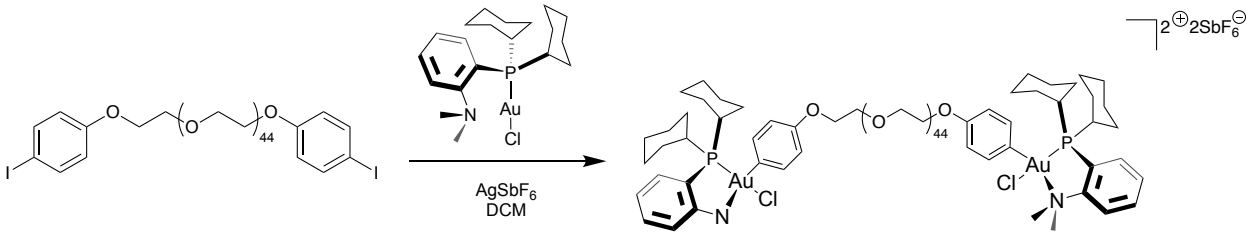

$AgSbF_6$ (5.9 mg, 3.5 eq) was added to a one-dram vial in the glovebox in the absence of light. This was removed from the glovebox, electrical taped, and charged with a stir bar. DCM (200 µL) was added to the vial, creating a clear solution. Separately, ((PCy$_2$)Me-DalPhos)Au^{I}Cl (9.5 mg, 3.5 eq) and *para*-iodobenzene PEG_{2000} (12.0 mg, 1 eq) were weighed out into a one-dram vial. This was dissolved in DCM (200 µL), creating a clear solution. Both reaction vials were added to the -20 ºC freezer for 1 min. The contents of the Au/ArI vial were transferred to the silver vial and stirred at 25 ºC for 18 h. The dark yellow/orange mixture was filtered through Celite, washed with DCM, and concentrated under vacuum to yield an orange oil. There was residual green material on the Celite. The concentrated orange oil was dissolved in minimal DCM and precipitated in diethyl ether 3 times. The material was concentrated under vacuum to yield an

orange oil in 81% yield. ^{1}H NMR (400 MHz, $CDCl_3$) δ 7.96 – 7.84 (m, 8H), 7.79 (d, *J* = 7.9 Hz, 3H), 7.55 – 7.50 (m, 2H), 7.12 (d, *J* = 8.6 Hz, 5H), 7.00 – 6.94 (d, 5H), 6.72 – 6.65 (m, 2H), 4.16 (dd, *J* = 5.7, 3.7 Hz, 5H), 4.08 (dd, *J* = 5.7, 4.0 Hz, 3H), 3.91 – 3.81 (m, 10H), 3.64 (s, 254H), 3.44 (s, 23H), 2.74 (d, *J* = 12.2 Hz, 5H), 1.75 (d, *J* = 38.8 Hz, 28H), 1.47 – 1.03 (m, 21H), 0.76 (d, *J* = 12.9 Hz, 6H). ^{31}P NMR (162 MHz, $CDCl_3$) δ 60.21.

Synthesis of bis *para*- Au (III) $(Ad)_2$ PEG_{2000} (2)

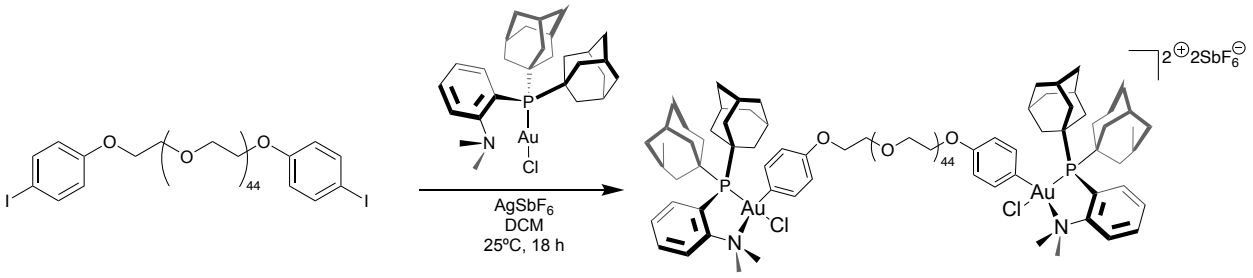

Adapted from Montgomery, et. al.[23] $AgSbF_6$ (25.6 mg, 3.5 eq) was added to a one-dram vial in the glovebox in the absence of light. This was removed from the glovebox, electrical taped, and charged with a stir bar. DCM (500 µL) was added to the vial, creating a clear solution. Separately, Me-DalPhos)AuCl (48.8 mg, 3.5 eq) and *para*-iodobenzene PEG_{2000} (30.0 mg, 1 eq) were weighed out into a one-dram vial. This was dissolved in DCM (500 µL), creating a clear solution. Both reaction vials were added to the -20 ºC freezer for 1 min. The contents of the Au/ArI vial were transferred to the silver vial and stirred at 25 ºC for 18 h. The dark yellow/orange mixture was filtered through Celite, washed with DCM, and concentrated under vacuum to yield a yellow oil. There was residual green material on the Celite. The concentrated orange oil was dissolved in minimal DCM and precipitated in diethyl ether 3 times. The material was concentrated under vacuum to yield a yellow oil in 84% yield.^{1}H NMR (400 MHz, $CDCl_3$) δ 8.04 – 7.89 (m, 6H), 7.77 (s, 2H), 7.31 (d, J = 8.9 Hz, 38H), 6.92 (d, J = 8.7 Hz, 4H), 4.15 (t, J = 4.7 Hz, 4H), 3.90 – 3.85

(m, 4H), 3.65 (s, 177H), 2.25 (d, J = 8.3 Hz, 12H), 2.11 (s, 27H), 1.75 (s, 25H). ^{31}P NMR (162 MHz, $CDCl_3$) δ 77.76.

Synthesis of divinyl sulfone PEG_{2000} (4)

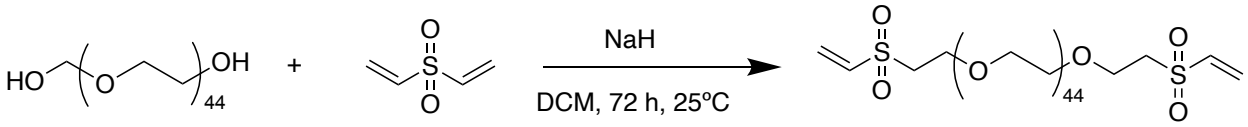

Adapted from Decker, et. al.[38] Sodium hydride (59.1 mg, 25 eq) was weighed into an oven-dried round-bottom flask equipped with a stir bar under argon. The flask was cooled in an ice-bath, and dry DCM (100 mL) was added. PEG_{2000} dihydroxy (200 mg, 1 eq), previously freeze-dried from benzene to remove water, was dissolved in dry DCM (50 mL). The PEG_{2000} dihydroxy was then added dropwise to the cooled slurry of sodium hydride and DCM. After hydrogen evolution (30 minutes stirring), (vinylsulfonyl)ethene (1.16 g, 989 μL, 100 eq) was added quickly. The solution was allowed to come to room temperature and stir for 3 days under argon. The solution was then neutralized with acetic acid, concentrated, and purified by precipitation into ice cold diethyl ether 5 times. The product was dried by vacuum to yield a light pink solid in quantitative yield. ^{1}H NMR (400 MHz, C_2D_6OS) δ 6.94 (dd, J = 16.6, 9.9 Hz, 2H), 6.29 – 6.14 (m, 4H), 3.73 (t, J = 5.9 Hz, 4H), 3.69 – 3.42 (m, 175H), 3.38 (t, J = 5.8 Hz, 6H).

3.5 Appendix II

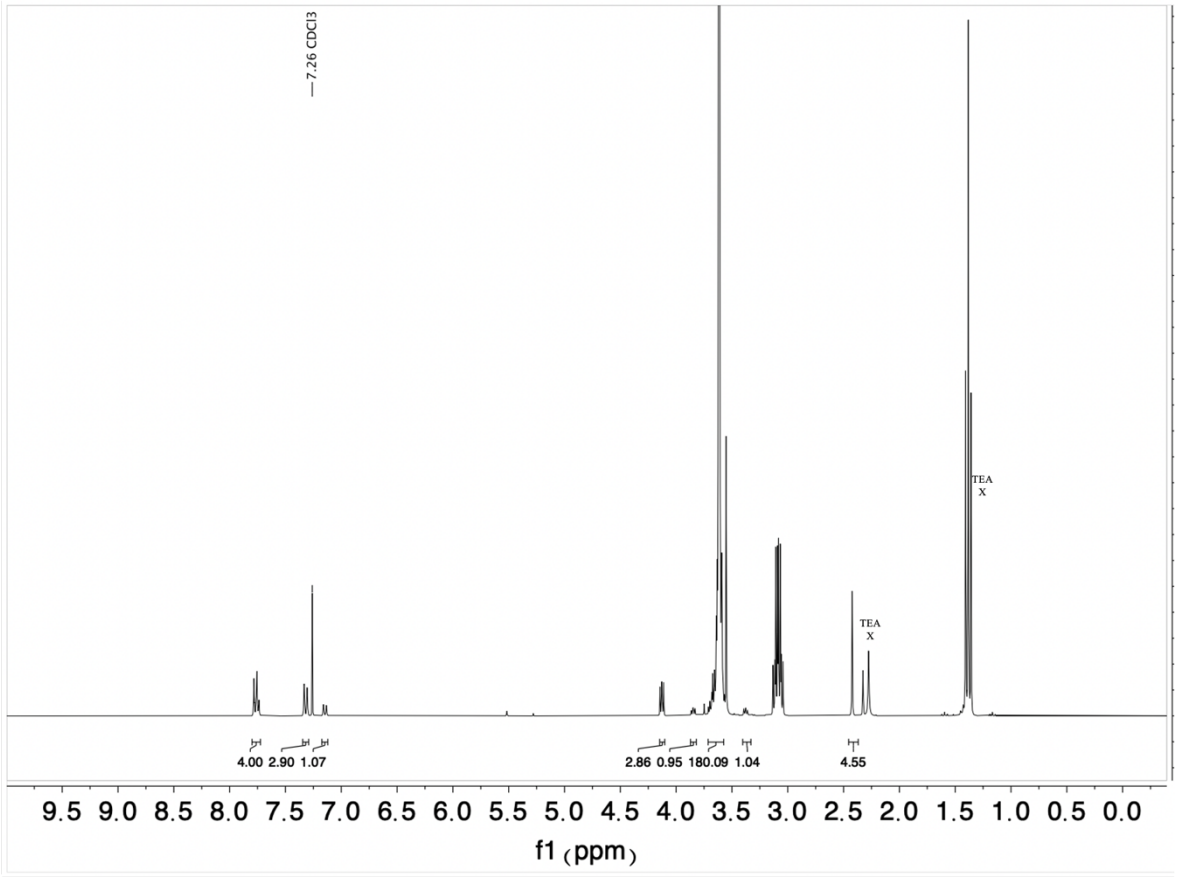

Figure 3.3. ^{1}H NMR of ditosyl PEG_{2000} in $CDCl_3$ at 23 ºC.

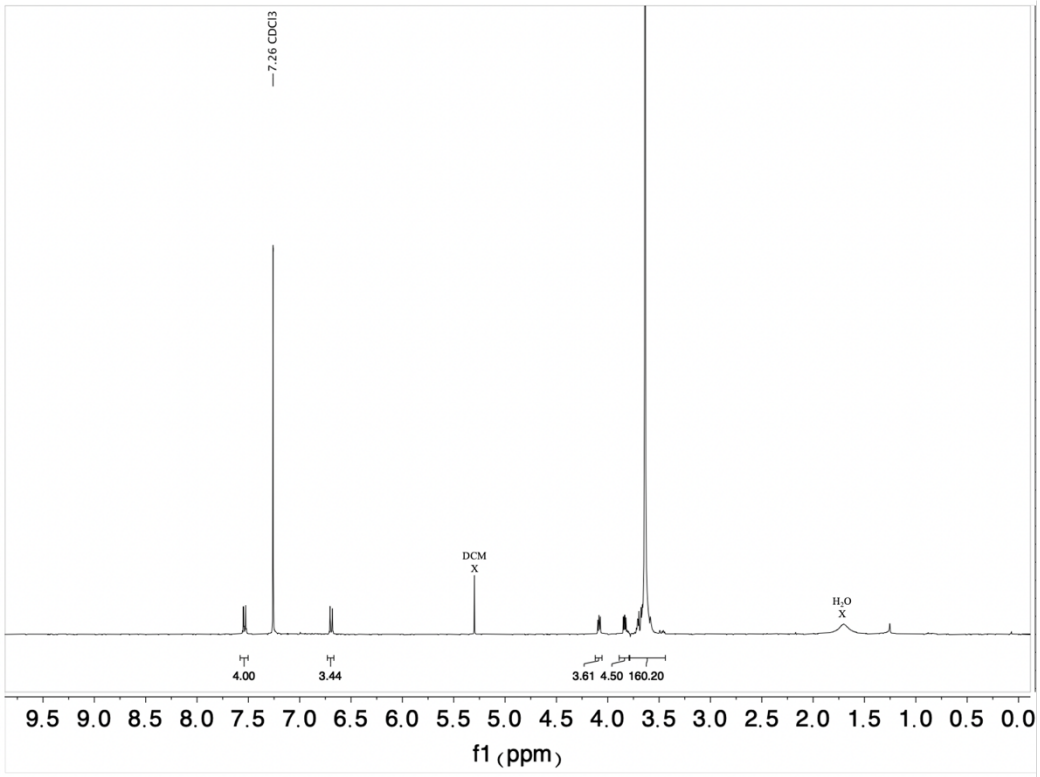

Figure 3.4. ^{1}H NMR of bis *para*-iodobenzene PEG_{2000} in $CDCl_3$ at 23 ºC.

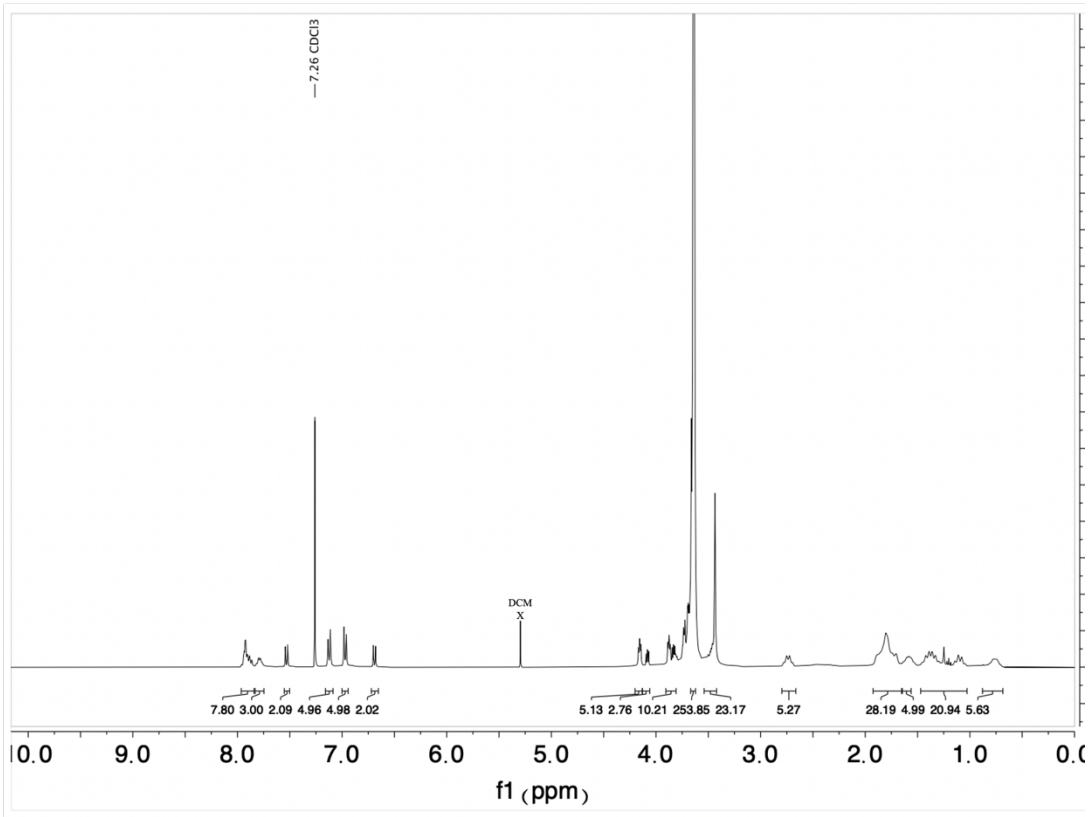

Figure 3.5. ^{1}H NMR of bis *para*- Au (III) $(Cy)_2$ PEG_{2000} **(1)** in $CDCl_3$ at 23 ºC.

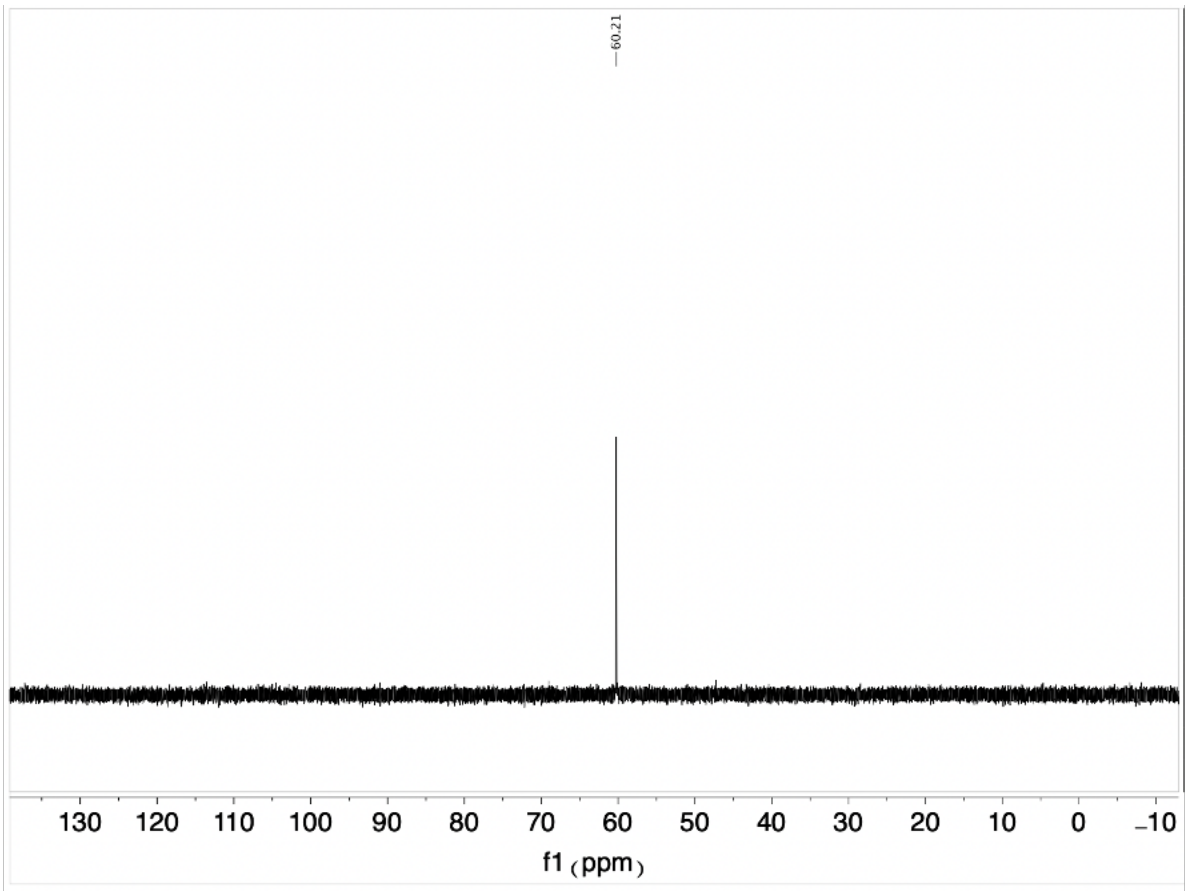

Figure 3.6. ^{31}P NMR of bis *para*- Au (III) $(Cy)_2$ PEG_{2000} **(1)** in $CDCl_3$ at 23 ºC.

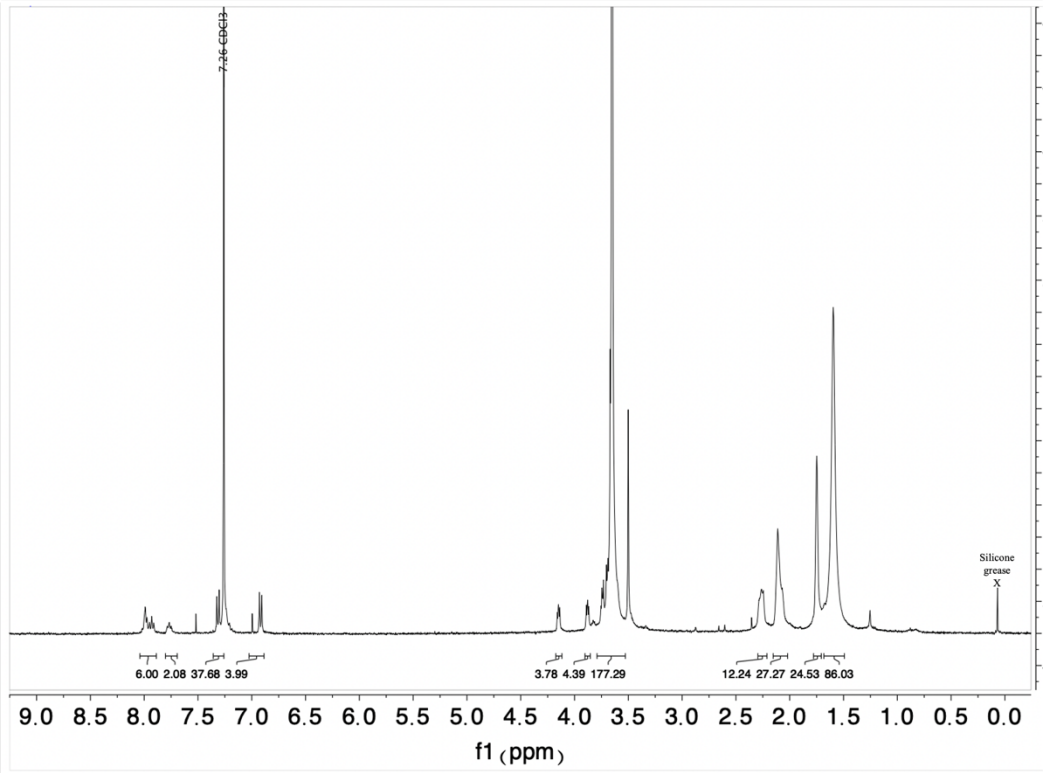

Figure 3.7. ^{1}H NMR of bis *para*- Au (III) $(Ad)_2$ PEG_{2000} **(2)** in $CDCl_3$ at 23 ºC.

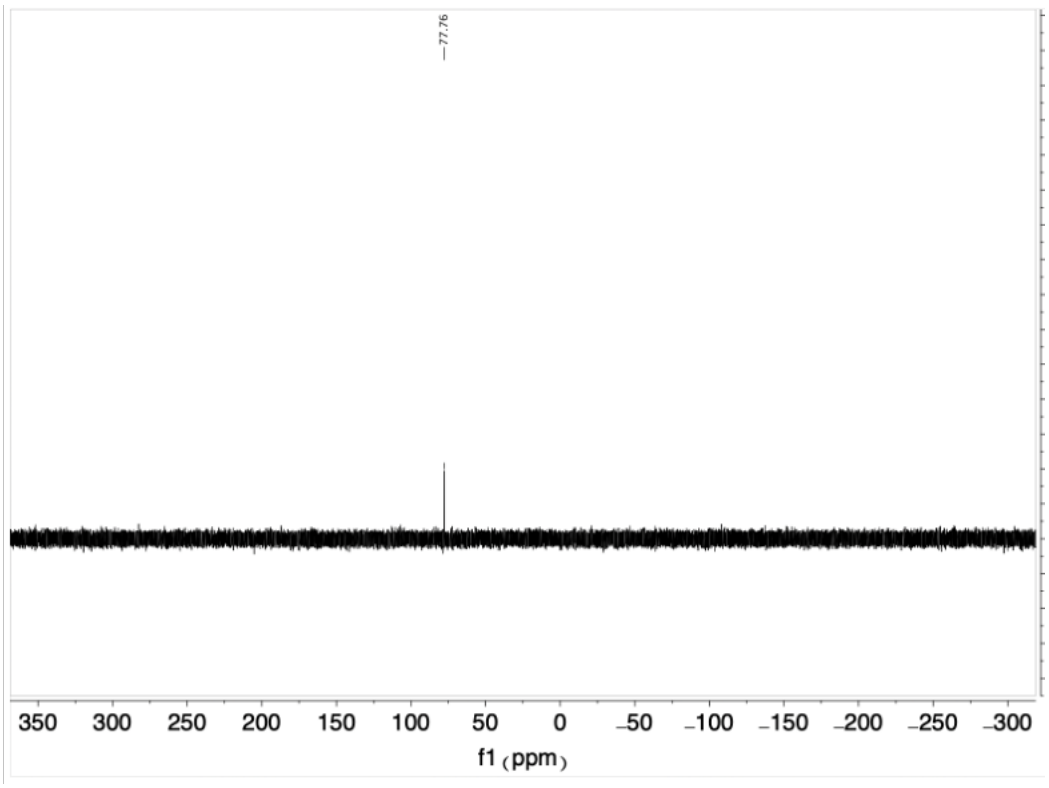

Figure 3.8. ^{31}P NMR of bis *para*- Au (III) $(Ad)_2$ PEG_{2000} **(2)** in $CDCl_3$ at 23 ºC.

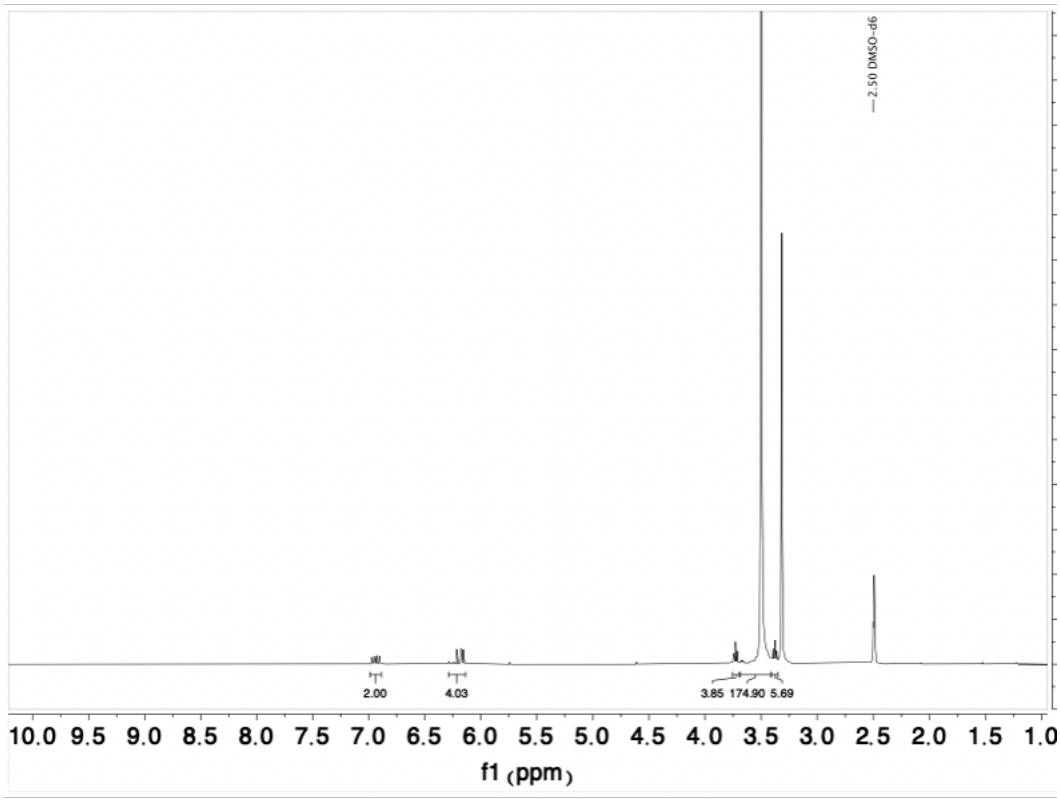

Figure 3.9. ^{1}H NMR of divinyl sulfone PEG_{2000} **(4)** in C_2D_6OS at 23 ºC.

Protein Dimerization Experiments

T4L-PEG-T4L Dimers

T4 Lysozyme V131C (T4L) Protein Expression

T4 lysozyme V131C (T4L) protein expression and purification was adapted from literature procedures.[5] T4 lysozyme V131C (T4L) Sequence (Calculated Mass: 18605.36 Da): MNIFEMLRIDEGLRLKIYKDTEGYYTIGIGHLLTKSPSLNAAKSELDKAIGRNTNGVITKD EAEKLFNQDVDAAVRGILRNAKLKPVYDSLDAVRRAALINMVFQMGETGVAGFTNSLR MLQQKRWDEAACNLAKSRWYNQTPNRAKRVITTFRTGTWDAYKNL.

E. coli host BL21(DE3) (Invitrogen) was used to express T4 lysozyme V131C (T4L) using an ampicillin resistant expression vector obtained from Prof. Wayne Hubbell (UCLA). To each of two 2 L flasks each containing 750 mL of previously autoclaved LB Broth (Miller) with ampicillin (50 μg/mL) was added 5 mL of a saturated 18 hour culture inoculated from a glycerol stock. The culture was grown at 37 °C with 250 rpm shaking for ca. 6 hours before the OD600 reached ~0.75 and the culture was induced with 1 mM isopropyl β- d-1-thiogalactopyranoside (IPTG). The culture continued to shake at 37 °C at 250 rpm for approximately 2 hours. The cultures were harvested by centrifugation at 4000 rpm for 15 min to yield a cell pellet. The pellet was resuspended in 20 mL lysis buffer (25 mM Tris, 25 mM MOPS, 0.2 mM EDTA, pH 7.6) by stirring vigorously. Spontaneous bacterial lysis occurred during resuspension as evident by increased viscosity of the suspension due to DNA release. Bacterial lysis was likely due to proteolytic activity of the lysozyme present in the bacteria. One subsequent freeze-thaw cycle ensured complete lysis of the bacteria. Benzoase (0.2 μL/mL) was then added to the solution and incubated at 25 °C for 15 min. Bacterial debris was then separated by centrifugation at 17,000 rpm for 25 min at 4 °C. The supernatant was loaded onto a 5 mL gravity SP Sepharose Fast Flow column (Cytiva) and

washed with 200 mL lysis buffer. The column was then washed with two column volumes of lysis buffer with increasing NaCl content (gradient from 0 M to 0.5 M in 0.1 M steps) to elute the desired protein. SDS-PAGE was run on all fractions and under reducing conditions with Coomassie Blue staining. Pure fractions were combined and solvent exchanged into storage buffer (20 mM PBS, pH 6.5) and concentrated to ~15 mL using an Amicon 3K Ultra-15 Centrifugal Filter (Millipore). Protein was further purified by preparative SEC-FPLC using an isocratic method in 20 mM PBS, pH 6.5. Pure fractions were concentrated and stored in storage buffer as described above. The purified protein was analyzed by LCMS and SDS-PAGE confirming sample purity and molecular weight (main text Figure 2). Concentration was determined by A280 (Extinction coefficient = 25,440 M^{-1} cm^{-1}) The protein sample was diluted with storage buffer to 76 µM and aliquots were flash frozen and stored in a -80 °C freezer.

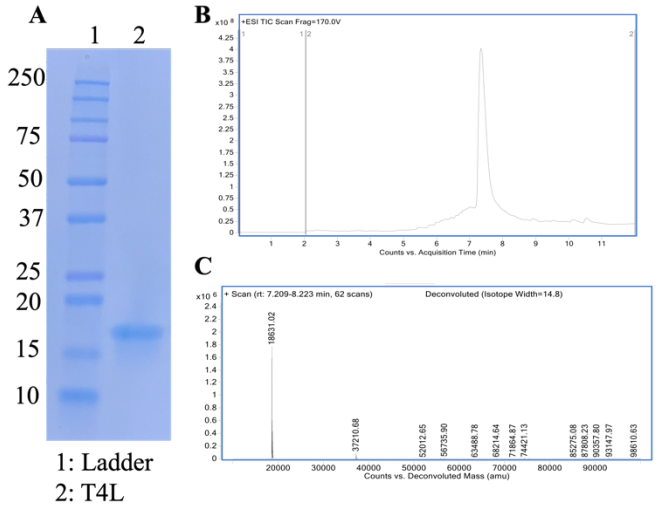

Figure 3.10. A) SDS-PAGE gel of T4 lysozyme following purification. B) LCMS total ion chromatogram (TIC) of T4 lysozyme following purification. C) LCMS deconvoluted mass of T4 lysozyme following purification m/z = 18.6 kDa.

Preparation of T4L-PEG-T4L Dimers

T4L-PEG-T4L Dimer Conditions Screening

All equivalent screenings are in relation to protein equivalents as 1. All reactions are done in reducing conditions unless otherwise noted.

General conditions for dimerizations are as follows: 70 μM T4L, Tris Buffer pH 6.0, 7.5 or pH 9.0 X equiv. TCEP·HCl, 4 equiv. (**1, 2, 3, or 4**) PEG_{2000} reagent, 12 h, 25 or 37 °C. To a 50 μL solution of T4L at 76 μM, 5 μL of a 3 mM TCEP·HCl (4 eq) solution in Tris Buffer was added. The protein underwent disulfide reduction for 1 hour at 37 ºC. Next, 5 μL of either **1, 2, 3** or **4** was added to the reaction mixture. Stock solutions of either **1, 2, 3** or **4** were prepared in MeCN prior to the procedure. After 12 h, the reaction was stopped by dilution in SDS-PAGE conditions (See below).

General SDS-PAGE Sample Preparation Procedure: 1 μL of a given reaction mixture was added to 19 μL of Laemmli loading buffer. For samples run under reducing conditions, the Laemmli loading buffer was prepared to contain 5% mercaptoethanol by volume and samples were heated at 90 ºC for five minutes prior to loading. Samples were loaded onto SDS-PAGE gel and run as described above in the general experimental information.

Temperature Screen: To a 50 μL solution of T4L at 76 μM, 5 μL of a 3 mM TCEP·HCl (4 eq) solution in PBS was added. The protein underwent disulfide reduction for 1 hour at 37 ºC. Next, 5 μL of either **1, 2, 3** or **4** were added to the solution at 0.5 eq with all PEG stock solutions prepared in MeCN. The reactions were allowed to proceed at either 23 ºC or 37 ºC 12 h. Then, the samples underwent the general SDS-PAGE sample preparation procedure as described above.

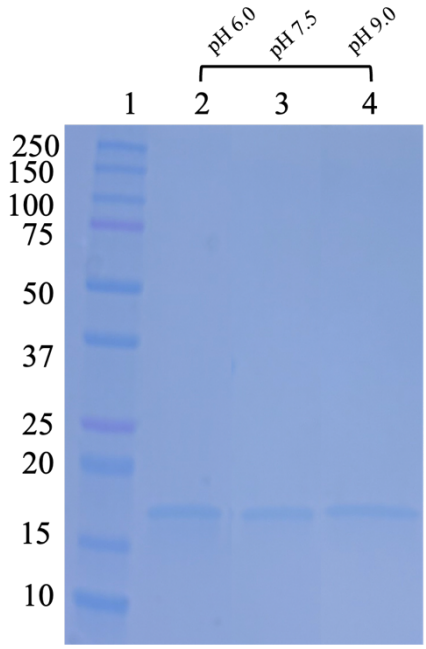

Figure 3.11. SDS-PAGE gel of T4L in Tris buffer pH 6.0, 7.5 and 9.0 at 37 ºC for 18 h in reducing conditions.

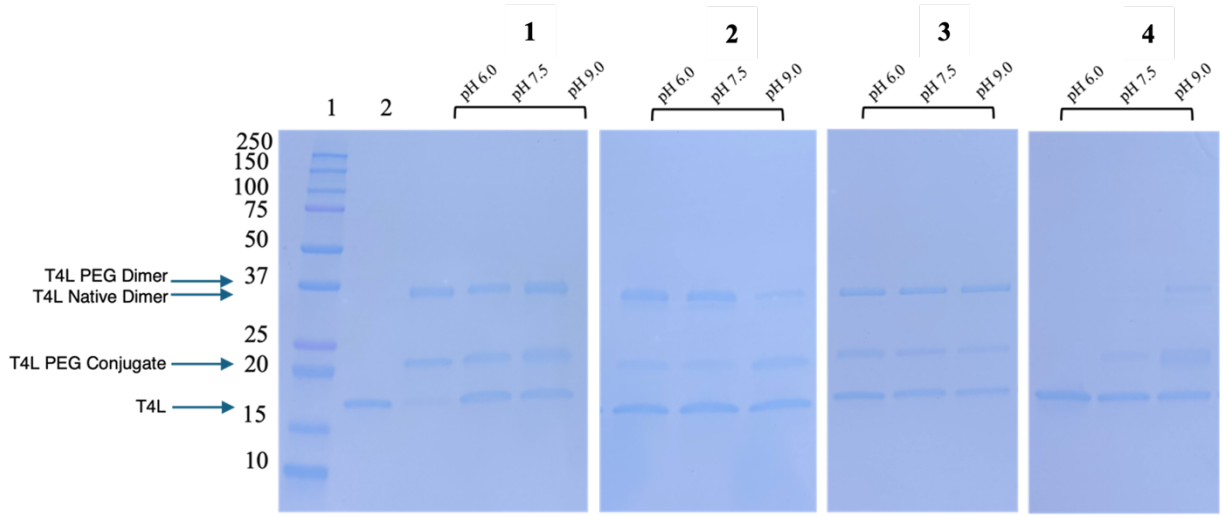

Figure 3.12. SDS-PAGE gel of T4L in Tris buffer with 0.5 eq **PEG reagent** at 25 ºC for 12 h in reducing conditions. Lane 1: ladder, Lane 2: T4L control. Highest % Conversion for each reagent: 71% pH 6.0 with **1**, 54% pH 6.0 with **2**, 43% pH 7.5 with **3**, 6% pH 9.0 with **4.**

PEG_{2000} Reagent	% Conversion pH 6.0	% Conversion pH 7.5	% Conversion pH 9.0
1	65- 71	51-54	47- 54
2	50 -54	41-44	3-6
3	34-37	41-43	38-40
4	0	0	4-6

Table 3.3. SDS-PAGE gel of T4L in Tris buffer with 0.5 eq **PEG reagent** at 25 ºC for 12 h in reducing conditions. Percent conversion calculated with ImageJ with n= 2 and therefore the range is listed.

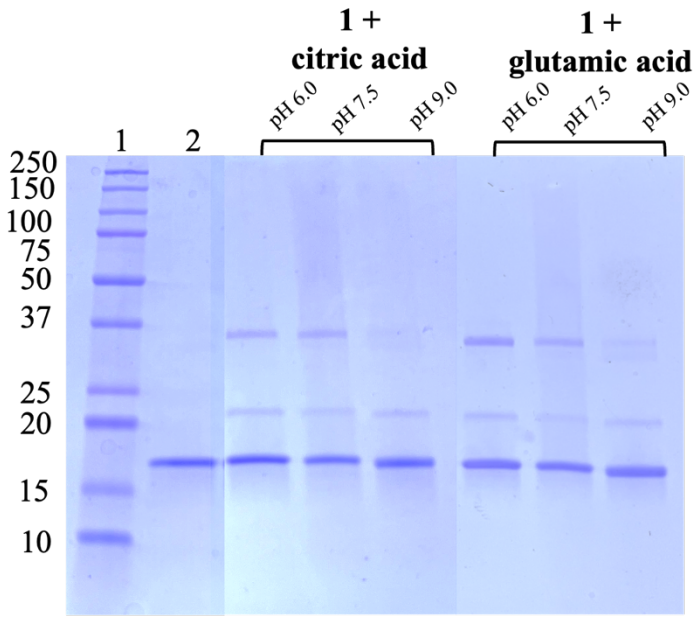

Figure 3.13. SDS-PAGE gel of T4L in Tris buffer with 0.5 eq **1 (left)**, **1 + citric acid (middle)**, and **1+ glutamic acid (right)** at 37 ºC for 12 h in reducing conditions.

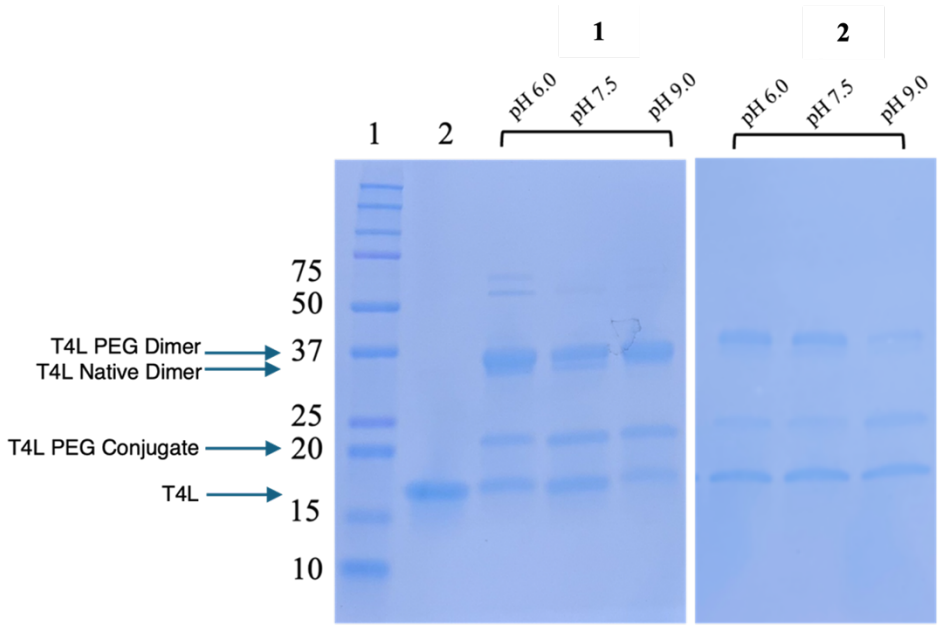

Figure 3.14. SDS-PAGE gel of T4L in Tris buffer with 0.5 eq **PEG reagent** at 37 ºC for 18 h in reducing conditions.

Characterization of S-arylated T4L-PEG-T4L Dimers

Stability Assessment in the Presence of Base, Acid, and Oxidation

The stability of the S-arylated T4L-PEG-T4L dimers was assessed with adaptation from previously reported literature.[5] Stability was measured by integrating the area under the curve of the samples using LC-MS.

Base reagent: K_2CO_3 (2 µL, 0.16 mM in H_2O)

Acid reagent: HCl (2 µL, 0.003 M in H_2O)

Oxidation reagent: H_5IO_6 (2 µL, 400 µM in H_2O)

Base and Acid Stability

S-arylated T4L-PEG-T4L was buffer exchanged to H_2O and prepared as 0.03 mM stock solutions for the stability experiments. S-arylated T4L-PEG-T4L (0.03 mM; 18 µL) and stability

test reagent (2 μL, in H_2O) were combined in a plastic Eppendorf and left at 25 ºC for 2 days, followed by 4 days at 37 °C. The reactions (20 uL) were quenched with a solution of 50% H_2O: 50% MeCN (v/v, 20 uL) and the resulting samples were analyzed by LC-MS.

Oxidation Stability

S-arylated T4L-PEG-T4L was buffer exchanged to H_2O and prepared as 0.03 mM stock solutions for the stability experiments. S-arylated T4L-PEG-T4L (0.03 mM; 18 μL) and stability test reagent (2 μL, in H_2O) were combined in a plastic Eppendorf and placed in an incubator at 37 ºC for 30 min. The reaction was quenched with a solution Na_2SO_3 (20 μL, 400 μM in H_2O). A solution of 50% H_2O: 50% MeCN (v/v, 20 uL) was added, and the resulting samples were analyzed by LC-MS.

3.6 References

(1) Matthews, J. M.; Sunde, M. Dimers, Oligomers, Everywhere. In *Protein Dimerization and Oligomerization in Biology*; Matthews, J. M., Ed.; Advances in Experimental Medicine and Biology; Springer: New York, NY, 2012; pp 1–18. https://doi.org/10.1007/978-1-4614-3229-6_1.

(2) Marianayagam, N. J.; Sunde, M.; Matthews, J. M. The Power of Two: Protein Dimerization in Biology. *Trends Biochem. Sci.* **2004**, *29* (11), 618–625. https://doi.org/10.1016/j.tibs.2004.09.006.

(3) Liu, C.; Luo, J. Protein Oligomer Engineering: A New Frontier for Studying Protein Structure, Function, and Toxicity. *Angew. Chem.* **2023**, *135* (23), e202216480. https://doi.org/10.1002/ange.202216480.

(4) Cai, X.; Wang, D.; Zhang, R.; Chen, Y.; Chen, J. The Transmembrane Domains of GPCR Dimers as Targets for Drug Development. *Drug Discov. Today* **2023**, *28* (1), 103419. https://doi.org/10.1016/j.drudis.2022.103419.

(5) Muhammad, T.; Strömstedt, A. A.; Gunasekera, S.; Göransson, U. Transforming Cross-Linked Cyclic Dimers of KR-12 into Stable and Potent Antimicrobial Drug Leads. *Biomedicines* **2023**, *11* (2), 504. https://doi.org/10.3390/biomedicines11020504.

(6) Zhong, X.; Guo, J.; Han, X.; Wu, W.; Yang, R.; Zhang, J.; Shao, G. Synthesis and Preclinical Evaluation of a Novel FAPI-04 Dimer for Cancer Theranostics. *Mol. Pharm.* **2023**, *20* (5), 2402–2414. https://doi.org/10.1021/acs.molpharmaceut.2c00965.

(7) Zhang, R.; Qin, H.; Prasad, R.; Fu, R.; Zhou, H.-X.; Cross, T. A. Dimeric Transmembrane Structure of the SARS-CoV-2 E Protein. *Commun. Biol.* **2023**, *6* (1), 1–10. https://doi.org/10.1038/s42003-023-05490-x.

(8) Nagano, M.; Kubota, K.; Sakata, A.; Nakamura, R.; Yoshitomi, T.; Wakui, K.; Yoshimoto, K. A Neutralizable Dimeric Anti-Thrombin Aptamer with Potent Anticoagulant Activity in Mice. *Mol. Ther. Nucleic Acids* **2023**, *33*, 762–772. https://doi.org/10.1016/j.omtn.2023.07.038.

(9) Wang, H.; Wu, J.; Sternke-Hoffmann, R.; Zheng, W.; Mörman, C.; Luo, J. Multivariate Effects of pH, Salt, and Zn2+ Ions on Aβ40 Fibrillation. *Commun. Chem.* **2022**, *5* (1), 1–12. https://doi.org/10.1038/s42004-022-00786-1.

(10) McLoughlin, N. M.; Albers, M. A.; Collado Camps, E.; Paulus, J.; Ran, Y. A.; Neubacher, S.; Hennig, S.; Brock, R.; Grossmann, T. N. Environment-Responsive Peptide Dimers Bind and Stabilize Double-Stranded RNA. *Angew. Chem.* **2023**, *135* (41), e202308028. https://doi.org/10.1002/ange.202308028.

(11) Sivasankaran, R. P.; Snell, K.; Kunkel, G.; Georgiou, P. G.; Puente, E. G.; Maynard, H. D. Polymer-Mediated Protein/Peptide Therapeutic Stabilization: Current Progress and Future Directions. *Prog. Polym. Sci.* **2024**, *156*, 101867. https://doi.org/10.1016/j.progpolymsci.2024.101867.

(12) Li, C.; Li, T.; Tian, X.; An, W.; Wang, Z.; Han, B.; Tao, H.; Wang, J.; Wang, X. Research Progress on the PEGylation of Therapeutic Proteins and Peptides (TPPs). *Front. Pharmacol.* **2024**, *15*. https://doi.org/10.3389/fphar.2024.1353626.

(13) Sanchez Armengol, E.; Unterweger, A.; Laffleur, F. PEGylated Drug Delivery Systems in the Pharmaceutical Field: Past, Present and Future Perspective. *Drug Dev. Ind. Pharm.* **2022**, *48* (4), 129–139. https://doi.org/10.1080/03639045.2022.2101062.

(14) Santhanakrishnan, K. R.; Koilpillai, J.; Narayanasamy, D. PEGylation in Pharmaceutical Development: Current Status and Emerging Trends in Macromolecular and Immunotherapeutic Drugs. *Cureus* **2024**. https://doi.org/10.7759/cureus.66669.

(15) *FDA Approved PEGylated Drugs By 2024 | Biopharma PEG*. https://www.biochempeg.com/article/58.html (accessed 2024-10-15).

(16) Cal, P. M. S. D.; Bernardes, G. J. L.; Gois, P. M. P. Cysteine-Selective Reactions for Antibody Conjugation. *Angew. Chem. Int. Ed.* **2014**, *53* (40), 10585–10587. https://doi.org/10.1002/anie.201405702.

(17) deGruyter, J. N.; Malins, L. R.; Baran, P. S. Residue-Specific Peptide Modification: A Chemist's Guide. *Biochemistry* **2017**, *56* (30), 3863–3873. https://doi.org/10.1021/acs.biochem.7b00536.

(18) Lyon, R. P.; Setter, J. R.; Bovee, T. D.; Doronina, S. O.; Hunter, J. H.; Anderson, M. E.; Balasubramanian, C. L.; Duniho, S. M.; Leiske, C. I.; Li, F.; Senter, P. D. Self-Hydrolyzing Maleimides Improve the Stability and Pharmacological Properties of Antibody-Drug Conjugates. *Nat. Biotechnol.* **2014**, *32* (10), 1059–1062. https://doi.org/10.1038/nbt.2968.

(19) Montgomery, H. R.; Spokoyny, A. M.; Maynard, H. D. Organometallic Oxidative Addition Complexes for *S* -Arylation of Free Cysteines. *Bioconjug. Chem.* **2024**, *35* (7), 883–889. https://doi.org/10.1021/acs.bioconjchem.4c00222.

(20) Rodriguez, J.; Dhanjee, H. H.; Pentelute, B. L.; Buchwald, S. L. Palladium Mediated Synthesis of Protein–Polyarene Conjugates. *J. Am. Chem. Soc.* **2022**, *144* (26), 11706–11712. https://doi.org/10.1021/jacs.2c03492.

(21) Doud, E. A.; Tilden, J. A. R.; Treacy, J. W.; Chao, E. Y.; Montgomery, H. R.; Kunkel, G. E.; Olivares, E. J.; Adhami, N.; Kerr, T. A.; Chen, Y.; Rheingold, A. L.; Loo, J. A.; Frost, C. G.;

Houk, K. N.; Maynard, H. D.; Spokoyny, A. M. Ultrafast Au(III)-Mediated Arylation of Cysteine. *J. Am. Chem. Soc.* **2024**. https://doi.org/10.1021/jacs.3c12170.

(22) Kunkel, G. E.; Zhou, Q.; Treacy, J. W.; Montgomery, H. R.; Salas-Ambrosio, P.; Ready, A. D.; Spokoyny, A. M.; Houk, K. N.; Maynard, H. D. Comparison of Cyclic and Linear PEG Conjugates. *Bioconjug. Chem.* **2024**, *35* (6), 744–749. https://doi.org/10.1021/acs.bioconjchem.4c00202.

(23) Montgomery, H. R.; Messina, M. S.; Doud, E. A.; Spokoyny, A. M.; Maynard, H. D. Organometallic S-Arylation Reagents for Rapid PEGylation of Biomolecules. *Bioconjug. Chem.* **2022**, *33* (8), 1536–1542. https://doi.org/10.1021/acs.bioconjchem.2c00280.

(24) Messina, M. S.; Stauber, J. M.; Waddington, M. A.; Rheingold, A. L.; Maynard, H. D.; Spokoyny, A. M. Organometallic Gold(III) Reagents for Cysteine Arylation. *J. Am. Chem. Soc.* **2018**, *140* (23), 7065–7069. https://doi.org/10.1021/jacs.8b04115.

(25) Vinogradova, E. V. Organometallic Chemical Biology: An Organometallic Approach to Bioconjugation. *Pure Appl. Chem.* **2017**, *89* (11), 1619–1640. https://doi.org/10.1515/pac-2017-0207.

(26) Kunkel, G. E.; Treacy, J. W.; Montgomery, H. R.; Puente, E. G.; Doud, E. A.; Spokoyny, A. M.; Maynard, H. D. Efficient End-Group Functionalization and Diblock Copolymer Synthesis *via* Au(III) Polymer Reagents. *Chem. Commun.* **2024**, *60* (1), 79–82. https://doi.org/10.1039/D3CC05350D.

(27) Garai, K.; Frieden, C. Quantitative Analysis of the Time Course of Aβ Oligomerization and Subsequent Growth Steps Using Tetramethylrhodamine-Labeled Aβ. *Proc. Natl. Acad. Sci.* **2013**, *110* (9), 3321–3326. https://doi.org/10.1073/pnas.1222478110.

(28) Chubarov, A.; Spitsyna, A.; Krumkacheva, O.; Mitin, D.; Suvorov, D.; Tormyshev, V.; Fedin, M.; Bowman, M. K.; Bagryanskaya, E. Reversible Dimerization of Human Serum Albumin. *Molecules* **2021**, *26* (1), 108. https://doi.org/10.3390/molecules26010108.

(29) Svilenov, H. L.; Kulakova, A.; Zalar, M.; Golovanov, A. P.; Harris, P.; Winter, G. Orthogonal Techniques to Study the Effect of pH, Sucrose, and Arginine Salts on Monoclonal Antibody Physical Stability and Aggregation During Long-Term Storage. *J. Pharm. Sci.* **2020**, *109* (1), 584–594. https://doi.org/10.1016/j.xphs.2019.10.065.

(30) Chiariello, M. G.; Grünewald, F.; Zarmiento-Garcia, R.; Marrink, S. J. pH-Dependent Conformational Switch Impacts Stability of the PsbS Dimer. *J. Phys. Chem. Lett.* **2023**, *14* (4), 905–911. https://doi.org/10.1021/acs.jpclett.2c03760.

(31) Tao, L.; Kaddis, C. S.; Ogorzalek Loo, R. R.; Grover, G. N.; Loo, J. A.; Maynard, H. D. Synthetic Approach to Homodimeric Protein–Polymer Conjugates. *Chem. Commun.* **2009**, No. 16, 2148. https://doi.org/10.1039/b822799c.

(32) Lorenzo, M. M.; Decker, C. G.; Kahveci, M. U.; Paluck, S. J.; Maynard, H. D. Homodimeric Protein-Polymer Conjugates via the Tetrazine-Trans-Cyclooctene Ligation. *Macromolecules* **2016**, *49* (1), 30–37. https://doi.org/10.1021/acs.macromol.5b02323.

(33) Zhang, J.; Desale, S. S.; Bronich, T. K. Polymer-Based Vehicles for Therapeutic Peptide Delivery. *Ther. Deliv.* **2015**, *6* (11), 1279–1296. https://doi.org/10.4155/tde.15.71.

(34) Nguyen, T. H.; Paluck, S. J.; McGahran, A. J.; Maynard, H. D. Poly(Vinyl Sulfonate) Facilitates bFGF-Induced Cell Proliferation. *Biomacromolecules* **2015**, *16* (9), 2684–2692. https://doi.org/10.1021/acs.biomac.5b00557.

(35) Nawrocka, D.; Krzyscik, M. A.; Opaliński, Ł.; Zakrzewska, M.; Otlewski, J. Stable Fibroblast Growth Factor 2 Dimers with High Pro-Survival and Mitogenic Potential. *Int. J. Mol. Sci.* **2020**, *21* (11), 4108. https://doi.org/10.3390/ijms21114108.

(36) Test, T. *Homobifunctional PEG Derivatives*. JenKem Technology USA. https://jenkemusa.com/homobifunctional-pegs (accessed 2024-10-28).

(37) Kunkel, G. E.; Treacy, J. W.; Polite, M. F.; Montgomery, H. R.; Doud, E. A.; Houk, K. N.; Spokoyny, A. M.; Maynard, H. D. Heterotelechelic Organometallic PEG Reagents Enable Modular Access to Complex Bioconjugates. *ACS Macro Lett.* **2024**, 1551–1557. https://doi.org/10.1021/acsmacrolett.4c00588.

(38) Decker, C. G.; Wang, Y.; Paluck, S. J.; Shen, L.; Loo, J. A.; Levine, A. J.; Miller, L. S.; Maynard, H. D. Fibroblast Growth Factor 2 Dimer with Superagonist in Vitro Activity Improves Granulation Tissue Formation during Wound Healing. *Biomaterials* **2016**, *81*, 157–168. https://doi.org/10.1016/j.biomaterials.2015.12.003.

(39) Vinogradova, E. V.; Zhang, C.; Spokoyny, A. M.; Pentelute, B. L.; Buchwald, S. L. Organometallic Palladium Reagents for Cysteine Bioconjugation. *Nature* **2015**, *526* (7575), 687–691. https://doi.org/10.1038/nature15739.

Chapter 4

FGF-2 Multimers Utilizing

Au (III) Bifunctional PEGylated Linkers

4.1 Introduction

According to the protein data bank, most proteins found in biology exist primarily in their oligomeric form compared to their monomer state.[1,2] Oligomerization improves protein stability against degradation and aggregation by exposure of surface residues to solvents, thus lowering the surface area to volume ratio.[2–4] In nature, proteins often form oligomeric or multimeric complexes that prove critical for effective activity and regulation.[5–7] Likewise, fixation of multiple proteins to a polymer scaffold can result in a conjugate that exhibits higher activities then the monomeric conjugate.[8] These multimeric complexes can allow for control over the accessibility and specificity of active sites; however, the chemistries to make these structures covalent are underexplored.[9] Consequently, development of highly efficient, yet biologically compatible protein dimerization is a growing subfield in chemical biology, medicine, and biotechnology.[10–19] It remains challenging to overcome the steric hindrance of proteins to reach full conjugation conversion at an acceptable kinetic rate and yield.[20]

FGF-2 is a growth factor protein that moderates cell proliferation, differentiation and migration, playing a critical role in wound healing, angiogenesis, bone regeneration, neuroregeneration, and can even result in scarless healing.[21,22] We have previously shown that FGF-2 dimers stimulated superior metabolic activity and migration in fibroblast and endothelial cells compared to FGF-2.[19] The optimal linker length was empirically determined to be that closest to the FGF-2:FGFR (FGF receptor) tetramer inter-cysteine distance, 70 Å, corresponding to a PEG_{2000}.[19] Furthermore, other groups have found that PEGylation of FGF-2 resulted in increased plasma lifetimes and decreased clearance through functionalization of the N-terminus.[23,24] We hypothesized that conjugation of FGF-2 with PEG_{2000} to create higher order oligomeric complexes, larger than dimers, could offer even greater activity and stability.

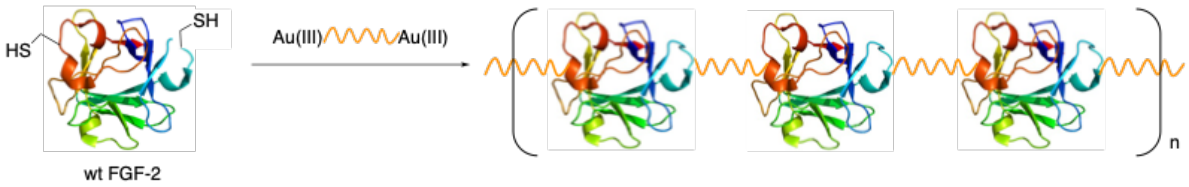

Figure 4.1 Multimerization of wt FGF-2 utilizing bifunctional Au (III) polymeric linkers.

Given the complex landscape presented at the biomolecule surface, the choice of conjugation chemistry at the biomolecule/polymer interface is of critical importance.[25] We have established that (Me-DalPhos)Au-substrates are highly efficient for cysteine arylation of proteins with polymers.[26–28] Bench stable and isolable polyethylene glycol PEG (Me-DalPhos)Au reagents were previously synthesized for the PEGylation of the model protein DARPin.[26] Thus, we hypothesized that the rapid bimolecular kinetics of the cysteine arylation approach will be amenable to the synthesis of multimeric FGF-2 scaffold utilizing the two accessible cysteine (Cys78 and Cys96) (**Figure 4.1**). FGF-2 is susceptible to degradation and aggregation after 1 h at 25 ºC and 30 min at 37 ºC, [29] thus, we anticipated that multimerization utilizing the rapid kinetics of Au (III) would be critical. The resulting S-aryl bonds also mitigates reversibility concerns compared to some other conjugation linkages such as thiol ethers formed from maleimides, which can be reversible *in vivo.* Herein are described efforts to synthesize a range of FGF-2 complexes from dimer, trimer, tetramer, and highest order multimers using bifunctional Au (III) PEGylated complexes. We prepared several Au (III) PEGylated complexes with different steric availability to explore the different conversions of higher order oligomers with each linker.

4.2 Results and Discussion

4.2.1 Synthesis of bifunctional Au (III) PEG_{2000} linkers.

PEG_{2000} bifunctional Au (III) linkers were synthesized through the general synthetic approach of ditosylation, arylation, and oxidative addition (OA). The Maynard and Spokoyny groups reported (Me-DalPhos)AuCl and more recently an ultrafast (dicyclohexPhos)AuCl reagent,

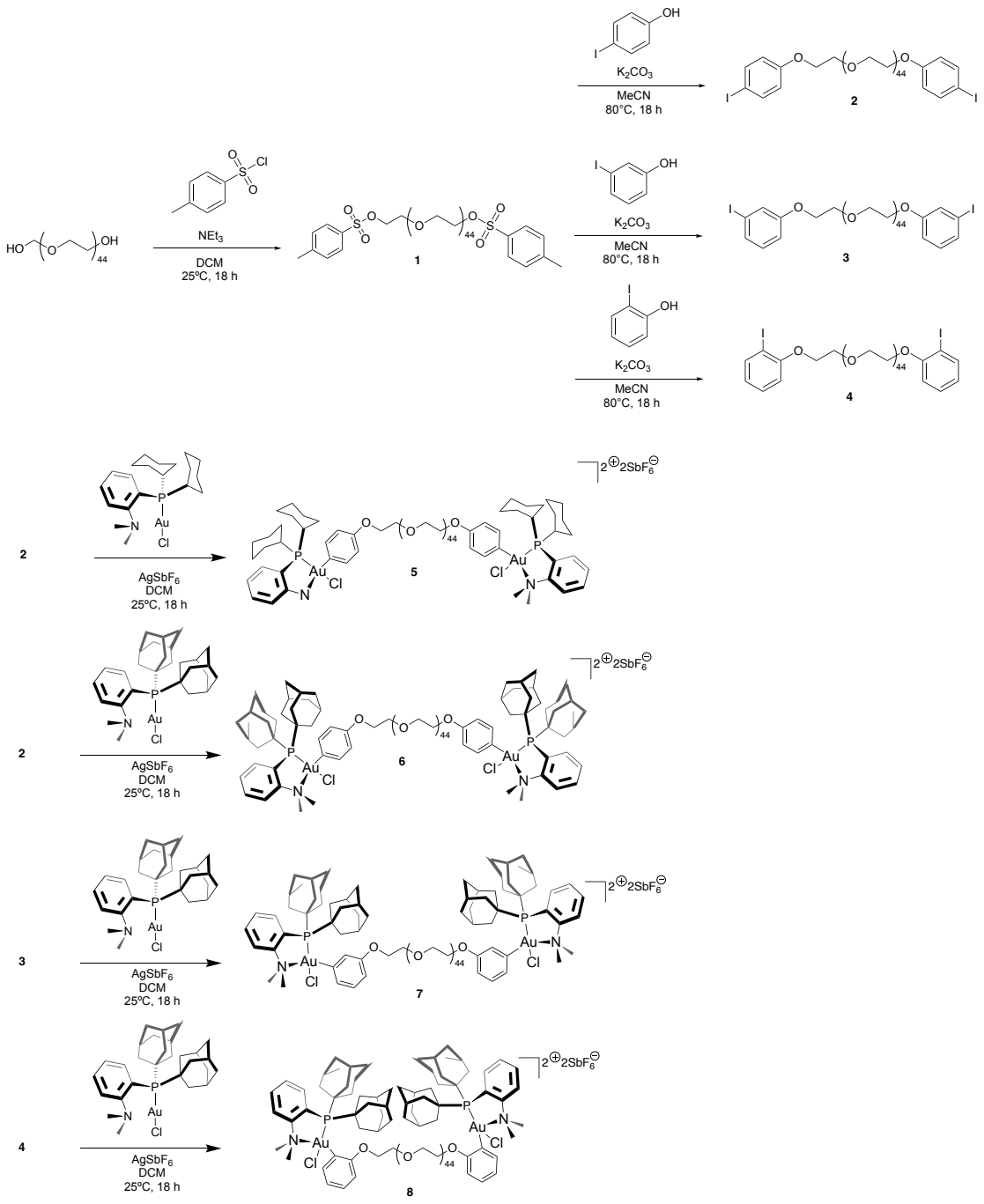

Figure 4.2. Synthetic approach towards a library of bifunctional Au (III) PEG_{2000}.

and both were tested.[28] The synthesis of a bifunctional dicyclohexyl Au (III) PEG_{2000} reagent (bis *para*- Au (III) $(Cy)_2$ $PEG_{2000,}$ **5**) was undertaken in 92% yield (**Figure 4.2**). Oxidative addition on **2** with (Me-DalPhos)AuCl yielded a bifunctional (Me-DalPhos) Au (III) PEG_{2000} reagent (bis *para*- Au (III) $(Ad)_2$ PEG_{2000}, **6)**. Additionally, we have recently demonstrated the ability to slow down the kinetics of S-arylation by sterically hindering the Au (III) sites.[30] Since the *para*- Au (III) position offers the greatest accessibility for reductive elimination (RE) of cysteines, we synthesized the *meta*- and *ortho*- Au(III) reagents from the respective 3-iodophenol and 2-iodophenol to afford **3** and **4**. OA of with (Me-DalPhos)AuCl **3** and **4** yielded Au (III) PEG_{2000} reagents **7** and **8**. We hypothesize **8** will provide the slowest conversion when exposed to FGF-2. This small toolbox of PEG_{2000} OA complexes was then used in the multimerization of FGF-2.

4.2.2 FGF-2 Multimerization by SDS-PAGE.

Before accessing higher order FGF-2 complexes, we utilized the mutant fibroblast growth factor 2 (mFGF-2) (C78S) to understand the dimerization conversion. Dimerization of mFGF-2 (2 eq) with **6** (1 eq) in Tris Buffer at pH 9.0 was monitored by SDS-PAGE, reaching 13 % after 1 h at 25 ºC (**Figure 4.3**). Due to the limited conversion of mFGF-2 to PEGylated dimer, the native FGF-2 was used for the future experiments.

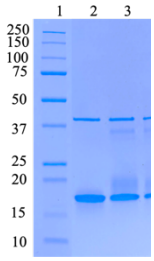

Figure 4.3. Dimerization of mFGF-2 (1 eq) with **6** (1 eq). Lane 1: ladder, Lane 2: mFGF-2, Lane 3: 60 min. By ImageJ optical densitometry, % Conversion from mFGF-2: 13 %.

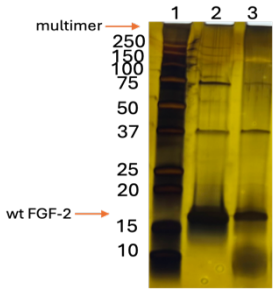

Figure 4.4. Conjugation of FGF-2 (1 eq) with **5** (1 eq). Lane 1: ladder, Lane 2: FGF-2, Lane 3: 1 min. By ImageJ optical densitometry, Lane 3 is 95% converted from the FGF-2 starting material.

RE of 1 eq of FGF-2 with 1 eq of **5** after 1 minute (**Figure 4.4**) gave 95% conversion of FGF-2 to multimeric structures by ImageJ optical densitometry analysis of SDS-PAGE exposed to silver stain. Due to the ultrafast kinetics of the (dicyclohexPhos)AuCl reagent, the multimeric complex of FGF-2 reached > 250 kDa by SDS-PAGE as indicated by the dark band at the top of the gel, visible by silver training. It is also possible these higher MW bands are due to aggregation of degraded products, as some protein degradation is observed in the gel below the FGF-2 band. RE of FGF-2 with 3 eq of **6** after 1 min yielded 76% conversion from monomeric FGF-2 with a distribution of dimer, pentamer, and multimers by SDS-PAGE (**Figure 4.20**). After 30 min (**Figure 4.5)**, monomeric FGF-2 was 91% converted to oligomeric structures, mostly visible by silver

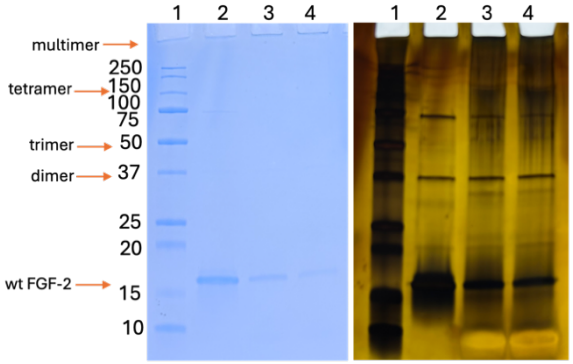

Figure 4.5. Conjugation of FGF-2 (1 eq) with **6** (3 eq). Lane 1: ladder, Lane 2: FGF-2, Lane 3: 10 min, Lane 4: 30 min. % Conversion from FGF-2: 83% Lane 3, 91% Lane 4.

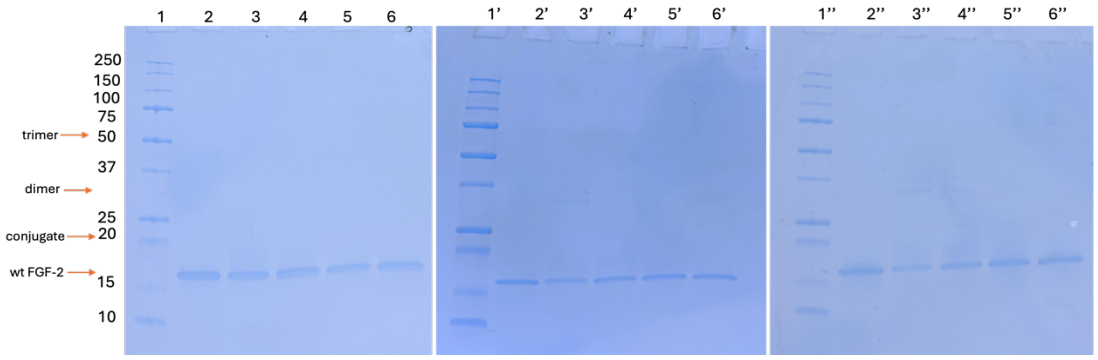

Figure 4.6. Equivalent screen of FGF-2 (1 eq) conjugation with **6** (2, 1, 0.5, or 0.25 eq) after 10 min (Lanes 1-6), 1 h (Lanes 1'-6'), 2 h (Lanes 1''-6''). Lane 1: ladder, Lane 2: FGF-2, Lane 3: 2 eq, Lane 4: 1 eq, Lane 5: 0.5 eq, Lane 6: 0.25 eq. % Conversion from FGF-2: 12% Lane 3, 6% Lane 4, 54% Lane 3', 26% Lane 4', 73% Lane 3'', 44% Lane 4'', 19% Lane 5'', 7% Lane 6''.

staining and quantified by ImageJ optical densitometry. Silver staining is a more sensitive staining technique compared to Coomassie, allowing the smaller multimeric complexes to be visible. The decreased band intensity of FGF-2 by Coomassie indicates that most of the FGF-2 converted to higher order multimeric complexes. Interestingly, the distribution between smaller oligomeric sizes was not equal. The highly reactive Au (III) reagents resulted in converion to higher order multimeric complexes. After 1 h with 3 eq of **6,** nearly quantitative conversion was reached with 99% of the monomeric FGF-2 converted to the highest order multimeric complex visible by the dark staining at the top of the gel **(Figure 4.21)**. Typically, with protein-polymer conjugation, excess polymer is added to increase conversion to the conjugate, however, we hypothesized adding excess protein, in this case, could help control the size of oligomeric complex. To 1 eq of FGF-2, 0.25- 2 eq of **6** was added and monitored over 2 h (**Figure 4.6**). After 10 min (**Lanes 1-6, Figure 4.6**), 12% conversion in Lane 3 was reached with 2 eq and 6% conversion in Lane 4 was reached with 1 eq. After 1 h (**Lanes 1'-6', Figure 4.6),** 54% conversion in Lane 3' was reached with 2 eq and 26% conversion in Lane 4' was reached with 1 eq. No conversion from monomeric FGF-2

was reached after 1 h with lower equivalents of 0.5 eq or 0.25 eq. However, after 2 h (**Lanes 1"-6", Figure 4.6**), the highest conversion was reached with 73% conversion in Lane 3", and improved conversion of 44% in Lane 4", 19% in Lane 5", and 7% in Lane 6". Not surprisingly, conversion from monomeric FGF-2 increased as the time of the reaction went on, and with higher equivalents of FGF-2. Silver staining of these conjugations was undertaken in attempt to visualize the multimeric structures (**Figure 4.22**).

Utilizing the more sterically hindered Au (III) PEG2000 reagents, OA with **8** and 7 at varying equivalents with time points up to 2 h was visualized by SDS-PAGE and % conversion only listed for the most converted lane for simplicity (**Figure 4.7**). A general trend was observed that with higher equivalents of polymer in this case and more time of either **8** or **7** yielded higher conversion of FGF-2. RE with 3 eq of **8** yielded 91% conversion after 1 h and 98% after 2 h and with 3 eq of **7** yielded 95% conversion after 1 h and 100% after 2 h. With these reagents, more mono conjugate is observed (FGF-2-PEG-Au (III)) before converting to higher order structures.

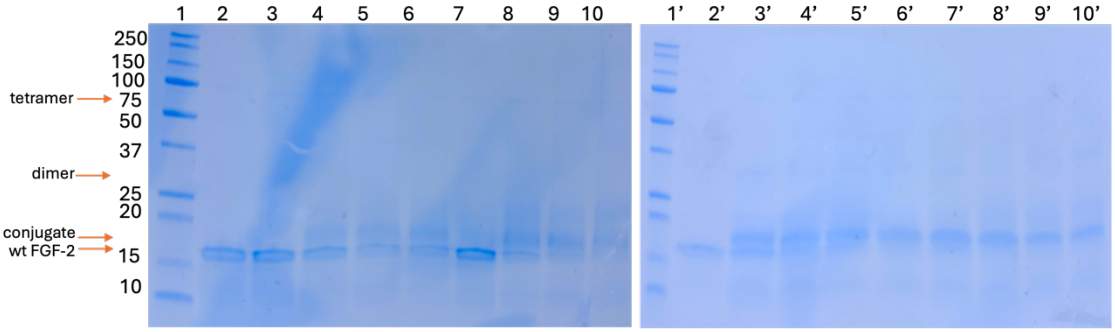

Figure 4.7. Equivalent screen of FGF-2 (1 eq) conjugation with **8** (Lanes 1-10) and **7** (Lanes 1'-10') (X eq) after X min. Lane 1: ladder, Lane 2: FGF-2, Lane 3: 1.3 eq 1 min, Lane 4: 1.3 eq 30 min, Lane 5: 1.3 eq 1 h, Lane 6: 1.3 eq 2 h, Lane 7: 3 eq 1 min, Lane 8: 3 eq 30 min, Lane 9: 3 eq 1 h, Lane 10: 3 eq 2 h. % Conversion from FGF-2: 91% Lane 9, 98% Lane 10, 95% Lane 9', 100% Lane 10'.

The multimeric conjugates are often smeared and therefore difficult to quantify. As a result, in all these cases, the decrease in FGF-2 in the SDS PAGE was quantified. Therefore, it cannot be certain that FGF-2 is converted completely into multimeric species. It could be that the FGF-2-polymer conjugate was formed (single protein) and this was observed in some cases. Or it could be that FGF-2 had degraded: after 1 h at 25 ºC, FGF-2 becomes susceptible to degradation and aggregation. Therefore, the balance between increasing conversion and preserving FGF-2 is a challenge. It can be concluded that control over the size of multimers formed utilizing bifunctional Au (III) reagents with equal reactivity will be difficult due to the accessibility of both Cys78 and Cys96 and reactivity of our reagents. Therefore, this approach was not pursued further. However, the work did provide interesting Au(III)-PEG-Au(III) linkers that could be utilized for dimerization of a mutant FGF-2 that contains one free cysteine or another proteins with free thiols.

4.3 Conclusion

Herein, multimeric complexes of FGF-2 utilizing Au (III) bifunctional PEG_{2000} linkers with a range of reactivity were synthesized and monitored by SDS-PAGE. Complete conversion of monomeric FGF-2 to multimers with sizes above 250 kDa, corresponding to oligomers of more than 7 FGF-2 units, was observed with 1 equivalent the of the (dicyclohexPhos)AuCl reagent, **5**, within 1 min. To slow multimer formation, the (Me-DalPhos)AuCl reagent was utilized, and by varying equivalents of **6**, 54% conversion was reached with 2 equivalents and 26% conversion with 1 equivalent after 1 h. For reagents **7** and **8**, 3 equivalents after 1 h yielded 95% and 91% conversion, however these reagents mostly converted to mono-conjugate rather than higher order structures. In conclusion, higher order oligomeric structures were synthesized and control over size was difficult to achieve.

4.4 Experimental

4.4.1 Materials

Unless otherwise noted, all materials were of analytical grade and purchased and used as received from Fisher Scientific, Acros Organics, Oakwood Chemicals or Sigma Aldrich. The silver hexafluoroantimonate ($AgSbF_6$) was stored in the glovebox under an atmosphere of N_2 and removed prior to use. Milli-Q water was used for all experiments. Fisher Water Optima™ LC-MS Grade and Fisher Acetonitrile Optima™ LC-MS Grade were used exclusively for LC-MS mobile phase solvents. Protein was expressed and purified from the plasmid pET29c(+)hFGF-2, which was kindly provided by Professor Thomas Scheper from the Helmholtz Centre for Infection Research (Braunschweig, Germany) according to Chen et al.[31]

4.4.2 Analytical Techniques

NMR spectra were recorded on AV 400 Bruker spectrometers at 400 MHz (^1H) and 121 MHz ($^{31}P\{^1H\}$). Spectra are reported in δ (parts per million) relative to residual proteo-solvent signals for ^1H and H_3PO_4 (δ 0.00 ppm) for $^{31}P\{^1H\}$. Deuterated solvents (Cambridge Isotope Laboratories) were used for all NMR experiments. ^1H NMR spectra for all polymers, spectra were acquired with a relaxation delay of 4 seconds. Data was analyzed using MestRenova v12 software. A Biotage Isolera Prime equipped with KP-SNAP Ultra Biotage columns was used for all flash column chromatography.

Protein and protein conjugates were purified by FPLC on a Bio-Rad BioLogic DuoFlow chromatography system. All purifications were carried out at 4 °C. All buffers were freshly prepared and filtered over a Thermo Scientific Nalgene 565-0020 Filter Unit, 0.2um PES prior to use. Size exclusion chromatography (SEC) purifications were performed using a Superdex 75 Increase 10/300 GL column. All protein purifications were monitored at wavelengths of 254 nm and 280 nm. A standard isocratic method was used for all sampled (20 mM Tris, 150 mM NaCl

buffer, pH 7.5 over 50 minutes). Protein concentration measurements were determined on a NanoDrop 2000 UV-Vis spectrophotometer at 280 nm (Extinction coefficient = 16,055 M^{-1} cm^{-1}).

Sodium dodecyl sulfate-polyacrylamide gel electrophoresis (SDS-PAGE) was carried out in a Mini-PROTEAN Tetra Cell system (Bio-Rad) connected to a PowerPac HC (BioRad) power supply using Bio-Rad Any kD™ Mini-PROTEAN® TGX™ Precast Gels at 195 V and 3 A for 30 minutes in a running buffer (25 mM Tris, 192 mM Glycine, 0.1% (w/v) SDS, pH 8.3). Precision Plus Protein™ Dual Xtra Prestained Protein Standards (2 µL) were used as protein ladder in all SDS-PAGE analysis. Laemmli 2x Concentrate (Sigma) containing 4% SDS, 20% glycerol, 0.004% bromophenol blue and 0.125 M Tris HCl at a pH of approximately 6.8 was used to load all protein and conjugate samples. Protein bands were visualized by staining the gels in an aqueous solution (0.1% Coomassie Brilliant Blue R 250, 45% MeOH, 9% acetic acid) and microwaving for 30 seconds followed by agitation for 15 minutes. Destaining was carried out by submerging the gels in an aqueous destaining solution (10% MeOH, 14% acetic acid), microwaving for 30 seconds, and agitating for several hours until the background of the gel became fully destained. ImageJ was used to calculate conversion by optical densitometry.

4.4.3 Methods

Synthesis of ditosyl PEG_{2000} (1)

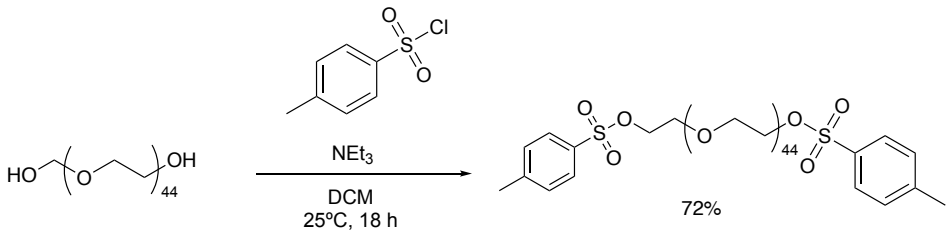

Adapted from Montgomery, et. al.[26] PEG_{2000} dihydroxy (1000 mg, 1 eq) was added to a round bottom equipped with a stir bar and DCM (10 mL). TEA (151.8 mg, 209 µL, 3 eq) was added slowly, stirred for 5 min, and subsequently cooled to 0 °C. 4-methylbenzenesulfonyl

chloride (286.0 mg, 3 eq) was dissolved in DCM (10 mL) and added dropwise to the reaction flask. The reaction was allowed to warm to 25 ºC and stir for 16 h. The reaction was concentrated under reduced pressure. The off-white sticky solid was dissolved in minimal DCM and purified by precipitation in ice cold diethyl ether 3 times. The white precipitate was dried by vacuum. ^{1}H NMR (300 MHz, $CDCl_3$) δ 7.76 (dd, J = 7.8, 5.9 Hz, 4H), 7.35 – 7.29 (m, 3H), 7.17 – 7.12 (m, 1H), 4.15 – 4.10 (m, 3H), 3.62 (s, 180H), 3.34 (s, 1H), 2.42 (s, 5H).

Synthesis of bis *para*-iodobenzene PEG$_{2000}$ (2)

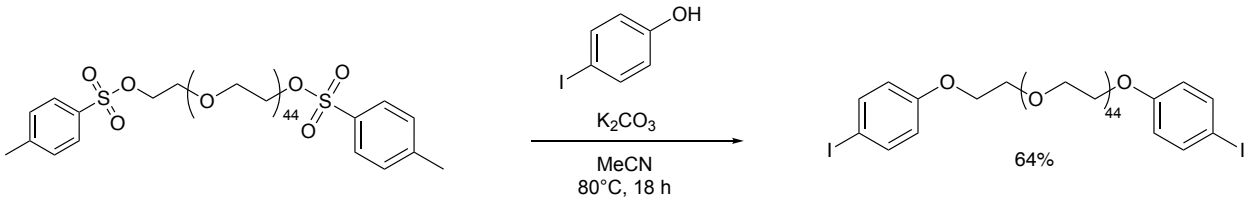

Adapted from Montgomery, et. al.[26] Ditosyl PEG$_{2000}$ (300 mg, 1 eq) and 4-iodophenol (278 mg, 10 eq) were added to an oven-dried round bottom flask with an appropriately sized stir bar and were dissolved in anhydrous MeCN (10 mL). To this solution was added K_2CO_3 (175 mg, 10 eq) while stirring. The reaction mixture was heated to 80 °C and was stirred for 12 hours at reflux. The solvent was removed under reduced pressure to afford an orange oil. The crude mixture was dissolved in DCM and filtered to remove excess carbonate. The DCM was removed under vacuum and the remaining solids were dissolved in a small amount of water, and the basic solution was neutralized to pH 7-8 with 1 M NH_4OAc buffer. The aqueous solution was removed on the lyophilizer to provide white solids. These solids were resuspended in DCM and filtered to remove undissolved salts. The DCM solution was concentrated under reduced pressure and precipitated from cold diethyl ether three times. The Biotage was then run using 100% DCM to elute the aryl/tosyl peaks and then a gradient to 10% MeOH to elute the product as a white solid. ^{1}H NMR

(400 MHz, $CDCl_3$) δ 7.58 – 7.50 (m, 4H), 6.73 – 6.67 (m, 3H), 4.08 (dd, *J* = 5.7, 4.0 Hz, 4H), 3.89 – 3.79 (m, 5H), 3.64 (s, 160H).

Synthesis of bis *meta*-iodobenzene PEG_{2000} (3)

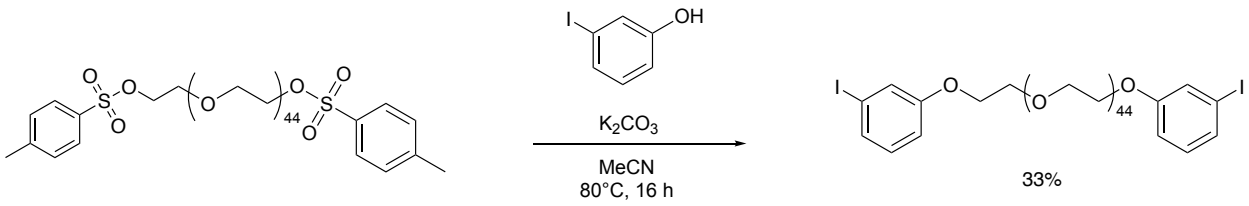

Ditosyl PEG_{2000} (300 mg, 1 eq) and 3-iodophenol (278 mg, 10 eq) were added to an oven-dried round bottom flask with an appropriately sized stir bar and were dissolved in anhydrous MeCN (10 mL). To this solution was added K_2CO_3 (175 mg, 10 eq) while stirring. The reaction mixture was heated to 80 °C and was stirred for 12 hours at reflux. The solvent was removed under reduced pressure to afford an orange oil. The crude mixture was dissolved in DCM and filtered to remove excess carbonate. The DCM was removed under vacuum and the remaining solids were dissolved in a small amount of water, and the basic solution was neutralized to pH 7-8 with 1 M NH_4OAc buffer. The aqueous solution was removed on the lyophilizer to provide white solids. These solids were resuspended in DCM and filtered to remove undissolved salts. The DCM solution was concentrated under reduced pressure and precipitated from cold diethyl ether three times. The biotage was then run using 100% DCM to elute the aryl/tosyl peaks and then a gradient to 10% MeOH to elute the product as a white solid. ^1H NMR (400 MHz, CD_3CN) δ 7.28 (ddd, *J* = 4.7, 2.1, 0.8 Hz, 2H), 7.02 (t, *J* = 8.2 Hz, 1H), 6.91 (ddd, *J* = 8.3, 2.4, 1.0 Hz, 1H), 4.09 – 4.03 (m, 2H), 3.75 – 3.71 (m, 2H), 3.70 – 3.38 (m, 142H).

Synthesis of bis *ortho*-iodobenzene PEG_{2000} (4)

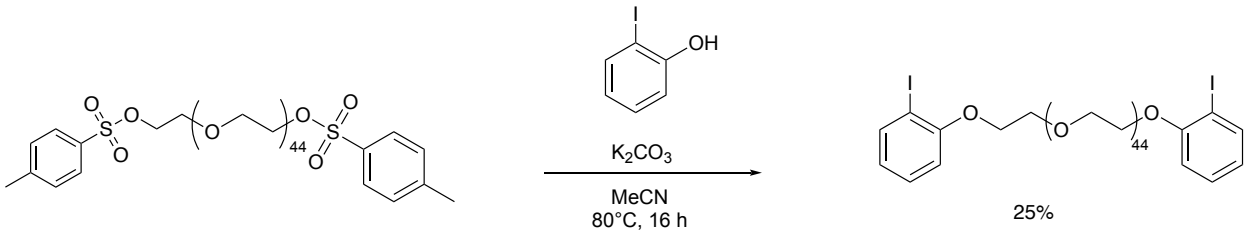

Ditosyl PEG_{2000} (300 mg, 1 eq) and 2-iodophenol (278 mg, 10 eq) were added to an oven-dried round bottom flask with an appropriately sized stir bar and were dissolved in anhydrous MeCN (10 mL). To this solution was added K_2CO_3 (175 mg, 10 eq) while stirring. The reaction mixture was heated to 80 °C and was stirred for 12 hours at reflux. The solvent was removed under reduced pressure to afford an orange oil. The crude mixture was dissolved in DCM and filtered to remove excess carbonate. The DCM was removed under vacuum and the remaining solids were dissolved in a small amount of water, and the basic solution was neutralized to pH 7-8 with 1 M NH_4OAc buffer. The aqueous solution was removed on the lyophilizer to provide white solids. These solids were resuspended in DCM and filtered to remove undissolved salts. The DCM solution was concentrated under reduced pressure and precipitated from cold diethyl ether three times. The biotage was then run using 100% DCM to elute the aryl/tosyl peaks and then a gradient to 10% MeOH to elute the product as a white solid. ^{1}H NMR (400 MHz, CD_3CN) δ 4.15 – 4.09 (m, 5H), 3.84 – 3.78 (m, 5H), 3.55 – 3.47 (m, 296H), 3.35 (s, 1H).

Synthesis of bis *para*-Au (III) $(Cy)_2$ PEG_{2000} (5)

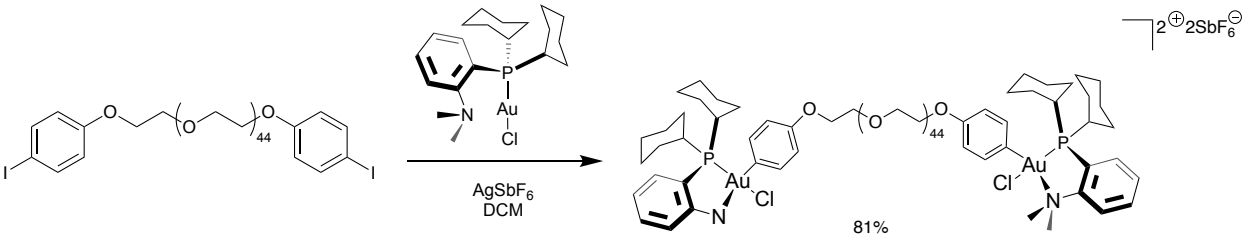

Adapted from Montgomery, et. al.[26] $AgSbF_6$ (5.9 mg, 3.5 eq) was added to a one dram vial in the glovebox in the absence of light. This was removed from the glovebox, electrical taped, and

charged with a stir bar. 500 µL of DCM was added to the vial, creating a clear solution. Separately, Au(I) cyclohexyl (9.5 mg, 3.5 eq) and **2** (12.0 mg, 1 eq) were weighed out into a one-dram vial. This was dissolved in 500 µL of DCM, creating a clear solution. Both reaction vials were added to the -20ºC freezer for 1 min. The contents of the Au/ArI vial were transferred to the silver vial and stirred at 25ºC for 18 h. The dark yellow/orange mixture was filtered through Celite, washing with DCM, and concentrated under vacuum to yield an orange oil. There was residual green material on the Celite. The concentrated orange oil was dissolved in minimal DCM and precipitated in diethyl ether three times. The material was concentrated under vacuum to yield an orange oil. ^{1}H NMR (400 MHz, $CDCl_3$) δ 7.96 – 7.84 (m, 8H), 7.79 (d, *J* = 7.9 Hz, 3H), 7.55 – 7.50 (m, 2H), 7.12 (d, *J* = 8.6 Hz, 5H), 7.00 – 6.94 (m, 5H), 6.72 – 6.65 (m, 2H), 4.16 (dd, *J* = 5.7, 3.7 Hz, 5H), 4.08 (dd, *J* = 5.7, 4.0 Hz, 3H), 3.91 – 3.81 (m, 10H), 3.64 (s, 254H), 3.44 (s, 23H), 2.74 (d, *J* = 12.2 Hz, 5H), 1.75 (d, *J* = 38.8 Hz, 28H), 1.47 – 1.03 (m, 21H), 0.76 (d, *J* = 12.9 Hz, 6H). ^{31}P NMR (162 MHz, $CDCl_3$) δ 60.21.

Synthesis of bis *para*-Au (III) $(Ad)_2$ PEG_{2000} (6)

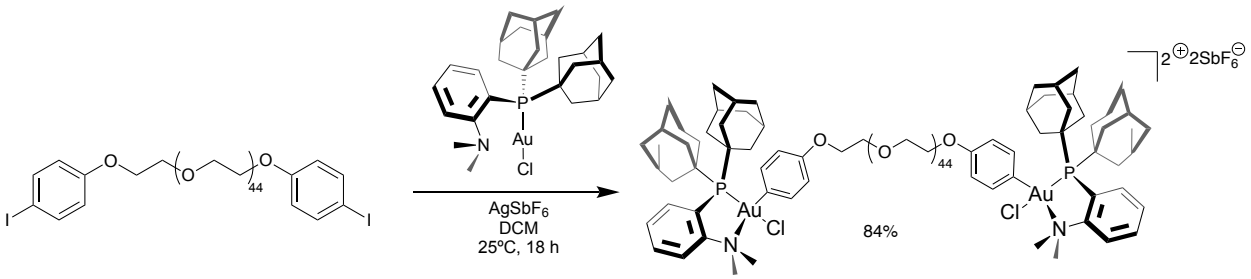

$AgSbF_6$ (25.6 mg, 3.5 eq) was added to a one-dram vial in the glovebox in the absence of light. This was removed from the glovebox, electrical taped, and charged with a stir bar. 500 µL of DCM was added to the vial, creating a clear solution. Separately, Me-DalPhos)AuCl (48.8 mg, 3.5 eq) and **2** (30.0 mg, 1 eq) were weighed out into a one-dram vial. This was dissolved in 500 µL of DCM, creating a clear solution. Both reaction vials were added to the -20ºC freezer for 1

min. The contents of the Au/ArI vial were transferred to the silver vial and stirred at 25ºC for 18 h. The dark yellow/orange mixture was filtered through Celite, washing with DCM, and concentrated under vacuum to yield a yellow oil. There was residual green material on the Celite. The concentrated orange oil was dissolved in minimal DCM and precipitated in diethyl ether three times. The material was concentrated under vacuum to yield a yellow oil.[1]H NMR (400 MHz, $CDCl_3$) δ 8.04 – 7.89 (m, 6H), 7.77 (s, 2H), 7.31 (d, J = 8.9 Hz, 38H), 6.92 (d, J = 8.7 Hz, 4H), 4.15 (t, J = 4.7 Hz, 4H), 3.90 – 3.85 (m, 4H), 3.65 (s, 177H), 2.25 (d, J = 8.3 Hz, 12H), 2.11 (s, 27H), 1.75 (s, 25H). [31]P NMR (162 MHz, $CDCl_3$) δ 77.76.

Synthesis of bis *meta*-Au (III) $(Ad)_2$ PEG_{2000} (7)

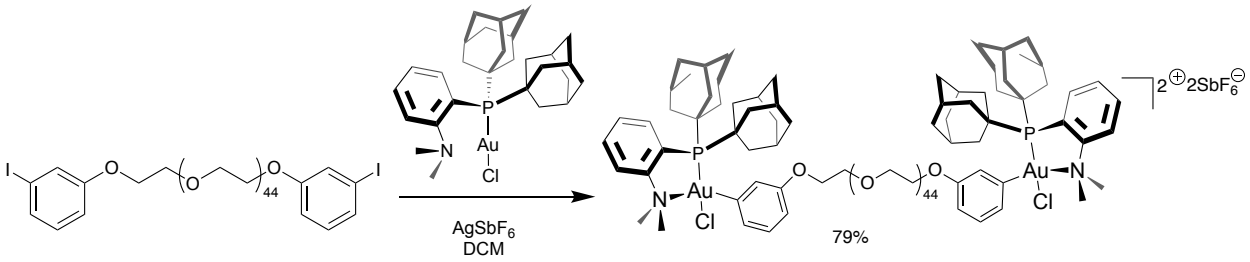

$AgSbF_6$ (25.6 mg, 3.5 eq) was added to a one-dram vial in the glovebox in the absence of light. This was removed from the glovebox, electrical taped, and charged with a stir bar. 500 µL of DCM was added to the vial, creating a clear solution. Separately, Me-DalPhos)AuCl (48.8 mg, 3.5 eq) and **3** (30.0 mg, 1 eq) were weighed out into a one-dram vial. This was dissolved in 500 µL of DCM, creating a clear solution. Both reaction vials were added to the -20ºC freezer for 1 min. The contents of the Au/ArI vial were transferred to the silver vial and stirred at 25ºC for 18 h. The dark yellow/orange mixture was filtered through Celite, washing with DCM, and concentrated under vacuum to yield a yellow oil. There was residual green material on the Celite. The concentrated orange oil was dissolved in minimal DCM and precipitated in diethyl ether three times. The material was concentrated under vacuum to yield a yellow solid. [1]H NMR

(400 MHz, Acetone) δ 8.37 – 8.32 (m, 1H), 8.27 – 8.21 (m, 1H), 7.33 – 7.21 (m, 3H), 6.91 – 6.83 (m, 1H), 4.16 (q, *J* = 5.1 Hz, 3H), 3.87 – 3.29 (m, 170H), 2.79 (d, *J* = 12.9 Hz, 14H), 2.49 (s, 9H), 2.27 (s, 11H), 1.84 (t, *J* = 11.6 Hz, 8H), 1.74 (d, *J* = 13.3 Hz, 10H). ^{31}P NMR (162 MHz, Acetone) δ 74.49.

Synthesis of bis *ortho*-Au (III) (Ad)$_2$ PEG$_{2000}$ (8)

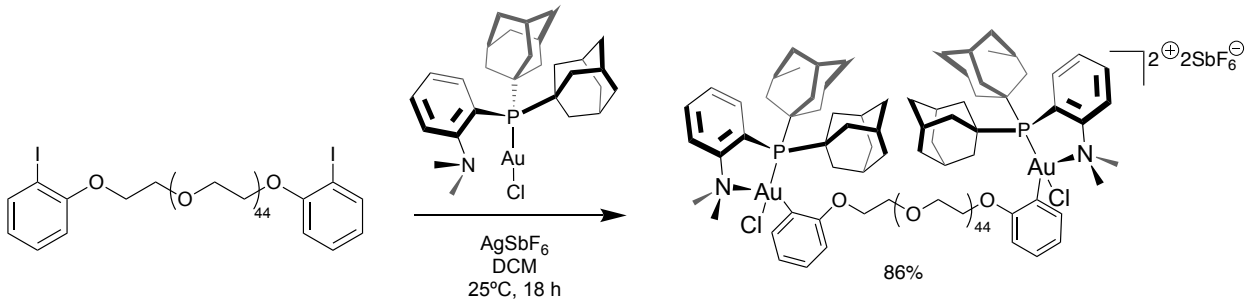

$AgSbF_6$ (25.6 mg, 3.5 eq) was added to a one-dram vial in the glovebox in the absence of light. This was removed from the glovebox, electrical taped, and charged with a stir bar. 500 µL of DCM was added to the vial, creating a clear solution. Separately, Me-DalPhos)AuCl (48.8 mg, 3.5 eq) and **4** (30.0 mg, 1 eq)) were weighed out into a one-dram vial. This was dissolved in 500 µL of DCM, creating a clear solution. Both reaction vials were added to the -20ºC freezer for 1 min. The contents of the Au/ArI vial were transferred to the silver vial and stirred at 25ºC for 18 h. The dark yellow/orange mixture was filtered through Celite, washing with DCM, and concentrated under vacuum to yield a yellow oil. There was residual green material on the Celite. The concentrated orange oil was dissolved in minimal DCM and precipitated in diethyl ether three times. The material was concentrated under vacuum to yield a dark orange oil. ^{1}H NMR (400 MHz, Acetone) δ 8.44 – 8.33 (m, 1H), 8.33 – 8.23 (m, 1H), 8.14 – 8.05 (m, 1H), 7.84 (ddd, *J* = 8.7, 7.1, 2.1 Hz, 1H), 7.60 – 7.51 (m, 1H), 7.37 – 7.26 (m, 1H), 7.09 – 7.02 (m, 1H), 7.00 (dd, *J* = 8.1, 1.4 Hz, 1H), 4.47 – 4.40 (m, 1H), 3.96 – 3.55 (m, 129H), 3.48 – 3.32 (m, 5H), 2.46 (t, *J* = 25.4 Hz, 10H), 2.17 (q, *J* = 3.5 Hz, 4H), 2.00 – 1.86 (m, 8H), 1.74 (dt, *J* = 37.4, 13.6 Hz, 11H).

^{31}P NMR (162 MHz, Acetone) δ 78.03, 69.09.

Mutant Basic Fibroblast Growth Factor 2 (mFGF-2 C78S) Protein Expression

Mutant FGF-2 (mutant C78S) protein expression and purification were adapted from literature procedures.6 mFGF-2 Sequence (Calculated Mass: 17106.36 Da): MAAGSITTLPALPEDGGSGAFPPGHFKDPKRLYCKNGGFFLRIHPDGRVDGVREKSDPHI KLQLQAEERGVVSIKGVCANRYLAMKEDGRLLASKCVTDECFFFERLESNNYNTYRSR KYTSWYVALKRTGQYKLGSKTGPGQKAILFLPMSAKS. Protein was expressed and purified from the plasmid pET29c(+)hFGF-2, which was kindly provided by Professor Thomas Scheper from the Helmholtz Centre for Infection Research (Braunschweig, Germany) according previously published literature.6 To each of two 5 mL of a saturated 18 hour culture inoculated from a glycerol stock. The culture was grown at 30 °C with 250 rpm shaking for about 6 hours before the OD600 reached ~0.75 and the culture was induced with 1 mM IPTG. The culture was continued to shake at 37 °C at 250 rpm for approximately 2 hours. The cultures were harvested by centrifugation at 4000 rpm for 15 min to yield a cell pellet. Cell pellets were frozen at -80ºC until further purified. To further purify, cells were suspended in lysis buffer (25 mM phosphate buffer, pH 7.5, 100 mM NaCl, 0.25 g/L MgCl2(7H2O), 3 mM DTT and 1 mM EDTA) at 40 g/L dry cell mass, and 1 protease inhibitor cocktail tablet per 50 mL at 25ºC for 15 min. Cells were homogenized. cells were centrifuged for 1 hour at 17,000G and 4 °C. The supernatant was loaded onto a 5 mL heparin Sepharose drip column. The supernatant was passed through the column 3 times and incubated at 4ºC for 12 h. The column was then washed with three column volumes of elution buffer (25 mM sodium phosphate buffer, pH 7.5, 3 mM DTT, 1 mM EDTA, and 0, 1.5 or 2 M NaCl) to elute the desired protein. SDS-PAGE was run on all fractions and under reducing conditions with Coomassie Blue staining. Pure fractions were combined, and solvent exchanged into storage buffer

(20 mM PBS, pH 6.5) and concentrated to ~15 mL using a using Amicon 3K Ultra-15 Centrifugal Filter (Millipore). Protein was further purified by preparative SEC FPLC using an isocratic method in 20 mM Tris-HCl buffer pH 7.5. Pure fractions were concentrated and stored in storage buffer (20 mM Tris-HCl buffer pH 9.0, 150 mM NaCl). The purified protein was analyzed by LC-MS and SDS-PAGE confirming sample purity and molecular weight. Concentration was determined by A280 (Extinction coefficient = 18,055 M-1 cm-1) The protein sample was diluted with storage buffer to 76 μM and aliquots were flash frozen and stored in a –80 °C freezer.

Basic Fibroblast Growth Factor 2 (wild type FGF-2) Expression

FGF-2 (wt) protein expression and purification were adapted from literature procedures.[31] Wt FGF-2 Sequence (Calculated Mass: 17691.55 Da): MAAGSITTLPALPEDGGSGAFPPGHFKDPKRLYCKNGGFFLRIHPDGRVDGVREKSDPHI KLQLQAEERGVVSIKGVCANRYLAMKEDGRLLASKCVTDECFFFERLESNNYNTYRSR KYTSWYVALKRTGQYKLGSKTGPGQKAILFLPMSAKS. Protein was expressed and purified from the plasmid pET29c(+)hFGF-2, which was provided by Professor Thomas Scheper from the Helmholtz Centre for Infection Research (Braunschweig, Germany) according previously published literature.[31] To each of two 5 mL of a saturated 18 hour culture inoculated from a glycerol stock. The culture was grown at 30 °C with 250 rpm shaking for about 6 hours before the OD600 reached ~0.75 and the culture was induced with 1 mM IPTG. The culture was continued to shake at 37 °C at 250 rpm for approximately 2 hours. The cultures were harvested by centrifugation at 4000 rpm for 15 min to yield a cell pellet. Cell pellets were frozen at -80ºC until further purified. To further purify, cells were suspended in lysis buffer (25 mM phosphate buffer, pH 7.5, 100 mM NaCl, 0.25 g/L $MgCl_2(7H_2O)$, 3 mM DTT and 1 mM EDTA) at 40 g/L dry cell mass, and 1 protease inhibitor cocktail tablet per 50 mL at 25ºC for 15 min. Cells were

homogenized. cells were centrifuged for 1 hour at 17,000G and 4°C. The supernatant was loaded onto a 5 mL heparin Sepharose drip column. The supernatant was passed through the column 3 times and incubated at 4ºC for 12 h. The column was then washed with three column volumes of elution buffer (25 mM sodium phosphate buffer, pH 7.5, 3 mM DTT, 1 mM EDTA, and 0, 1.5 or 2M NaCl) to elute the desired protein. SDS-PAGE was run on all fractions and under reducing conditions with Coomassie Blue staining. Pure fractions were combined, and solvent exchanged into storage buffer (20 mM PBS, pH 6.5) and concentrated to ~15 mL using a using Amicon 3K Ultra-15 Centrifugal Filter (Millipore). Protein was further purified by preparative SEC FPLC using an isocratic method in 20 mM Tris-HCl buffer pH 7.5. Pure fractions were concentrated and stored in storage buffer (20 mM Tris-HCl buffer pH 9.0, 150 mM NaCl). The purified protein was analyzed by LC-MS and SDS-PAGE confirming sample purity and molecular weight. Concentration was determined by A280 (Extinction coefficient = 16,055 M^{-1} cm^{-1}) The protein sample was diluted with storage buffer to 76 μM and aliquots were flash frozen and stored in a –80 °C freezer.

Representative Reductive Elimination Experiment of FGF-2 with Au(III) linkers

Adapted from previously reported literature.[26] 50 μL of a solution of 76 μM FGF-2 in 20 mM Tris-HCl buffer pH 9.0, 150 mM NaCl (1 eq) was reduced with 5 μL of a 3mM sock solution of TCEP•HCl (4 eq) in MilliQ H_2O at 25ºC for 1 h to reduce disulfide bonds formed during storage. Then, 5 μL of a X mM (0.19, 0.38, 0.76, 0.99, 1.1, 1.5, or 1.8 mM) stock solution of Au(III) PEG reagent (0.25, 0.5, 1, 1.3, 1.5, 2, 3 equivalents, respectively) in MeCN was added, gently flicked to mix and allowed to react for one minute at 25ºC. After one minute, the reaction was stopped by dilution in appropriate media for analysis (see below).

Representative SDS-PAGE Procedure

After X min, 1 µL of the reaction mixture was diluted into 19 µL Laemmli loading buffer (5% BME) in preparation for SDS-PAGE analysis. Samples were loaded onto SDS-PAGE gel and run at 195 V for 30 min and Coomassie stained and/or silver stained. Approximate sizes of PEGylated FGF-2 complexes: FGF-PEG_{2000}: 19.2 kDa, Dimer: 36.4 kDa, Dimer + PEG_{2000}: 38.4 kDa, Trimer: 55.6 kDa, Trimer + PEG_{2000}: 57.6 kDa, Tetramer: 74.8 kDa, Tetramer + PEG_{2000}: 76.8 kDa, Pentamer FGF: 94.0 kDa, Pentamer FGF + PEG_{2000}: 96.0 kDa, Hexamer FGF: 113.2 kDa, Hexamer FGF+ PEG_{2000}: 115.2 kDa, Heptamer FGF: 132.4 kDa, Heptamer FGF + PEG_{2000}: 134.4 kDa.

4.5 Appendix III

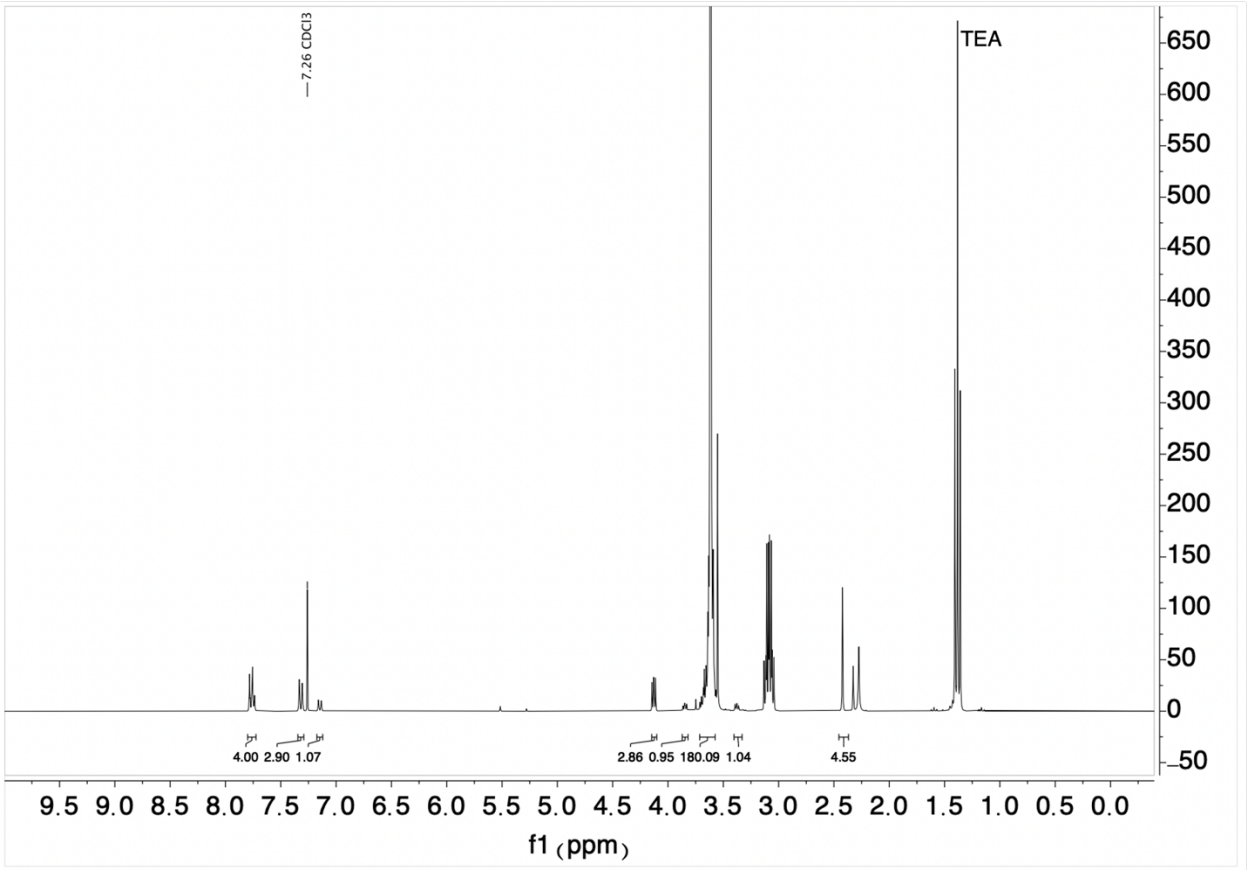

Figure 4.8. ^1H NMR spectrum of ditosyl PEG_{2000} (400 MHz in $CDCl_3$).

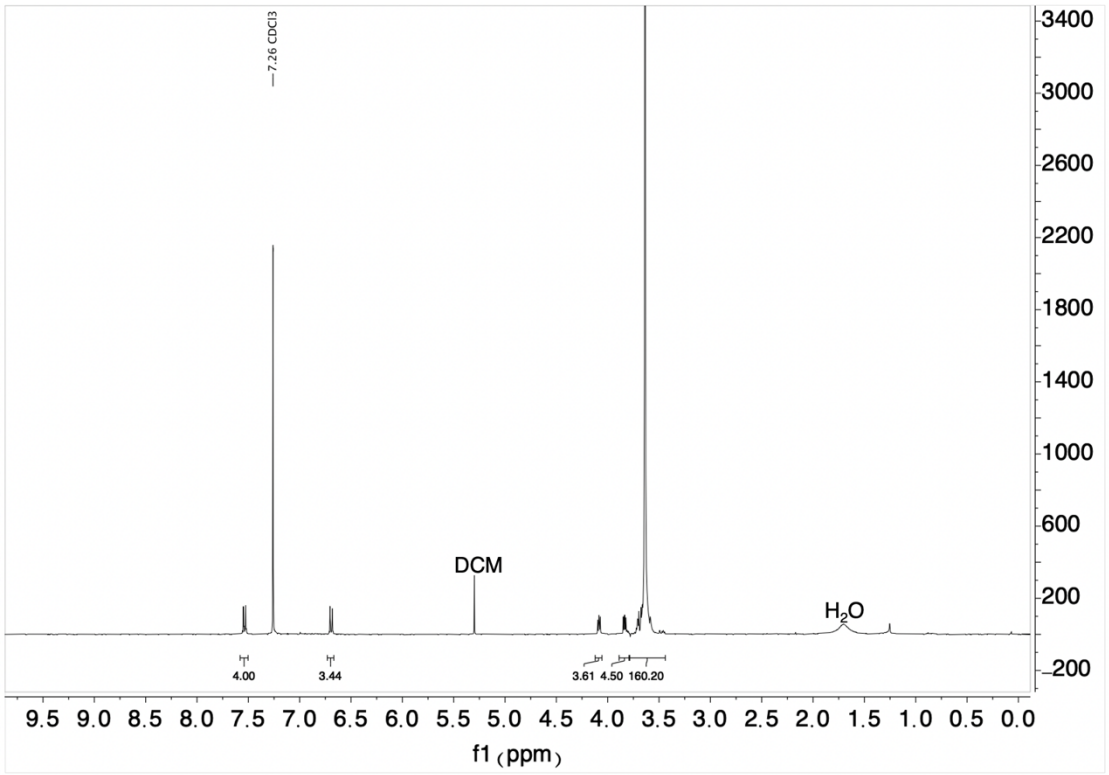

Figure 4.9. ^{1}H NMR spectrum of bis *para*- diiodobenzene- PEG_{2000} (400 MHz in $CDCl_3$).

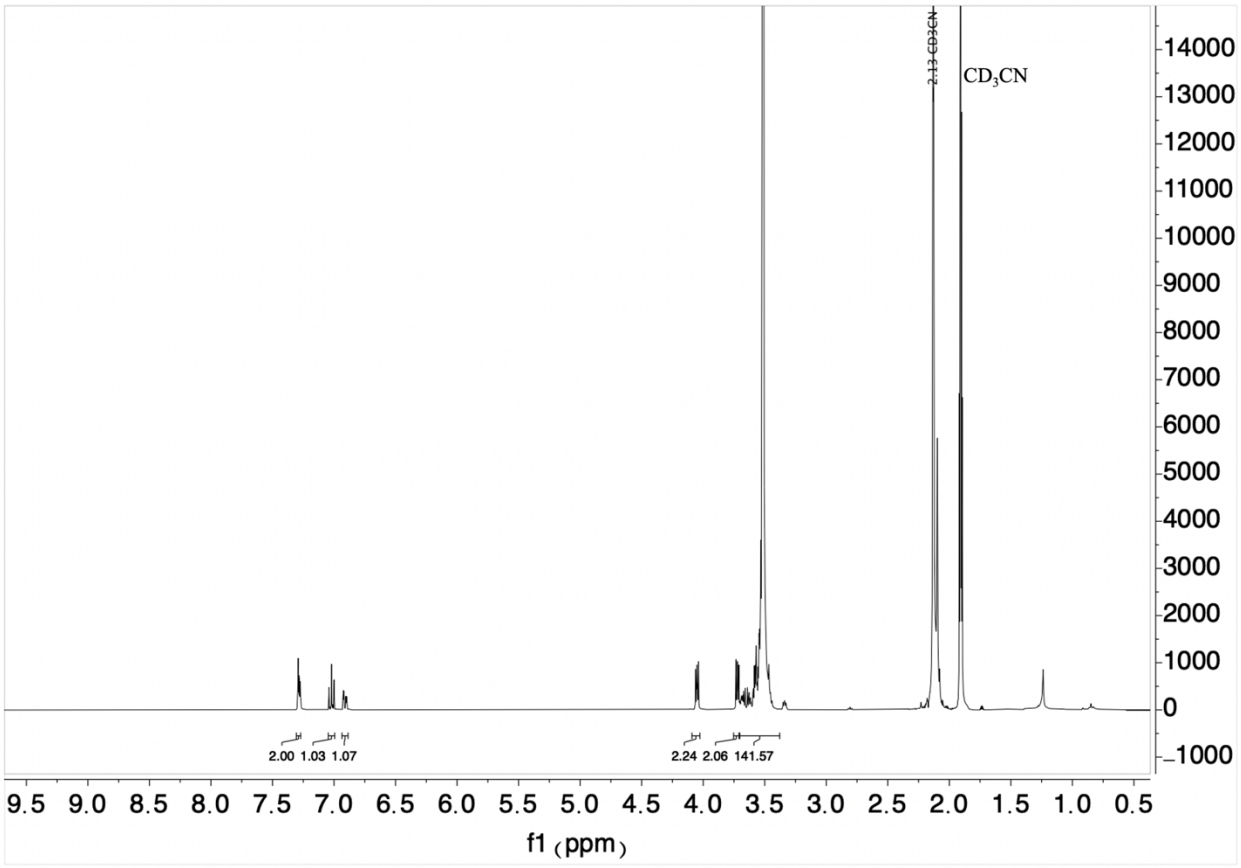

Figure 4.10. ^{1}H NMR spectrum of bis *meta*- diiodobenzene-PEG_{2000} (400 MHz in CD_3CN).

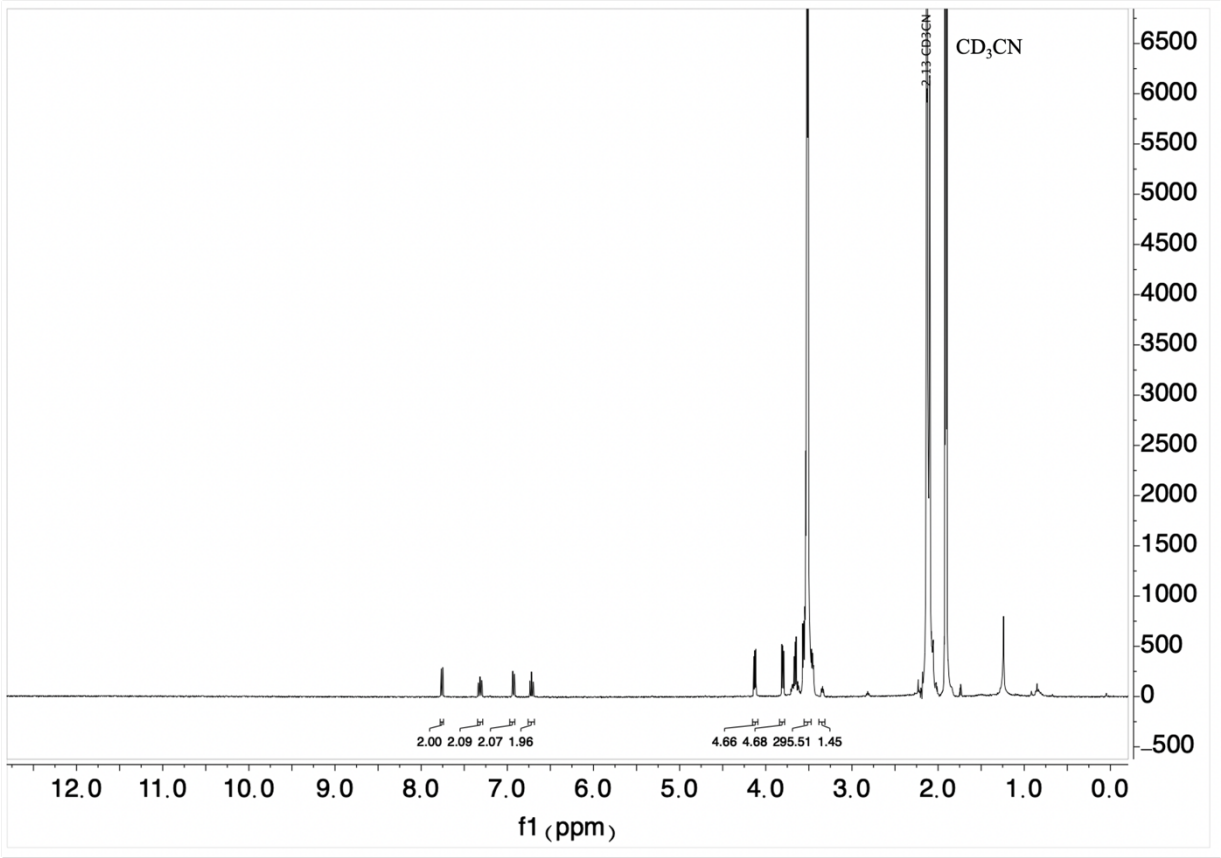

Figure 4.11. ^{1}H NMR spectrum of bis *ortho*- diiodobenzene- PEG_{2000} (400 MHz in CD_3CN).

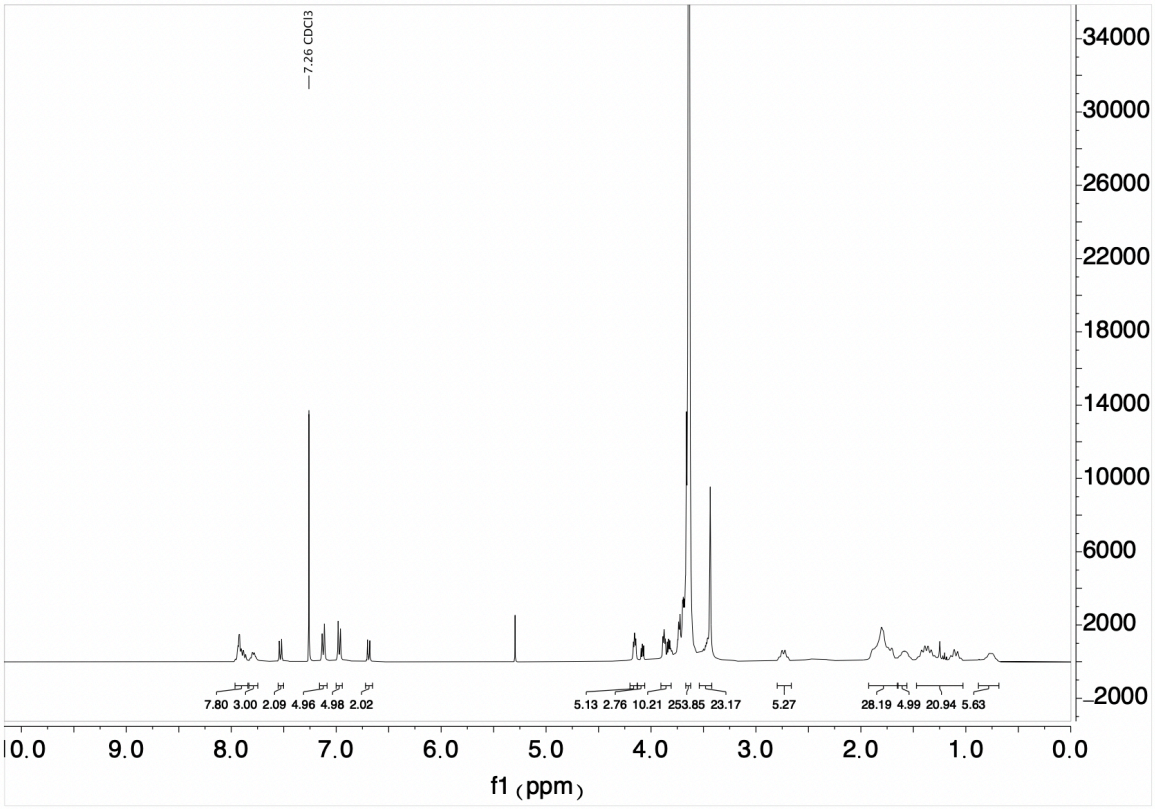

Figure 4.12. ^{1}H NMR spectrum of bis *para*- Au (III) $(Cy)_2$ PEG_{2000} (400 MHz in $CDCl_3$).

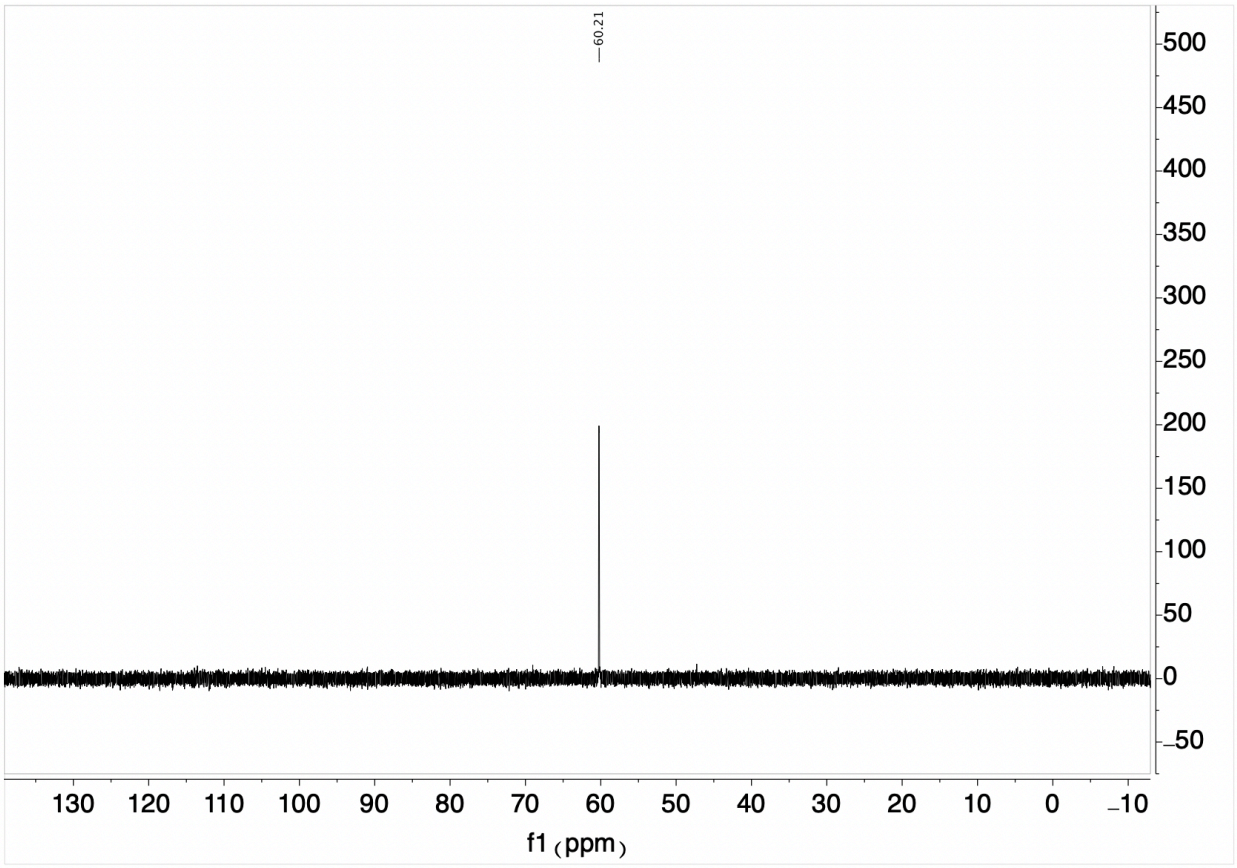

Figure 4.13. ^{31}P NMR spectrum of bis *para*- Au (III) $(Cy)_2$ PEG_{2000} (400 MHz in $CDCl_3$).

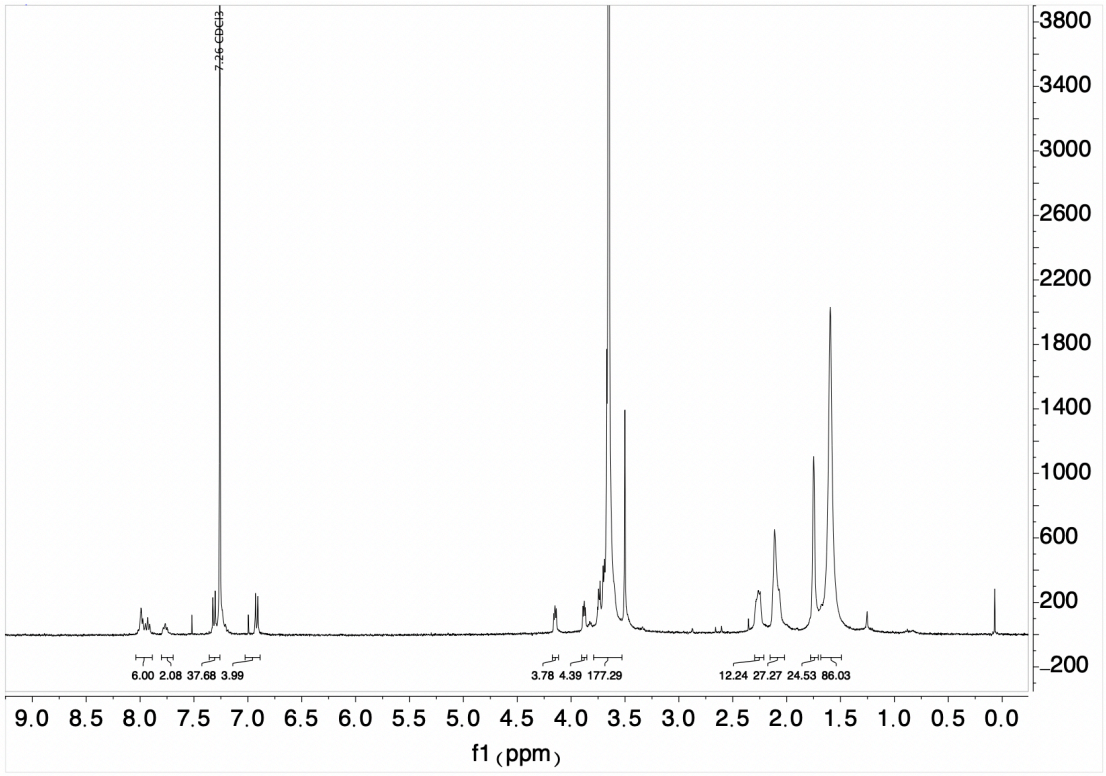

Figure 4.14. ^{1}H NMR spectrum of bis *para*- Au (III) $(Ad)_2$ PEG_{2000} (400 MHz in $CDCl_3$).

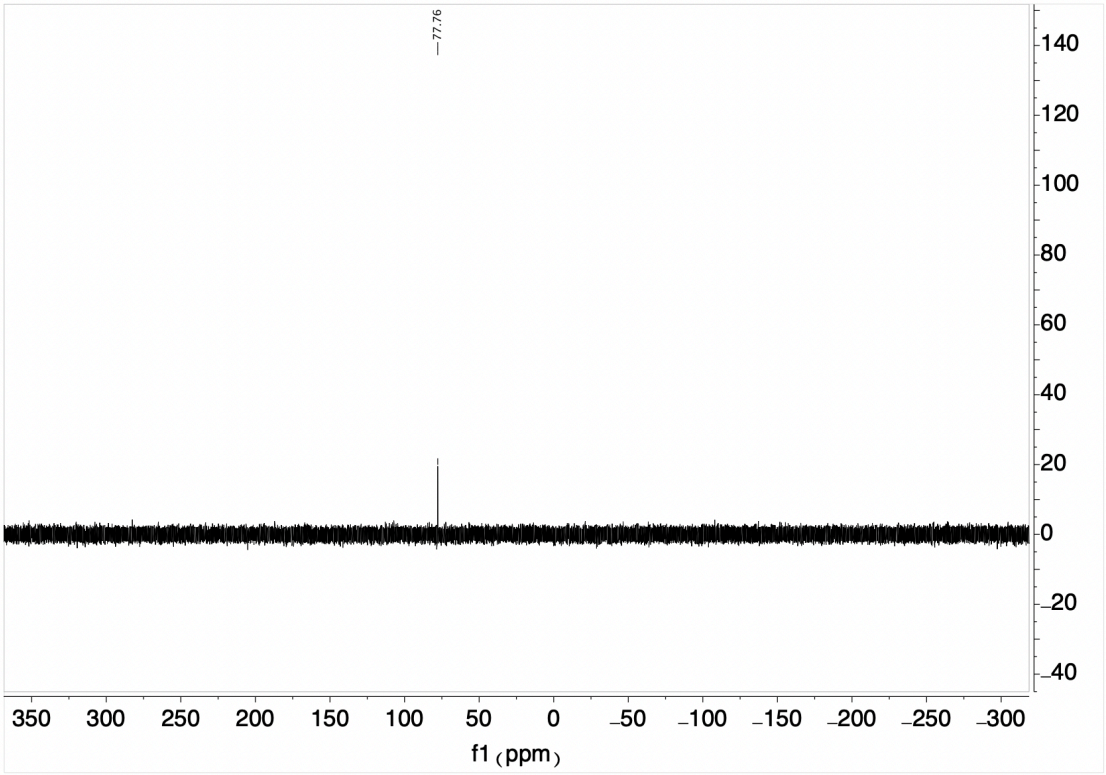

Figure 4.15. ^{31}P NMR spectrum of bis *para*- Au (III) $(Ad)_2$ PEG_{2000} (400 MHz in $CDCl_3$).

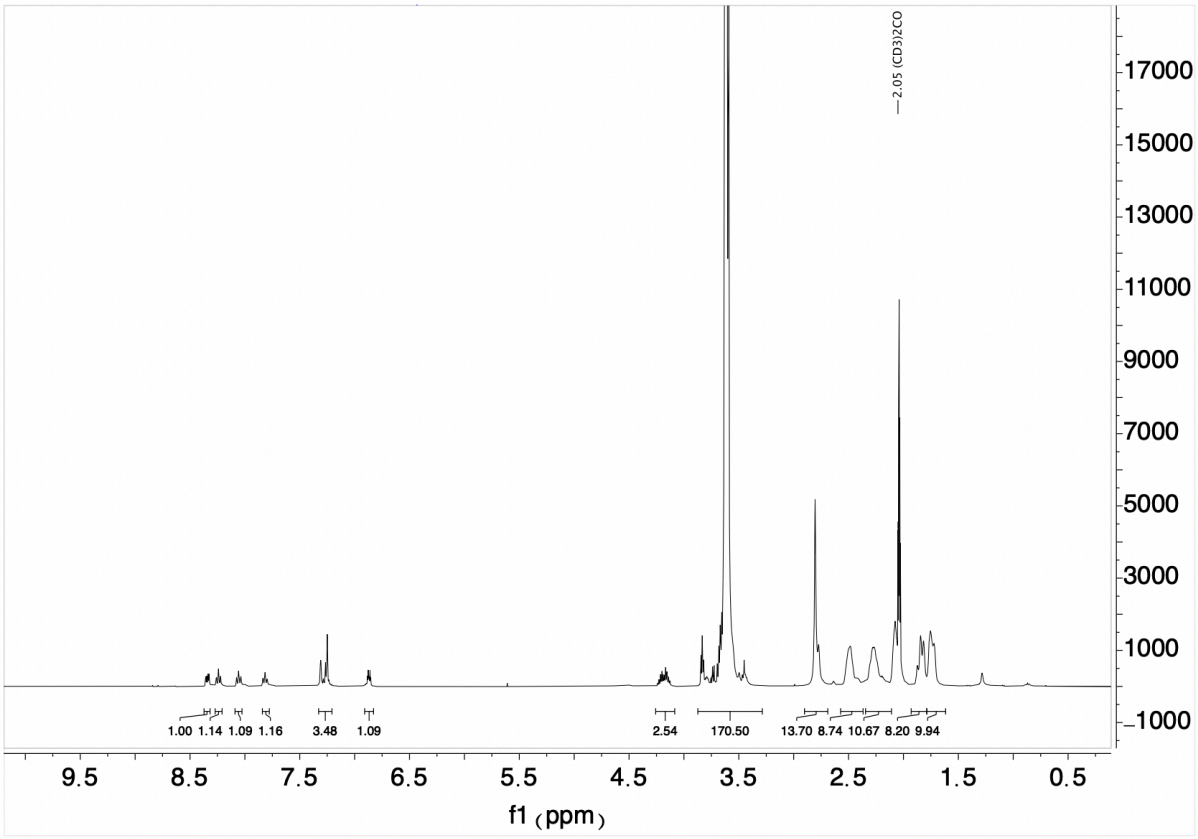

Figure 4.16. ^{1}H NMR spectrum of bis *meta*- Au (III) $(Ad)_2$ PEG_{2000} (400 MHz in $(CD_3)_2CO$).

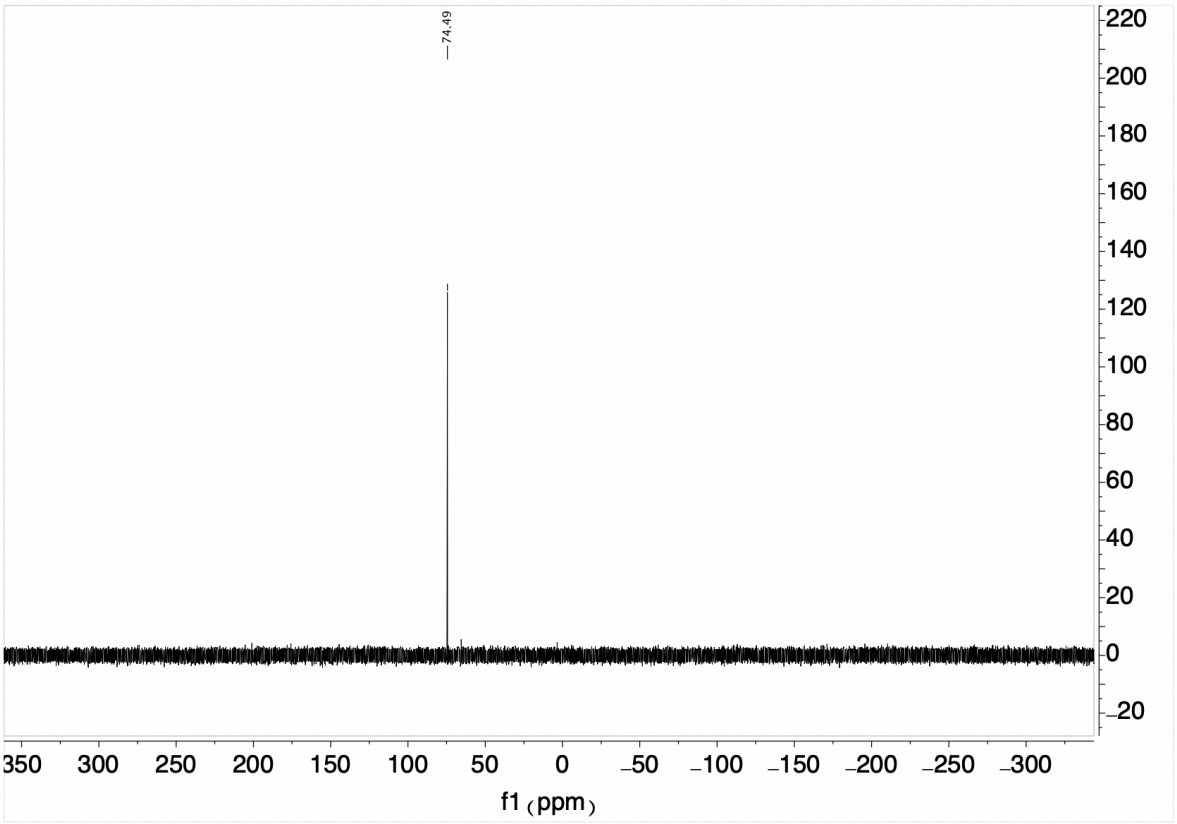

Figure 4.17. ^{31}P NMR spectrum of bis *meta*- Au (III) $(Ad)_2$ PEG_{2000} (400 MHz in $(CD_3)_2CO$).

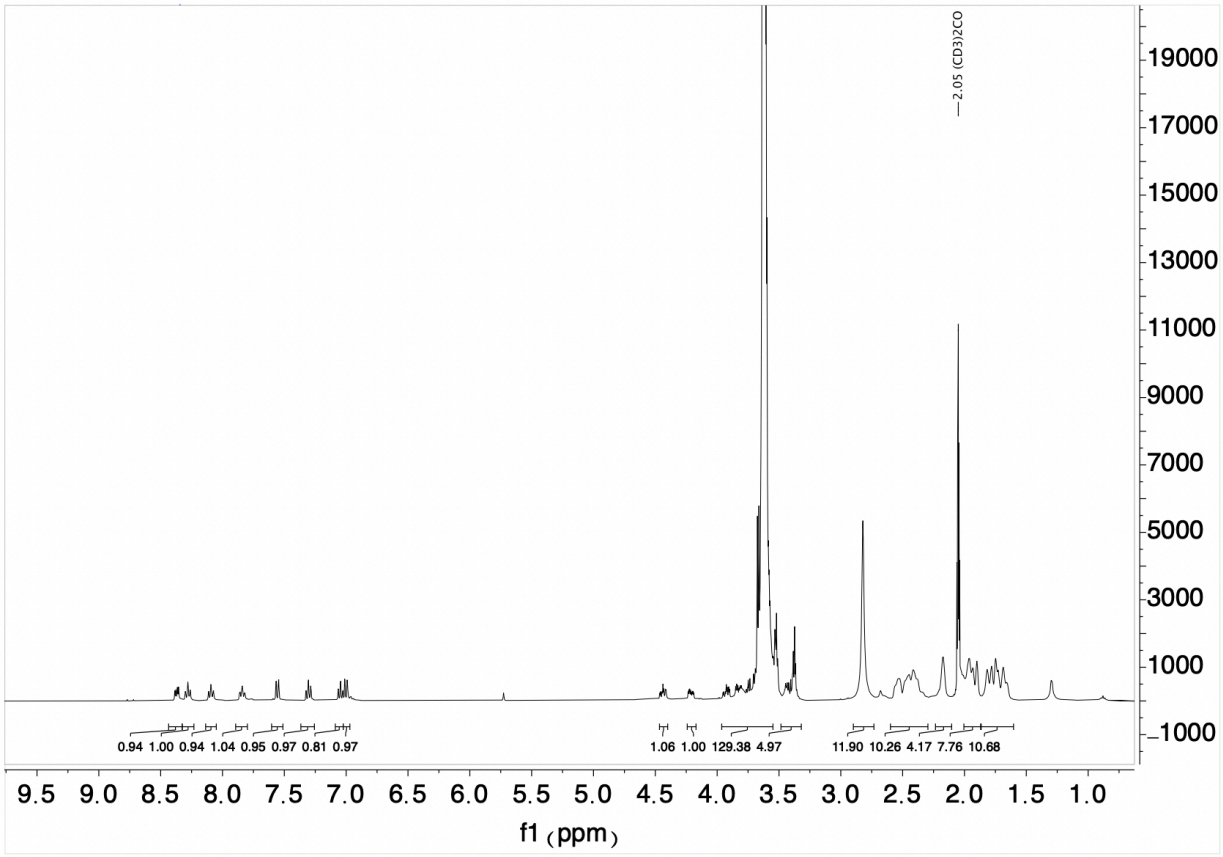

Figure 4.18. ^{1}H NMR spectrum of bis *ortho*- Au (III) $(Ad)_2$ PEG_{2000} (400 MHz in $(CD_3)_2CO$).

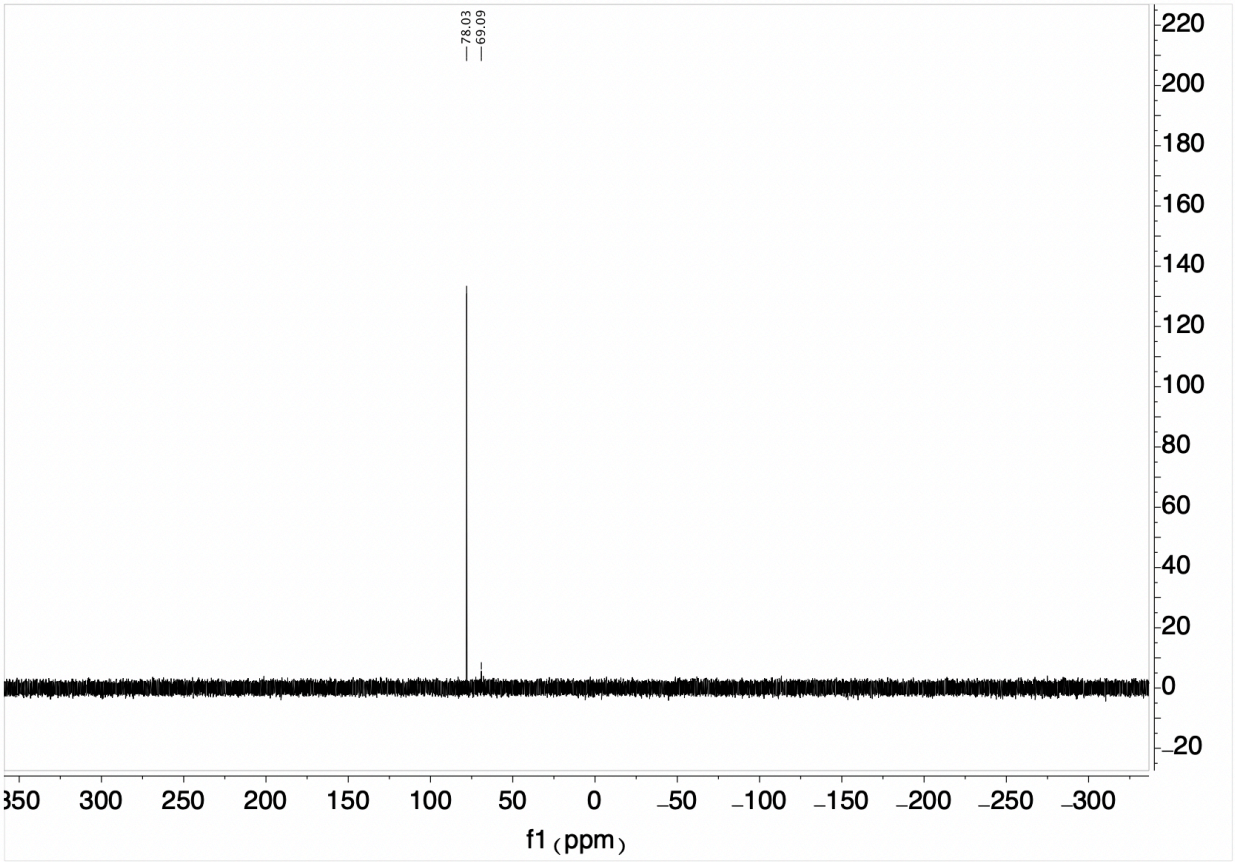

Figure 4.19. ^{31}P NMR spectrum of bis *ortho*- Au (III) $(Ad)_2$ PEG_{2000} (400 MHz in $(CD_3)_2CO$).

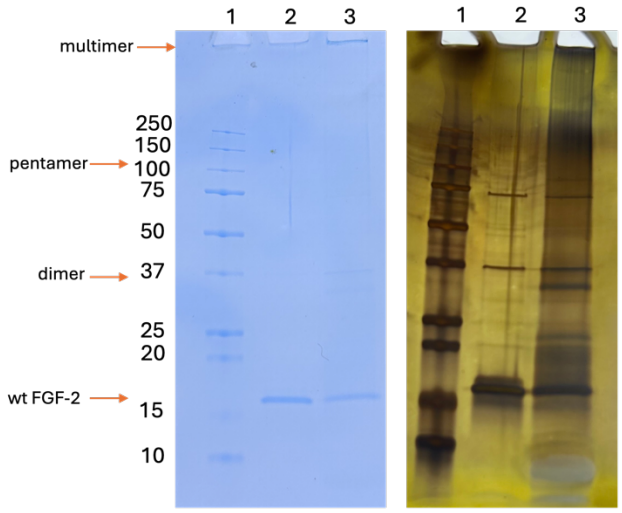

Figure 4.20. 1: Reductive elimination of FGF-2 (1 eq) with 3 eq of **6**. Lane 1: ladder, Lane 2: FGF-2, Lane 3: 1 min. % Conversion from FGF-2: 76%.

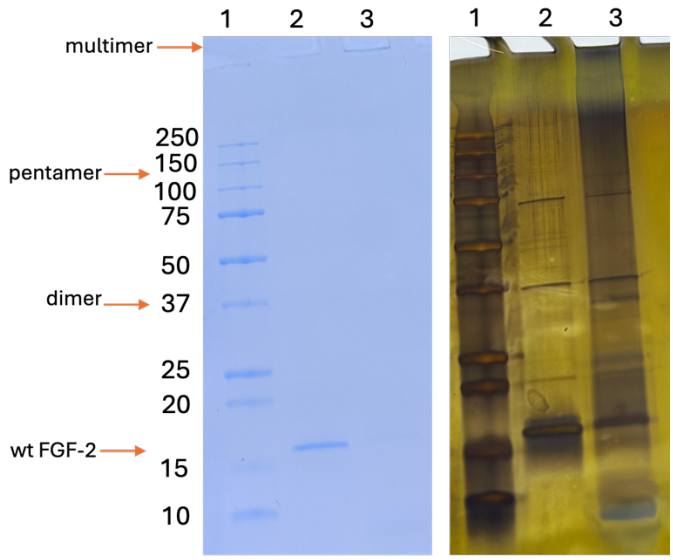

Figure 4.21. 1: Reductive elimination of FGF-2 (1 eq) with 3 eq **6**. Lane 1: ladder, Lane 2: FGF-2, Lane 3: 1 h. % Conversion from FGF-2: 99%.

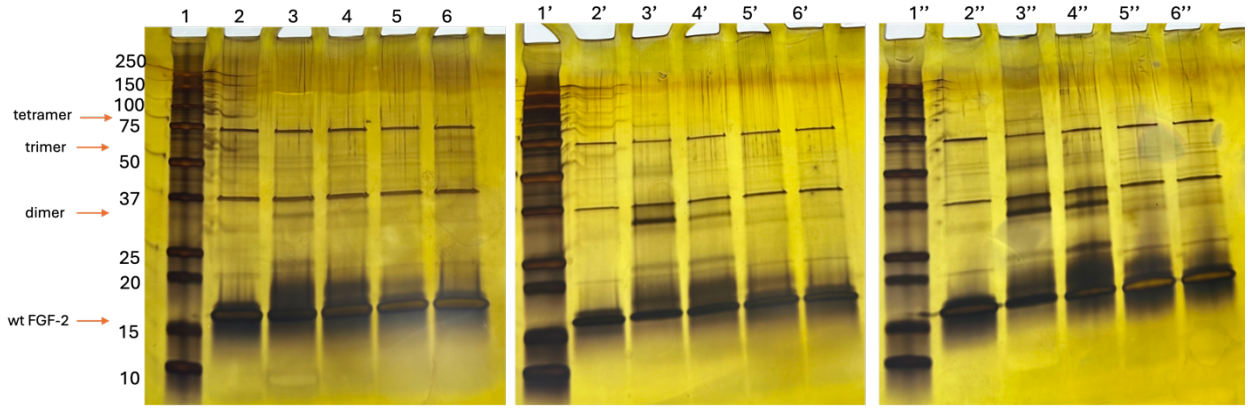

Figure 4.22. Silver stain of Figure 4.5 Reductive elimination of FGF-2 (1 eq) equivalents screen after 10 min (Lanes 1-6), 1 h (Lanes 1'-6'), 2 h (Lanes 1''-6'') with **6**. Lane 1: ladder, Lane 2: FGF-2, Lane 3: 2 eq, Lane 4: 1 eq, Lane 5: 0.5 eq, Lane 6: 0.25 eq.

4.6 References

(1) Goodsell, D. S.; Olson, A. J. Structural Symmetry and Protein Function. *Annu. Rev. Biophys. Biomol. Struct.* **2000**, *29* (1), 105–153. https://doi.org/10.1146/annurev.biophys.29.1.105.

(2) Ali, M. H.; Imperiali, B. Protein Oligomerization: How and Why. *Bioorg. Med. Chem.* **2005**, *13* (17), 5013–5020. https://doi.org/10.1016/j.bmc.2005.05.037.

(3) Johnson, R. L.; Blaber, H. G.; Evans, T.; Worthy, H. L.; Pope, J. R.; Jones, D. D. Designed Artificial Protein Heterodimers With Coupled Functions Constructed Using Bio-Orthogonal Chemistry. *Front. Chem.* **2021**, *9*.

(4) Gwyther, R. E. A.; Jones, D. D.; Worthy, H. L. Better Together: Building Protein Oligomers Naturally and by Design. *Biochem. Soc. Trans.* **2019**, *47* (6), 1773–1780. https://doi.org/10.1042/BST20190283.

(5) Klemm, J. D.; Schreiber, S. L.; Crabtree, G. R. DIMERIZATION AS A REGULATORY MECHANISM IN SIGNAL TRANSDUCTION. *Annu. Rev. Immunol.* **1998**, *16* (1), 569–592. https://doi.org/10.1146/annurev.immunol.16.1.569.

(6) Mammen, M.; Choi, S.-K.; Whitesides, G. M. Polyvalent Interactions in Biological Systems: Implications for Design and Use of Multivalent Ligands and Inhibitors. *Angew. Chem. Int. Ed.* **1998**, *37* (20), 2754–2794. https://doi.org/10.1002/(SICI)1521-3773(19981102)37:20<2754::AID-ANIE2754>3.0.CO;2-3.

(7) Matthews, J. M.; Sunde, M. Dimers, Oligomers, Everywhere. In *Protein Dimerization and Oligomerization in Biology*; Matthews, J. M., Ed.; Advances in Experimental Medicine and Biology; Springer: New York, NY, 2012; pp 1–18. https://doi.org/10.1007/978-1-4614-3229-6_1.

(8) Griffith, B. R.; Allen, B. L.; Rapraeger, A. C.; Kiessling, L. L. A Polymer Scaffold for Protein Oligomerization. *J. Am. Chem. Soc.* **2004**, *126* (6), 1608–1609. https://doi.org/10.1021/ja037646m.

(9) Marianayagam, N. J.; Sunde, M.; Matthews, J. M. The Power of Two: Protein Dimerization in Biology. *Trends Biochem. Sci.* **2004**, *29* (11), 618–625. https://doi.org/10.1016/j.tibs.2004.09.006.

(10) Thomas, T. P.; Shukla, R.; Kotlyar, A.; Liang, B.; Ye, J. Y.; Norris, T. B.; Baker, J. R. Dendrimer−Epidermal Growth Factor Conjugate Displays Superagonist Activity. *Biomacromolecules* **2008**, *9* (2), 603–609. https://doi.org/10.1021/bm701185p.

(11) Krueger, A. T.; Kroll, C.; Sanchez, E.; Griffith, L. G.; Imperiali, B. Tailoring Chimeric Ligands for Studying and Biasing ErbB Receptor Family Interactions. *Angew. Chem. Int. Ed.* **2014**, *53* (10), 2662–2666. https://doi.org/10.1002/anie.201307869.

(12) Brown, K. A.; Zou, Y.; Shirvanyants, D.; Zhang, J.; Samanta, S.; Mantravadi, P. K.; Dokholyan, N. V.; Deiters, A. Light-Cleavable Rapamycin Dimer as an Optical Trigger for Protein Dimerization. *Chem. Commun.* **2015**, *51* (26), 5702–5705. https://doi.org/10.1039/C4CC09442E.

(13) Lin, H.; Abida, W. M.; Sauer, R. T.; Cornish, V. W. Dexamethasone−Methotrexate: An Efficient Chemical Inducer of Protein Dimerization In Vivo. *J. Am. Chem. Soc.* **2000**, *122* (17), 4247–4248. https://doi.org/10.1021/ja9941532.

(14) Gendreizig, S.; Kindermann, M.; Johnsson, K. Induced Protein Dimerization in Vivo through Covalent Labeling. *J. Am. Chem. Soc.* **2003**, *125* (49), 14970–14971. https://doi.org/10.1021/ja037883p.

(15) Erhart, D.; Zimmermann, M.; Jacques, O.; Wittwer, M. B.; Ernst, B.; Constable, E.; Zvelebil, M.; Beaufils, F.; Wymann, M. P. Chemical Development of Intracellular Protein Heterodimerizers. *Chem. Biol.* **2013**, *20* (4), 549–557. https://doi.org/10.1016/j.chembiol.2013.03.010.

(16) Rakhit, R.; Navarro, R.; Wandless, T. J. Chemical Biology Strategies for Posttranslational Control of Protein Function. *Chem. Biol.* **2014**, *21* (9), 1238–1252. https://doi.org/10.1016/j.chembiol.2014.08.011.

(17) Sainlos, M.; Tigaret, C.; Poujol, C.; Olivier, N. B.; Bard, L.; Breillat, C.; Thiolon, K.; Choquet, D.; Imperiali, B. Biomimetic Divalent Ligands for the Acute Disruption of Synaptic AMPAR Stabilization. *Nat. Chem. Biol.* **2011**, *7* (2), 81–91. https://doi.org/10.1038/nchembio.498.

(18) Griffith, B. R.; Allen, B. L.; Rapraeger, A. C.; Kiessling, L. L. A Polymer Scaffold for Protein Oligomerization. *J. Am. Chem. Soc.* **2004**, *126* (6), 1608–1609. https://doi.org/10.1021/ja037646m.

(19) Decker, C. G.; Wang, Y.; Paluck, S. J.; Shen, L.; Loo, J. A.; Levine, A. J.; Miller, L. S.; Maynard, H. D. Fibroblast Growth Factor 2 Dimer with Superagonist in Vitro Activity Improves Granulation Tissue Formation during Wound Healing. *Biomaterials* **2016**, *81*, 157–168. https://doi.org/10.1016/j.biomaterials.2015.12.003.

(20) Lorenzo, M. M.; Decker, C. G.; Kahveci, M. U.; Paluck, S. J.; Maynard, H. D. Homodimeric Protein–Polymer Conjugates via the Tetrazine–Trans-Cyclooctene Ligation. *Macromolecules* **2016**, *49* (1), 30–37. https://doi.org/10.1021/acs.macromol.5b02323.

(21) Bikfalvi, A.; Klein, S.; Pintucci, G.; Rifkin, D. B. Biological Roles of Fibroblast Growth Factor-2. *Endocr. Rev.* **1997**, *18* (1), 26–45. https://doi.org/10.1210/edrv.18.1.0292.

(22) Akita, S.; Akino, K.; Hirano, A. Basic Fibroblast Growth Factor in Scarless Wound Healing. *Adv. Wound Care* **2013**, *2* (2), 44–49. https://doi.org/10.1089/wound.2011.0324.

(23) Alconcel, S. N. S.; Baas, A. S.; Maynard, H. D. FDA-Approved Poly(Ethylene Glycol)–Protein Conjugate Drugs. *Polym. Chem.* **2011**, *2* (7), 1442–1448. https://doi.org/10.1039/C1PY00034A.

(24) Lühmann, T.; Gutmann, M.; Moscaroli, A.; Raschig, M.; Béhé, M.; Meinel, L. Biodistribution of Site-Specific PEGylated Fibroblast Growth Factor-2. *ACS Biomater. Sci. Eng.* **2020**, *6* (1), 425–432. https://doi.org/10.1021/acsbiomaterials.9b01248.

(25) Ko, J. H.; Maynard, H. D. A Guide to Maximizing the Therapeutic Potential of Protein–Polymer Conjugates by Rational Design. *Chem. Soc. Rev.* **2018**, *47* (24), 8998–9014. https://doi.org/10.1039/C8CS00606G.

(26) Montgomery, H. R.; Messina, M. S.; Doud, E. A.; Spokoyny, A. M.; Maynard, H. D. Organometallic S-Arylation Reagents for Rapid PEGylation of Biomolecules. *Bioconjug. Chem.* **2022**, *33* (8), 1536–1542. https://doi.org/10.1021/acs.bioconjchem.2c00280.

(27) Kunkel, G. E.; Zhou, Q.; Treacy, J. W.; Montgomery, H. R.; Salas-Ambrosio, P.; Ready, A. D.; Spokoyny, A. M.; Houk, K. N.; Maynard, H. D. Comparison of Cyclic and Linear PEG Conjugates. *Bioconjug. Chem.* **2024**, *35* (6), 744–749. https://doi.org/10.1021/acs.bioconjchem.4c00202.

(28) Doud, E. A.; Tilden, J. A. R.; Treacy, J. W.; Chao, E. Y.; Montgomery, H. R.; Kunkel, G. E.; Olivares, E. J.; Adhami, N.; Kerr, T. A.; Chen, Y.; Rheingold, A. L.; Loo, J. A.; Frost, C. G.; Houk, K. N.; Maynard, H. D.; Spokoyny, A. M. Ultrafast Au(III)-Mediated Arylation of Cysteine. *J. Am. Chem. Soc.* **2024**. https://doi.org/10.1021/jacs.3c12170.

(29) Benington, L. R.; Rajan, G.; Locher, C.; Lim, L. Y. Stabilisation of Recombinant Human Basic Fibroblast Growth Factor (FGF-2) against Stressors Encountered in Medicinal Product Processing and Evaluation. *Pharmaceutics* **2021**, *13* (11), 1762. https://doi.org/10.3390/pharmaceutics13111762.

(30) Kunkel, G. E.; Treacy, J. W.; Polite, M. F.; Montgomery, H. R.; Doud, E. A.; Houk, K. N.; Spokoyny, A. M.; Maynard, H. D. Heterotelechelic Organometallic PEG Reagents Enable Modular Access to Complex Bioconjugates. *ACS Macro Lett.* **2024**, 1551–1557. https://doi.org/10.1021/acsmacrolett.4c00588.

(31) Chen, R.; John, J.; Lavrentieva, A.; Müller, S.; Tomala, M.; Zhao, Y.; Zweigerdt, R.; Beutel, S.; Hitzmann, B.; Kasper, C.; Martin, U.; Rinas, U.; Stahl, F.; Scheper, T. Cytokine Production Using Membrane Adsorbers: Human Basic Fibroblast Growth Factor Produced by *Escherichia Coli*. *Eng. Life Sci.* **2012**, *12* (1), 29–38. https://doi.org/10.1002/elsc.201100045.

Chapter 5

Degradable Sulfonate Polymers by Thiol-ene Click Chemistry

5.1 Introduction

Biodegradable materials offer a promising solution to address the global plastic waste crisis. Polymers that degrade into non-toxic compounds when exposed to water, air, and microbes are in high demand due to their biocompatibility and abundance.[1,2] They can be found in nature or synthetically derived from renewable materials, bio-based precursors, and microorganisms. Biodegradable polymers have many biomedical applications including implantable large devices, medical delivery, and tissue engineering.[3–5] The susceptibility of these polymers to degradation is significantly influenced by various factors, such as polymer type, crystallinity, molecular weight, and functional groups, which ultimately affect their resultant applications.[6]

Aliphatic polyesters such as poly (ϵ-caprolactone) (pCL) are notable for their degradability and compatibility in biomedical applications.[7] PCL's flexible mechanical properties such as semi-crystallinity and low glass transition temperature (Tg), Young's modulus, and yield stress make it a suitable polymer for tissue engineering, drug delivery, and implantable biomaterials.[8,9] The physical, chemical, and mechanical properties of pCL can be modified by co-polymerization or blending with other polymers to afford changes in crystallinity, solubility, and degradation.[10] Another technique for altering properties is to install functional groups at the end group or side chains of pCL via alkynyl-azide, allyl-thiol, and sulfhydryl-maleimide reactions.[11–14] Hydrophilic polymers or small molecules are often used to increase hydrophilicity of pCL while still maintaining its mechanical properties in order to expand applications.

Hydrophilic moieties such a sulfonate groups are incorporated in polymeric biomaterials like hydrogels, scaffolds, and nanoparticles to improve cellular responses such as adhesion, proliferation, and differentiation.[15] Sulfonate groups have also been shown to improve chitosan properties and mimic heparin activity.[15–18] PCL has been previously grafted from with

poly(sodium styrene sulfonate), however these surfaces can films and electrospun surfaces have uneven distributions and can be difficult to control.[19–22] Poly (ally-caprolactone) pCL-allyl has been utilized to install functional groups thiol-ene reactions.[12,23,24] Herein, we demonstrate a simple approach to access pCL-sulfonate polymers of varying molecular weight (MW).[25] pCL-allyl with varying MWs were synthesized *via* anionic ring-opening polymerization (ROP). Sulfonate side chains were attached to pCL-allyl via thiol-ene click chemistry to yield polymers between 10 kilodaltons (kDa) and 160 kDa. The mechanical properties and degradation were investigated.

5.2 Results and Discussion

5.2.1 Synthesis of pCL-allyl *via* ROP.

First, pCL-allyl of different molecular weights were synthesized from ally caprolactone utilizing ROP (Figure 1A). ROP of allyl caprolactone has been previously reported using the thiourea catalyst 1-(3,5-bis(trifluoromethyl)phenyl)-3-cyclohexylthiourea (3-O) and base 7-methyl-1,5,7-triazabicyclo(4.4.0)dec-5-ene (MTBD).[12,23,24] Therefore, this catalyst system was first utilized and pCL-allyl was synthesized with DP 40 (**1**) and 135 (**2**) (**Table 5.1**).[26] For the synthesis of 2, an elevated temperature of 50 °C was required to achieve a polymer of this DP with dispersity (Đ) <1.5. Polymerizations of DP larger than 135 were attempted at 20 °C and 50 °C at 2 M or 4M monomer concentration; however, the percent conversion did not exceed 67% by ^{1}H NMR (entries 7 - 10) (**Table 5.3).**

To access higher molecular weights while maintaining relatively low dispersity, an alternative catalyst was used. The Waymouth group has expanded the field of ROP urea anion catalysts, including 1-cyclohexyl-3-phenylurea, or Urea 7 catalyst.[27] ROP of unmodified caprolactone with Urea 7 yielded 89 % conversion and a MW of 17.9 kDa after 12 s with $Đ$ <1.2.27

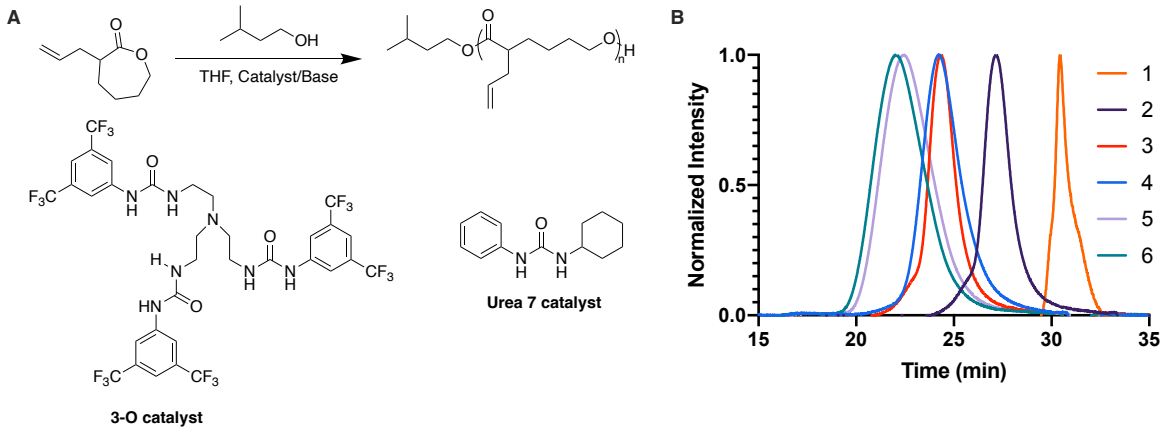

Figure 5.1. (A) ROP of allyl caprolactone general scheme using either 3-O with MTBD or Urea 7 with NaH. (B) DMF Size Exclusion Chromatography (SEC) of 1, 2, 3, 4, 5, and 6.

We first tested the Urea 7/NaH system to prepare lower MW pCL-allyl, 10 kDa and 20 kDa. Although full conversion was achieved within 30 min and 1 h, respectively, the dispersities were slightly higher than with the 3-O/MTBD system with values of 1.2 (entry **9** and **10** respectively, **Table 5.3**). For a higher DP of 285, the Urea 7/NaH system achieved 92% conversion after 3 h to give a 50 kDa pCL-allyl (entry **3**, **Table 5.1**) using 2 M of monomer. When attempting to access DP 400, 450, and 500 with the same monomer concentration, the conversions were limited to a maximum of 65 %, 45 % and 39 % respectively (entry **13, 14, 15, Table 5.3**). When increasing the monomer concentration from 2M to 4M, DPs of approximately 370, 472, and 528 were reached with conversions > 80 % (entry **4 - 6, Table 5.1**) with greater than 80% conversion and $Đ$ of 1.36, 1.42, and 1.57, respectively. By varying the catalyst/base, monomer concentration, and temperature, a range of molecular weights from 6.3 kDa to 81.2 kDa was achieved with a slight increase in $Đ$ as DP increased; DMF size exclusion chromatography (SEC) traces are shown in **Figure 5.1B.**

Table 5.1. ROP conditions for pCL-allyl$_{40}$, pCL-allyl$_{135}$, pCL-allyl$_{285}$, pCL-allyl$_{370}$, pCL-allyl$_{472}$, pCL-allyl$_{528}$. All polymers were synthesized using a 1: 1.19: 1.19 ratio of initiator: catalyst: base in THF at 25 °C. 3-methyl 1-butanol was used to initiate all polymerizations. [a]Temperature at 50 °C. M_n values reported in kDa. Expected M_n is calculated from H^1 NMR observed conversion.

PCL-allyl	**Catalyst /Base**	**Time (h)**	**Concentration (M)**	**% Conversion M_n (H^1 NMR)**	**Expected M_n**	**DP (H^1 NMR)**	**M_n (SEC)**	**$Đ$ (SEC)**
1	3-O/MTBD	2.5	2	100	6.3	40	7.4	1.06
2[A]	3-O /MTBD	5	2	84.4	21.0	135	22.3	1.18
3	Urea 7/NaH	3	2	92.1	44.1	285	50.1	1.31
4	Urea 7/NaH	4	4	89.3	57.2	370	73.0	1.36
5	Urea 7/NaH	8	4	85.9	73.0	472	92.5	1.42
6	Urea 7/NaH	12	4	81.2	81.2	528	125.0	1.57

5.2.2 pCL-allyl functionalization *via* thiol-ene.

To install the sulfonate group, thiol-ene click chemistry was employed between the library of pCL-allyl and 3-mercaptopropane sulfonate (**Figure 5.2**). This reaction was challenging because pCL-allyl is hydrophobic and 3-mercaptopropane sulfonate is soluble in water. To remedy this, the phase transfer catalyst (PTC) tetrabutylammonium bromide was employed, which allowed for successful thiol-ene in immiscible solvents. pCL-allyl and the photoinitiator dimethoxyphenylacetophenone (DMPA) were dissolved in DCM and 3-mercaptopropane sulfonate in H_2O with the addition of the PTC. After exposure to UV light for 30 minutes, complete conversion from allyl was not achieved. We found that reducing 3-mercaptopropane sulfonate

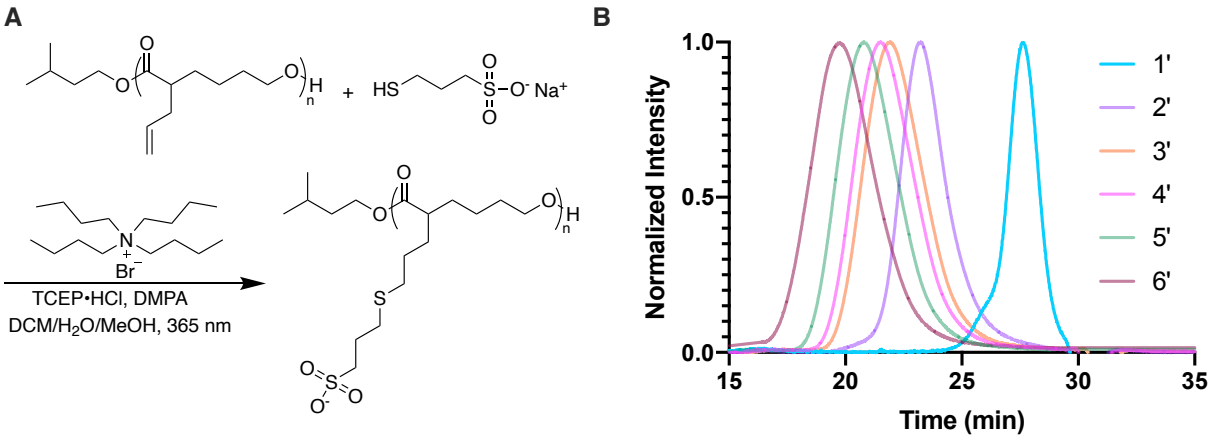

Figure 5.2. (A) Thiol-ene of pCL-ally to yield pCL-sulfonate general scheme. (B) DMF SEC of **1, 2, 3, 4, 5,** and **6** denoted with a ‘ to indicate the sulfonated version.

immediately before use with TCEP·HCl for 1 h at 25 °C was crucial to ensure full conversion from the allylated polymer. Additionally, if the polymer was left exposed to UV light for too long, DMPA incorporation into the backbone was observed by H^1 NMR. After performing kinetics of this reaction, we determined that at 0.3 mM polymer, 30 minutes was the optimal time for all the polymers to reach full conversion without any photo initiator incorporation. The pCL-sulfonate polymer library resulted in polymers from 12.2 kDa to 163.3 kDa with $1.1 \leq Đ \leq 1.6$, approximately similar dispersities as the starting pCL-ally (**Table 5.2**). A clear shift in MW can be seen when overlayed by SEC, further providing evidence of the conversion from the pCL-allyl to the pCL-sulfonate (**Figure 5.18**). It was possible that when lowering the ratio of 3-mercapropropane

Table 5.2. pCL-sulfonate of varying MW determined by ^{1}H NMR and DMF SEC.

PCL-SULFONATE	M_n (^{1}H NMR)	M_n (SEC)	$Đ$ (SEC)
1’	12.2	**10.8**	1.14
2’	**41.8**	**39.5**	1.21
3’	**88.2**	**76.3**	1.37
4’	**114.4**	**105.6**	1.40
5’	**146.0**	143.5	1.56
6’	**163.3**	152.1	1.63

sulfonate to polymer, partial functionalization of the ally polymer to the corresponding sulfonate could be targeted (**Figure 5.19**). Thus, if desired for an application, partial sulfonation would be possible.

5.2.3 Thermogravimetric analysis (TGA).

Thermogravimetric analysis of the pCL-sulfonate polymers were assessed **(1'-5') (Figure 5.3A**). Due to the polymers being very hydroscopic, the temperature was initially held at 100 °C to remove any excess water. Differential scanning calorimetry shows there is no glass transition before the degradation temperature is reached, and thus the polymer decomposes prior to melting (**Figure 5.20**). The lower MW polymers show a slightly faster initial % weight loss compared to the higher MW polymers (**Figure 5.3B**). However, as the temperature increases, these changes become insignificant to one another as seen by the variability in 50% weight loss (**Figure 5.3C**).

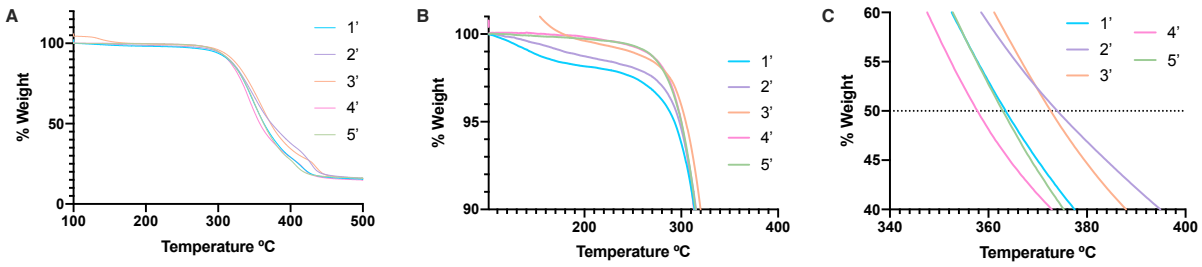

Figure 5.3. (A) TGA of pCL-sulfonate. (B) Zoomed in TGA of pCL-sulfonate at the initial weight loss. (C) Zoomed in TGA of pCL-sulfonate at 50 % weight. Temperature (°C) at 50% weight loss for 1'-5' respectively: 363.59, 374.18, 373.85, 358.11, 363.29. A) Thiol-ene of pCL-ally to yield pCL-sulfonate general scheme. (B) DMF SEC of **1, 2, 3, 4, 5,** and **6** denoted with a ' to indicate the sulfonated version.

5.2.4 Hydrolytic Degradation.

To confirm that functionalization with the sulfonate side chain still allowed for degradation of the pCL backbone, the library of pCL-sulfonate polymers, soluble in water, were treated with

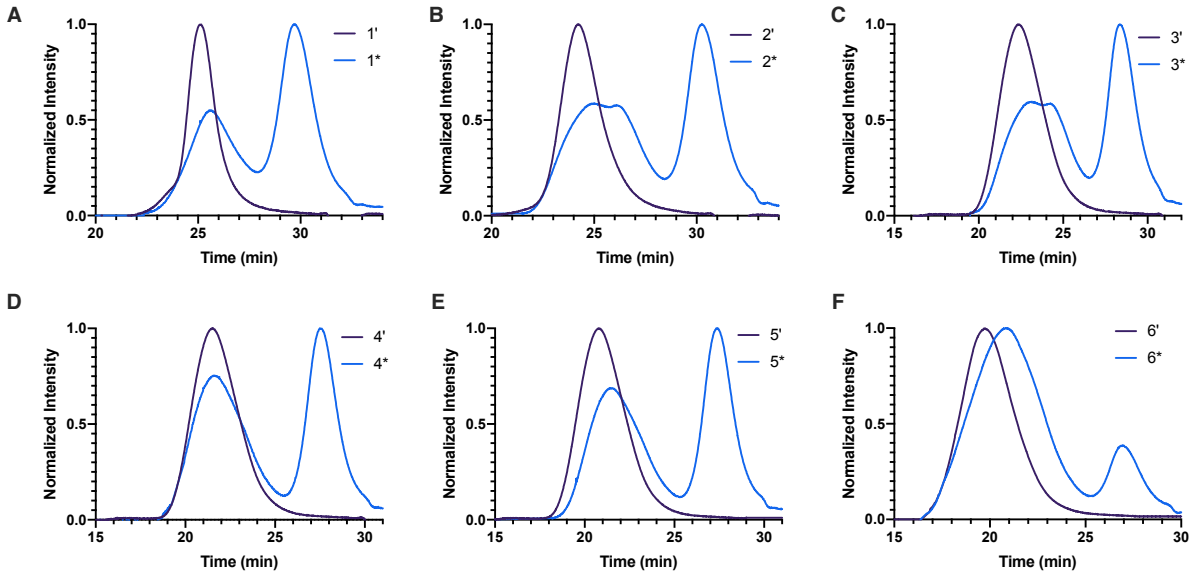

Figure 5.4. DMF SEC degradation after treatment with 5% KOH for 24 h at 4 °C of pCL-sulfonate. A * indicates the degraded trace of the polymer. A) TGA of pCL-sulfonate. B) Zoomed in TGA of pCL-sulfonate at the initial weight loss. C) Zoomed in TGA of pCL-sulfonate at 50 % weight. Temperature (°C) at 50% weight loss for **1'-5'** respectively: 363.59, 374.18, 373.85, 358.11, 363.29.

5% KOH to hydrolytically cleave the backbone.[12] After treatment for 24 h, the degraded polymers were analyzed by DMF SEC (**Figure 5.4**). All of the polymers showed a lower molecular weight peak corresponding to smaller degraded products. However, the smaller polymers appeared to be degraded more than the larger polymers at this time point; longer time points would be needed to reach full degradation. Yet the results did demonstrate that the polymers modified with sulfonate groups could degrade in water.

5.3 Conclusion

In conclusion, pCL-allyl with molecular weights ranging from 6.3 kDa – 81.2 kDa was synthesized by ROP. The pCL-ally polymers were successfully functionalized via thiol-ene to yield pCL-sulfonate polymers from 12.2 kDa to 163.3 kDa, with minimal increase in dispersity. The

pCL-sulfonate polymers showed no significant dependence on molecular weight loss with regard to temperature induced degradation. However, there was a molecular weight loss dependence on degradation. Yet all the polymers were degradable with time.

5.4 Experimental

5.4.1 Materials

Unless otherwise stated, all materials were purchased and used as received from Fisher Scientific, Acros, Alfa Aesar, Oakwood Chemicals, or Sigma Aldrich. Polymerization reagents were stored in a glovebox maintained under a nitrogen atmosphere prior to use. Milli-Q water was used for all experiments. Anhydrous tetrahydrofuran (THF) was distilled from sodium benzophenone and stored under argon prior to use. Allyl bromide, ε- caprolactone, 7-methyl-1,5,7-triazabicyclo(4.4.0)dec-5-ene (MTBD), and 2-methyl 1-butanol were distilled under vacuum over activated 4 Å molecular sieves prior to use.

Polymerizations were performed in a Vacuum Atmospheres Genesis stainless steel glovebox under anhydrous nitrogen atmosphere. Allyl caprolactone was synthesized as previously described,[26] purified by distillation under reduced pressure before use, and polymerized as previously described.[12] Sodium hydride (NaH) (60% in mineral oil) was rinsed five times with hexanes and dried under reduced pressure before use. The thiourea catalyst 1-(3,5-bis(trifluoromethyl)phenyl)-3-cyclohexylthiourea (3-O) was synthesized as previously described.[28] The thiourea catalyst Urea 7 was synthesized as previously described.[27] Ultraviolet irradiation was carried out in a Photochemical Safety Reaction Cabinet from Ace Glass Incorporated at 365 nm. Spectra/Por3® regenerated cellulose membrane (MWCO 3.5 kDa) was purchased from Spectrum Chemical (New Brunswick, NJ) for polymer dialysis.

5.4.2 Analytical Techniques

NMR spectra were recorded on the following: AV400 Bruker spectrometer at 400 (^{1}H); Spectra are reported in δ (parts per million) relative to residual proteo-solvent signals for ^{1}H and H_3PO_4 (δ 0.00 ppm) for $^{31}P\{^{1}H\}$. The following abbreviations were used to explain multiplicities: s = singlet, d = doublet, t = triplet, q = quartet, m = multiplet. Deuterated solvents were purchased from Cambridge Isotope Laboratories and used as received for all NMR experiments. ^{1}H NMR spectra for all polymers, spectra were acquired with a relaxation delay of 4 seconds. Data was analyzed using MestReNova v12 software.

DMF Size Exclusion Chromatography (SEC)/Gel Permeation Chromatography (GPC) was conducted on an Agilent 1260 Infinity II high performance liquid chromatography (HPLC) system with a Wyatt Optilab (RI and MALS detection), one Polymer Laboratories PLgel guard column, and two Polymer Laboratories PLgel 5 μm mixed D columns. The eluent was DMF (HPLC Grade, 99.7+%, Thermo Scientific Chemicals) containing LiBr (0.1 M) at 40 °C (Flow rate: 0.6 mL/min). Molecular weight information was determined for data collected using a PMMA (Agilent Technologies, EasiVial PMMA, pre-weighed calibration kit) conventional calibration analysis.

Thermal degradation measurements were carried out using a PerkinElmer Thermogravimetric Analyzer (TGA) 8000. Temperature programs were run from 30 to 500 °C at a heating rate of 10°C/min. TGA tests were performed in alumina crucibles where solid samples (5-10 mg) were placed without any previous treatment and experiments were run immediately. All TGA tests were carried out in a nitrogen environment using a flow rate 20 ml/min to prevent oxidation.

Thermal properties of the sample were evaluated using a PerkinElmer Differential Scanning Calorimeter (DSC) 8000. Approximately 5–10 mg of the sample was accurately weighed and sealed in an aluminum pan. An empty aluminum pan was used as the reference. The sample

was subjected to a heating-cooling cycle under a nitrogen atmosphere with a flow rate of 20 ml/min to prevent oxidation. The sample was heated from 0 °C to 500 °C at a rate of 10°C/min and cooled at a rate of 20 °C/min.

5.4.3 Methods

Ring-opening polymerization (ROP) of allyl caprolactone

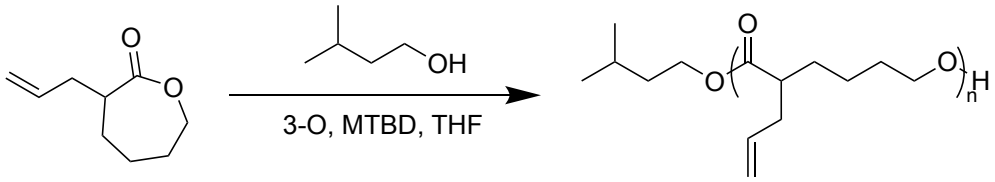

The general procedure for ROP of allyl-caprolactone was adapted from previously reported literature.[12,23,24,26]

General Procedure for ROP utilizing 3-O/MTBD system

In a nitrogen-filled glovebox, a dram vial was charged with a stir bar, 3-O, MTBD, THF, and 2-methyl 1-butanol. Allyl-caprolactone was added to initiate the polymerization. Polymerization was allowed to proceed at 20 °C for 6.3 kDa and 20.8 kDa polymers. For the 20.8 kDa polymer, the dram vial and its contents were fully assembled and sealed, then removed from the box and allowed to polymerize at 50 °C in an oil bath. Reaction was monitored by ^{1}H NMR. After 2.5 h (6.3 kDa) and 5 h (20.8 kDa) the polymerization was quenched with either acetic acid or benzoic acid in toluene outside of the glovebox. The conversions were 96% and 84% respectively. Percent Conversion was determined by the disappearance of the allyl monomer proton at 5.81 ppm (1H) and appearance of the ally polymer proton at 5.71 ppm (1H) using ^{1}H NMR (monomer proton/polymer proton x 100). Polymers were purified by precipitation five times in ice cold hexanes and dried under reduced pressure to give the polymer as a colorless oil.

Representative ROP (pCL-allyl$_{40}$):

In a nitrogen-filled glovebox, For the synthesis of pCL-allyl$_{40}$ (2M) a dram vial was charged with a stir bar, 3-O (17.5 mg, 1.19 eq, 0.019 mmol), MTBD (2.76 µL, 1.19 eq, 0.019 mmol), THF (227.1 µL), and 2-methyl 1-butanol (1.76 µL, 1 eq, 0.016 mmol). Allyl-caprolactone (97.1µL, 40 eq, 0.65 mmol) was added to initiate the polymerization. Polymerization was allowed to proceed at 20 °C for 6.3 kDa at 2.5 h. The polymerization was quenched with acetic acid outside of the glovebox. Polymers were purified by precipitation five times in ice cold hexanes and dried under reduced pressure to give the polymer as a colorless oil in 95.6% yield (97.0 mg).

6.3 kDa pCL-allyl40 (1): ^{1}H NMR (400 MHz, $CDCl_3$) δ 5.72 (ddt, *J* = 16.9, 10.1, 6.8 Hz, 39H), 5.09 – 4.97 (m, 80H), 4.13 – 3.96 (m, 81H), 2.47 – 2.28 (m, 83H), 2.22 (dddd, *J* = 12.7, 5.9, 3.5, 1.2 Hz, 40H), 1.69 – 1.57 (m, 122H), 1.57 – 1.44 (m, 78H), 1.40 – 1.27 (m, 81H), 0.92 (d, *J* = 6.6 Hz, 6H). M_n (DMF SEC) = 7,400 Da; $Đ$ = 1.06. % Conversion (by ^{1}H NMR): 100%. Yield: 97.0 mg, 95.6 %.

21.0 kDa pCL-allyl$_{135}$ (2): ^{1}H NMR (400 MHz, $CDCl_3$) δ 5.71 (ddt, J = 16.8, 9.9, 6.8 Hz, 136H), 5.09 – 4.95 (m, 275H), 4.04 (tdd, J = 6.5, 3.6, 1.6 Hz, 295H), 2.44 – 2.27 (m, 342H), 2.26 – 2.15 (m, 139H), 1.68 – 1.55 (m, 578H), 1.48 (ddd, J = 13.4, 10.5, 6.5 Hz, 148H), 1.34 (dp, J = 15.1, 7.1 Hz, 348H), 0.91 (d, J = 6.6 Hz, 6H). M_n (DMF SEC) = 22,300 Da; $Đ$ = 1.18. % Conversion (by ^{1}H NMR): 84.4%. Yield: 82.0 mg, 81.7 %.

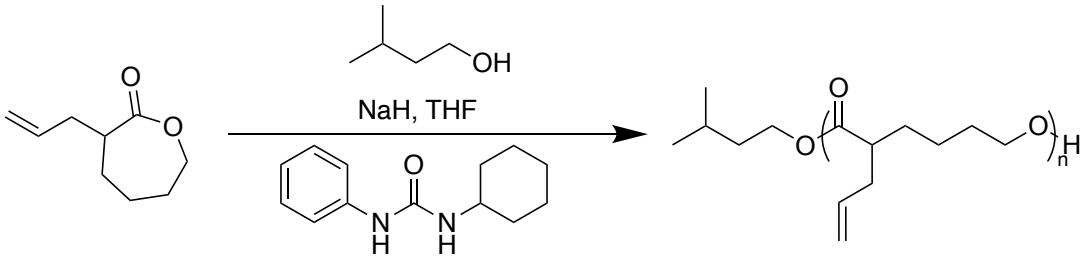

General Procedure for ROP utilizing Urea 7/NaH system:

In a nitrogen-filled glovebox, a dram vial was charged with a stir bar, Urea 7, NaH, THF, and 2-methyl 1-butanol. Stock solutions were made of Urea 7, NaH, and 2-methyl-butanol in THF. Polymerization of the 43.0 kDa polymer was at 2M and for the 57 kDa, 70 kDa, and at 4M for the 81 kDa. Allyl-caprolactone was added to initiate the polymerization. Polymerization was allowed to proceed at 20 °C. Reaction was monitored by ^{1}H NMR. After 3 h (44 kDa), 4 h (57 kDa), and 8 h (73 kDa), 12 h (81 kDa) the polymerization was quenched with either acetic acid or benzoic acid in toluene outside of the glovebox. The conversions were 92%, 90%, 86% and 81%, respectively. % Conversion was determined by the disappearance of the allyl monomer proton at 5.81 ppm (^{1}H) and appearance of the ally polymer proton at 5.71 ppm (^{1}H) using ^{1}H NMR (monomer proton/polymer proton x 100). Polymers were purified by precipitation five times in ice cold hexanes and dried under reduced pressure to give the polymer as a colorless oil.

Representative ROP (pCL-allyl$_{285}$):

In a nitrogen-filled glovebox, a dram vial was charged with a stir bar, Urea 7 (0.54 mg, 1.19 eq, 0.0025 mmol), NaH (0.06 mg, 1.19 eq, 0.0025 mmol), THF (227.1 µL), and 2-methyl 1-butanol (0.23 µL, 1 eq, 0.0021 mmol) were added. Allyl-caprolactone (97.1µL, 310 eq, 0.65 mmol) was added to initiate the polymerization. Polymerization was allowed to proceed at 20 °C for 43.0 kDa at 3 h. The polymerization was quenched with acetic acid outside of the glovebox. Polymers were purified by precipitation five times in ice cold hexanes and dried under reduced pressure to give the polymer as a colorless oil (89.0 mg) in 88.8% yield.

44.1 kDa pCL-allyl$_{285}$ (3): ^{1}H NMR (400 MHz, $CDCl_3$) δ 5.72 (ddt, J = 16.9, 10.1, 6.8 Hz, 283H), 5.09 – 4.98 (m, 577H), 4.05 (dddt, J = 13.2, 10.8, 6.6, 3.3 Hz, 572H), 2.46 – 2.29 (m, 582H), 2.23 (td, J = 13.3, 6.7 Hz, 318H), 1.72 – 1.44 (m, 1845H), 1.34 (h, J = 7.0 Hz, 613H). 0.84 (d, J = 6.5 Hz, 6H).; M_n (DMF SEC) = 50,100 Da, $Đ$ = 1.31% Conversion (by ^{1}H NMR): 92.1%. Yield: 89.0 mg, 88.8 %.

57.2 kDa pCL-allyl$_{370}$ (4): ^{1}H NMR (400 MHz, $CDCl_3$) δ 5.71 (ddt, J = 16.9, 10.1, 6.8 Hz, 369H), 5.09 – 4.96 (m, 743H), 4.11 – 3.96 (m, 739H), 2.47 – 2.28 (m, 751H), 2.21 (dt, J = 13.6, 6.3 Hz, 375H), 1.69 – 1.55 (m, 1184H), 1.54 – 1.42 (m, 406H), 1.33 (p, J = 7.4 Hz, 749H). 0.89 (d, J = 6.5 Hz, 6H). M_n (DMF SEC) = 73,000; $Đ$ = 1.36. % Conversion (by ^{1}H NMR): 89.3%. Yield: 87.2 mg, 87.1 %.

73.0 kDa pCL-allyl$_{472}$ (5): ^{1}H NMR (400 MHz, $CDCl_3$) δ 5.71 (ddt, J = 16.9, 10.2, 6.8 Hz, 472H), 5.13 – 4.90 (m, 961H), 4.15 – 3.92 (m, 956H), 2.45 – 2.28 (m, 964H), 2.21 (dt, J = 14.2, 6.0 Hz, 477H), 1.69 – 1.56 (m, 1431H), 1.48 (tdd, J = 12.9, 9.1, 5.0 Hz, 506H), 1.33 (p, J = 7.4 Hz, 971H). 0.90 (d, J = 6.5 Hz, 6H). M_n (DMF SEC) = 92,500 Da; $Đ$ = 1.42. % Conversion (by ^{1}H NMR): 85.9%. Yield: 81.0 mg, 80.9%.

81.2 kDa pCL-allyl$_{528}$ (6): ^{1}H NMR (400 MHz, $CDCl_3$) δ 5.70 (ddt, J = 16.9, 10.1, 6.8 Hz, 528H), 5.11 – 4.92 (m, 1079H), 4.13 – 3.91 (m, 1085H), 2.36 (dtt, J = 28.6, 8.1, 6.2 Hz, 1096H), 2.25 – 2.15 (m, 530H), 1.67 – 1.54 (m, 1634H), 1.48 (dtd, J = 13.3, 8.0, 5.2 Hz, 566H), 1.32 (p, J = 7.4 Hz, 1087H). 0.90 (d, J = 6.5 Hz, 6H). M_n (DMF SEC) = 125,00 Da; $Đ$ = 1.57. % Conversion (by ^{1}H NMR): 81.3%. Yield: 79.6 mg, 79.5 %.

General Procedure for thiol-ene:

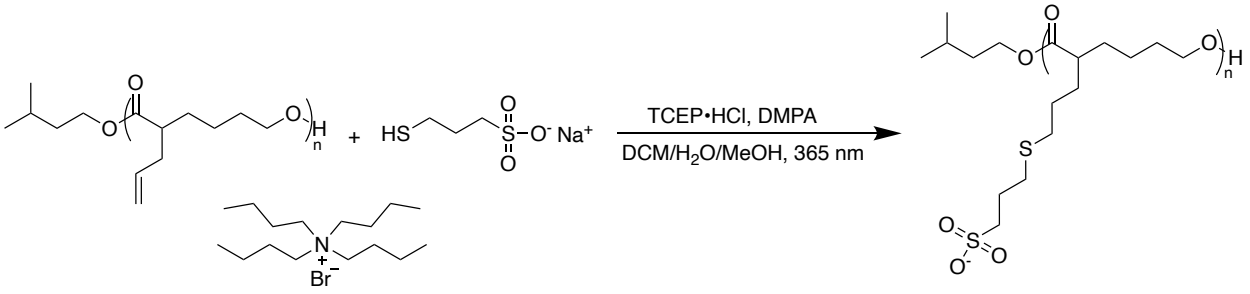

In a dram vial, sodium 3-mercaptopropane sulfonate was reduced with TCEP·HCl in H_2O for 1 h at 25 ºC. Separately, pCL-allyl, dimethoxyphenylacetophenone (DMPA), and tetrabutylammonium bromide were combined in a dram vial equipped with a stir bar and DCM. The reduced thiol and MeOH were added to the polymer vial. The mixture was degassed by sparging for 30 min with argon and then placed in the UV reactor on a stir plate with vigorous mixing and exposed to 365 nm UV light. After 30 min, the solution was opened and dialyzed against 3.5 kDa MWCO in acetone/ H_2O for 24 h and then H_2O for 24 h. After 48 h, the resulting solution was then lyophilized to yield a sticky light yellow solid. Yields were quantitative.

Representative synthesis of functional polyesters via thiol-ene reaction (pCL-sulfonate$_{40}$):

In a dram vial, sodium 3-mercaptopropane sulfonate (85.4 mg, 3 equivalents per alkene, 479 μmol) was reduced with TCEP·HCl (137.4 mg, 3 equivalents per alkene, 479 μmol) in H_2O (1.0 mL) for 1 h at 25 ºC. Separately, pCL-allyl$_{40}$ (25.0 mg, 1 eq, 4.0 μmol), DMPA (20.5 mg, 0.5 eq, 79.9 μmol), and tetrabutylammonium bromide (51.5 mg, 1 eq, 160 μmol) were combined in a dram vial equipped with a stir bar and DCM (1.0 mL). The reduced thiol and MeOH (200 μL) were added to the polymer vial. Final concentration of polymer was 0.3 mM. The mixture was degassed by sparging for 30 min with argon and then placed in the UV reactor on a stir plate with vigorous mixing and exposed to 365 nm UV light. After 30 min, the solution was opened and

dialyzed against 3.5 kDa MWCO in acetone/ H_2O for 24 h and then H_2O for 24 h. After 48 h, the resulting solution was then lyophilized to yield a sticky light yellow solid (quantitative yield).

12.4 kDa pCL-sulfonate$_{40}$ (1'): ^{1}H NMR (400 MHz, D_2O) δ 4.15 (s, 72H), 3.24 (d, J = 10.5 Hz, 93H), 3.00 (s, 69H), 2.66 (d, J = 32.8 Hz, 148H), 2.46 (s, 42H), 2.05 (s, 68H), 1.65 (d, J = 36.1 Hz, 412H), 1.41 (t, J = 7.4 Hz, 189H), 1.00 (t, J = 7.2 Hz, 148H). IR: ν = 2915, 1720, 1152, 1033 cm^{-1}. M_n (DMF SEC) = 10,800 Da; $Đ$ = 1.14.

41.8 kDa pCL-sulfonate$_{135}$ (2'): ^{1}H NMR (400 MHz, D_2O) δ 4.16 (s, 198H), 3.24 (s, 178H), 3.01 (s, 167H), 2.66 (d, J = 32.2 Hz, 349H), 2.45 (s, 135H), 1.65 (d, J = 35.8 Hz, 954H), 1.41 (d, J = 7.1 Hz, 432H), 0.99 (t, J = 7.3 Hz, 282H). IR: ν = 2921, 1721, 1150, 1029 cm^{-1}. M_n (DMF SEC) = 39,500 Da; $Đ$ = 1.21.

88.2 kDa pCL-sulfonate$_{285}$ (3'): ^{1}H NMR (400 MHz, D_2O) δ 4.15 (s, 538H), 3.25 (s, 610H), 3.00 (s, 555H), 2.66 (d, J = 33.7 Hz, 1142H), 2.45 (s, 285H), 2.05 (s, 542H), 1.65 (d, J = 37.2 Hz, 2935H), 1.50 – 1.28 (m, 1237H), 1.00 (t, J = 7.1 Hz, 875H). IR: ν = 2912, 1718, 1149, 1031 cm^{-1}. M_n (DMF SEC) = 76,300 Da; $Đ$ = 1.37.

114.4 kDa pCL-sulfonate$_{370}$ (4'): ^{1}H NMR (400 MHz, D_2O) δ 4.14 (s, 577H), 3.26 (s, 606H), 3.00 (s, 571H), 2.66 (d, J = 34.0 Hz, 1124H), 2.45 (s, 370H), 2.05 (s, 578H), 1.65 (d, J = 36.9 Hz, 2959H), 1.42 (d, J = 6.4 Hz, 1225H), 1.00 (t, J = 7.1 Hz, 811H). IR: ν = 2917, 1721, 1157, 1032 cm^{-1}. M_n (DMF SEC) = 105,600 Da; $Đ$ = 1.40.

146.0 kDa pCL-sulfonate$_{472}$ (5'): ^{1}H NMR (400 MHz, D_2O) δ 4.15 (s, 808H), 3.25 (t, J = 8.1 Hz, 1087H), 3.00 (s, 846H), 2.79 – 2.54 (m, 1682H), 2.45 (s, 472H), 2.05 (s, 838H), 1.65 (d, J = 36.8 Hz, 4476H), 1.41 (p, J = 7.4 Hz, 2005H), 1.00 (t, J = 7.2 Hz, 1626H). IR: ν = 2913, 1716, 1151, 1031 cm^{-1}. M_n (DMF SEC) = 143,500 Da; $Đ$ = 1.56.

163.3 kDa pCL-sulfonate$_{528}$ (6'): ^{1}H NMR (400 MHz, D_2O) δ 4.15 (s, 967H), 3.25 (d, J = 9.9 Hz, 1056H), 3.00 (s, 887H), 2.66 (d, J = 33.5 Hz, 1764H), 2.45 (s, 528H), 2.05 (s, 864H), 1.65 (d, J = 37.0 Hz, 4980H), 1.42 (dd, J = 14.6, 7.5 Hz, 2252H), 1.00 (t, J = 7.2 Hz, 1604H). IR: ν = 2912, 1724, 1149, 1036 cm^{-1}. M_n (DMF SEC) = 152,100 Da; $Đ$ = 1.63.

pCL-allyl$_{249}$-sulfonate$_{249}$: ^{1}H NMR (400 MHz, D_2O) δ 5.75 (s, 250H), 5.04 (s, 731H), 4.07 (s, 528H), 3.26 (s, 374H), 2.77 – 2.12 (m, 1359H), 1.69 (s, 1550H), 1.42 (s, 712H), 1.00 (s, 454H). *0.5 equivalent 3-mercaptopropane sulfonate used for this polymer only

Degradation of pCL-sulfonate:

The general procedure for the degradation experiments was adapted from previously reported literature.[12]

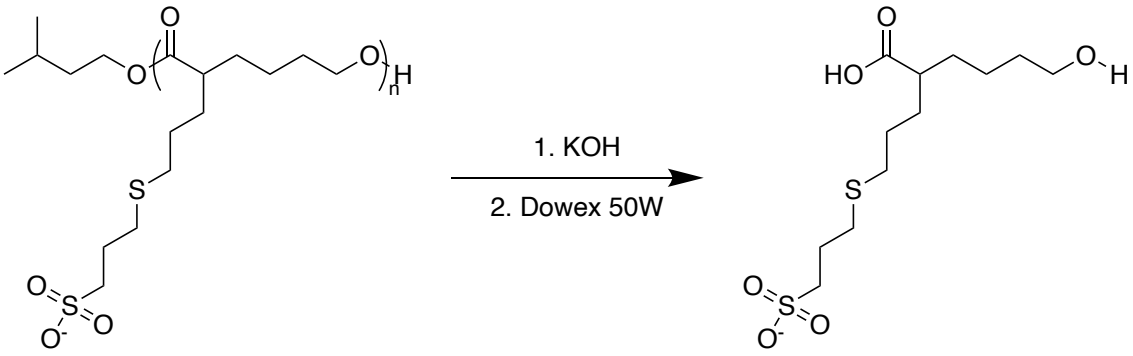

General Experimental Information

pCL-sulfonate (3 mg) was dissolved in 5% aqueous KOH (1 mL) and placed on a rotating place at 4 ºC. Aliquots (300 µL) were removed after 24 hours, neutralized with a strong cationic resin (Dowex 50W-8x200), lyophilized to remove solvent, and analyzed by DMF SEC to assess degradation.

5.5 Appendix IV

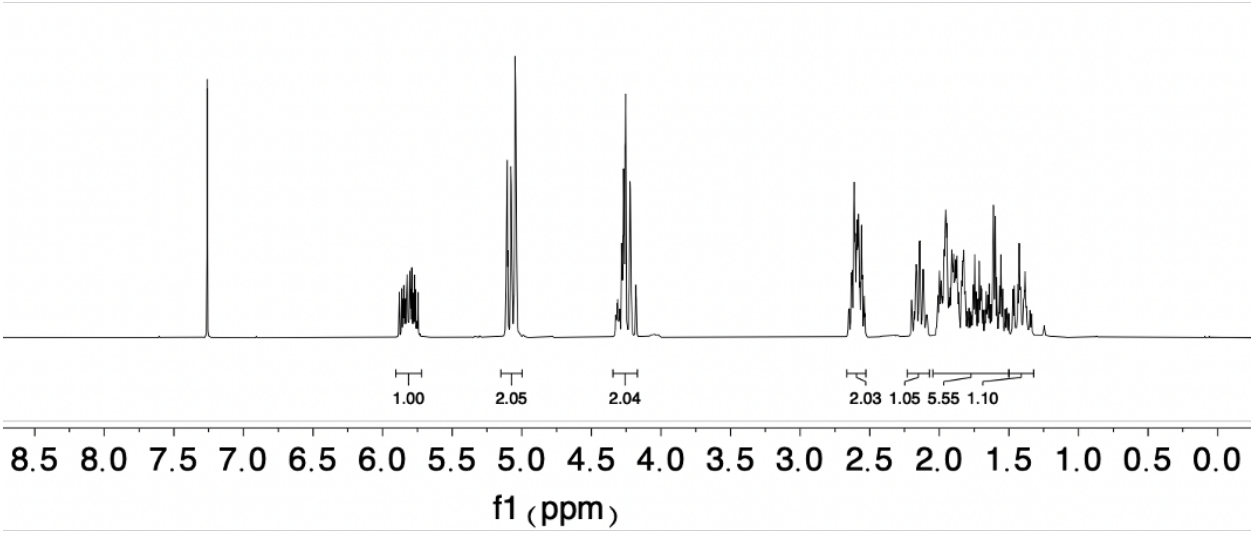

Figure 5.5. ^{1}H NMR spectrum allyl caprolactone (400 MHz, $CDCl_3$) at 23 ºC.

ENTRY	Catalyst/Base	Time (h)	Temperature °C	Concentration (M)	Target DP	%Conversion M_n (H^1 NMR)	DP (H^1 NMR)	M_n (H^1 NMR)
7	3-O/MTBD	5	20	2	150	66.7	100	15.5
8	3-O/MTBD	8	20	2	250	46.8	117	18.1
9	3-O/MTBD	8	50	2	250	53.7	134	20.8
10	3-O/MTBD	5	50	4	250	60.9	152	23.5
11	Urea 7/NaH	0.5	20	2	70	99.8	70	10.1
12	Urea 7/NaH	1	20	2	140	98.9	140	21.2
13	Urea 7/NaH	4	20	2	400	65.1	260	40.2
14	Urea 7/NaH	8	20	2	450	45.2	203	31.4
15	Urea 7/NaH	12	20	2	500	39.2	196	30.3

Table 5.3. ROP conditions screening. Initiator: Catalyst: Base Ratio: 1: 1.19: 1.19. 2-methyl 1-butanol was used to initiate all polymerizations in THF.

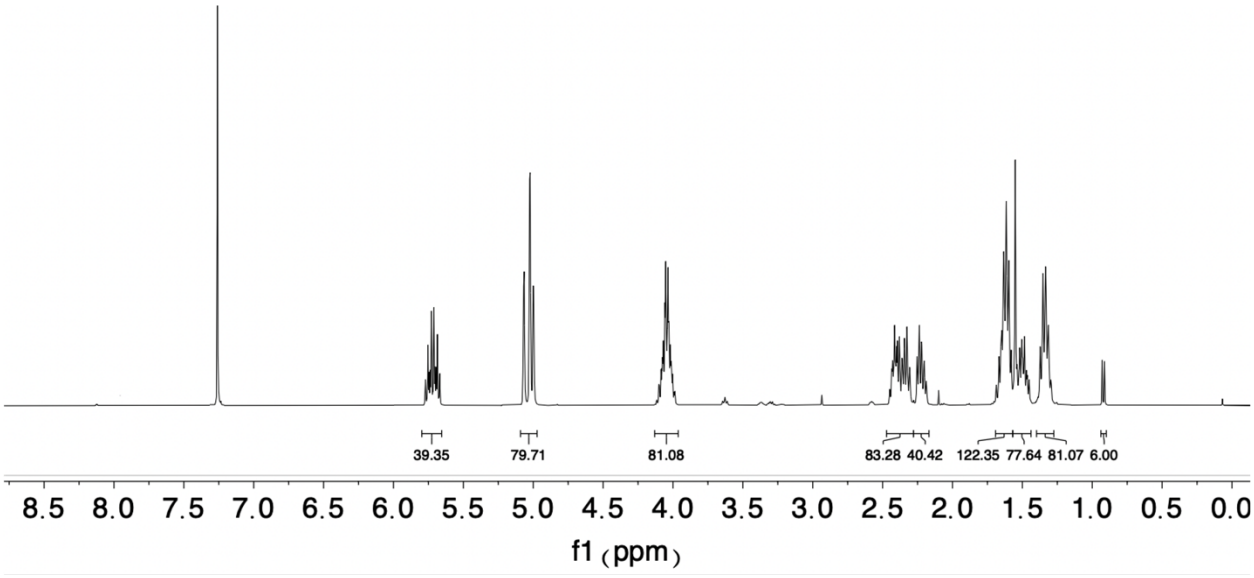

Figure 5.6. ^{1}H NMR spectrum pCL-allyl$_{40}$ (**1**) (400 MHz, $CDCl_3$) at 23 ºC.

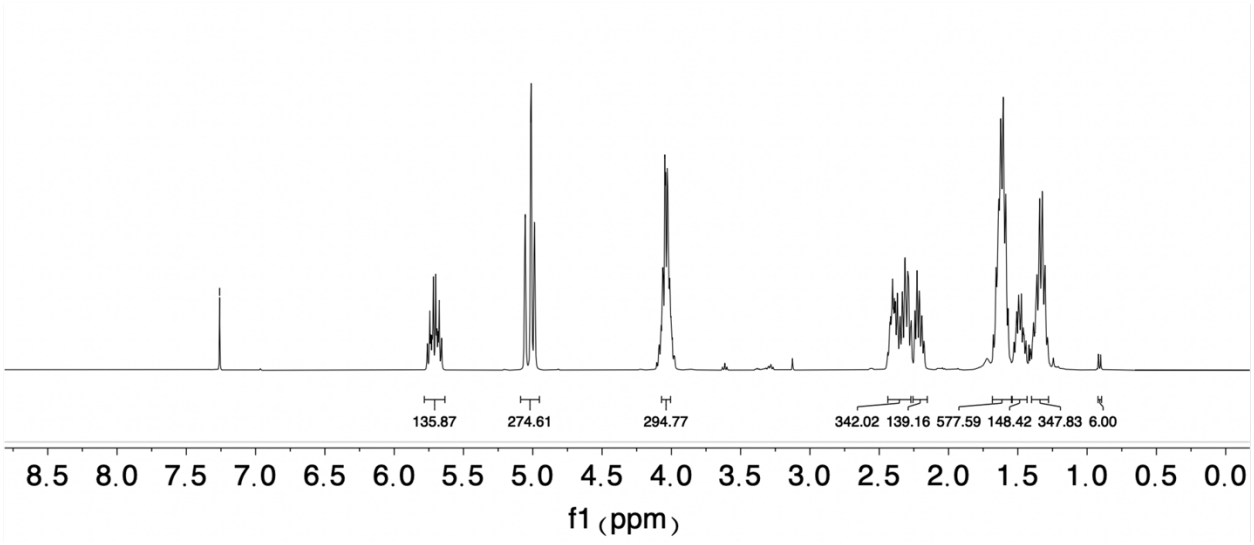

Figure 5.7. ^{1}H NMR spectrum pCL-allyl$_{135}$ (**2**) (400 MHz, $CDCl_3$) at 23 ºC.

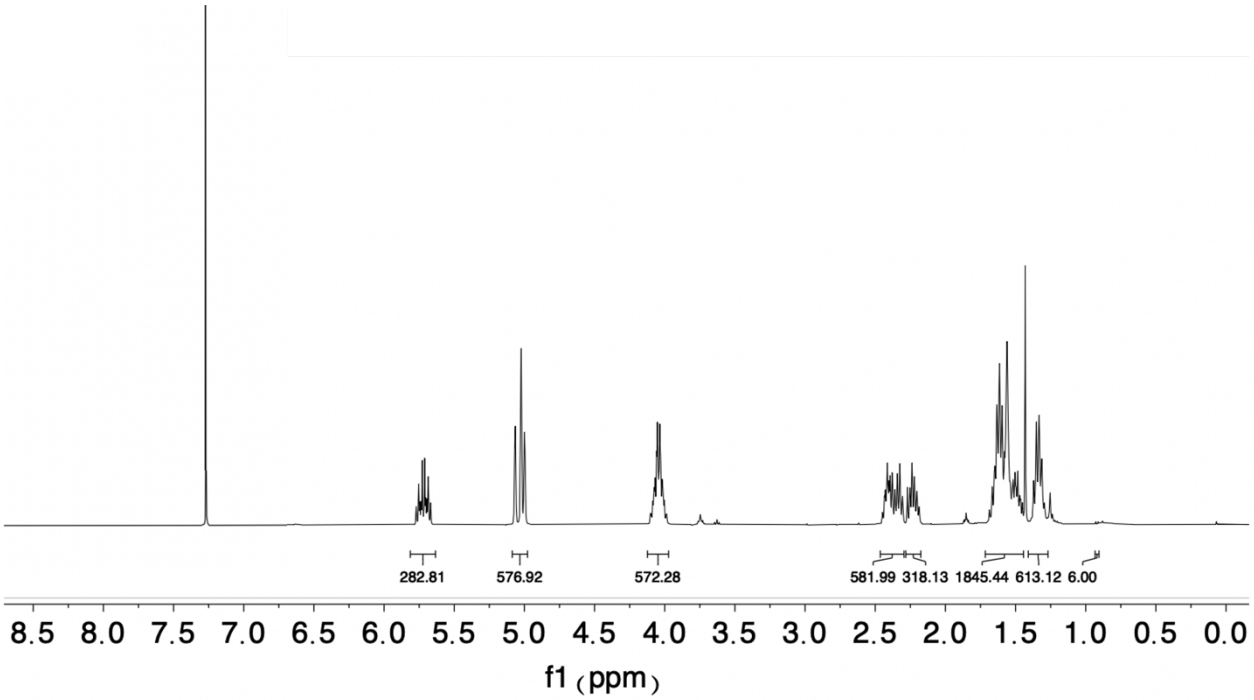

Figure 5.8. ^{1}H NMR spectrum pCL-allyl$_{285}$ (**3**) (400 MHz, $CDCl_3$) at 23 ºC.

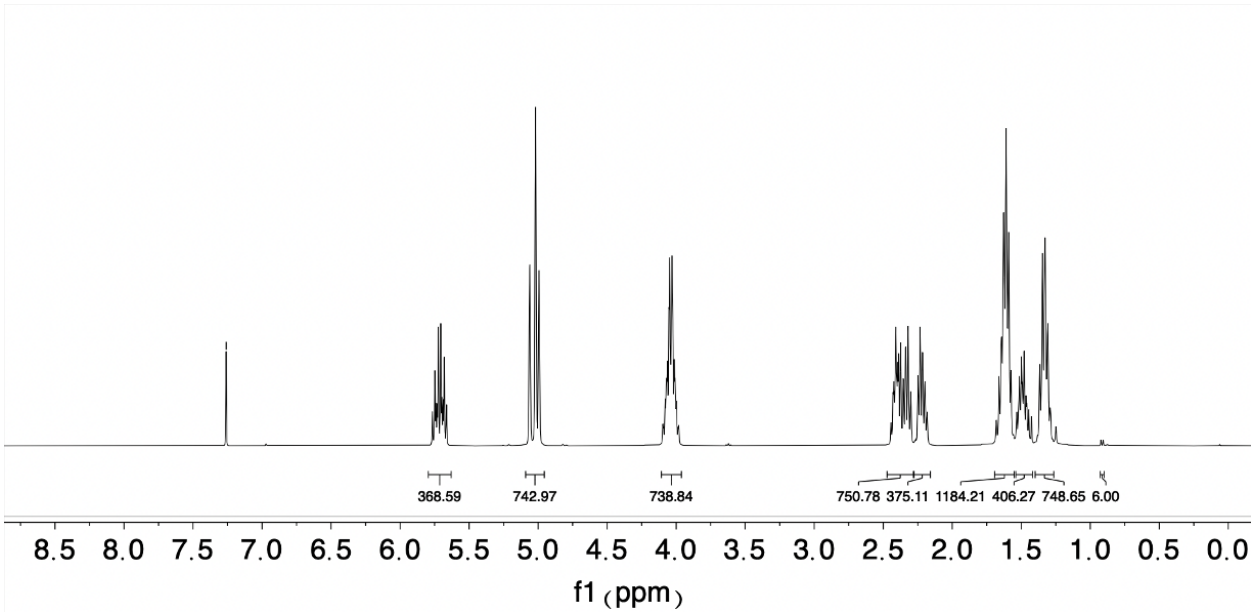

Figure 5.9. ^{1}H NMR spectrum pCL-allyl$_{370}$ (**4**) (400 MHz, $CDCl_3$) at 23 ºC.

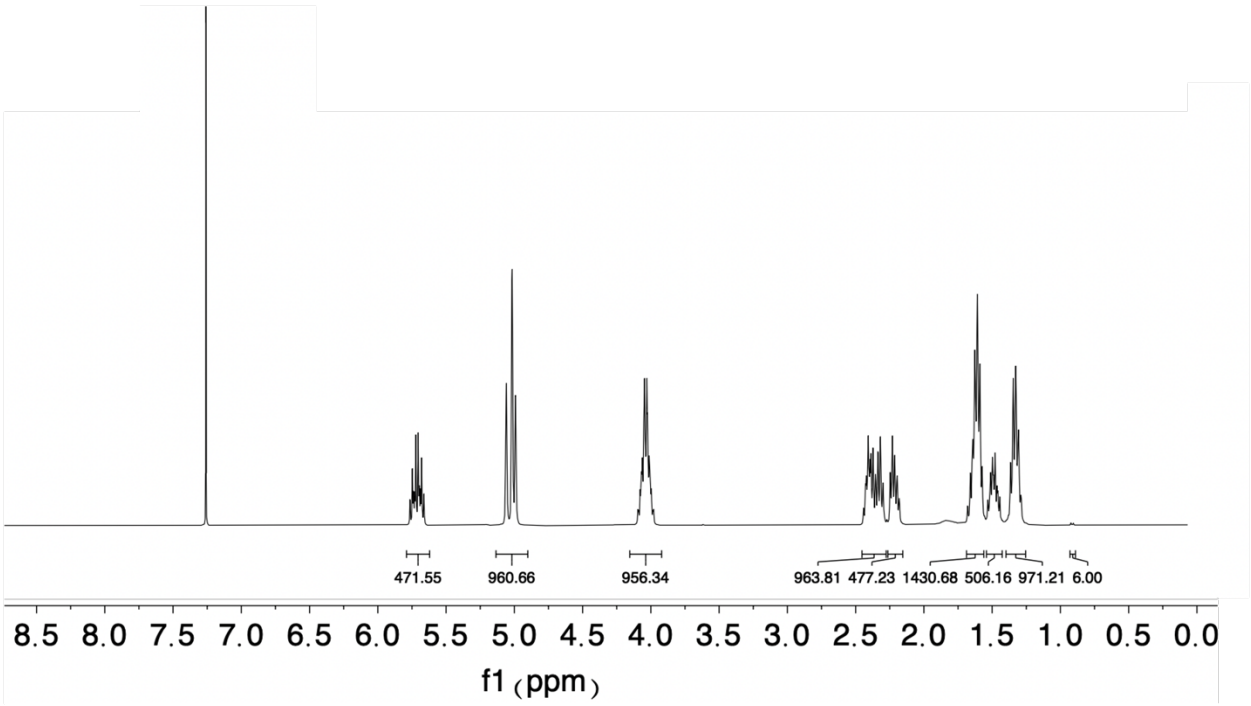

Figure 5.10. ^{1}H NMR spectrum pCL-allyl$_{472}$ (**5**) (400 MHz, $CDCl_3$) at 23 ºC.

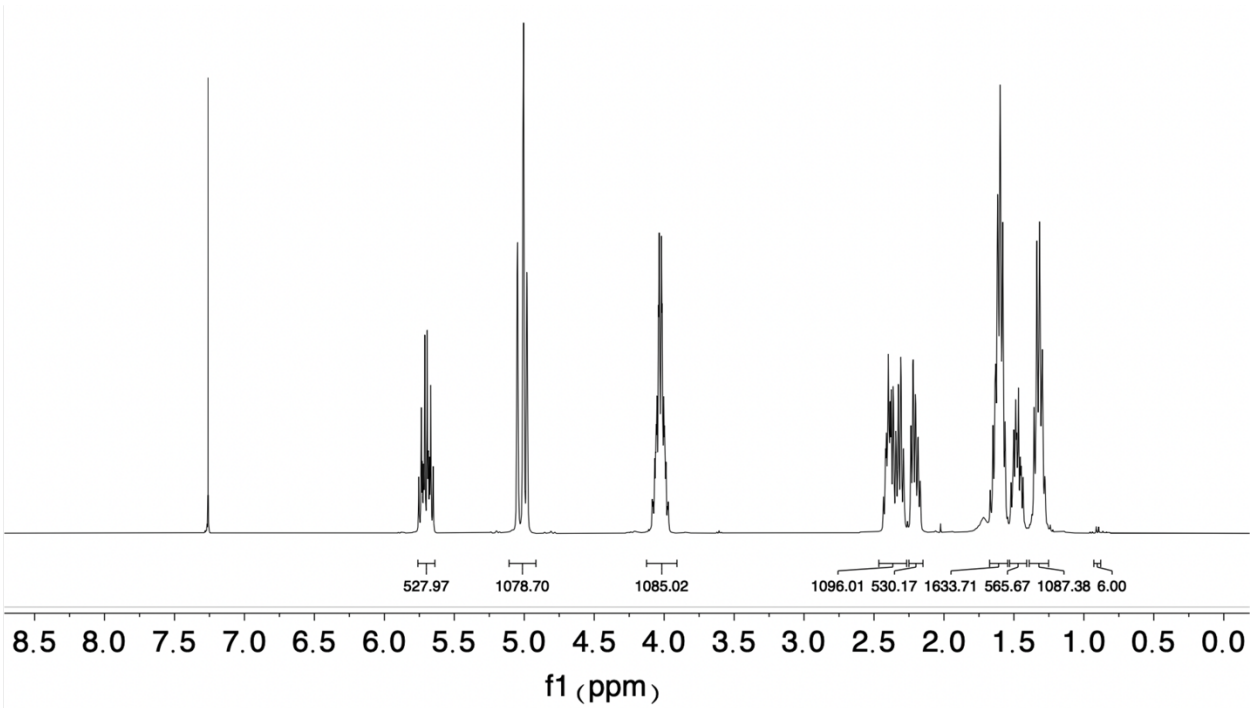

Figure 5.11. ^{1}H NMR spectrum pCL-allyl$_{528}$ (**6**) (400 MHz, $CDCl_3$) at 23 ºC.

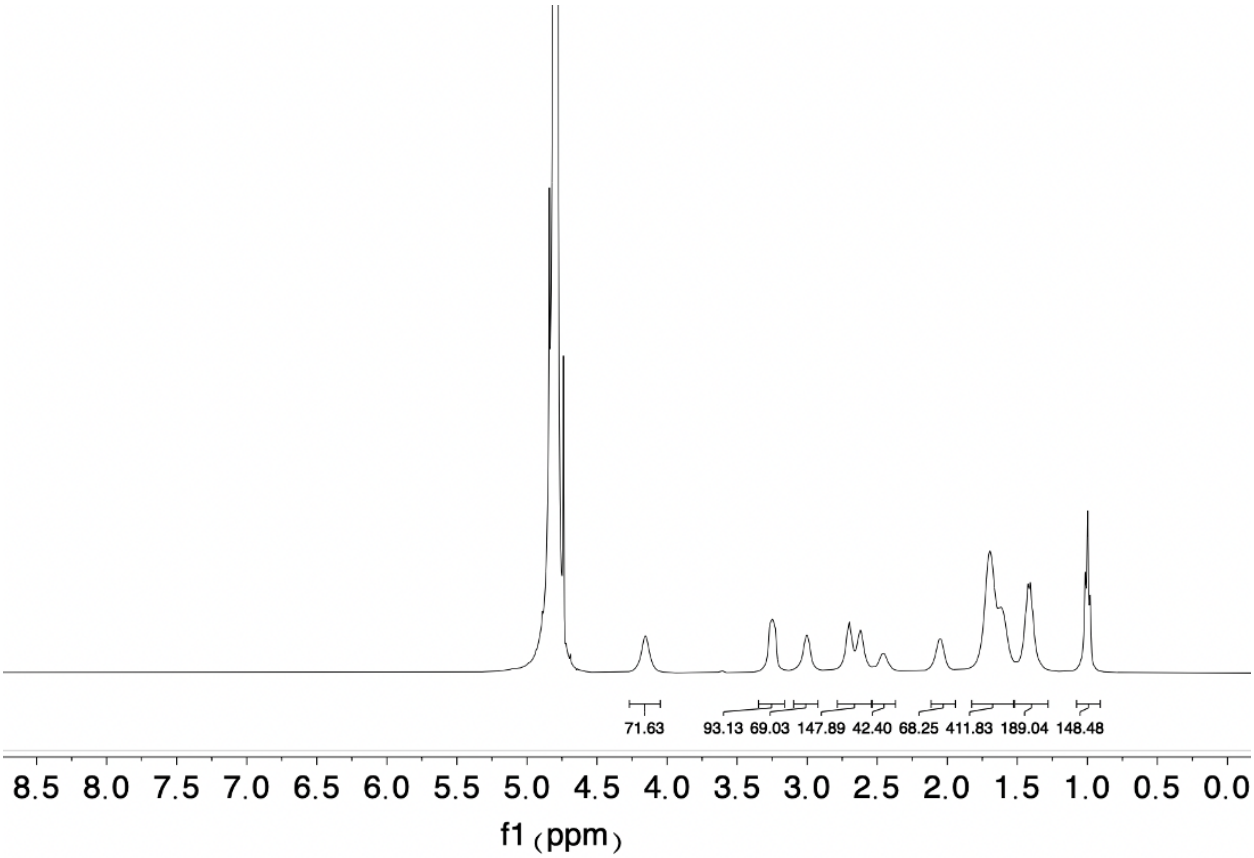

Figure 5.12. ^{1}H NMR spectrum pCL-sulfonate$_{40}$ (**1'**) (400 MHz, D_2O) at 23 ºC.

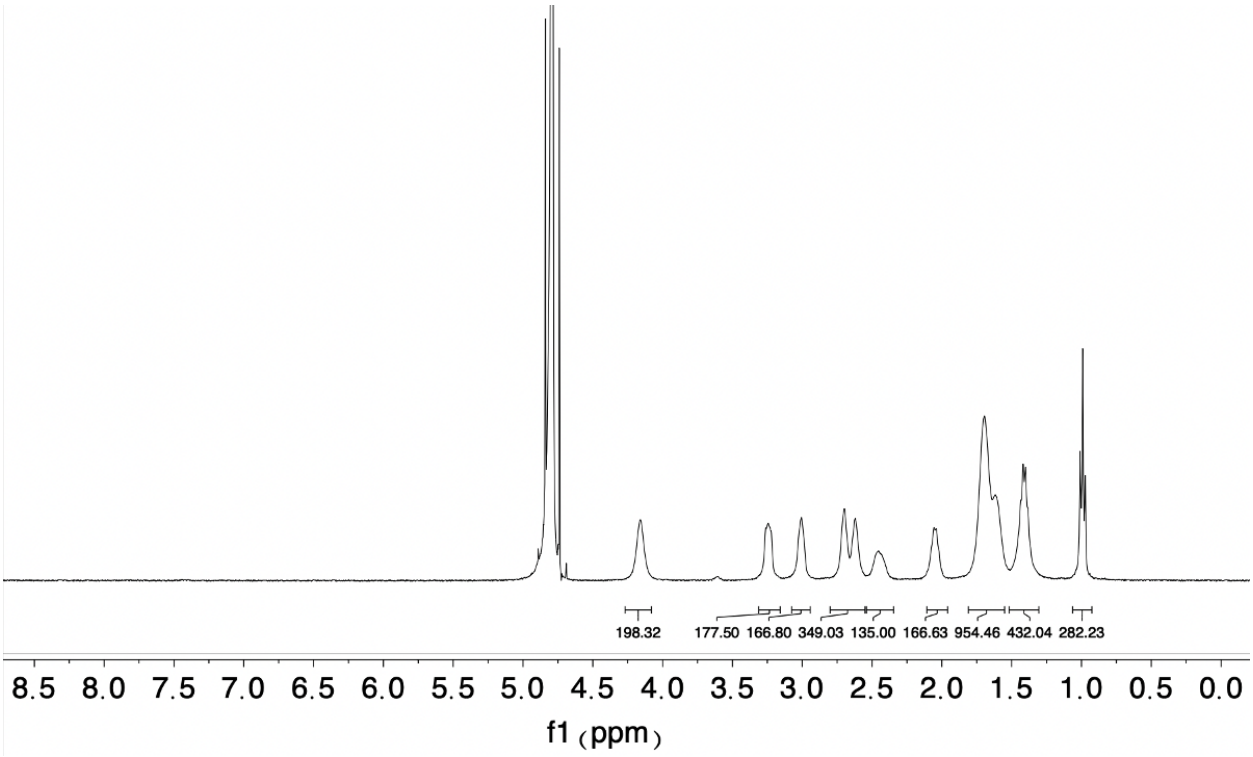

Figure 5.13. ^{1}H NMR spectrum pCL-sulfonate$_{135}$ (**2'**) (400 MHz, D_2O) at 23 ºC.

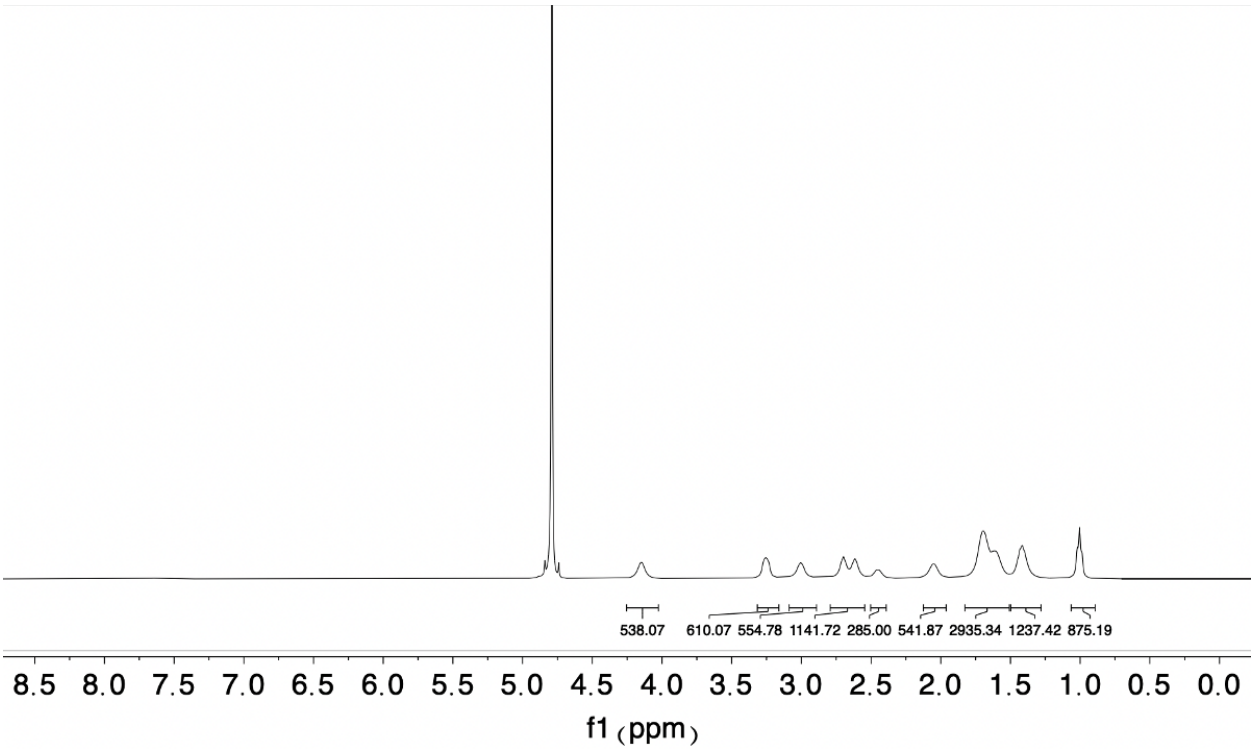

Figure 5.14. ^{1}H NMR spectrum pCL-sulfonate$_{285}$ (**3'**) (400 MHz, D_2O) at 23 ºC.

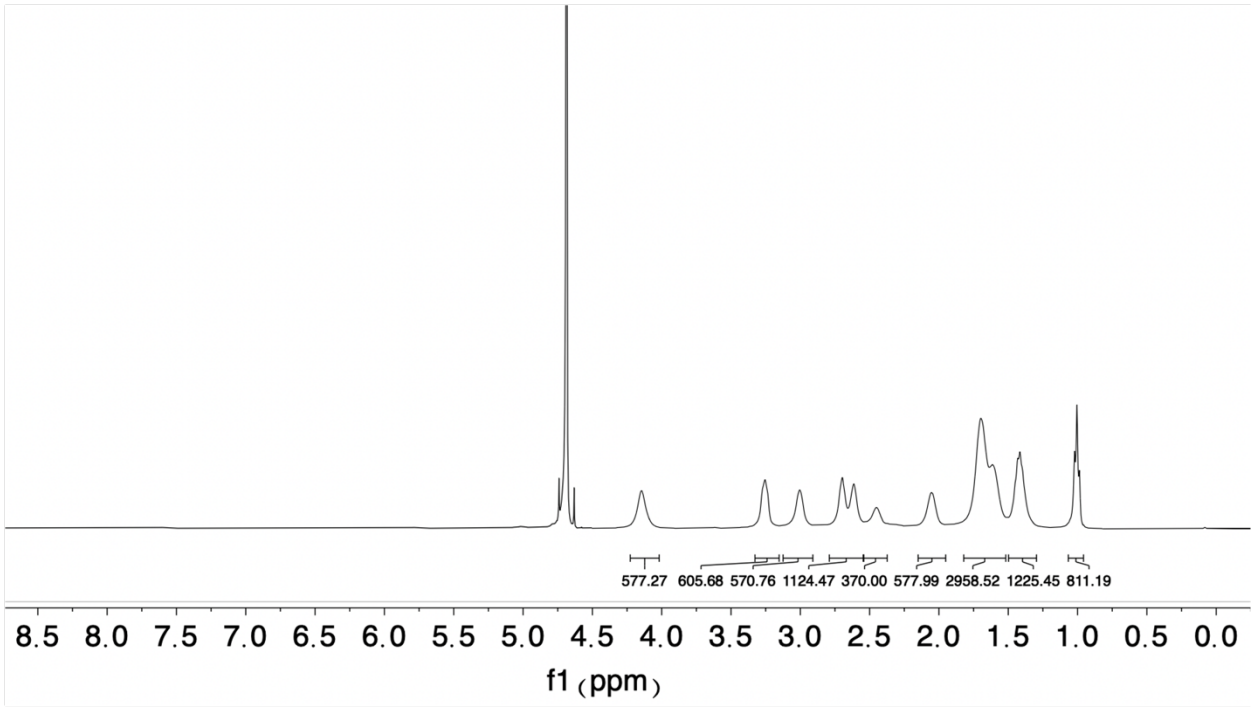

Figure 5.15. ^{1}H NMR spectrum pCL-sulfonate$_{370}$ (**4'**) (400 MHz, D_2O) at 23 ºC.

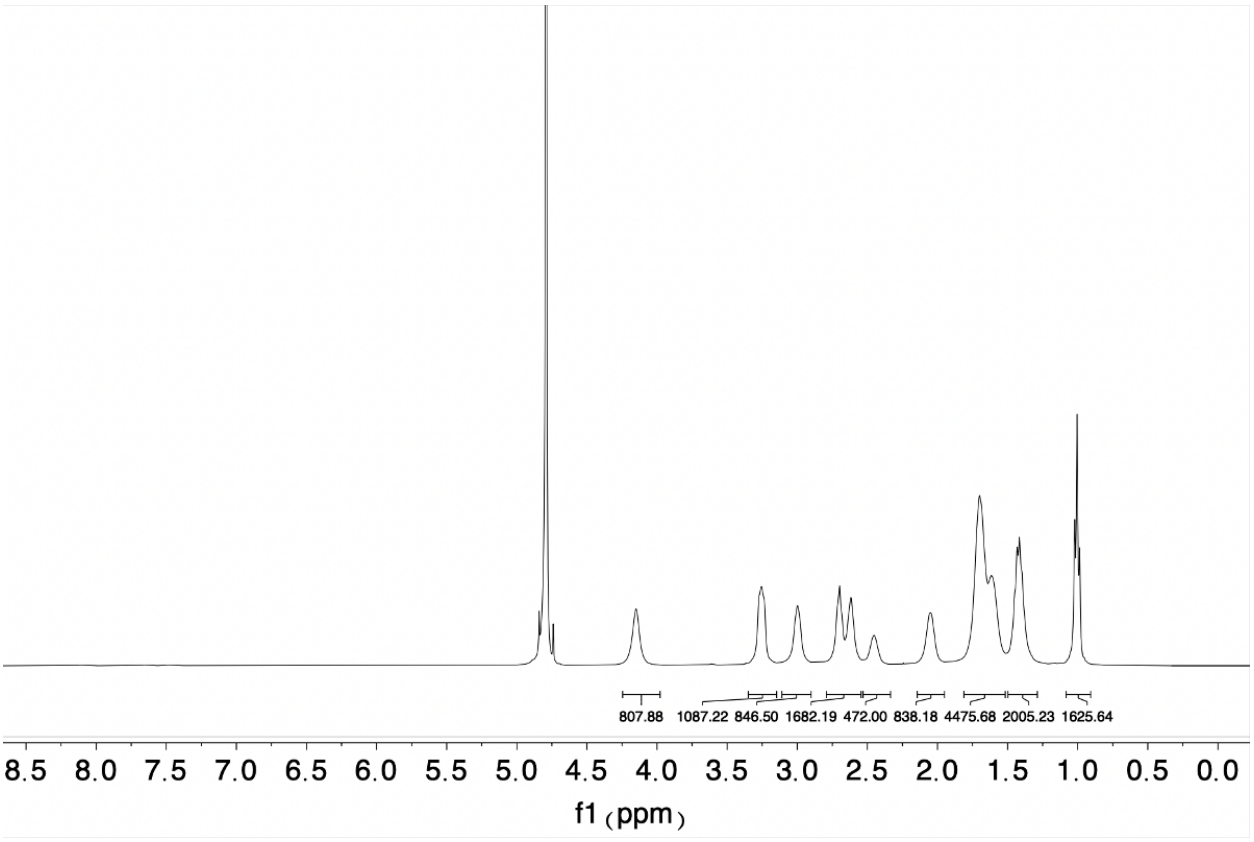

Figure 5.16. ^{1}H NMR spectrum pCL-sulfonate$_{472}$ (**5'**) (400 MHz, D_2O) at 23 ºC.

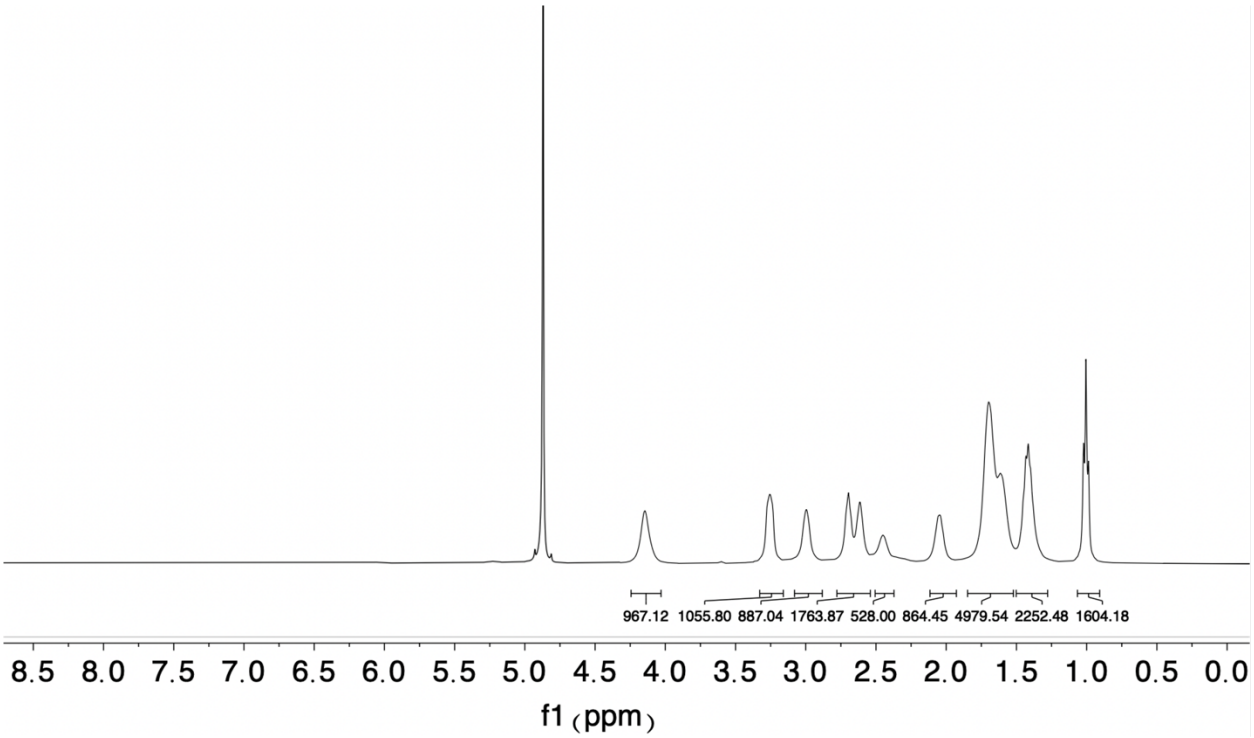

Figure 5.11. ^{1}H NMR spectrum pCL-sulfonate$_{528}$ (**6'**) (400 MHz, D_2O) at 23 ºC.

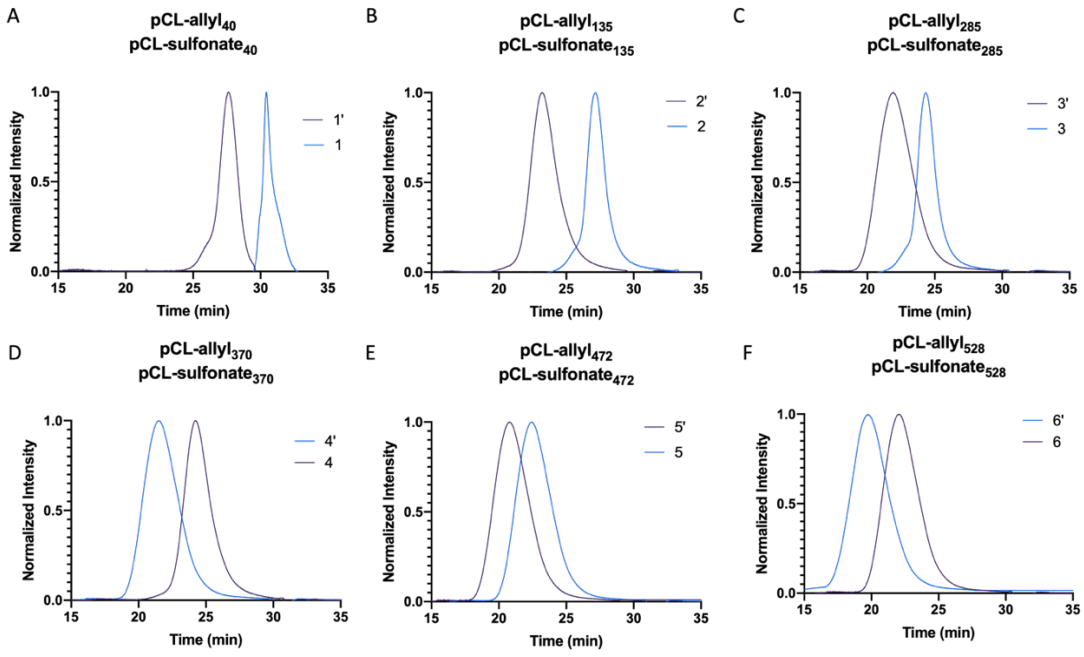

Figure 5.18. DMF Size exclusion chromatography of pCL-sulfonate$_n$ overlayed with pCL-allyl$_n$. (A) n= 40 (B) n= 135, (C) n= 285, (D) n= 370, (E) n= 472, (F) n= 528.

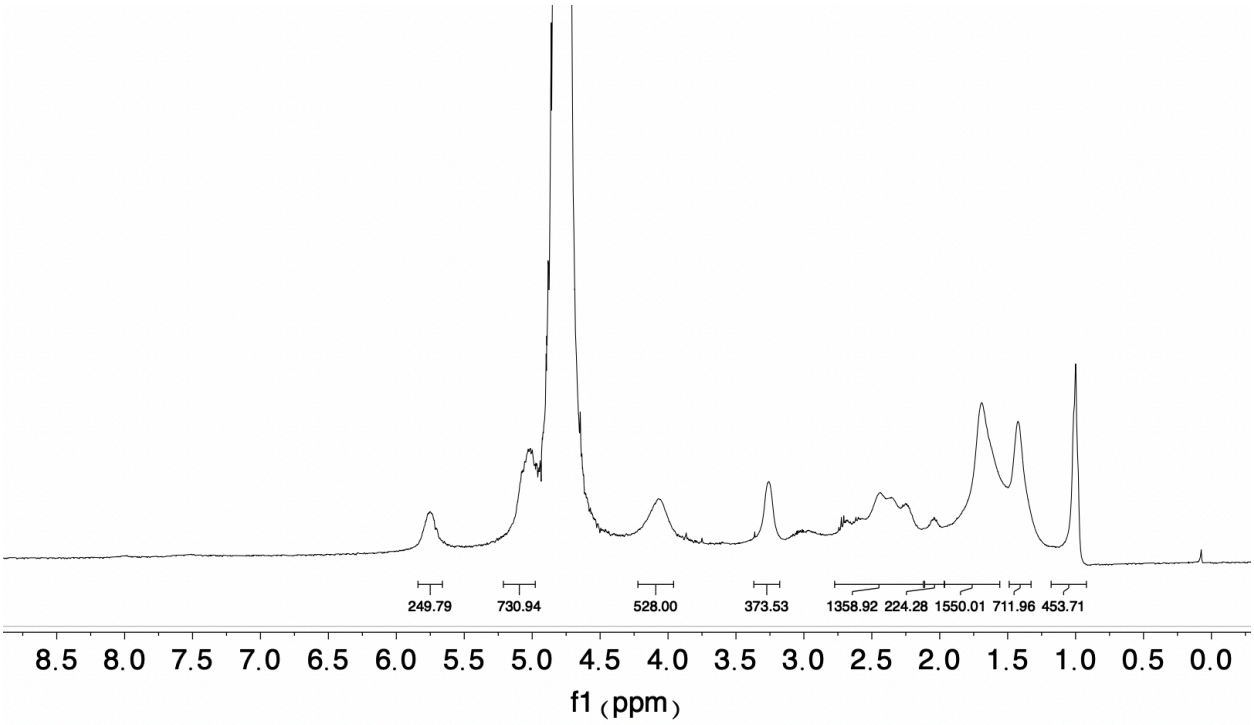

Figure 5.19. ^{1}H NMR spectrum pCL-allyl$_{249}$-sulfonate$_{249}$ (400 MHz, D_2O) at 23 ºC.

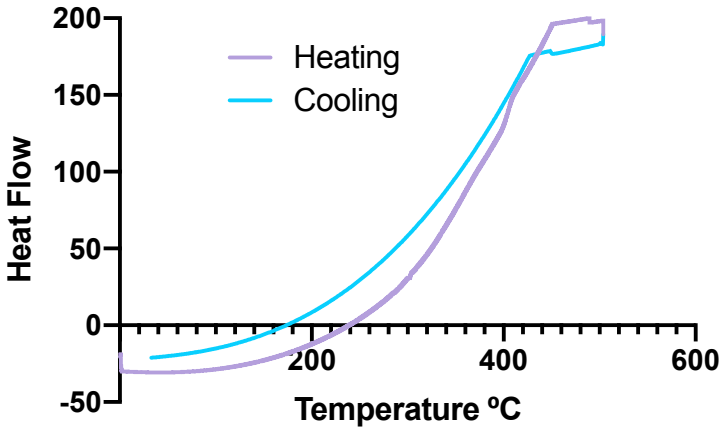

Figure 5.20. Representative DSC of pCL-sulfonate$_{524}$.

5.6 References

(1) La Fuente, C. I. A.; Maniglia, B. C.; Tadini, C. C. Biodegradable Polymers: A Review about Biodegradation and Its Implications and Applications. *Packag. Technol. Sci.* **2023**, *36* (2), 81–95. https://doi.org/10.1002/pts.2699.

(2) Sushma, M. V.; kadam, A.; Kumar, D.; Mutreja, I. Biodegradable Polymers. In *Biomaterials and Biopolymers*; Domb, A., Mizrahi, B., Farah, S., Eds.; Springer International Publishing: Cham, 2023; pp 33–54. https://doi.org/10.1007/978-3-031-36135-7_2.

(3) Alaswad, S. O.; Mahmoud, A. S.; Arunachalam, P. Recent Advances in Biodegradable Polymers and Their Biological Applications: A Brief Review. *Polymers* **2022**, *14* (22), 4924. https://doi.org/10.3390/polym14224924.

(4) *Biomedical Applications of Biodegradable Polyesters*. https://www.mdpi.com/2073-4360/8/1/20 (accessed 2024-10-23).

(5) *Biodegradable Polymers: Medical Applications - Kunduru - Major Reference Works - Wiley Online Library*. https://onlinelibrary.wiley.com/doi/full/10.1002/0471440264.pst027.pub2 (accessed 2024-10-23).

(6) Hakvåg, S.; Brakstad, O. G.; Kubowicz, S.; Booth, A. M. Chapter 2 - Composition, Properties and Other Factors Influencing Plastics Biodegradability. In *Biodegradability of Conventional Plastics*; Sarkar, A., Sharma, B., Shekhar, S., Eds.; Elsevier, 2023; pp 17–45. https://doi.org/10.1016/B978-0-323-89858-4.00014-2.

(7) Manavitehrani, I.; Fathi, A.; Badr, H.; Daly, S.; Shirazi, A. N.; Dehghani, F. Biomedical Applications of Biodegradable Polyesters. *Polymers* **2016**, *8* (1), 20. https://doi.org/10.3390/polym8010020.

(8) Porter, J. R.; Henson, A.; Popat, K. C. Biodegradable Poly(ε-Caprolactone) Nanowires for Bone Tissue Engineering Applications. *Biomaterials* **2009**, *30* (5), 780–788. https://doi.org/10.1016/j.biomaterials.2008.10.022.

(9) Emadi, H.; Karevan, M.; Masoudi Rad, M.; Sadeghzade, S.; Pahlevanzadeh, F.; Khodaei, M.; Khayatzadeh, S.; Lotfian, S. Bioactive and Biodegradable Polycaprolactone-Based Nanocomposite for Bone Repair Applications. *Polymers* **2023**, *15* (17), 3617. https://doi.org/10.3390/polym15173617.

(10) Dash, T. K.; Konkimalla, V. B. Poly-ϵ-Caprolactone Based Formulations for Drug Delivery and Tissue Engineering: A Review. *J. Controlled Release* **2012**, *158* (1), 15–33. https://doi.org/10.1016/j.jconrel.2011.09.064.

(11) Kunkel, G. E.; Treacy, J. W.; Montgomery, H. R.; Puente, E. G.; Doud, E. A.; Spokoyny, A. M.; Maynard, H. D. Efficient End-Group Functionalization and Diblock Copolymer Synthesis *via* Au(III) Polymer Reagents. *Chem. Commun.* **2024**, *60* (1), 79–82. https://doi.org/10.1039/D3CC05350D.

(12) Pelegri-O'Day, E. M.; Paluck, S. J.; Maynard, H. D. Substituted Polyesters by Thiol–Ene Modification: Rapid Diversification for Therapeutic Protein Stabilization. *J. Am. Chem. Soc.* **2017**, *139* (3), 1145–1154. https://doi.org/10.1021/jacs.6b10776.

(13) Öztürk, T.; Meyvacı, E.; Arslan, T. Synthesis and Characterization of Poly(Vinyl Chloride-g-ε-Caprolactone) Brush Type Graft Copolymers by Ring-Opening Polymerization and "Click" Chemistry. *J. Macromol. Sci. Part A* **2020**, *57* (3), 171–180. https://doi.org/10.1080/10601325.2019.1680253.

(14) Qin, X.; Wu, Y.; Liu, S.; Yang, L.; Yuan, H.; Cai, S.; Flesch, J.; Li, Z.; Tang, Y.; Li, X.; Zhuang, Y.; You, C.; Liu, C.; Yu, C. Surface Modification of Polycaprolactone Scaffold With

Improved Biocompatibility and Controlled Growth Factor Release for Enhanced Stem Cell Differentiation. *Front. Bioeng. Biotechnol.* **2022**, *9*. https://doi.org/10.3389/fbioe.2021.802311.

(15) Akram, A.; Iqbal, M.; Yasin, A.; Zhang, K.; Li, J. Sulfonated Molecules and Their Latest Applications in the Field of Biomaterials: A Review. *Coatings* **2024**, *14* (2), 243. https://doi.org/10.3390/coatings14020243.

(16) Dimassi, S.; Tabary, N.; Chai, F.; Blanchemain, N.; Martel, B. Sulfonated and Sulfated Chitosan Derivatives for Biomedical Applications: A Review. *Carbohydr. Polym.* **2018**, *202*, 382–396. https://doi.org/10.1016/j.carbpol.2018.09.011.

(17) Hoffmann, M.; Snyder, N. L.; Hartmann, L. Polymers Inspired by Heparin and Heparan Sulfate for Viral Targeting. *Macromolecules* **2022**, *55* (18), 7957–7973. https://doi.org/10.1021/acs.macromol.2c00675.

(18) Paluck, S. J.; Nguyen, T. H.; Maynard, H. D. Heparin-Mimicking Polymers: Synthesis and Biological Applications. *Biomacromolecules* **2016**, *17* (11), 3417–3440. https://doi.org/10.1021/acs.biomac.6b01147.

(19) Amokrane, G.; Humblot, V.; Jubeli, E.; Yagoubi, N.; Ramtani, S.; Migonney, V.; Falentin-Daudré, C. Electrospun Poly(ε-Caprolactone) Fiber Scaffolds Functionalized by the Covalent Grafting of a Bioactive Polymer: Surface Characterization and Influence on in Vitro Biological Response. *ACS Omega* **2019**, *4* (17), 17194–17208. https://doi.org/10.1021/acsomega.9b01647.

(20) Leroux, A.; Ngoc Nguyen, T.; Rangel, A.; Cacciapuoti, I.; Duprez, D.; Castner, D. G.; Migonney, V. Long-Term Hydrolytic Degradation Study of Polycaprolactone Films and

Fibers Grafted with Poly(Sodium Styrene Sulfonate): Mechanism Study and Cell Response. *Biointerphases* **2020**, *15* (6), 061006. https://doi.org/10.1116/6.0000429.

(21) Rohman, G.; Huot, S.; Vilas-Boas, M.; Radu-Bostan, G.; Castner, D. G.; Migonney, V. The Grafting of a Thin Layer of Poly(Sodium Styrene Sulfonate) onto Poly(ε-Caprolactone) Surface Can Enhance Fibroblast Behavior. *J. Mater. Sci. Mater. Med.* **2015**, *26* (7), 206. https://doi.org/10.1007/s10856-015-5539-7.

(22) Nguyen, T. N.; Rangel, A.; Migonney, V. Kinetic and Degradation Reactions of Poly (Sodium 4-Styrene Sulfonate) Grafting "from" Ozonized Poly (ϵ-Caprolactone) Surfaces. *Polym. Degrad. Stab.* **2020**, *176*, 109154. https://doi.org/10.1016/j.polymdegradstab.2020.109154.

(23) Pelegri-O'Day, E. M.; Bhattacharya, A.; Theopold, N.; Ko, J. H.; Maynard, H. D. Synthesis of Zwitterionic and Trehalose Polymers with Variable Degradation Rates and Stabilization of Insulin. *Biomacromolecules* **2020**, *21* (6), 2147–2154. https://doi.org/10.1021/acs.biomac.0c00133.

(24) Yang, J.; Gelb, M. B.; Tamshen, K.; Forsythe, N. L.; Ko, J. H.; Puente, E. G.; Pelegri-O'Day, E.; Jamieson, S. M. F.; Perry, J. K.; Maynard, H. D. Site-Selective Zwitterionic Poly(Caprolactone-Carboxybetaine)-Growth Hormone Receptor Antagonist Conjugate: Synthesis and Biological Evaluation. *Biomacromolecules* **2024**. https://doi.org/10.1021/acs.biomac.4c00828.

(25) Shen, J.; Yuan, W.; Badv, M.; Moshaverinia, A.; Weiss, P. S. Modified Poly(ε-Caprolactone) with Tunable Degradability and Improved Biofunctionality for Regenerative Medicine. *ACS Mater. Au* **2023**, *3* (5), 540. https://doi.org/10.1021/acsmaterialsau.3c00027.

(26) Parrish, B.; Quansah, J. K.; Emrick, T. Functional Polyesters Prepared by Polymerization of A-allyl(Valerolactone) and Its Copolymerization with E-caprolactone and Δ-valerolactone. *J. Polym. Sci. Part Polym. Chem.* **2002**, *40* (12), 1983–1990. https://doi.org/10.1002/pola.10277.

(27) Lin, B.; Waymouth, R. M. Urea Anions: Simple, Fast, and Selective Catalysts for Ring-Opening Polymerizations. *J. Am. Chem. Soc.* **2017**, *139* (4), 1645–1652. https://doi.org/10.1021/jacs.6b11864.

(28) Pratt, R. C.; Lohmeijer, B. G. G.; Long, D. A.; Lundberg, P. N. P.; Dove, A. P.; Li, H.; Wade, C. G.; Waymouth, R. M., Hedrick, J. L. Organic Catalysis for Ring-Opening Polymerization. *Macromolecules*, **2006**, 39, 7863–7871. https://doi.org/10.1021/mz3005956.